The Quantized Velocity Finite Element Method

Charles M. Cook

Dissertation submitted to the faculty of the
Virginia Polytechnic Institute and State University
in partial fulfillment of the requirements for the degree of

Doctor of Philosophy
in
Engineering Mechanics

Rakesh K. Kapania
Justin Kauffman
Luca Massa
Mark A. Stremler

November 28, 2023
Blacksburg, Virginia

Keywords:
Computational Fluid Dynamics
Finite Element Methods
Compressible Flow
Lattice Boltzmann Methods

The Quantized Velocity Finite Element Method

Charles M. Cook

ABSTRACT

The Euler and Navier-Stokes-Fourier equations will be directly expressed as distribution evolution equations, where a new and proper continuum prescription will be derived. These equations of motion will be numerically solved with the development of a new and unique finite element formulation. Out of this framework, the 7D phasetime element has been born. To provide optimal stability, a new quantization procedure is established based on the principles of quantum theory. The entirety of this framework has been coined the "quantized velocity finite element method" (QVFEM). The work performed herein lays the foundational development of what is hoped to become a new paradigm shift in computational fluid dynamics.

The Quantized Velocity Finite Element Method

Charles M. Cook

GENERAL AUDIENCE ABSTRACT

To model any of the four fundamental states of matter, for practical engineering applications, we must first recognize the complexity of such states. In consequence, a new and novel approach is presented on how to numerically simulate the dynamics of a gas using both the Euler and Navier-Stokes-Fourier equations of continuum mechanics and thermodynamics. In contrast to direct numerical simulation, a statistical mechanical prescription will be given where the equations of motion will be quantized using methods taken from the study of quantum mechanics. This newly developed discretization of the phase space and time, or phasetime, provides optimal stability for compressible flow simulations. From the newly proposed framework, the 7D phasetime element has been born.

The Quantized Velocity Finite Element Method

Charles M. Cook

DEDICATION

I would like to dedicate this work to the three people who wrote and submitted letters of recommendation, on my behalf, while applying to graduate programs:

Sunil Saigal, Ph.D., P.E.

Ryan Brownell, P.E.

Professor Eric Compton

I applied to exactly twenty graduate schools and was accepted into four; one being Virginia Tech. Dr. Saigal and Prof. Compton were two of my favorite professors whose classes I still remember quite distinctly. I would also like to give Prof. Lisa Hailey a shout-out. Several years after obtaining my bachelors degree, Dr. Saigal became a mentor of mine. While I was applying to graduate schools, we would meet at local coffee shops where he would give me advice on where to apply, what to say and write, and overall career advice. This is a man whom I very much admire and appreciate. When the time comes, I will do the same for others.

Ryan was one of the many professional engineers I worked under during my time at French and Parrello Associates (FPA). He was hard-working, well-organized, and always made time to properly explain what was needed on the plans and to answer any questions I had. In fact, I almost left graduate school to go and work for him again. Our lives are finite, and unfortunately, Ryan's was cut short. I wish I could show you what you've helped me accomplish.

I would lastly like to thank all of my dogs for all the love and support throughout the years:

Lady
Leo
Tracey
Cooper

Whenever I'm working, there is always a dog laying by my side for moral support. Throughout my final year at graduate school, Cooper spent about as much time as I did in my office. I stand on the shoulders of James Clerk Maxwell.

The Quantized Velocity Finite Element Method

Charles M. Cook

TABLE OF CONTENTS

Chapter 1 – Prelude

1.1 Background

The core governing field equations, which model the dynamics of fluids and gases, have long been established due to the collective work by Newton [1], Euler [2], Navier [3], Stokes [4], and among others such as Cauchy, Poisson, and Saint-Venant [5,6]. The famous momentum transport equations are known as the Navier-Stokes (NS) equations, which are a viscous extension to the inviscid Euler equations. Since their final development in the early-to-mid 1800s, general solutions have remained unattainable. In fact, on the date of May 24, 2000 the Clay Mathematics Institute of Cambridge, Massachusetts announced seven millennium prize problems; one being the incompressible NS equations[1].

The act of numerically approximating these sets of equations has become a science in itself, which is otherwise known as computational fluid dynamics (CFD). This computational science only became viable with the invention of the programmable computer and remains an active area of research today. Approximate solutions to any set of field equations, which may describe the dynamics and/or behavior of any of the four fundamental states of matter, have and will most likely continue to serve as a critical engineering design tool. For example, in structural mechanics, finite element analysis has had much success and is the leading methodology used in commercial software such as Nastran, Abaqus, and Ansys packages.

1.2 Tensor Notation

Before discussing some of the current research trends in CFD, it will be beneficial to briefly review the adopted notation. To represent tensor quantities, index notation will be used throughout. Additionally, the Einstein summation convention may replace the summation operator. In general, lowercase letters which are bold, e.g. $\boldsymbol{a}$, or with one index, e.g. a_i, will represent a vector or rank 1 tensor while uppercase letters which are bold, e.g. $\mathbf{A}$, or with multiple indices, e.g. A_{ij}, will represent higher order tensors. The inner product between two vectors is then:

$$\boldsymbol{a} \cdot \boldsymbol{b} = \sum_i a_i b_i = a_i b_i \tag{1}$$

Which produces a scalar quantity while the outer product, i.e. $\boldsymbol{a} \otimes \boldsymbol{b}$ or $a_i b_j$, forms a rank 2 tensor. The trace operation, represented by $\mathrm{tr}(\boldsymbol{a} \otimes \boldsymbol{b})$, is equal to the inner product. A commonly used rank 2 tensor, in this work, is the Kronecker delta tensor defined as:

$$\delta_{ij} = \begin{cases} 1 & \text{if } \; i = j \\ 0 & \text{if } \; i \neq j \end{cases} \tag{2}$$

Higher order versions exist in even ranks. For example, the rank 4 Kronecker delta tensor is:

$$\delta_{ijkl} = \delta_{ij}\delta_{kl} + \delta_{ik}\delta_{jl} + \delta_{il}\delta_{jk} \tag{3}$$

[1] https://www.claymath.org/millennium/navier-stokes-equation/

Chapter 2 – Literature Review

The quantized velocity finite element method (QVFEM) originates from the lattice Boltzmann method (LBM) [7,8] whose precursor is the lattice gas cellular automata (LGCA). Therefore, the LBM will herein be reviewed. To do so, we must first derive the Boltzmann equation.

2.1 The Generalized Boltzmann Equation

To begin, let us define a system of n molecules each with a center of mass assigned to a cartesian coordinate $\mathbf{x}_i \ \forall \ i = 1,2,\dots,n$ measured from the stationary reference point $\mathbf{x}_\mathrm{o}$. The set of all positions within the 3D Euclidean space is then $\mathbf{x}_1, \mathbf{x}_2, \dots, \mathbf{x}_n$ whose associated velocities are denoted $\dot{\mathbf{x}}_1, \dot{\mathbf{x}}_2, \dots, \dot{\mathbf{x}}_n$. To relate the molecules via their relative positions $\boldsymbol{\delta}_i$, the molecular network will be defined from the recursive formula: $\mathbf{x}_i = \mathbf{x}_{i-1} + \boldsymbol{\delta}_i$. Upon writing out each term, one may express the position of each molecule as a function of the relative positions:

$$\mathbf{x}_i = \mathbf{x}_\mathrm{o} + \textstyle\sum_{k=1}^{i} \boldsymbol{\delta}_k \tag{4}$$

Since the reference position is arbitrary, then for simplicity, will be set equal to the origin location, i.e. $\mathbf{x}_\mathrm{o} = \langle 0,0,0 \rangle$. Generalized coordinates will next be introduced as $\boldsymbol{q}_i = \boldsymbol{\delta}_i$ so that (4) simplifies to $\mathbf{x}_i = \sum_{k=1}^{i} \boldsymbol{q}_k$. We've now created a hierarchy in the sense that $\mathbf{x}_1 = \boldsymbol{q}_1$, $\mathbf{x}_2 = \boldsymbol{q}_1 + \boldsymbol{q}_2$, ... ,

$$\mathbf{x}_n = \boldsymbol{q}_1 + \boldsymbol{q}_2 + \cdots + \boldsymbol{q}_n \tag{5}$$

From which we may now work with the set of generalized coordinates $\boldsymbol{q}_1, \boldsymbol{q}_2, \dots, \boldsymbol{q}_n$ and the associated generalized velocities $\dot{\boldsymbol{q}}_1, \dot{\boldsymbol{q}}_2, \dots, \dot{\boldsymbol{q}}_n$. This is known as the Lagrangian formalism. Upon defining a Lagrangian, i.e. $\mathrm{L} \equiv \mathrm{K} - \Pi$, the equations of motion (EOM) may be directly derived from Lagrange's equations. Their derivation stems from Hamilton's principle of stationary action; formally stated as [9; ch.2]:

$$\delta \mathbb{S} = \int_{t_1}^{t_2} \mathfrak{D}\mathrm{L} \, \mathbb{d}t = 0 \tag{6}$$

Where $\mathbb{S}$ is Hamilton's action and $\mathfrak{D}\mathrm{L}$ is the first order variation in the Lagrangian. The Lagrangian will now be defined in the following manner:

$$\mathrm{L}(\dot{\boldsymbol{q}}_1, \dot{\boldsymbol{q}}_2, \dots, \dot{\boldsymbol{q}}_n, \boldsymbol{q}_1, \boldsymbol{q}_2, \dots, \boldsymbol{q}_n, t) = \mathrm{K}(\dot{\boldsymbol{q}}_1, \dot{\boldsymbol{q}}_2, \dots, \dot{\boldsymbol{q}}_n) - \Pi(\boldsymbol{q}_1, \boldsymbol{q}_2, \dots, \boldsymbol{q}_n, t) \tag{7}$$

The kinetic energy differential, per molecule, is defined as the rate of momentum projected along the path taken, i.e. $\mathbb{d}\mathrm{K}_i = m_i \ddot{\mathbf{x}}_i \cdot \mathbb{d}\mathbf{x}_i$ (no summation). Upon integrating, the total kinetic energy of the system of molecules, is found through summing over each individual:

$$\mathrm{K} = \sum_{i=1}^{n} m_i \int \ddot{\mathbf{x}}_i \cdot \mathbb{d}\mathbf{x}_i = \frac{1}{2} \sum_{i=1}^{n} m_i |\dot{\mathbf{x}}_i|^2 \tag{8}$$

To define the total potential energy, let us first define the force acting on each molecule [10; p.190]:

$$\mathfrak{f}_i(\boldsymbol{q}_1, \boldsymbol{q}_2, \dots, \boldsymbol{q}_n, t) = \mathbf{f}_i(\mathbf{x}_i, t) + \sum_{j=1}^{n} \mathbf{F}_{ij}(|\mathbf{x}_i - \mathbf{x}_j|) \tag{9}$$

Where the term $\mathbf{f}_i$ accounts for forces acting on each molecule from outside the system and the second term incorporates intermolecular repulsive/attractive forces between the molecules. The total potential energy may now be found in a similar manner to (8):

$$\Pi = \sum_{i=1}^{n} \int \mathbf{f}_i \cdot \mathbb{d}\mathbf{x}_i + \sum_{i=1}^{n} \int \sum_{j=1}^{n} \mathbf{F}_{ij} \cdot \mathbb{d}\mathbf{x}_i \tag{10}$$

Now that the Lagrangian has been established, the equations of motion may be directly derived from Lagrange's equations. However, obtaining solutions for these types of systems (when n is "large"), becomes a daunting task. The initial conditions are also unknown. If boundary conditions exist, then we must incorporate nonholonomic constraints. On another note, the model is not necessarily complete. In addition to translational degrees of freedom (DoF), the molecules may also rotate and vibrate. One may also want to incorporate the electronic structures. If this is the case, quantum theory must be utilized. So in contrary to direct molecular simulation (DMS), we are going to take an alternate route. To overcome these difficulties, we'll turn to the realm of probability theory [11; ch.1-4]. To begin, we will switch the formalism to the Hamiltonian one through introducing the set of generalized momenta, defined from the Lagrangian:

$$\mathbf{p}_1, \mathbf{p}_2, \dots, \mathbf{p}_n = \frac{\partial \mathrm{L}}{\partial \dot{\boldsymbol{q}}_1}, \frac{\partial \mathrm{L}}{\partial \dot{\boldsymbol{q}}_2}, \dots, \frac{\partial \mathrm{L}}{\partial \dot{\boldsymbol{q}}_n} \tag{11}$$

The Hamiltonian may now be formally defined from the following Legendre transformation:

$$\mathrm{H}(\mathbf{p}_1, \mathbf{p}_2, \dots, \mathbf{p}_n, \boldsymbol{q}_1, \boldsymbol{q}_2, \dots, \boldsymbol{q}_n, t) = \sum_{i=1}^{n} \mathbf{p}_i \cdot \dot{\boldsymbol{q}}_i(\mathbf{p}_1, \mathbf{p}_2, \dots, \mathbf{p}_n) - \text{Ł} \tag{12}$$

Where Ł is the Lagrangian (7) reformed into $\mathrm{L}(\mathbf{p}_1, \mathbf{p}_2, \dots, \mathbf{p}_n, \boldsymbol{q}_1, \boldsymbol{q}_2, \dots, \boldsymbol{q}_n, t)$. It will be noted that the equations of motion may now be equivalently derived from Hamilton's equations:

$$\dot{\boldsymbol{q}}_i = \frac{\partial \mathrm{H}}{\partial \mathbf{p}_i}, \qquad \dot{\mathbf{p}}_i = -\frac{\partial \mathrm{H}}{\partial \boldsymbol{q}_i} \tag{13}$$

Using this formalism, a generalized probability functional, containing all necessary information to describe the system, will be introduced in the form:

$$\mathfrak{F}[\mathbf{p}_1(t), \mathbf{p}_2(t), \dots, \mathbf{p}_n(t), \boldsymbol{q}_1(t), \boldsymbol{q}_2(t), \dots, \boldsymbol{q}_n(t), t] \tag{14}$$

The idea is to now develop an equation of motion which describes the evolution of $\mathfrak{F}$, from which we may extract the evolved bulk quantities through generating moments (or expectations) over the phase space Γ. Defining $\mathcal{G}(\mathbf{p}_1, \mathbf{p}_2, \dots, \mathbf{p}_n, \boldsymbol{q}_1, \boldsymbol{q}_2, \dots, \boldsymbol{q}_n)$, this operation will take the form:

$$\bar{\mathfrak{F}}[\mathcal{G}] = \prod_{i=1}^{n} \int_{\Gamma_i} \mathcal{G}\mathfrak{F}\, d\mathcal{P}_i d\mathcal{Q}_i \tag{15}$$

The total differential change, with respect to time, is then found through using the chain rule of multivariable differential calculus [12; p.117]:

$$\frac{\mathbb{d}\mathfrak{F}}{\mathbb{d}t} = \frac{\partial \mathfrak{F}}{\partial t} + \sum_{i=1}^{n} \left(\frac{\partial \mathfrak{F}}{\partial \boldsymbol{q}_i} \cdot \frac{\partial \mathrm{H}}{\partial \mathbf{p}_i} - \frac{\partial \mathfrak{F}}{\partial \mathbf{p}_i} \cdot \frac{\partial \mathrm{H}}{\partial \boldsymbol{q}_i} \right) = \dot{\mathfrak{F}} + \{\mathfrak{F}, \mathrm{H}\} \tag{16}$$

Where $\{\mathfrak{F}, \mathrm{H}\}$ is known as a Poisson bracket [13; p.284]. To enforce continuity, we must require:

$$\frac{\mathbb{d}\mathfrak{F}}{\mathbb{d}t} + \sum_{i=1}^{n} \left(\frac{\partial \cdot \dot{\boldsymbol{q}}_i}{\partial \boldsymbol{q}_i} + \frac{\partial \cdot \dot{\mathbf{p}}_i}{\partial \mathbf{p}_i} \right) \mathfrak{F} = 0 \tag{17}$$

Well, under the Hamiltonian formalism, it can easily be shown that:

$$\sum_{i=1}^{n} \left(\frac{\partial \cdot \dot{\boldsymbol{q}}_i}{\partial \boldsymbol{q}_i} + \frac{\partial \cdot \dot{\mathbf{p}}_i}{\partial \mathbf{p}_i} \right) \mathfrak{F} = \sum_{i=1}^{n} \left[\frac{\partial}{\partial \boldsymbol{q}_i} \cdot \left(\frac{\partial \mathrm{H}}{\partial \mathbf{p}_i} \right) - \frac{\partial}{\partial \mathbf{p}_i} \cdot \left(\frac{\partial \mathrm{H}}{\partial \boldsymbol{q}_i} \right) \right] \mathfrak{F} = 0 \tag{18}$$

As a result, $\dot{\mathfrak{F}} = -\{\mathfrak{F}, \mathrm{H}\}$, which is otherwise known as Liouville's equation [14; ch.1]. To uncover the Boltzmann equation, (17) will first be written in the form:

$$\frac{\partial \mathfrak{F}}{\partial t} + \dot{\boldsymbol{q}}_1 \cdot \frac{\partial \mathfrak{F}}{\partial \boldsymbol{q}_1} + \dot{\mathbf{p}}_1 \cdot \frac{\partial \mathfrak{F}}{\partial \mathbf{p}_1} + \sum_{i=2}^{n} \{\mathfrak{F}, \mathrm{H}\}_i = 0 \tag{19}$$

We must now recognize the total functional $\mathfrak{F}$ as a joint probability density [11; p.144] or joint PDF. The 1st marginal PDF [11; p.145] is then found through integrating over all generalized positions and momenta assigned within the range $i = 2,3, \dots, n$:

$$\mathfrak{F}_1 = \mathfrak{F}(\mathbf{p}_1, \boldsymbol{q}_1, t) = \prod_{i=2}^{n} \int_{\Gamma_i} \mathfrak{F}\, d\mathcal{P}_i d\mathcal{Q}_i \tag{20}$$

Thus obtaining the so-called "single particle" probability density. Before performing the same integration over (19), the generalized velocities $\dot{\boldsymbol{q}}_i$ will be solved for in terms of the generalized momenta $\mathbf{p}_i$ through utilizing (11). It is found that $m_1 \dot{\boldsymbol{q}}_1 = \mathbf{p}_1 - \mathbf{p}_2$ for any integer value of $n \geq 2$. Similarly, the generalized forces $\dot{\mathbf{p}}_i$ can be obtained as functions of the generalized coordinates $\boldsymbol{q}_i$ and time t through utilizing (13). Upon defining $\Pi = \pi_1(\boldsymbol{q}_1, t) + \pi_n(\boldsymbol{q}_1, \boldsymbol{q}_2, \dots, \boldsymbol{q}_n, t)$, we find:

$$\dot{\mathbf{p}}_1 = -\frac{\partial \pi_1}{\partial \boldsymbol{q}_1} - \frac{\partial \pi_n}{\partial \boldsymbol{q}_1} \tag{21}$$

Where π_1 is associated with the external force acting on molecule #1. Upon substituting $\dot{\boldsymbol{q}}_1(\mathbf{p}_1, \mathbf{p}_2)$ and $\dot{\mathbf{p}}_1(\boldsymbol{q}_1, \boldsymbol{q}_2, \dots, \boldsymbol{q}_n, t)$ into (19), one finds:

$$\frac{\partial \mathfrak{F}}{\partial t}+\frac{\mathbf{p}_1}{m_1}\cdot\frac{\partial \mathfrak{F}}{\partial \boldsymbol{q}_1}-\frac{\partial \pi_1}{\partial \boldsymbol{q}_1}\cdot\frac{\partial \mathfrak{F}}{\partial \mathbf{p}_1}=\frac{\mathbf{p}_2}{m_1}\cdot\frac{\partial \mathfrak{F}}{\partial \boldsymbol{q}_1}+\frac{\partial \pi_n}{\partial \boldsymbol{q}_1}\cdot\frac{\partial \mathfrak{F}}{\partial \mathbf{p}_1}-\sum_{k=2}^{n}\{\mathfrak{F},\mathrm{H}\}_k \tag{22}$$

The next step is to perform the same integration as in (20) thus unveiling the generalized Boltzmann equation [14; ch.2] (under the Hamiltonian formalism):

$$\frac{\partial \mathfrak{F}_1}{\partial t}+\frac{\mathbf{p}_1}{m_1}\cdot\frac{\partial \mathfrak{F}_1}{\partial \boldsymbol{q}_1}-\frac{\partial \pi_1}{\partial \boldsymbol{q}_1}\cdot\frac{\partial \mathfrak{F}_1}{\partial \mathbf{p}_1}+\mathcal{J}=0 \tag{23}$$

$$\mathcal{J}=\prod_{i=2}^{n}\int_{\Gamma_i}\left[\sum_{k=2}^{n}\left(\dot{\boldsymbol{q}}_k\cdot\frac{\partial \mathfrak{F}}{\partial \boldsymbol{q}_k}+\dot{\mathbf{p}}_k\cdot\frac{\partial \mathfrak{F}}{\partial \mathbf{p}_k}\right)-\frac{\mathbf{p}_2}{m_1}\cdot\frac{\partial \mathfrak{F}}{\partial \boldsymbol{q}_1}-\frac{\partial \pi_n}{\partial \boldsymbol{q}_1}\cdot\frac{\partial \mathfrak{F}}{\partial \mathbf{p}_1}\right]d\mathcal{P}_i d\mathcal{Q}_i \tag{24}$$

Where $\mathcal{J}$ is the generalized interaction integral. An equivalent formulation may be found using the Lagrangian formalism. Before performing the transformation, it will be more convenient to first reorganize the generalized coordinates in the following way:

$$\overbrace{q_1,q_2,q_3}^{\boldsymbol{q}_1},\overbrace{q_4,q_5,q_6}^{\boldsymbol{q}_2},\dots,\overbrace{q_{3n-2},q_{3n-1},q_{3n}}^{\boldsymbol{q}_n} \tag{25}$$

Referring back to (17), the terms containing the set of generalized forces $\dot{\mathbf{p}}_1,\dot{\mathbf{p}}_2,\dots,\dot{\mathbf{p}}_n$ will now expand through identifying the dependence $\mathbf{p}_i(\dot{\boldsymbol{q}}_1,\dot{\boldsymbol{q}}_2,\dots,\dot{\boldsymbol{q}}_n)$ per generalized momenta:

$$-\sum_{i=1}^{n}\frac{\partial \mathfrak{F}}{\partial \mathbf{p}_i}\cdot\frac{\partial \mathrm{H}}{\partial \boldsymbol{q}_i}=\sum_{i=1}^{3n}\dot{\mathrm{p}}_i\frac{\partial \mathfrak{F}}{\partial \mathrm{p}_i}=\sum_{i=1}^{3n}\sum_{j=1}^{3n}\frac{\partial \mathfrak{F}}{\partial \mathrm{p}_i}\frac{\partial \mathrm{p}_i}{\partial \dot{q}_j}\ddot{q}_j=\sum_{i=1}^{n}\ddot{\boldsymbol{q}}_i\cdot\frac{\partial \mathfrak{F}}{\partial \dot{\boldsymbol{q}}_i} \tag{26}$$

In consequence, the Liouville equation may equivalently be represented in the form:

$$\frac{\partial \mathfrak{F}}{\partial t}+\dot{\boldsymbol{q}}_1\cdot\frac{\partial \mathfrak{F}}{\partial \boldsymbol{q}_1}+\ddot{\boldsymbol{q}}_1\cdot\frac{\partial \mathfrak{F}}{\partial \dot{\boldsymbol{q}}_1}+\sum_{i=2}^{n}\left(\dot{\boldsymbol{q}}_i\cdot\frac{\partial \mathfrak{F}}{\partial \boldsymbol{q}_i}+\ddot{\boldsymbol{q}}_i\cdot\frac{\partial \mathfrak{F}}{\partial \dot{\boldsymbol{q}}_i}\right)=0 \tag{27}$$

Using Lagrange's equations, the generalized accelerations $\ddot{\boldsymbol{q}}_i$ may be solved for as functions of the generalized coordinates $\boldsymbol{q}_i$ and time t. For any integer $n\geq 2$, one obtains the EOM:

$$m_1\ddot{\boldsymbol{q}}_1=\frac{\partial \Pi}{\partial \boldsymbol{q}_2}-\frac{\partial \Pi}{\partial \boldsymbol{q}_1} \tag{28}$$

Upon feeding this result into (27) and integrating, we yet again uncover the generalized Boltzmann equation, however now, under the Lagrangian formalism:

$$\frac{\partial \mathfrak{F}_1}{\partial t}+\dot{\boldsymbol{q}}_1\cdot\frac{\partial \mathfrak{F}_1}{\partial \boldsymbol{q}_1}-\frac{1}{m_1}\frac{\partial \pi_1}{\partial \boldsymbol{q}_1}\cdot\frac{\partial \mathfrak{F}_1}{\partial \dot{\boldsymbol{q}}_1}+\mathcal{J}=0 \tag{29}$$

$$\mathcal{J}=\prod_{i=2}^{n}\int_{\Gamma_i}\left[\sum_{k=2}^{n}\left(\dot{\boldsymbol{q}}_k\cdot\frac{\partial \mathfrak{F}}{\partial \boldsymbol{q}_k}+\ddot{\boldsymbol{q}}_k\cdot\frac{\partial \mathfrak{F}}{\partial \dot{\boldsymbol{q}}_k}\right)+\frac{1}{m_1}\left(\frac{\partial \pi_n}{\partial \boldsymbol{q}_2}-\frac{\partial \pi_n}{\partial \boldsymbol{q}_1}\right)\cdot\frac{\partial \mathfrak{F}}{\partial \dot{\boldsymbol{q}}_1}\right]d\dot{\mathcal{Q}}_i d\mathcal{Q}_i \tag{30}$$

We have now concluded our introduction to the Boltzmann equation. On a final note, if $\mathfrak{F}$ depends on time implicitly, then the analytical solution to $\{\mathfrak{F}, \mathrm{H}\} = 0$, is given by [15; p.376]:

$$\mathfrak{F}(\mathbf{p}_1, \mathbf{p}_2, \dots, \mathbf{p}_n, \boldsymbol{q}_1, \boldsymbol{q}_2, \dots, \boldsymbol{q}_n) = \zeta^{-1} \exp[-\beta \mathrm{H}(\mathbf{p}_1, \mathbf{p}_2, \dots, \mathbf{p}_n, \boldsymbol{q}_1, \boldsymbol{q}_2, \dots, \boldsymbol{q}_n)] \tag{31}$$

Where β is coined "thermodynamic beta" which nondimensionalizes the Hamiltonian and ζ is the partition function:

$$\zeta = \prod_{i=1}^{n} \int_{\Gamma_i} \exp(-\beta \mathrm{H}) \, d\mathcal{P}_i d\mathcal{Q}_i \tag{32}$$

Therefore, $1/\zeta$ acts as the normalizing coefficient.

2.2 Introduction to the Boltzmann Collision Integral

Various forms of the interaction integral, found within (24) and (30), have been used to predict transport coefficients associated to phenomena such as mass diffusion, viscosity, and thermal conductivity. These predictions were originally formulated by Chapman and Enskog [15] in the early 1900s. This is not the primary focus of this dissertation, however, their methodology will newly be incorporated into both deriving and solving the Navier-Stokes-Fourier (NSF) equations. To gain a larger perspective on the theory of the Boltzmann equation, a brief introduction to the collision integral will be given.

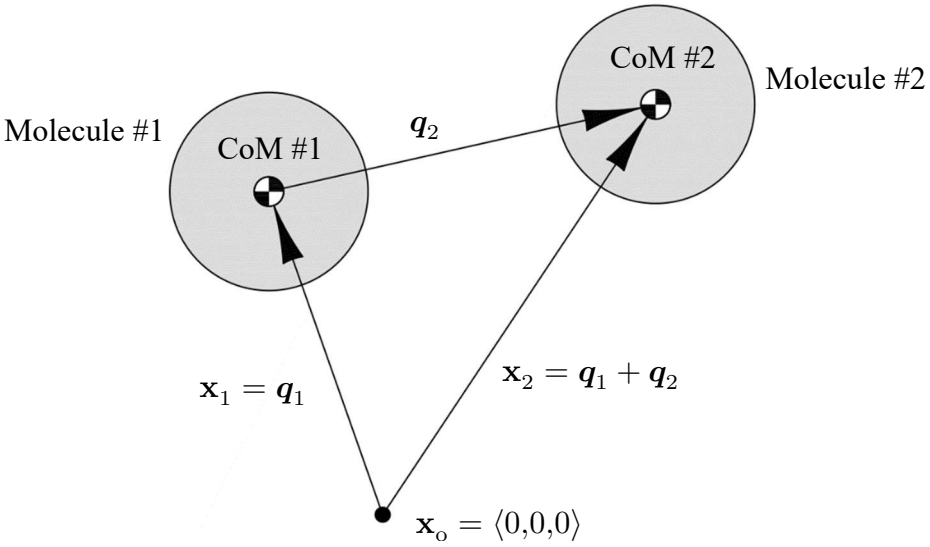

Figure 1 Two-body system

We'll estimate the coefficient of shearing viscosity of an argon gas assuming collisional events are perfectly elastic [10; p.211]. Two-body collisions will be assumed to be dominant within a constant potential energy field; see Figure 1. The interaction integral (30) will now take the following collisional form:

$$\mathcal{J} = \int_{\Gamma_2} \dot{\boldsymbol{q}}_2 \cdot \frac{\partial \mathfrak{F}}{\partial \boldsymbol{q}_2} d\dot{\mathcal{Q}}_2 d\mathcal{Q}_2 = \int_{\mathcal{A}} \int_{\mathbb{R}^3} (\dot{\boldsymbol{q}}_2 \cdot \mathbf{e}_2) \delta \mathfrak{F} \, d\dot{\mathcal{Q}}_2 d\mathrm{A} \tag{33}$$

Where the basis vector is defined as $\mathbf{e}_2 = \dot{\boldsymbol{q}}_2/|\dot{\boldsymbol{q}}_2|$ therefore $\dot{\boldsymbol{q}}_2 \cdot \mathbf{e}_2 = |\dot{\boldsymbol{q}}_2|$. The molecular chaos hypothesis, a.k.a. the stosszahlansatz [14; p.22], will next be adopted and applied, such that:

$$\delta\mathfrak{F} = \mathfrak{F}(\dot{\mathbf{x}}_1', \dot{\mathbf{x}}_2') - \mathfrak{F}(\dot{\mathbf{x}}_1, \dot{\mathbf{x}}_2) = \mathfrak{F}' - \mathfrak{F} \tag{34}$$

Where $\dot{\mathbf{x}}_1'$ and $\dot{\mathbf{x}}_2'$ are the post-collisional velocity vectors of molecules "1" and "2" respectively. The generalized Boltzmann equation (29) will now take on a less general form:

$$\int_{\mathcal{A}} \int_{\mathbb{R}^3} |\dot{\boldsymbol{q}}_2| \delta\mathfrak{F} \, d\dot{\mathcal{Q}}_2 d\mathrm{A} = 0 \tag{35}$$

It will be noted that if we multiply (35) by $d\dot{\mathcal{Q}}_1$ and integrate once more, then a change of variables may be performed such that $d\dot{\mathcal{Q}}_1 d\dot{\mathcal{Q}}_2 = d\dot{\mathcal{X}}_1 d\dot{\mathcal{X}}_2$, where the Jacobian of the transformation is unity. The system as a whole is assumed to be in a state of equilibrium therefore the stationary solution (31) is then valid. Upon making β specific through absorbing m, the normalized solution is:

$$\mathfrak{F}(\dot{\mathbf{x}}_1, \dot{\mathbf{x}}_2) = \frac{1}{(2\pi\beta^{-1})^3} \exp\left(-\frac{1}{2}\beta|\dot{\mathbf{x}}_1|^2\right) \exp\left(-\frac{1}{2}\beta|\dot{\mathbf{x}}_2|^2\right) \tag{36}$$

When $\mathfrak{F}$ is expressed in terms of the molecular velocities $\dot{\mathbf{x}}_1$ and $\dot{\mathbf{x}}_2$, the distribution is isotropic and separatable such that $\mathfrak{F}(\dot{\mathbf{x}}_1, \dot{\mathbf{x}}_2) = \mathfrak{F}(\dot{\mathbf{x}}_1)\mathfrak{F}(\dot{\mathbf{x}}_2)$. However, when $\dot{\mathbf{x}}_1 = \dot{\boldsymbol{q}}_1$ and $\dot{\mathbf{x}}_2 = \dot{\boldsymbol{q}}_1 + \dot{\boldsymbol{q}}_2$, meaning $\mathfrak{F}$ is expressed in terms of the generalized velocities, the distribution becomes anisotropic, as shown in Figure 2. In this case, the distribution is not separatable since $\mathfrak{F}(\dot{\boldsymbol{q}}_1, \dot{\boldsymbol{q}}_2) \neq \mathfrak{F}(\dot{\boldsymbol{q}}_1)\mathfrak{F}(\dot{\boldsymbol{q}}_2)$ because there exists a correlation between the velocities of the two molecules.

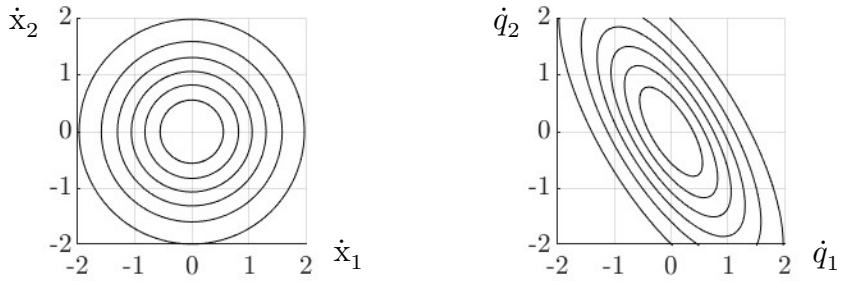

Figure 2 Contour plots of $\mathfrak{F}(\dot{\mathrm{x}}_1, \dot{\mathrm{x}}_2)$ (left) and $\mathfrak{F}(\dot{q}_1, \dot{q}_2)$ (right)

The provided derivation of (35) is ad hoc and not necessarily mathematically rigorous. A more formal derivation can be performed through using a balance principle [16; ch.11], stated as:

$$\mathfrak{F}' d\mathrm{V}' - \mathfrak{F} d\mathrm{V} = 0 \tag{37}$$

The objective is to now relate the pre- and post-collision differential volumes based on the geometry of the molecular encounter so that $d\mathrm{V} = d\mathrm{V}'$. We'll begin with first defining:

$$d\mathrm{V} = (\dot{\boldsymbol{q}}_2 dt) \cdot \mathbf{e}_2 d\mathrm{A} = dl d\mathrm{A} \tag{38}$$

Where $dl = |\dot{\boldsymbol{q}}_2|dt$ is the differential length of the collision cylinder. The differential area will be defined as $d\mathrm{A} = rdrd\phi$ which represents the collision cross-section as shown in Figure 3, in regards to two colliding "hard" spheres:

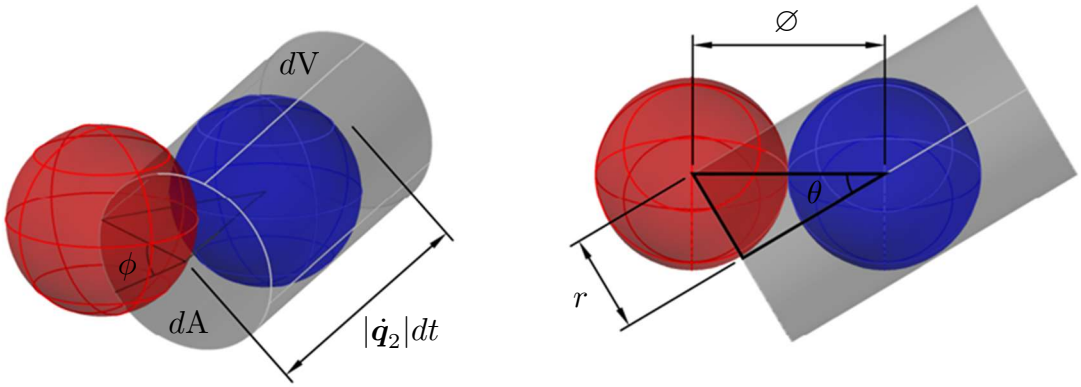

Figure 3 Two-body collision geometry (hard sphere scattering)

The relation $r = \varnothing \sin\theta$ is found using simple trigonometry therefore $dr = \varnothing \cos\theta \, d\theta$ where $\varnothing$ is the van der Waals diameter. As a result, $d\mathrm{A} = |g|^2 d\Omega$ where $d\Omega = \sin\theta \, d\theta d\phi$ and $|g|^2 = \varnothing^2 \cos\theta$ is the scattering probability valid in this circumstance $\forall \; 0 \leq \theta \leq \pi/2$; which relates the collision cross-section of the incoming molecule to the solid angle which the molecule is reflected into so that $d\mathrm{A} = d\mathrm{A}'$. Upon combining, the post-collision differential volume element is expressed as:

$$d\mathrm{V}' = (\dot{\boldsymbol{q}}_2' dt) \cdot \mathbf{e}_2' d\mathrm{A}' = \varnothing^2 |\dot{\boldsymbol{q}}_2'| \cos\theta \sin\theta \, d\theta d\phi dt \tag{39}$$

Where the area of the collision cross-section is easily obtained from:

$$\int_{\mathcal{A}} d\mathrm{A} = \int_0^{2\pi} d\phi \int_0^{\pi/2} |g|^2 \sin\theta \, d\theta = \pi \varnothing^2 \tag{40}$$

In order to make $d\mathrm{V}' = d\mathrm{V}$, the magnitude $|\dot{\boldsymbol{q}}_2'|$ must be equal to $|\dot{\boldsymbol{q}}_2|$ therefore must be a constant of the motion. Well from Newton's third law of motion (3rd LoM), we may state that $\ddot{\mathbf{x}}_1 = -\ddot{\mathbf{x}}_2$ and $\dot{\mathrm{K}}_1 = -\dot{\mathrm{K}}_2$. Integrating over time provides the following balance relations:

$$\dot{\mathbf{x}}_1 + \dot{\mathbf{x}}_2 = \dot{\mathbf{x}}_1' + \dot{\mathbf{x}}_2' \tag{41}$$

$$|\dot{\mathbf{x}}_1|^2 + |\dot{\mathbf{x}}_2|^2 = |\dot{\mathbf{x}}_1'|^2 + |\dot{\mathbf{x}}_2'|^2 \tag{42}$$

$$\dot{\mathbf{x}}_1 \cdot \dot{\mathbf{x}}_2 = \dot{\mathbf{x}}_1' \cdot \dot{\mathbf{x}}_2' \tag{43}$$

Multiplying (41) by m yields the momentum balance and multiplying (42) by $m/2$ yields the kinetic energy balance. Combining these two balance equations provides the projection relation (43). Since $m_1 = m_2$, the center of mass (CoM) is given by $\mathbf{x}_\oplus = \frac{1}{2}(\mathbf{x}_1 + \mathbf{x}_2)$ which is the average of the two positions. It so happens that $\dot{\mathbf{x}}_\oplus$, $\mathrm{K}_\oplus$, and $|\dot{\boldsymbol{q}}_2|$ are all constants of the motion:

$$\dot{\mathbf{x}}_{\oplus} = \tfrac{1}{2}(\dot{\mathbf{x}}_1 + \dot{\mathbf{x}}_2) = \tfrac{1}{2}(\dot{\mathbf{x}}_1' + \dot{\mathbf{x}}_2') = \dot{\mathbf{x}}_{\oplus}' \tag{44}$$

$$|\dot{\boldsymbol{q}}_2|^2 = |\dot{\mathbf{x}}_1|^2 - 2\dot{\mathbf{x}}_1 \cdot \dot{\mathbf{x}}_2 + |\dot{\mathbf{x}}_2|^2 = |\dot{\mathbf{x}}_1'|^2 - 2\dot{\mathbf{x}}_1' \cdot \dot{\mathbf{x}}_2' + |\dot{\mathbf{x}}_2'|^2 = |\dot{\boldsymbol{q}}_2'|^2 \tag{45}$$

$$|\dot{\mathbf{x}}_{\oplus}|^2 = \tfrac{1}{4}|\dot{\mathbf{x}}_1|^2 + \tfrac{1}{2}\dot{\mathbf{x}}_1 \cdot \dot{\mathbf{x}}_2 + \tfrac{1}{4}|\dot{\mathbf{x}}_2|^2 = \tfrac{1}{4}|\dot{\mathbf{x}}_1'|^2 + \tfrac{1}{2}\dot{\mathbf{x}}_1' \cdot \dot{\mathbf{x}}_2' + \tfrac{1}{4}|\dot{\mathbf{x}}_2'|^2 = |\dot{\mathbf{x}}_{\oplus}'|^2 \tag{46}$$

In consequence, $|\dot{\boldsymbol{q}}_2| = |\dot{\boldsymbol{q}}_2'|$ therefore $d\mathrm{V} = d\mathrm{V}'$ ✓. As a result of (42), the master balance relation (37) is now automatically satisfied since $\mathfrak{F} = \mathfrak{F}'$ ✓. It will be noted that the vector parallelogram rule may be used to prove that $|\dot{\boldsymbol{q}}_2|$ is equivalent to $2|\dot{\mathbf{x}}_{\oplus}|$ in regards to two colliding vectors. Therefore, the use of the speed $|\dot{\mathbf{x}}_2 - \dot{\mathbf{x}}_1|$, within (38) and (39), is just as valid as $|\dot{\mathbf{x}}_1 + \dot{\mathbf{x}}_2|$.

Let us now use the current two-body model to extend the framework to a system of n molecules, where there is approximately n^2 possible collision pairs. This will be done through first denoting the number density as $\cancel{n} = n/\cancel{v} = \rho/m$ where $\cancel{v}$ is the total volume which contains all n molecules and ρ is the mass density. A number density velocity distribution will next be defined in terms of two separate and independent distributions as $\hat{n} = \hat{n}_1\hat{n}_2 = \cancel{n}^2\mathfrak{F}$. We'll now return to (37), i.e. $\delta\mathfrak{F}d\mathrm{V} = 0$, divide by dt, multiply by $\cancel{n}^2 d\dot{\mathcal{X}}_1 d\dot{\mathcal{X}}_2$, then integrate to obtain:

$$\delta\dot{\cancel{n}}_{\mathrm{c}} = \int_{\mathbb{R}^3}\int_{\mathbb{R}^3}\int_{\mathcal{A}} \delta\hat{n}\,|\dot{\boldsymbol{q}}_2|d\mathrm{A}d\dot{\mathcal{X}}_1 d\dot{\mathcal{X}}_2 = 0 \tag{47}$$

Where $\dot{\cancel{n}}_{\mathrm{c}}$ is the number of collisions per unit volume per unit time and is treated as a conserved quantity. It is worth mentioning that this formulation is probabilistically "Lagrangian." To explain this statement, let us first recall that $\mathrm{L} = \mathrm{K} - \Pi = \mathrm{E} - 2\Pi$. Using set notation, it has already been established that $\hat{n}(\dot{\mathbf{x}}_1 \cap \dot{\mathbf{x}}_2) = \hat{n}_1\hat{n}_2$ which means $\dot{\mathbf{x}}_1$ and $\dot{\mathbf{x}}_2$ are statistically independent. Based on the axiom of finite additivity [11; p.9], then we may also say $\hat{n}(\dot{\mathbf{x}}_1 \cup \dot{\mathbf{x}}_2) = \hat{n}_1 + \hat{n}_2$ so that:

$$\delta\hat{n} = \hat{n}(\dot{\mathbf{x}}_1' \cap \dot{\mathbf{x}}_2') - \hat{n}(\dot{\mathbf{x}}_1 \cap \dot{\mathbf{x}}_2) = \hat{n}_1'\hat{n}_2' - \hat{n}_1\hat{n}_2 \tag{48}$$

$$= \hat{n}[(\dot{\mathbf{x}}_1' \cap \dot{\mathbf{x}}_2') \cup (\dot{\mathbf{x}}_1 \cap \dot{\mathbf{x}}_2)] - 2\hat{n}(\dot{\mathbf{x}}_1 \cap \dot{\mathbf{x}}_2)$$

Since $\dot{\cancel{n}}_{\mathrm{c}}^{\mathrm{out}} - \dot{\cancel{n}}_{\mathrm{c}}^{\mathrm{in}} = 0$, where both terms are equal to $\dot{\cancel{n}}_{\mathrm{c}}$, then the total number of collisions per unit volume per unit time may be expressed as:

$$\dot{\cancel{n}}_{\mathrm{c}} = \pi\varnothing^2 \int_{\mathbb{R}^3}\int_{\mathbb{R}^3} |\dot{\boldsymbol{q}}_2|\hat{n}\, d\dot{\mathcal{X}}_1 d\dot{\mathcal{X}}_2 \tag{49}$$

To perform the integration over the two-fold velocity space, the energy balance (42) will first be rewritten in terms of the constants of motion $|\dot{\boldsymbol{q}}_2|$ and $|\dot{\mathbf{x}}_{\oplus}|$:

$$\tfrac{1}{2}|\dot{\boldsymbol{q}}_2|^2 + 2|\dot{\mathbf{x}}_{\oplus}|^2 = \tfrac{1}{2}|\dot{\boldsymbol{q}}_2'|^2 + 2|\dot{\mathbf{x}}_{\oplus}'|^2 \tag{50}$$

Since $\frac{1}{4}|\dot{\boldsymbol{q}}_2|^2 + |\dot{\mathbf{x}}_{\oplus}|^2 = \frac{1}{2}|\dot{\mathbf{x}}_1|^2 + \frac{1}{2}|\dot{\mathbf{x}}_2|^2$, then (36) may undergo a change of variables from $\dot{\mathbf{x}}_1$

and $\dot{\mathbf{x}}_2$ to $\dot{\boldsymbol{q}}_2$ and $\dot{\mathbf{x}}_\oplus$. These cartesian velocity coordinates will next be transformed into spherical coordinates. So in general, $d\dot{\mathcal{X}} = |\dot{\mathbf{x}}|^2 \sin\vartheta \, d|\dot{\mathbf{x}}| d\vartheta d\varphi$ and (36) will now take the form [15; ch.5]:

$$\mathfrak{F}(|\dot{\boldsymbol{q}}_2|, |\dot{\mathbf{x}}_\oplus|) = (2\pi\beta^{-1})^{-3} \exp(-\tfrac{1}{4}\beta|\dot{\boldsymbol{q}}_2|^2) \exp(-\beta|\dot{\mathbf{x}}_\oplus|^2) \tag{51}$$

Noting that the solid angle is equal to 4π, the zeroth order moment (or expectation) is computed as:

$$\prod_{i=1}^{2} \int_{\mathbb{R}^3} \mathfrak{F}(\dot{\mathbf{x}}_i) \, d\dot{\mathcal{X}}_i = 16\pi^2 \int_0^\infty |\dot{\boldsymbol{q}}_2|^2 \mathfrak{F}(|\dot{\boldsymbol{q}}_2|) \, d|\dot{\boldsymbol{q}}_2| \int_0^\infty |\dot{\mathbf{x}}_\oplus|^2 \mathfrak{F}(|\dot{\mathbf{x}}_\oplus|) \, d|\dot{\mathbf{x}}_\oplus| = 1 \tag{52}$$

We'll next return to (49), perform the change of variables, then perform the integration to find:

$$\dot{\text{n}}_\text{c} = 16\pi^3 \varnothing^2 \int_0^\infty |\dot{\boldsymbol{q}}_2|^3 \hat{n}(|\dot{\boldsymbol{q}}_2|) \, d|\dot{\boldsymbol{q}}_2| \int_0^\infty |\dot{\mathbf{x}}_\oplus|^2 \hat{n}(|\dot{\mathbf{x}}_\oplus|) \, d|\dot{\mathbf{x}}_\oplus| = \frac{4\pi^{1/2}\varnothing^2\rho^2}{m^2\beta^{1/2}} \tag{53}$$

Since $\dot{\text{n}}_\text{c}$ is independent of time, it will be inferred that the cumulative number of collisions, per unit volume, has a linear dependence upon time such that $\text{n}_\text{c} = \dot{\text{n}}_\text{c} t$. It will next be assumed that the average time interval between successive collisions, denoted t_c, is constant. In effect, we will hypothesize that the collision rate is equal to $\dot{\text{n}}_\text{c} = \text{n}/t_\text{c}$ therefore $\text{n}_\text{c} = (\text{n}/t_\text{c})t$. The collision interval may now be computed through utilizing (53) to obtain $t_\text{c} = m\beta^{1/2}/4\pi^{1/2}\varnothing^2\rho$. The average distance traveled over the time interval t_c, or mean-free path length, will next be expressed as $\ell_\text{c} = \overline{v} t_\text{c}$, where $\overline{v}$ represents the mean molecular speed. The associated distribution is the stationary mass density velocity distribution, whose derivation in based on (31):

$$\hat{\rho}(\dot{\mathbf{x}}) = \rho(2\pi/\beta)^{-3/2} \exp(-\tfrac{1}{2}\beta|\dot{\mathbf{x}}|^2) \tag{54}$$

From which the mean speed may be computed from the following moment:

$$\overline{v} = \frac{1}{\rho} \int_{\mathbb{R}^3} |\dot{\mathbf{x}}| \hat{\rho}(\dot{\mathbf{x}}) \, d\dot{\mathcal{X}} = \frac{1}{\rho} \int_0^{2\pi} d\varphi \int_0^\pi \sin\vartheta \, d\vartheta \int_0^\infty |\dot{\mathbf{x}}|^3 \hat{\rho}(|\dot{\mathbf{x}}|) \, d|\dot{\mathbf{x}}| = \frac{2\sqrt{2}}{\sqrt{\pi\beta}} \tag{55}$$

In consequence, the mean-free path length computes to $\ell_\text{c} = m(\sqrt{2}\pi\varnothing^2\rho)^{-1}$. This is a classic result as found in [17; p.6-57]. We must now relate our findings from the collision integral to the coefficient of shearing viscosity, denoted μ $(\text{Pa}\cdot\text{s})$. It will be assumed that the causal mechanism of viscous dissipation is molecular diffusion. So in contrary to the stationary distribution (54), let us consider the mass density distribution $\hat{\rho}(\mathbf{x}, t)$; which is in a state of nonequilibrium due to the explicit dependence upon time. The total temporal derivative is then:

$$\frac{\mathrm{d}}{\mathrm{d}t} \hat{\rho}[\mathbf{x}(t), t] = \frac{\partial\hat{\rho}}{\partial t} + \dot{\mathbf{x}} \cdot \frac{\partial\hat{\rho}}{\partial\mathbf{x}} \tag{56}$$

Continuity will once again be enforced such that $\mathrm{d}\hat{\rho} = -\hat{\rho}(\boldsymbol{\nabla}\cdot\dot{\mathbf{x}})\mathrm{d}t$, where the gradient operator is denoted $\boldsymbol{\nabla} = \partial/\partial\mathbf{x}$. As a result, the governing continuity equation is $\partial\hat{\rho} = -\boldsymbol{\nabla}\cdot(\hat{\rho}\dot{\mathbf{x}})$. For ease

of notation, the temporal derivative $\partial\hat{\rho}/\partial t$ has simply been replaced with $\partial\hat{\rho}$. Intermolecular collisions will be hypothesized as the causal mechanism of mass diffusion. Therefore, the diffusion velocity will be defined as $\dot{\mathbf{x}} = \mathbf{x}/\tau$, where $\tau \propto t_{\mathrm{c}}$. The continuity equation, which is an advection transport equation, will next be transformed into a diffusion transport equation through first defining $\hat{\rho}(\mathbf{x}, t) = \mathcal{G}(\mathbf{x})\mathcal{Q}(t)$. In reference to (54), it is natural to define the spatial contribution as $\mathcal{G} = \exp(-\frac{1}{2}\beta|\dot{\mathbf{x}}|^2)$ where $\dot{\mathbf{x}}$ is now dependent upon $\mathbf{x}$. The resulting velocity operator relation is $\dot{\mathbf{x}}\hat{\rho} = -\nu\boldsymbol{\nabla}\hat{\rho}$, where the coefficient of kinematic viscosity is identified as $\nu = \tau/\beta$; having units of specific action (m^2/s). Upon feeding the newly found gradient relation into the continuity equation, one uncovers the mass diffusion equation: $\partial\hat{\rho} = \nu\nabla^2\hat{\rho}$. In contrary to the method provided, one may also refer to Einstein's theory of Brownian movement [18].

To uncover the fundamental solution, the principle of superposition will be utilized. The partial solution will then be given through using the method of separation of variables [19; ch.2] as $\hat{\rho}(\boldsymbol{k}, \mathbf{x}, t) = a(\boldsymbol{k})\psi(\boldsymbol{k}, \mathbf{x})f(\boldsymbol{k}, t)$ where $\boldsymbol{k}$ is the vector of wave numbers. The resulting eigen-equations are $\dot{f} = -\omega f$ and $\nabla^2\psi = -k^2\psi$ where $\omega = \nu k^2$. The solution to the time-dependent ODE is simply $f(\boldsymbol{k}, t) = \exp(-\omega t)$ and the solution to the Helmholtz equation is provided as $\psi(\boldsymbol{k}, \mathbf{x}) = \exp(i\boldsymbol{k}\cdot\mathbf{x})$. Given the initial condition $\hat{\rho}_{\mathrm{o}}(\mathbf{x}) = \rho\delta(\mathbf{x})$, where $\delta(\mathbf{x})$ is the Dirac delta function centered about $\mathbf{x} = \mathbf{0}$, the fundamental solution is obtained through using the theory of continuous Fourier transforms [19; ch.10]:

$$a(\boldsymbol{k}) = \frac{1}{(2\pi)^3}\int_{\mathbb{R}^3}\hat{\rho}_{\mathrm{o}}(\mathbf{x})\psi^*(\boldsymbol{k}, \mathbf{x})\, d\mathcal{X} = \frac{\rho}{(2\pi)^3} \tag{57}$$

$$\hat{\rho}(\mathbf{x}, t) = \int_{\mathbb{R}^3} a(\boldsymbol{k})\psi(\boldsymbol{k}, \mathbf{x})f(\boldsymbol{k}, t)\, d\mathcal{K} = \frac{\rho}{(4\pi\nu t)^{3/2}}\exp\left(-\frac{1}{4\nu t}|\mathbf{x}|^2\right) \tag{58}$$

Where ψ^* denotes the complex conjugate stationary wave function. Integrating (58) over the infinite spatial domain shows that the zeroth order moment upholds the condition of constancy of mass [20]. The moment of interest is now the second order central moment which provides an expression for the mean-squared-displacement of mass as a linear function of time:

$$\ell^2(t) = \frac{1}{3\rho}\int_{\mathbb{R}^3}|\mathbf{x}|^2\hat{\rho}(\mathbf{x}, t)\, d\mathcal{X} = 2\nu t \tag{59}$$

To gain some further insight, let us now consider a random walk process for a molecule confined within a cubic domain of volume $(2\ell_{\mathrm{c}})^3$ over the time interval t_{c}. The molecule will initially be located within the center of the domain therefore can travel a distance of $\pm\ell_{\mathrm{c}}$ in each orthogonal direction. The motion per dimension is then restricted to the integer lattice $\mathcal{z}_\alpha = \{-1, +1\}$ so that the stepping vector may be expressed as $\mathbf{x}_\alpha = \boldsymbol{\mathcal{z}}_\alpha\ell_{\mathrm{c}}$. The stepping probability is next provided in the form of the discrete set of weights $w_\alpha = \{1/2\,, 1/2\}$, which is a discrete analog to (58). The mean-squared-displacement is then found from the equivalent second order central moment:

$$2\nu t_{\mathrm{c}} = \frac{1}{3}\sum_{\alpha=1}^{2}|\mathbf{x}_\alpha|^2 w_\alpha = \ell_{\mathrm{c}}^2 \tag{60}$$

As a result, the coefficient of kinematic viscosity may be expressed as $\nu = \frac{1}{2}\ell_{\mathrm{c}}^2/t_{\mathrm{c}}$. The associated kinetic energy is identified as $\frac{1}{2}\overline{v}^2 = (\tau/t_{\mathrm{c}})\beta^{-1}$ therefore $\tau = (4/\pi)t_{\mathrm{c}}$. As a final result, the coefficient of shearing viscosity ($\mu = \rho\nu$) is obtained in the form:

$$\mu = \frac{1}{2}\rho\overline{v}\ell_{\mathrm{c}} = \frac{m}{\pi\varnothing^2\sqrt{\pi\beta}} \tag{61}$$

To complete the derivation, we must find an expression for β using the axioms of thermodynamics. It will first be recognized that within the solution (58): $|\mathbf{x}|^2/4\nu t = \beta(|\mathbf{x}|^2/4\tau t)$. Well, in reference to (54), the kinetic energy may now be identified whose moment yields the internal energy:

$$\varepsilon = \frac{1}{4\rho\tau t}\int_{\mathbb{R}^3} |\mathbf{x}|^2\hat{\rho}(\mathbf{x},t)\,d\mathcal{X} = \frac{3}{2\beta} \tag{62}$$

Using this knowledge, the specific Lagrangian, denoted $\mathcal{L} = |\mathbf{x}|^2/4\tau t - \varepsilon$, may next be found through multiplying the mass diffusion equation by the specific action quantity t/β:

$$\int_{\mathbb{R}^3} \mathcal{L}\hat{\rho}\,d\mathcal{X} = \frac{t}{\beta}\int_{\mathbb{R}^3}\frac{\partial\hat{\rho}}{\partial t}d\mathcal{X} = \frac{\nu t}{\beta}\int_{\mathbb{R}^3}\sum_{i=1}^{3}\frac{\partial^2\hat{\rho}}{\partial \mathrm{x}_i^2}d\mathcal{X} = 0 \tag{63}$$

It will be noted that all Gaussian distributions contain the minimization property as shown in (63). Using the equipartition theorem, we may now declare $\beta = \Theta^{-1}$. The thermal energy is denoted $\Theta = R\mathrm{T}$ where R is the specific gas constant and T is the temperature.

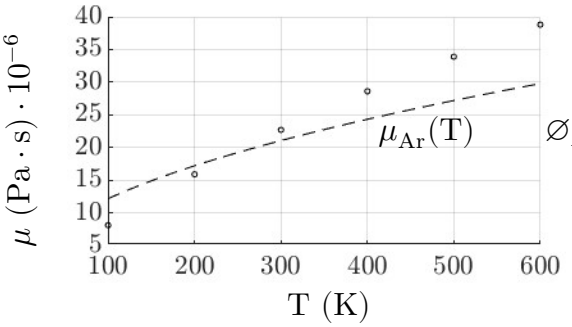

$\varnothing_{\mathrm{Ar}} = 376$ pm [17; p.9-49]

Figure 4 Comparison of predicted viscosity curve against experimental data [17; p.6-229]

The results shown in Figure 4 are somewhat reasonable around 200 K. The theoretical prediction (black dashed curve) begins to diverge from the experimental data around 300 K. One way to obtain more accurate results is to include intermolecular forces, e.g. $\mathbf{F}_{12}(|\boldsymbol{q}_2|)$, which will then affect the scattering probability. To do so, one must define the potential energy between molecules.

2.3 Overview of the Lattice Boltzmann Method

At this current point in the dissertation, the generalized Boltzmann equation has been derived using principles from analytical mechanics. The Boltzmann collision integral was next reviewed through

predicting the coefficient of shearing viscosity of an argon gas. Let us now consider the scalar velocity distribution field $\mathrm{F}(\boldsymbol{\xi}, \mathbf{x}, t)$ whose total temporal derivative expands as:

$$\frac{\mathbb{d}}{\mathbb{d}t}\mathrm{F}[\boldsymbol{\xi}(t), \mathbf{x}(t), t] = \frac{\partial \mathrm{F}}{\partial t} + \boldsymbol{\xi} \cdot \frac{\partial \mathrm{F}}{\partial \mathbf{x}} + \boldsymbol{a} \cdot \frac{\partial \mathrm{F}}{\partial \boldsymbol{\xi}} \tag{64}$$

Where $\boldsymbol{\xi}$ is the random velocity vector field and $\boldsymbol{a}$ denotes the acceleration vector field; related to the presence of a body force, i.e. $\boldsymbol{b} = \rho \boldsymbol{a}$. Due to intermolecular collisions, the general EOM is:

$$\mathbb{d}\mathrm{F}/\mathbb{d}t = -\mathfrak{C}[\mathrm{F}] \tag{65}$$

Where $\mathfrak{C}[\mathrm{F}]$ denotes the general collision operator. It will be noted that (65) is an equivalent field equation in comparison to (29), which is expressed in terms of the generalized coordinates $\boldsymbol{q}_i$ and the generalized velocities $\dot{\boldsymbol{q}}_i \ \forall \ i = 1,2, \dots, n$. The standard within the LB framework is the BGK[2] collision operator [21]: $\mathfrak{C}_{\mathrm{BGK}}[\mathrm{F}] = (\mathrm{F} - \mathrm{M})/\tau$, where M indicates the local equilibrium velocity distribution [14; p.72] and τ is referred to as the "relaxation" time. The general Boltzmann field equation (65), in the absence of a body force, will now take the single relaxation (SR) form:

$$\dot{\mathrm{F}} + \boldsymbol{\xi} \cdot \boldsymbol{\nabla}\mathrm{F} = -(\mathrm{F} - \mathrm{M})/\tau \tag{66}$$

To gain further insight, let us consider $\mathrm{F}(\boldsymbol{\xi}, t)$ therefore (66) reduces to $\mathrm{M} = \mathrm{F} + \tau\dot{\mathrm{F}}$. Holding M fixed, the solution is $\mathrm{F} = \mathrm{M} + (\mathrm{O} - \mathrm{M})\exp(-\mathfrak{t})$ where the initial condition is $\mathrm{O} = \mathrm{F}(t = 0)$ and the nondimensional time is denoted $\mathfrak{t} = t/\tau$. It can now be inferred that this formulation assumes the system is in a state of nonequilibrium, which will naturally "relax" towards an equilibrium state [15; p.72], at a rate governed by τ. Based on the homogenous analytical solution, the distribution never quite reaches equilibrium but approaches this state in a nonlinear fashion. Upon reforming (66) into $\mathrm{M} = \mathrm{F} + \tau(\mathbb{d}\mathrm{F}/\mathbb{d}t)$, the general solution is provided in the form [22]:

$$\mathrm{F}[\mathbf{x}(t), t] = \mathrm{F}(\mathbf{x}_{\mathrm{o}}, t_{\mathrm{o}}) - \frac{1}{\tau}\int_{t_1}^{t_2} (\mathrm{F}[\mathbf{x}(t), t] - \mathrm{M}[\mathbf{x}(t), t])\, \mathbb{d}t \tag{67}$$

Where the motion is given by $\mathbf{x}(t) = \mathbf{x}_{\mathrm{o}} + \boldsymbol{\xi}\delta t$, the time is defined as $t = t_{\mathrm{o}} + \delta t$, the initial time is set to $t_{\mathrm{o}} = 0$, and τ is assumed constant. The lattice Boltzmann equation (LBE) can be obtained through applying a one-point rectangular rule to the integral: $\tau^{-1}\int(\mathrm{F} - \mathrm{M})\,\mathbb{d}t \approx \mathfrak{t}(\mathrm{F}_{\mathrm{o}} - \mathrm{M}_{\mathrm{o}})$. As a result, the solution (67) will take the approximate form:

$$\mathrm{F}(\mathbf{x}_{\mathrm{o}} + \boldsymbol{\xi}\delta t, t_{\mathrm{o}} + \delta t) = (1 - \mathfrak{t})\mathrm{F}(\mathbf{x}_{\mathrm{o}}, t_{\mathrm{o}}) + \mathfrak{t}\mathrm{M}(\mathbf{x}_{\mathrm{o}}, t_{\mathrm{o}}) \tag{68}$$

It will be noted that if we expand the exponential within the homogenous solution, using a first order Taylor series about the initial time, i.e. $\exp(-\mathfrak{t}) = 1 - \mathfrak{t} + \mathcal{O}(t^2)$, then upon substituting, an equivalent result to (68) is found. Therefore, the approach to equilibrium now has a linear dependence upon time such that $\mathrm{F}[\mathbf{x}(\tau), \tau] = \mathrm{M}(\mathbf{x}_{\mathrm{o}}, t_{\mathrm{o}})$. This linearized formulation is directly

[2] The abbreviation "BGK" stands for the developers: Bhatnagar-Gross-Krook

analogous to applying a first order Taylor series expansion to the solution about the initial time:

$$\mathrm{F}[\mathbf{x}(t),t] = \mathrm{F}(\mathbf{x}_\mathrm{o},t_\mathrm{o}) + (\dot{\mathrm{F}} + \boldsymbol{\xi}\cdot\boldsymbol{\nabla}\mathrm{F})\big|_{t_\mathrm{o}}\delta t + \mathcal{O}(\delta t^2) \tag{69}$$

If we evaluate (66) at $t = t_\mathrm{o}$, then upon substituting $\mathrm{d}\mathrm{F}/\mathrm{d}t|_{t_\mathrm{o}} \approx (\mathrm{F}-\mathrm{F}_\mathrm{o})/\delta t$ from (69), the LBE (68) is once again found. This is known as the first order approximation. Now taking this one step further, the integral within the solution (67) will be approximated using a two-point trapezoidal rule: $\tau^{-1}\int(\mathrm{F}-\mathrm{M})\,\mathrm{d}t \approx \frac{1}{2}\mathfrak{t}(\mathrm{F}_\mathrm{o}-\mathrm{M}_\mathrm{o}+\mathrm{F}-\mathrm{M})$. Upon defining $\mathrm{G} = \mathrm{F}+\frac{1}{2}\mathfrak{t}(\mathrm{F}-\mathrm{M})$ and $\mathrm{G}_\mathrm{o} = \mathrm{F}_\mathrm{o}+\frac{1}{2}\mathfrak{t}(\mathrm{F}_\mathrm{o}-\mathrm{M}_\mathrm{o})$, the second order approximate solution is obtained in the form:

$$\mathrm{G}(\mathbf{x}_\mathrm{o}+\boldsymbol{\xi}\delta t, t_\mathrm{o}+\delta t) = (1-\mathfrak{t}')\mathrm{G}(\mathbf{x}_\mathrm{o},t_\mathrm{o}) + \mathfrak{t}'\mathrm{M}(\mathbf{x}_\mathrm{o},t_\mathrm{o}) \tag{70}$$

Where the nondimensional time is redefined as $\mathfrak{t}' = t/\tau'$ given $\tau' = \tau + \frac{1}{2}t$. We can now observe that (70) is analogous to (68). There are indirect ways to recover the Navier-Stokes (NS) equations through expanding the solution via a second order Taylor series then applying a perturbation analysis [23]. This methodology is ad hoc and does not replicate the computations performed within LB codes; see [60; p.13] and [61; ch.2.6].

Within the algorithm, initializing F is not a straightforward task due to the lack of an analytical expression. An example procedure can be found in [24]. The most simple action is to set $\mathrm{F}(\mathbf{x},0) = \mathrm{M}(\mathbf{x},0)$ as was done in [25]. For this reason, boundary conditions must be derived and employed directly onto the distribution function itself; in contrary to typical CFD procedures. For more details, please refer to the textbooks [7,8], which also discusses and provides references to state-of-the-art research trends regarding the LBM. For an overall literature review, the reader is referred to [21,26,27].

The collision-streaming algorithm, which may be extracted from (68) or (70), is used in other statistical molecular simulation methods, such as the LGCA and the direct simulation Monte Carlo (DSMC) method [28; p.366]. The same concept is sometimes applied to the finite difference LBM [29] and the finite volume LBM [30]. For compressible flows [29,31,32,33,34,35,36], (66) has typically been discretized in space using a finite volume formulation where each flux, located at the associated cell interface, is reconstructed based on the surrounding nodal values. The ENO[3] family, including the WENO [37] methodology, is commonly used in the effort to achieve stability. Otherwise, a total variation diminishing (TVD) constraint is applied. Upwind finite difference schemes have also been used, however, are less commonly found in the literature.

The spatial discretization within the FDLBM and FVLBM is not a unique feature. However, the temporal schemes applied to these two closely related frameworks, are a bit more specialized due to the collision operator and the associated constraints [15; p.50,109]:

$$\int_{\mathbb{R}^3} \phi(\boldsymbol{\xi})\mathfrak{C}[\mathrm{F}(\boldsymbol{\xi})]\,d\Xi = 0 \;\forall\; \phi = 1, \boldsymbol{\xi}, |\boldsymbol{\xi}|^2 \tag{71}$$

[3] The abbreviation “ENO” stands for “essentially non-oscillatory” and “WENO” refers to the “weighted” extension

The general EOM (65), in the absence of a body force, will next be multiplied by ϕ (representing a "summational invariant") then integrated over the velocity space. Upon applying (71), we obtain:

$$\int_{\mathbb{R}^3} (\mathrm{d}\mathrm{F}/\mathrm{d}t + \mathfrak{C}[\mathrm{F}])\phi \, d\Xi = \int_{\mathbb{R}^3} (\dot{\mathrm{F}} + \boldsymbol{\xi} \cdot \boldsymbol{\nabla}\mathrm{F})\phi \, d\Xi = 0 \tag{72}$$

One can now observe that the collision term redistributes the values assigned to F in such a way to cause a zero net effect. At the beginning of an arbitrary time step, the initial distribution will first be established as $\mathrm{F}_0 = \mathrm{F}(\mathbf{x}, 0)$. For ease of notation, the advection operator will be declared $\mathfrak{A}[\mathrm{F}] = \boldsymbol{\xi} \cdot \boldsymbol{\nabla}\mathrm{F}$ so that the governing EOM may be expressed in the form: $\dot{\mathrm{F}} + \mathfrak{A}[\mathrm{F}] + \mathfrak{C}[\mathrm{F}] = 0$. In many of the previously cited references, a multistage IMEX[4] Runge-Kutta [38] scheme is adopted, given $\mathfrak{n}$ stages per time step. This formulation treats the advection term explicitly while the collision term is treated implicitly, so that the stage values are computed from:

$$\mathrm{F}_\beta = \mathrm{F}_0 - t \sum_{\alpha=1}^{\beta} (\mathrm{A}_{\alpha\beta}\mathfrak{A}[\mathrm{F}_\alpha] + \mathrm{B}_{\alpha\beta}\mathfrak{C}[\mathrm{F}_\alpha]) \tag{73}$$

Where $\mathrm{A}_{\alpha\beta}$ and $\mathrm{B}_{\alpha\beta}$ are both matrices which apply weights to the advection and collision terms respectively. The advection terms are explicit because all diagonal terms within $\mathrm{A}_{\alpha\beta}$ are zero, i.e. $\mathrm{A}_{11} = \mathrm{A}_{22} = \cdots = \mathrm{A}_{\mathfrak{n}\mathfrak{n}} = 0$. The BGK collision term, per stage, is $\mathfrak{C}_{\mathrm{BGK}}[\mathrm{F}_\alpha] = (\mathrm{F}_\alpha - \mathrm{M}_\alpha)/\tau$ (assuming τ is constant) which will now replace the general collision operator within (73). We'll next multiply (73) by ϕ then generate the moment, while applying (71), to yield:

$$\int_{\mathbb{R}^3} \phi \mathrm{M}_\beta \, d\Xi = \int_{\mathbb{R}^3} \phi \mathrm{M}_0 \, d\Xi - t \sum_{\alpha=1}^{\beta} \mathrm{A}_{\alpha\beta} \int_{\mathbb{R}^3} \phi \mathfrak{A}[\mathrm{F}_\alpha] \, d\Xi \tag{74}$$

As a result, (74) is used to determine the equilibrium stage values so that (73) becomes explicit:

$$(1 + \mathfrak{t}\mathrm{B}_{11})\mathrm{F}_1 = \mathrm{F}_0 + \mathfrak{t}\mathrm{B}_{11}\mathrm{M}_1 \tag{75}$$

$$(1 + \mathfrak{t}\mathrm{B}_{\beta\beta})\mathrm{F}_\beta = \mathrm{F}_0 + \sum_{\alpha=1}^{\beta} (\mathfrak{t}\mathrm{B}_{\alpha\beta}\mathrm{M}_\alpha - t\mathrm{A}_{\alpha\beta}\mathfrak{A}[\mathrm{F}_\alpha]) - \mathfrak{t} \sum_{\alpha=1}^{\beta-1} \mathrm{B}_{\alpha\beta}\mathrm{F}_\alpha \tag{76}$$

After computing all stage values, the temporally advanced value is obtained from:

$$\mathrm{F} = \mathrm{F}_0 - t \sum_{\beta=1}^{\mathfrak{n}} (\mathrm{a}_\beta \mathfrak{A}[\mathrm{F}_\beta] + \mathrm{b}_\beta \mathfrak{C}[\mathrm{F}_\beta]) \tag{77}$$

Where a_β and b_β are vectors of weights, similar to their matrix counterparts. Within the algorithm, the integrals shown in (74) are in actuality finite summations. Some examples of discretizing F and M, in the velocity space, can be found in [39,40,41]. Multiple methods exist which include the

[4] The abbreviation "IMEX" stands for "implicit-explicit"

use of the Gauss-Hermite quadrature, the Gram-Schmidt orthogonalization procedure, and the entropic method.

To end the literature review, a simple 2D simulation will be performed. Viscosity and thermal conductivity will be neglected therefore the governing EOM is the freestream version of (66). A double distribution function approach will be utilized; one for the mass and momentum evolutions, expanded up to and including the fourth order Hermite polynomial ($\mathrm{D2Q9^2}$), and one for the total energy evolution, expanded up to and including the second order Hermite polynomial ($\mathrm{D2Q5^2}$). It will be noted that if the velocity distribution contained a nonequilibrium part, then typically two relaxation terms would be used within the energy evolution equation. The more general model is known as the multiple relaxation time (MRT) formulation, in contrary to the SRT form (66).

Similar to the Sod shock tube [47,48], a shock box [32] will be simulated whose inner and outer regions, at $t = 0$, contain different densities, temperatures, and pressures. In both regions, the gas will initially be at rest whose specific heat ratio is that of a diatomic perfect gas, i.e. $\gamma = 7/5$. Over a uniform spatial grid, the streaming algorithm will be implemented. Along the boundaries, the distributions will be held fixed to their initial values. Therefore, we've indirectly applied the no-slip boundary condition. The results of the simulation are shown in Figures 5 & 6.

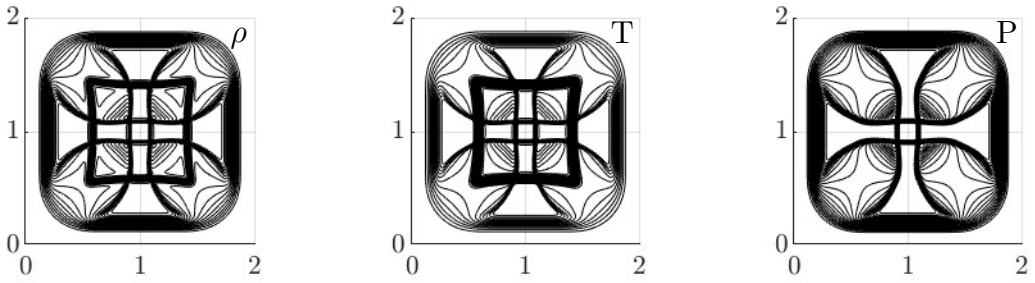

Figure 5 Shock box lattice Boltzmann simulation

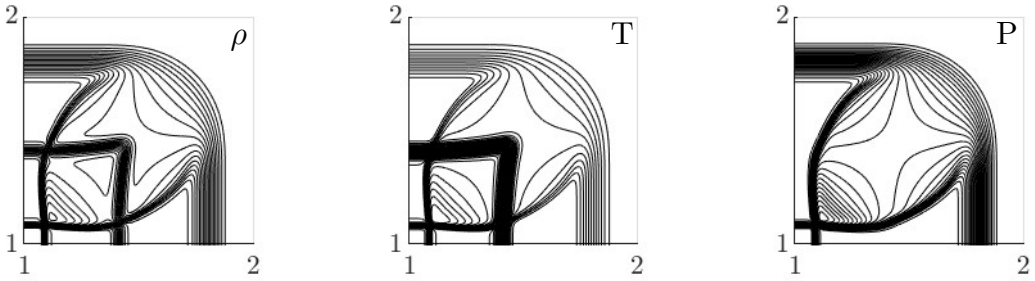

Figure 6 Shock box lattice Boltzmann simulation (upper RHS)

As one can observe from the results, the overall methodology of the LBM has serious potential to become a leading commercial software CFD algorithm. However, there are major fundamental flaws which first need reconciling. It is critical to note that due to the velocity discretization method used, being the Gauss-Hermite quadrature, there only exists a small collection of initial conditions which produce a stable shock box simulation. This is due to the fact that the Hermite-expanded

Gaussian is not a true representation of the Gaussian function itself, in contrary to the Taylor series expansion. This type of polynomial form often violates the first Kolmogorov axiom of probability [11; p.7]. If the velocity distribution is interpreted not that of a probability density, but of how the mass or total energy is dispersed over a time step, then the polynomial form often violates the basic definitions of mass and energy. For a visualization, please see Figure 7, where v is the mean velocity in one spatial dimension. In this regard, the Gram-Schmidt and entropic methods are no better.

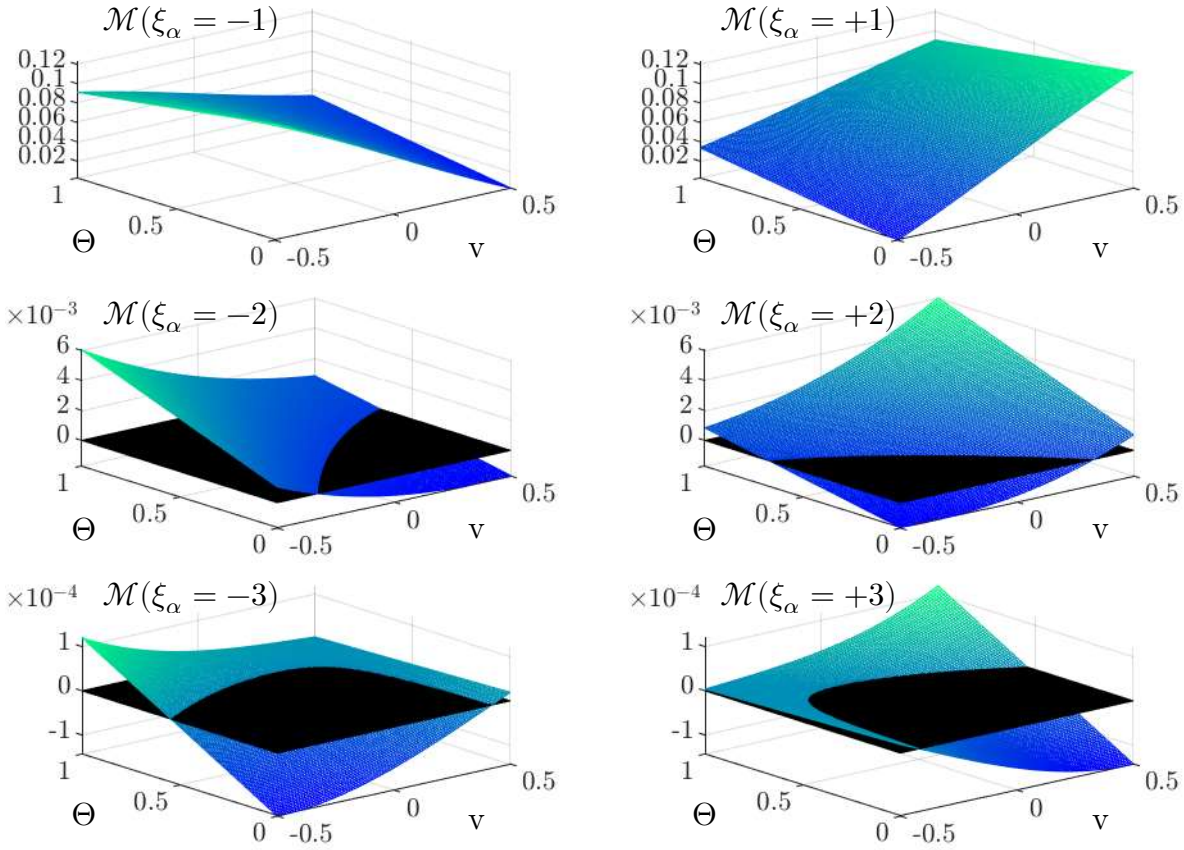

Figure 7 Hermite-expanded (3rd order) discrete Maxwellian (D1Q7)

In addition to the lack of positivity preservation resulting from the current velocity discretization methods, another major fundamental flaw, as previously mentioned, is that the EOM (66) cannot directly reproduce the Navier-Stokes equations. The indirect method is to apply the Chapman-Enskog perturbation analysis [15; ch.7]. It is vital to note that the work performed by these two scientists, along with Cowling, was aimed at predicting transport coefficients; in contrast to Grad's moment method [14; ch.7]. The main purpose of this dissertation is to resolve these two problems.

To explain the upcoming format, chapter 3 is a reformatted version of a paper I've been writing to be submitted to the American Institute of Aeronautics and Astronautics (AIAA) for peer-review publication. Initially, this work was geared towards hypersonics research due to the need of an accurate and stable CFD algorithm to properly capture shock wave development. Over time, I've realized that the QVFEM is a general framework; not specific to hypersonics. Overall, chapter 3 lays the groundwork and chapter 4 covers nonequilibrium extensions.

Chapter 3 – The QVFEM: Part I

The growing desire for high-speed flight vehicles has introduced numerous challenges to engineers; one being accurate predictions of mechanical and thermal loads acting on the outer mold surface of a flight vehicle body. To perform these calculations from a continuum standpoint, one must numerically solve the governing flowfield equations which tend to become highly unstable in the presence of shock wave development at flight speeds greater than the local speed of sound. This chapter will both review the statistical derivation and propose a new computational scheme to be applied to the compressible Euler equations of gas dynamics. The method has been coined the "quantized velocity finite element method" (QVFEM) which proves to be numerically stable during shock wave development without the use of artificial dissipation.

3.1 Introduction

Over the past several years, the field of hypersonics has been reawakened in the United States due to recent advances in hypersonic technology in countries such as Russia and China [42]. Besides military applications, there now exists research in the development of hypersonic vehicles for civil use, such as the Hermeus prototype plane: Quarterhorse[5]. One of the many challenges in the design of hypersonic vehicles is accurate prediction of the mechanical and thermal loads which act on the surface of the flight vehicle body. The determination of these loadings are a critical component in the structural design to ensure survivability of the structure, payload, and most importantly the passengers aboard. Additionally, to optimize the lift-to-drag ratio, a computational analysis tool is necessary for aerodynamic design. This specific problem has highlighted a major hole in modern-day computational fluid dynamics. To support this claim, William Gilbert Strang (1934-) during an interview in 2013 once made a remark saying[6]:

> "*All numerical methods are waiting to be improved. The finite elements came first for structural problems and that's a class of equations where nothing is going to move too far; where the bridge just moves a little bit and it's important to know how much. But think of the difference between that and fluid problems … a river is flowing, a jet engine is sending jet out (it's creating shock waves); much, much harder problems. The frontier (the difficult problems) are really those where there is a velocity involved … and for that we need new finite elements that are adapted to fast movement and to the appearance of shock waves. So you could say for solid mechanics we're good, for fluid mechanics we have much work to do, and for gas mechanics we have much, much work to do.*"

This quote sums up the major motivation of this work. Traditional computational methods will be expanded upon and modern-day so-called "shock-capturing" numerical schemes will be deemed unnecessary within the proposed QVFEM. One example is the family of essentially non-oscillatory (ENO) schemes which include the weighted (WENO) and targeted (TENO) methodologies [43], which approximate spatial gradients over structured grids; formulated within a finite volume framework. The temporal scheme is independent of the spatial where typically a strong stability preserving Runge-Kutta method is used. There has also been work in applying this methodology to unstructured grids [44]. Additionally, for these types of irregular nodal layouts, methods such

[5] https://www.hermeus.com/quarterhorse
[6] https://youtu.be/WwgrAH-IMOk

as the total variation bounded (TVB) discontinuous Galerkin finite element method [58] have been used in the past to stabilize the spatial gradients. Again, space and time are treated independently where a finite difference scheme is typically applied to the temporal derivative operator. In this work, space and time will be coupled into a single unified numerical scheme and the use of any artificial dissipation will not be needed. The prescription provided by the laws of the governing nonrelativistic physics will prove to be satisfactory and will not require any additional buffering terms or complex shock-capturing schemes to provide stability in the algorithm.

The method proposed in this chapter is Part I of a multipart series. Part I will introduce the QVFEM applied to the Euler equations which is an inviscid adiabatic flowfield model. Part II will entail the application to the Navier-Stokes-Fourier (NSF) equations to include viscous interactions and thermal conductivity. Multiple branches of physics will be utilized including classical mechanics, analytical mechanics, continuum mechanics, and thermodynamics with the binding glue being statistical mechanics. Once the equations of motion are formulated, the system being analyzed will be quantized based on the axioms of quantum mechanics. A new interpretation of quantum theory will be proposed to allow both classical and quantum theories to exist in harmony with one another. To accomplish such a task, multiple branches of calculus will be exploited including variational, distributional, and tensor calculus where index notation and the Einstein summation convention will, for the most part, be adopted.

One may also notice that the proposed methodology is not only inspired by traditional finite element methods but also by the lattice Boltzmann method (LBM). For example [31,32,33] uses a double distribution function approach where time is treated with an IMEX-RK scheme and space with a WENO [31], TVD [32], or upwind difference [33] scheme. There are however major deviations between the QVFEM and the LBM which will be discussed in more detail here within Part I as well as Part II, where physical dissipative and diffusive effects are taken into account. Within this work, the total energy density velocity distribution will be extended from a perfect gas to an ideal gas model. Additionally, the proposed framework will utilize a triple distribution function approach. Well as Dr. Strang said, "*... we have much work to do ...*" so let's get to it.

A complete reorganization of the Euler equations will be performed using statistical mechanics. Before doing so, the motivation will first be discussed. To begin, Sir Isaac Newton (1643-1727) gave us the ability to model the motion of discrete mechanical systems through the following Newtonian equation of motion [1; p.83, Law II]:

$$\mathrm{d}\mathbf{v}(t)/\mathrm{d}t = \dot{\mathbf{v}} = -(1/m)\boldsymbol{\nabla}\Pi \tag{78}$$

Where $\boldsymbol{\nabla} = \partial/\partial\mathbf{x}$, the velocity vector is $\mathbf{v}(t) = \dot{\mathbf{x}}(t)$, and $\mathbf{x}(t)$ is the position of a single point being the centroid of an identifiable object with mass m. Changes in the rate of motion, with respect to time, are governed by the spatial gradient in the potential energy field Π. To apply this methodology to a flowfield, one would need to have knowledge of the number of molecules within the domain of interest, the initial positions of the molecules, molecular geometry, internal forces amongst the constituent molecules, etc. The motion would then be found through solving a system of differential equations, whose size is proportional to n. These types of physical systems in nature are typically composed of enormous amounts of smaller subsystems being, as mentioned previously, molecules and atoms. For example, in a $500\ \mathrm{mL}$ bottle of water, there are

approximately $1.6 \cdot 10^{25}$ H_2O molecules occupying that volume. Therefore, the Newtonian EOM is not optimal for these types of analyses.

What is desirable is a model where the physics are described in terms of densities rather than individual molecules. For high-speed flows (above the local speed of sound), the distance at which a single molecule or a density of molecules will travel over a "small" time interval is enormous. Therefore, it is also desirable to track the evolution of the system through stationary viewing windows or control volumes; in contrast to tracking the actual motion of the bodies. As a result, Leonhard Euler (1707-1783) extended Newton's framework to a continuum field formulation through the following Eulerian equation of motion [2; p.286]:

$$\mathrm{d}\mathbf{v}(\mathbf{x},t)/\mathrm{d}t = \dot{\mathbf{v}} + (\mathbf{v}\cdot\boldsymbol{\nabla})\mathbf{v} = -(1/\rho)\boldsymbol{\nabla}\mathrm{P} \tag{79}$$

The velocity and position are now vector fields and the operator $\mathrm{d}/\mathrm{d}t$ is what's known as the "material" derivative; see [45; p.80-82] and [46; p.66-67]. This operation includes a multistep process where the function being operated on is first written in terms of the reference configuration $\mathbf{x}_\mathrm{o}$ and absolute time t. The derivative operation is next performed then lastly the function is converted back into the current configuration $\mathbf{x}$. In this work, we'll refer to this operator as the mapping derivative (MD) where the motion at every point in spacetime is given by the one-to-one mapping function $\boldsymbol{\varphi}$ [45; p.61-63]. The following notation will be used for the mapping:

$$\mathbf{x} = \boldsymbol{\varphi}(\mathbf{x}_\mathrm{o},t) \;\leftrightarrow\; \mathbf{x}_\mathrm{o} = \boldsymbol{\varphi}^{-1}(\mathbf{x},t) \tag{80}$$

So, the velocity field $\mathbf{v}(\mathbf{x},t)$ is first converted to the functional $\mathbf{v}[\boldsymbol{\varphi}(\mathbf{x}_\mathrm{o},t),t]$. The operator $\mathrm{d}/\mathrm{d}t$ is next applied holding $\mathbf{x}_\mathrm{o}$ fixed then finally mapped back into the current configuration:

$$\mathrm{d}\mathbf{v}(\mathbf{x},t)/\mathrm{d}t = \dot{\mathbf{v}}(\mathbf{x},t) + \dot{\boldsymbol{\varphi}}(\mathbf{x}_\mathrm{o},t)\cdot\boldsymbol{\nabla}|_{\mathbf{x}_\mathrm{o}=\boldsymbol{\varphi}^{-1}(\mathbf{x},t)}\mathbf{v}(\mathbf{x},t) \tag{81}$$

As a result, an expression for the velocity field is obtained as $\mathbf{v}(\mathbf{x},t) = \dot{\boldsymbol{\varphi}}[\boldsymbol{\varphi}^{-1}(\mathbf{x},t),t]$. What we have now is a prescription for how information is transported over a spacetime continuum field. When dealing with high-speed flows, i.e. $\mathrm{M} = |\mathbf{v}|/\mathbb{c} \geq 1$, the leading cause in numerical instabilities in CFD algorithms is the advection operator $\mathbf{v}\cdot\boldsymbol{\nabla}$ where $|\mathbf{v}| \geq \mathbb{c}$. Since $\mathbf{v} \approx \delta\boldsymbol{\varphi}/\delta t$, the idea is to have $\delta\boldsymbol{\varphi} \leq \delta\mathbf{x}$ to ensure proper conveyance of information. For example, let us consider the MD of a general scalar function denoted as $\mathrm{F}(\mathbf{x},t)$. A first order forwards Taylor series in time and a first order backwards Taylor series in space will be applied, which yields respectively:

$$\mathrm{F}(\mathbf{x},t+\delta t) = \mathrm{F}(\mathbf{x},t) + \dot{\mathrm{F}}(\mathbf{x},t)\delta t + \mathcal{O}(\delta t^2) \tag{82}$$

$$\mathrm{F}(\mathbf{x}-\mathbf{v}\delta t,t) = \mathrm{F}(\mathbf{x},t) - \mathbf{v}\cdot\boldsymbol{\nabla}\mathrm{F}(\mathbf{x},t)\delta t + \mathcal{O}(\delta t^2) \tag{83}$$

From which an approximation to the MD is obtained in the form of a first order upwind scheme:

$$\mathrm{dF}/\mathrm{d}t = \dot{\mathrm{F}} + \mathbf{v}\cdot\boldsymbol{\nabla}\mathrm{F} \approx [\mathrm{F}(\mathbf{x},t+\delta t) - \mathrm{F}(\mathbf{x}-\mathbf{v}\delta t,t)]/\delta t \tag{84}$$

The discrete form (84) is only valid if $\delta\boldsymbol{\varphi} = \delta\mathbf{x}$. In the case that $\delta\boldsymbol{\varphi} < \delta\mathbf{x}$, then:

$$\frac{\mathrm{dF}}{\mathrm{d}t} \approx \frac{\mathrm{F}(x_i, y_j, z_k, t_{l+1}) - \mathrm{F}(x_i, y_j, z_k, t_l)}{t_{l+1} - t_l} \pm |u| \frac{\mathrm{F}(x_i, y_j, z_k, t_l) - \mathrm{F}(x_{i\mp1}, y_j, z_k, t_l)}{x_i - x_{i\mp1}}$$

$$\pm|v| \frac{\mathrm{F}(x_i, y_j, z_k, t_l) - \mathrm{F}(x_i, y_{j\mp1}, z_k, t_l)}{y_j - y_{j\mp1}} \pm |w| \frac{\mathrm{F}(x_i, y_j, z_k, t_l) - \mathrm{F}(x_i, y_j, z_{k\mp1}, t_l)}{z_k - z_{k\mp1}} \tag{85}$$

Where the chosen stencil depends upon the sign of the velocity component, or in other words, the direction of the "wind." For $\mathrm{dF}/\mathrm{d}t = \mho$, the temporally advanced value, denoted F', is given by:

$$\mathrm{F}' \approx \mathrm{F} - (u\delta t/\delta x)\delta_x \mathrm{F} - (v\delta t/\delta y)\delta_y \mathrm{F} - (w\delta t/\delta z)\delta_z \mathrm{F} + \mho\delta t \tag{86}$$

To maintain stability in the algorithm and for the output results to be physically meaningful, we must require that $\mathbf{v}\delta t \leq \delta\mathbf{x}$. If this inequality is not satisfied, the information being carried by the advection stream is brought outside the stencil domain and is therefore lost. The Courant number, per dimension, must be greater than zero and less than or equal to unity:

$$\langle 0,0,0 \rangle < \langle u\delta t/\delta x \, , v\delta t/\delta y \, , w\delta t/\delta z \rangle \leq \langle 1,1,1 \rangle \tag{87}$$

Otherwise, there is a loss of information which violates the balance laws of mass, momentum, and energy. For reference, we refer to the von Neumann stability analysis of the discretized one-dimensional linear advection equation performed in [49; p.161-162]. To note, the CFL requirement may vary depending on the discretization scheme used. In this work, however, (87) will always be a governing inequality.

Due to the importance of this condition, one more example will be provided. Let's envision a one-dimensional information stream within an element of length ℓ, over the time interval τ, traveling at a constant rate of $\mathbb{c}$. If $\mathbb{c} \leq \ell/\tau$, then at $t = \tau$, the information remains contained within the domain of the element. However, if $\mathbb{c} > \ell/\tau$, then the information will reach a point in space beyond the domain of the element by the end of the time step. As a result, the information is lost due to loss of containment. When the velocity components u, v, and/or w become "large," the constraint (87) is often not satisfied.

To make matters worse, the Eulerian EOM (79) is nonlinear due to the advection operator operating on the velocity field: $(\mathbf{v} \cdot \boldsymbol{\nabla})\mathbf{v}$. To overcome these difficulties, a reorganization becomes necessary. One additional remark will be made. The velocity $\mathbf{v}$ is a mean value of the molecular velocities $\mathbf{v}_\alpha \ \forall \ \alpha = 1,2, \ldots, n$ per control volume. Since these equations are statistical in nature, it will herein be proven that it's most optimal to treat them as such from both theoretical and computational standpoints; which leads us into the realm of probability theory.

3.2 The Equilibrium Distribution of Molecular Velocities

The mass density ρ will be decomposed into a distribution of states denoted $\hat{\rho}(\dot{\boldsymbol{q}}, \boldsymbol{q}) \ \forall \ \Gamma \in \mathbb{R}^6$, which must satisfy the following conditions based on the Kolmogorov axioms of probabilities and the calculus of distributions [11; p.5-7]:

I. The mass density will be decomposed in such a manner so that $\hat{\rho} \subset \mathbb{R}^{+}$ thus implying non-negativity of mass therefore $\hat{\rho} \geq 0$.

II. The distribution $\hat{\rho}$ shall be normalized so that ρ may be recovered upon summing over all possible velocity states $\boldsymbol{\xi}\ \forall\ \Xi \in \mathbb{R}^3$ and positions $\boldsymbol{y}\ \forall\ \Lambda \in \mathbb{R}^3$. The mass density is then:

$$\rho \equiv \int_{\mathbb{R}^6} \hat{\rho}[\dot{\boldsymbol{q}}(\boldsymbol{\xi}), \boldsymbol{q}(\boldsymbol{y})]\, d\Gamma \tag{88}$$

III. For (88) to be valid, each possible velocity state and position must be unique so that the intersection of states forms an empty set. The union of states is equal to $\Gamma \in \mathbb{R}^6$ so that the collection of all states forms a partition of the phase space. In this work, the phase space refers to velocity and position in contrary to momentum and position.

Perturbations in velocity and position will be analyzed through introducing the virtual time τ so that the variational time may be defined as $t^* = t + \tau$. Applying a first order Taylor series expansion to the generalized coordinate and velocity vectors yields the following variational quantities respectively:

$$\boldsymbol{q}^* = \boldsymbol{q}(t+\tau) = \boldsymbol{q}(t) + \dot{\boldsymbol{q}}\tau \tag{89}$$

$$\dot{\boldsymbol{q}}^* = \dot{\boldsymbol{q}}(t+\tau) = \dot{\boldsymbol{q}}(t) + \ddot{\boldsymbol{q}}\tau \tag{90}$$

Where in the limit as $\tau \to 0$ recovers the exact definition of how these quantities change with respect to time:

$$\dot{\boldsymbol{q}} = \frac{\partial \boldsymbol{q}^*}{\partial \tau} = \lim_{\tau \to 0} \frac{\boldsymbol{q}(t+\tau) - \boldsymbol{q}(t)}{\tau} \tag{91}$$

$$\ddot{\boldsymbol{q}} = \frac{\partial \dot{\boldsymbol{q}}^*}{\partial \tau} = \lim_{\tau \to 0} \frac{\dot{\boldsymbol{q}}(t+\tau) - \dot{\boldsymbol{q}}(t)}{\tau} \tag{92}$$

As time marches forwards over the increment $\tau \equiv \delta t$, the information stored within $\hat{\rho}$ transmits via the functional:

$$\hat{\rho}^* = \hat{\rho}(\dot{\boldsymbol{q}}^*, \boldsymbol{q}^*) = \hat{\rho}(\dot{\boldsymbol{q}} + \ddot{\boldsymbol{q}}\tau, \boldsymbol{q} + \dot{\boldsymbol{q}}\tau) \tag{93}$$

The perturbed distribution changes with respect to the virtual time in the following manner, through using the chain rule of multivariable differential calculus [12; p.117]:

$$\frac{\partial \hat{\rho}^*}{\partial \tau} = \frac{\partial \hat{\rho}^*}{\partial q_i^*}\frac{\partial q_i^*}{\partial \tau} + \frac{\partial \hat{\rho}^*}{\partial \dot{q}_i^*}\frac{\partial \dot{q}_i^*}{\partial \tau} = \dot{q}_i \frac{\partial \hat{\rho}^*}{\partial q_i^*} + \ddot{q}_i \frac{\partial \hat{\rho}^*}{\partial \dot{q}_i^*} \tag{94}$$

Taking the limit as $\tau \to 0$ provides the definition of the temporal rate of change in the distribution $\hat{\rho}$ through the following variational operation, otherwise known as the Gâteaux operator [46; p.46-47, 372-374]:

$$\frac{\mathrm{d}\hat{\rho}}{\mathrm{d}t} = \lim_{\tau \to 0} \frac{1}{\tau}(\hat{\rho}^* - \hat{\rho}) = \left.\frac{\partial \hat{\rho}^*}{\partial \tau}\right|_{\tau=0} = \dot{q}_i \frac{\partial \hat{\rho}}{\partial q_i} + \ddot{q}_i \frac{\partial \hat{\rho}}{\partial \dot{q}_i} \tag{95}$$

$$= \frac{\partial \hat{\rho}}{\partial q_i}\frac{\partial \mathcal{E}}{\partial \dot{q}_i} - \frac{\partial \hat{\rho}}{\partial \dot{q}_i}\frac{\partial \mathcal{E}}{\partial q_i} = \{\hat{\rho}, \mathcal{E}\}$$

Where the specific total energy and associated Lagrangian are defined as:

$$\mathcal{E}(\dot{\boldsymbol{q}}, \boldsymbol{q}) = \tfrac{1}{2}|\dot{\boldsymbol{q}}|^2 + \phi(\boldsymbol{q}) \tag{96}$$

$$\mathcal{L}(\dot{\boldsymbol{q}}, \boldsymbol{q}) = \tfrac{1}{2}|\dot{\boldsymbol{q}}|^2 - \phi(\boldsymbol{q}) \tag{97}$$

As a result, the total derivative with respect to time may be written in terms of a Poisson bracket: $\mathrm{d}\hat{\rho}/\mathrm{d}t = \{\hat{\rho}, \mathcal{E}\}$. We'll seek a solution for which the distribution is stationary. Solving $\{\hat{\rho}, \mathcal{E}\} = 0$ obtains the following analytical solution [15; p.376]:

$$\hat{\rho}(\dot{\boldsymbol{q}}, \boldsymbol{q}) = \rho\zeta^{-1}\exp[-\beta\mathcal{E}(\dot{\boldsymbol{q}}, \boldsymbol{q})] \tag{98}$$

Where ζ is the partition function, therefore $1/\zeta$ acts as the normalizing coefficient, and β is the nondimensionalizing specific energy coefficient, having units of $\mathrm{kg/J}$ in this circumstance. Since $\mathrm{d}\hat{\rho}/\mathrm{d}t = 0$, then the finite change over a specified time interval must also equate to zero:

$$\delta\hat{\rho} = \int_{\delta t} \{\hat{\rho}, \mathcal{E}\}\,\mathrm{d}t = 0 \tag{99}$$

Applying the method of integration by parts unveils the Beltrami identity:

$$\int_{\delta t}\left[\frac{\mathrm{d}}{\mathrm{d}t}\left(\frac{\partial \hat{\rho}}{\partial \dot{q}_i}\right) - \frac{\partial \hat{\rho}}{\partial q_i}\right]\dot{q}_i\,\mathrm{d}t = \left(\frac{\partial \hat{\rho}}{\partial \dot{q}_i}\dot{q}_i - \hat{\rho}\right)\Big|_{\delta t} \tag{100}$$

Since $\partial\hat{\rho}/\partial\boldsymbol{q} = -(\partial\mathcal{E}/\partial\boldsymbol{q})\beta\hat{\rho}$ and $\partial\hat{\rho}/\partial\dot{\boldsymbol{q}} = -(\partial\mathcal{E}/\partial\dot{\boldsymbol{q}})\beta\hat{\rho}$, then (100) simplifies to:

$$\int_{\delta t}(\ddot{q}_i + \partial\phi/\partial q_i)\dot{q}_i\hat{\rho}\,\mathrm{d}t = \int_{\delta t}\dot{\mathcal{E}}\hat{\rho}\,\mathrm{d}t = 0 \tag{101}$$

Therefore recovering a variational form of Newton's specific EOM, where $\dot{\mathcal{E}} = 0$. It is now quite obvious that what makes the solution (98) stationary, is Newton's 2nd law of motion (LoM). This distribution is otherwise known as the generalized Maxwellian, named after James Clerk Maxwell (1831-1879). The generalized velocity vector will next be declared as $\dot{\boldsymbol{q}} = \boldsymbol{\xi} - \mathbf{v}$. This vector quantity resembles the relative velocity between a possible velocity state $\boldsymbol{\xi}$ and the mean or observable velocity $\mathbf{v}$. Similarly, the generalized position vector will be established as $\boldsymbol{q} = \boldsymbol{y} - \mathbf{x}$, where $\boldsymbol{y}$ is a possible position and $\mathbf{x}$ is the mean or path observed. To finalize (98), the partition function will be defined from the condition (88):

$$\zeta \equiv \int_{\mathbb{R}^6}\exp(-\beta\mathcal{E})\,d\Gamma \equiv \int_{\mathbb{R}^3}\exp(-\beta|\dot{\boldsymbol{q}}|^2/2)\,d\Xi\int_{\mathbb{R}^3}\exp(-\beta\phi)\,d\Lambda \tag{102}$$

Since the kinetic energy is only a function of $\dot{\boldsymbol{q}}$ and the potential energy is only a function of $\boldsymbol{q}$, then (102) may be separated as shown. As a result, the partition function may be decomposed as $\zeta = \zeta_{\text{ki}}\zeta_{\text{po}}$. Upon defining a potential energy function, the mean potential energy or internal translational energy is:

$$\varepsilon \equiv \frac{1}{\zeta_{\text{po}}} \int_{\mathbb{R}^3} \phi \exp(-\beta\phi)\, d\Lambda \tag{103}$$

The development of a potential energy function is beyond the scope of this work due to the fact that intermolecular forces will be neglected under the ideal gas assumption. The associated mean will be derived in the next subsection based on thermodynamical principles. To determine the nondimensionalizing coefficient, the following minimization principle will be enforced:

$$\vec{\rho}[\mathcal{L}] \equiv \int_{\mathbb{R}^6} \mathcal{L}\hat{\rho}\, d\Gamma \equiv \frac{1}{2}\int_{\mathbb{R}^3} |\dot{\boldsymbol{q}}|^2 \hat{\rho}(\dot{\boldsymbol{q}})\, d\Xi - \rho \int_{\mathbb{R}^3} \phi(\boldsymbol{q})\hat{p}(\boldsymbol{q})\, d\Lambda \equiv 0 \tag{104}$$

Where the phase space distribution is separated as $\hat{\rho}(\dot{\boldsymbol{q}}, \boldsymbol{q}) = \hat{\rho}(\dot{\boldsymbol{q}})\hat{p}(\boldsymbol{q})$. From here on out, the operator $\vec{\rho}$ will no longer refer to integration over the phase space but only the velocity space. So, (104) simplifies to $\vec{\rho}[\mathcal{L}(\dot{\boldsymbol{q}})] = \frac{1}{2}\vec{\rho}[\dot{\boldsymbol{q}} \cdot \dot{\boldsymbol{q}}] - \rho\varepsilon = 0$, where $\mathcal{L}(\dot{\boldsymbol{q}}) = \frac{1}{2}|\dot{\boldsymbol{q}}|^2 - \varepsilon$. Upon solving for ζ_{ki} and β using the previously noted conditions, an isotropic Gaussian distribution is obtained as:

$$\hat{\rho}(\boldsymbol{\xi}; \mathbf{v}|\varepsilon) = \frac{\rho}{(4\pi\varepsilon/3)^{3/2}} \exp(-3|\dot{\boldsymbol{q}}|^2/4\varepsilon) \tag{105}$$

Where $\beta = 3(2\varepsilon)^{-1}$ and $\zeta_{\text{ki}} = (2\pi/\beta)^{3/2}$, thus concluding the derivation of the equilibrium velocity distribution. The notation for $\hat{\rho}(\boldsymbol{\xi}; \mathbf{v}|\varepsilon)$ uses the Green's function notation from [19] and the quantity to the RHS of the bar identifies the variance, similar to the notation used in [11].

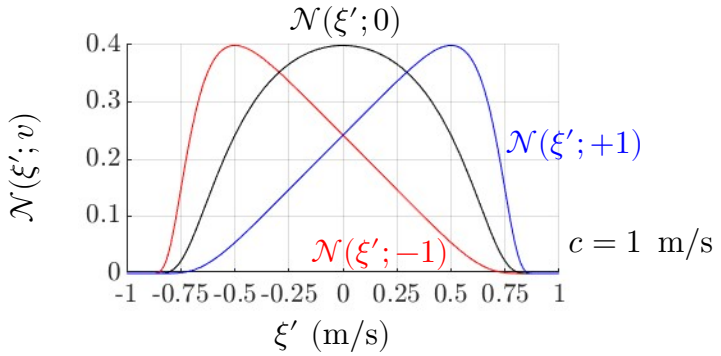

Figure 8 Unit normal velocity distribution with maximum speed c

For a quick purely academic exercise, let us suppose there is a limiting value on the velocity, denoted c. In one spatial dimension on a Minkowski diagram, the horizontal axis represents the distance traveled by light, denoted ct, and the vertical axis represents the distance traveled by a particle or point mass, denoted ξt. An angle will next be introduced as θ, such that $\xi = c\tan\theta$, where $\theta = b\xi'$ and $bc = \pi/2$. The total differential of ξ is then $d\xi = (\pi/2)\sec^2(b\xi')\, d\xi'$ so that

integration over $f(\xi)$ will now take the following form:

$$\int_{\mathbb{R}} f(\xi)\, d\xi = \frac{\pi}{2} \lim_{\mathcal{s} \to c} \int_{-\mathcal{s}}^{+\mathcal{s}} \sec^2(b\xi')\, f(\xi')\, d\xi' \tag{106}$$

The distribution is now anisotropic when the mean velocity is other than zero, i.e. $\upsilon \neq 0$. This means there is a "preferred" direction as shown on the transformed unit normal distribution plotted in Figure 8. This transformation was found with the help of my advisor, Dr. Kapania.

Now that the Maxwellian has been derived ab initio of mechanics, we'll next explore the underlying thermodynamic process built into (105).

3.3 The Resulting Thermodynamics of a Monatomic Perfect Gas

The attention will now turn from the phase space to the thermodynamic state space. For example, the constraint (104) reappears in the following partial differential equation:

$$\int_{\mathbb{R}^3} \mathcal{L}\hat{\rho}\, d\Xi = \frac{\varepsilon}{\beta} \int_{\mathbb{R}^3} \frac{\partial \hat{\rho}}{\partial \varepsilon} d\Xi = \frac{\varepsilon}{3\beta} \sum_{i=1}^{3} \int_{\mathbb{R}^3} \frac{\partial^2 \hat{\rho}}{\partial \xi_i^2} d\Xi = 0 \tag{107}$$

The governing PDE is then $\partial\hat{\rho}/\partial\varepsilon = \frac{1}{3}\dot{\nabla}^2\hat{\rho}$ which provides the mass dispersion prescription. As one can observe, most of the mass moves with velocity $\mathbf{v}$. However, based on the internal energy, varying amounts of mass travel with velocity $\boldsymbol{\xi} \neq \mathbf{v}$. The fundamental thermodynamic relation may next be obtained through applying the natural logarithm to (105), multiplying by $-\upsilon R\hat{\rho}$, then integrate over the velocity space [46; ch.7]:

$$\mathrm{s}(\varepsilon, \upsilon) = -\upsilon R\vec{\rho}[\ln \hat{\rho}] = \mathrm{c}_{\upsilon} \ln \varepsilon + R \ln \upsilon + \mathrm{c}_{\upsilon}(1 + \ln 4\pi/3) \tag{108}$$

The specific heat coefficient at constant volume is $\mathrm{c}_{\upsilon} = 3R/2$ which will be derived shortly in a more rigorous fashion. To note, the specific gas constant is given by $R = k_{\mathrm{B}}/m$ and the specific volume is $\upsilon = 1/\rho$. The following two Maxwell relations provide the definition of temperature and an expression for the thermodynamic pressure, respectively:

$$\mathrm{T} = (\partial\varepsilon/\partial\mathrm{s})_{\upsilon} \tag{109}$$

$$\mathrm{P} = (\partial\varepsilon/\partial\mathrm{s})_{\upsilon}(\partial\mathrm{s}/\partial\upsilon)_{\varepsilon} \tag{110}$$

The internal energy is found to be a linear function of temperature: $\varepsilon = \mathrm{c}_{\upsilon}\mathrm{T}$, and the pressure falls under the ideal gas equation of state: $\mathrm{P} = \rho\Theta$, where the specific thermal energy is $\Theta = R\mathrm{T}$. The specific volume may now be expressed as $\upsilon = \Theta/\mathrm{P}$ so that the Gibbs relation may be directly found from the fundamental relation (108):

$$\mathrm{ds} = (\partial\mathrm{s}/\partial\upsilon)_{\varepsilon}\mathrm{d}\upsilon + (\partial\mathrm{s}/\partial\varepsilon)_{\upsilon}\mathrm{d}\varepsilon = R\mathrm{d}\upsilon/\upsilon + \mathrm{c}_{\upsilon}\mathrm{d}\varepsilon/\varepsilon \tag{111}$$

$$\mathrm{d}\varepsilon = \delta q + \delta w = \mathrm{T}\mathrm{d}\mathrm{s} - \mathrm{P}\mathrm{d}\upsilon \tag{112}$$

The term $\delta q = \mathrm{T}\mathrm{d}\mathrm{s}$ represents the heat supplied to or transferred out of the system while the term $\delta w = -\mathrm{P}\mathrm{d}\upsilon$ represents the work done on the system. Using Newton's 3rd LoM, the work response may be equal and opposite (not always). Under the 2nd law of thermodynamics (LoT), the entropy production must be greater or equal to zero. To note, the differential $\mathrm{d}\mathrm{s}$ is not subjected to this inequality constraint. Please refer to chapter 4 for an in-depth discussion. Overall, the Gibbs relation (112) represents the 1st law of thermodynamics, which shows the balance of energy. To uncover expressions for the specific heat coefficients, the entropy will be expressed as a function of temperature-volume, temperature-pressure, and pressure-volume respectively:

$$\mathrm{s}(\mathrm{T}, \upsilon) = \mathrm{c}_{\upsilon} \ln \Theta + R \ln \upsilon + \mathrm{s}_{\mathrm{o}} \tag{113}$$

$$\mathrm{s}(\mathrm{T}, \mathrm{P}) = \mathrm{c}_{\mathrm{P}} \ln \Theta - R \ln \mathrm{P} + \mathrm{s}_{\mathrm{o}} \tag{114}$$

$$\mathrm{s}(\mathrm{P}, \upsilon) = \mathrm{c}_{\upsilon} \ln \mathrm{P} + \mathrm{c}_{\mathrm{P}} \ln \upsilon + \mathrm{s}_{\mathrm{o}} \tag{115}$$

Where the entropy constant is $\mathrm{s}_{\mathrm{o}} = \mathrm{c}_{\upsilon}(1 + \ln 2\pi)$ and the specific heat coefficient at constant pressure is given by the Mayer relation $\mathrm{c}_{\mathrm{P}} = \mathrm{c}_{\upsilon} + R$. From the above transformations, the specific heat coefficients may formally be derived as:

$$\mathrm{c}_{\upsilon} = \mathrm{T}(\partial \mathrm{s}/\partial \mathrm{T})_{\upsilon} = \mathrm{P}(\partial \mathrm{s}/\partial \mathrm{P})_{\upsilon} = \partial \varepsilon/\partial \mathrm{T} = 3R/2 \tag{116}$$

$$\mathrm{c}_{\mathrm{P}} = \mathrm{T}(\partial \mathrm{s}/\partial \mathrm{T})_{\mathrm{P}} = \upsilon(\partial \mathrm{s}/\partial \upsilon)_{\mathrm{P}} = \partial h/\partial \mathrm{T} = 5R/2 \tag{117}$$

The enthalpy is then $h = \mathrm{c}_{\mathrm{P}}\mathrm{T} = \varepsilon + \upsilon \mathrm{P}$ so that the total differential yields $\mathrm{d}h = \mathrm{T}\mathrm{d}\mathrm{s} + \upsilon \mathrm{d}\mathrm{P}$, being the equivalent form of (112). Using (115), the total differential expands similarly to (111):

$$\mathrm{d}\mathrm{s} = (\partial \mathrm{s}/\partial \mathrm{P})_{\upsilon} \mathrm{d}\mathrm{P} + (\partial \mathrm{s}/\partial \upsilon)_{\mathrm{P}} \mathrm{d}\upsilon = \mathrm{c}_{\upsilon} \mathrm{d}\mathrm{P}/\mathrm{P} + \mathrm{c}_{\mathrm{P}} \mathrm{d}\upsilon/\upsilon \tag{118}$$

Assuming an isentropic process, i.e. $\mathrm{d}\mathrm{s} = 0$, then (118) may be used to find the isentropic speed of sound (squared):

$$\mathbb{a}^2 = \mathrm{d}\mathrm{P}/\mathrm{d}\rho = \gamma \mathrm{P}/\rho = \gamma \Theta \tag{119}$$

Where the specific heat ratio is $\gamma = \mathrm{c}_{\mathrm{P}}/\mathrm{c}_{\upsilon} = 5/3$ so the specific heat coefficients may now be expressed as:

$$\mathrm{c}_{\upsilon} = R/(\gamma - 1)\,, \qquad \mathrm{c}_{\mathrm{P}} = \gamma R/(\gamma - 1) \tag{120}$$

At this point, it may be concluded that the derived distribution (105) is representative of the perfect gas model. In summary, the internal energy and enthalpy are linear functions of temperature therefore the specific heat coefficients are constant. These computed quantities fall under the category of a perfect monatomic gas, such as the noble gas argon (Ar). The mass of which will be provided in both Daltons and kilograms [17; p.1-11]:

$$m = 39.948\ \mathrm{u} = 39.948 \cdot 1.66053906660 \cdot 10^{-27}\ \mathrm{kg} \approx 6.6335 \cdot 10^{-26}\ \mathrm{kg} \tag{121}$$

From the National Institute of Standards and Technology (NIST), the exact value for Boltzmann's constant is provided as[7] $k_{\mathrm{B}} = 1.380649 \cdot 10^{-23}\ \ \mathrm{J/K}$. The universal gas constant is $\mathfrak{R} = N_{\mathrm{A}} k_{\mathrm{B}}$ where the exact value for Avogadro's number is $N_{\mathrm{A}} = 6.02214076 \cdot 10^{23}/\mathrm{mol}$ (also provided by NIST). The specific gas constant is then found via:

$$R = \mathfrak{R}/(mN_{\mathrm{A}}) = k_{\mathrm{B}}/m \approx 208.1321\ \ \mathrm{J/(kg \cdot K)} \tag{122}$$

Based on NIST-JANAF, the specific heat coefficient at constant pressure is:

$$\mathrm{c_P^{ex}} = 20.786/(mN_{\mathrm{A}}) \approx 520.3264\ \ \mathrm{J/(kg \cdot K)}\ \ \forall\ 100\ \mathrm{K} \leq \mathrm{T} \leq 6000\ \mathrm{K} \tag{123}$$

Where the theoretical prediction is once again $\mathrm{c_P^{th}} = 5R/2$, which is almost identical to the results obtained from experiment over an extremely large temperature range at $\mathrm{P} = 1\ \mathrm{bar} = 100\ \mathrm{kPa}$. As we know, Earth's atmosphere is composed mainly of molecular nitrogen $\mathrm{N_2}$ (~78%) and molecular oxygen $\mathrm{O_2}$ (~21%). These chemical species are diatomic molecules whose specific heat coefficients, at minimum, vary as a function of temperature. The treatment for such scenarios will be prescribed within ch.3.5.

3.4 Application to Inviscid Adiabatic Continuum Transport

Since $\varepsilon \equiv \frac{3}{2}\upsilon\mathrm{P}$, the distribution (105) will now take the following form:

$$\hat{\rho}(\boldsymbol{\xi}; \mathbf{v}|\upsilon\mathrm{P}) = \frac{\rho}{(2\pi\upsilon\mathrm{P})^{3/2}} \exp\left[-\frac{\rho}{2\mathrm{P}}(\boldsymbol{\xi} - \mathbf{v})^{\intercal} \cdot (\boldsymbol{\xi} - \mathbf{v})\right] \tag{124}$$

Even though the ideal gas pressure relation will be used throughout this work, (124) shows a more generalized model where any equation of state (EOS) for the pressure may be used. The zeroth order moment is once again $\vec{\rho} = \rho$ and the first to third order raw moments are provided below; being the momentum density vector, momentum density flux or energy density (rank 2) tensor, and energy density flux (rank 3) tensor respectively:

$$\vec{\rho}[\xi_i] = \rho \mathrm{v}_i \tag{125}$$

$$\vec{\rho}[\xi_i \xi_j] = \rho \mathrm{v}_i \mathrm{v}_j + \mathrm{P}\delta_{ij} \tag{126}$$

$$\vec{\rho}[\xi_i \xi_j \xi_k] = \rho \mathrm{v}_i \mathrm{v}_j \mathrm{v}_k + \mathrm{P}(\mathrm{v}_i \delta_{jk} + \mathrm{v}_j \delta_{ik} + \mathrm{v}_k \delta_{ij}) \tag{127}$$

The total stress tensor is defined from the second order central moment: $\vec{\rho}[\dot{q}_i \dot{q}_j] \equiv \mathrm{P}\delta_{ij} - \sigma_{ij}$, where σ_{ij} is the viscous stress tensor. Additionally, the heat flux vector is defined from the third order central moment: $\mathrm{q}_i \equiv \frac{1}{2}\vec{\rho}[\dot{q}_l \dot{q}_l \dot{q}_i]$. Using the previously derived equilibrium distribution (124), the hydrostatic pressure tensor is recovered as $\vec{\rho}[\dot{q}_i \dot{q}_j] = \mathrm{P}\delta_{ij}$ and the heat flux computes to zero: $\frac{1}{2}\vec{\rho}[\dot{q}_l \dot{q}_l \dot{q}_i] = 0$. To note, all odd order central moments of the Gaussian compute to zero,

[7] https://physics.nist.gov/cgi-bin/cuu/Value?k|search_for=Boltzmann

whether isotropic or the more general anisotropic form, whose off-diagonal covariance matrix components are non-zero entries. From (124), the momentum density velocity distribution will be defined simply as $\hat{\mathbf{p}} = \hat{\rho}\boldsymbol{\xi}$, whose associated "kinetic" energy distribution is $\widehat{\mathrm{K}} = \frac{1}{2}\hat{\upsilon}|\hat{\mathbf{p}}|^2 = \frac{1}{2}\hat{\rho}|\boldsymbol{\xi}|^2$. The resulting energy density and energy density flux vector is computed from the following two moments respectively:

$$\overrightarrow{\mathrm{K}} = \rho(\varrho + \varepsilon_{\mathrm{tr}}) \tag{128}$$

$$\overrightarrow{\mathrm{K}}[\xi_i] = \rho(\varrho + \varepsilon_{\mathrm{tr}} + \upsilon\mathrm{P})\mathrm{v}_i \tag{129}$$

Where the kinetic energy is denoted $\varrho = \frac{1}{2}|\mathbf{v}|^2$ and the translational internal energy is $\varepsilon_{\mathrm{tr}} = \frac{3}{2}\Theta$, given $\upsilon\mathrm{P} = \Theta$. Molecules such as N_2 and O_2 may also posses rotational, vibrational, and (but not limited to) electronic energies. This concept will be explained in more detail within ch.3.5 where the total energy density distribution will be derived. The form to be used within the QVFEM is provided as:

$$\hat{\upsilon}\hat{\mathrm{E}} = \tfrac{1}{2}|\boldsymbol{\xi}|^2 + \overline{\varepsilon} \tag{130}$$

Where $\overline{\varepsilon} \equiv \varepsilon_{\mathrm{ro}} + \varepsilon_{\mathrm{vi}} + \varepsilon_{\mathrm{el}}$ is the non-translational internal energy contribution. It will be found in Part II that this scalar quantity gives rise to the coefficient of dilatational viscosity. These concepts will be discussed in more detail when considering viscous interactions and thermal conductivity. Moving forwards, the zeroth and first order moments of (130) are computed as:

$$\overrightarrow{\mathrm{E}} = \rho e \tag{131}$$

$$\overrightarrow{\mathrm{E}}[\xi_i] = (\rho e + \mathrm{P})\mathrm{v}_i \tag{132}$$

Where the total energy is denoted $e = \varrho + \varepsilon$ and the total internal energy is the sum of the translational and non-translational contributions: $\varepsilon = \varepsilon_{\mathrm{tr}} + \overline{\varepsilon}$. The Reynolds transport theorem will next provide the following continuum equations of motion showing the balance of mass, momentum, energy, and entropy respectively; see [45; p.113] and [46; p.139]:

$$\frac{\partial\vec{\rho}}{\partial t} = -\frac{\partial\vec{\rho}[\xi_i]}{\partial \mathrm{x}_i}, \qquad \frac{\partial\vec{\mathrm{p}}_i}{\partial t} = -\frac{\partial\vec{\mathrm{p}}_i[\xi_l]}{\partial \mathrm{x}_l} \tag{133}$$

$$\frac{\partial\overrightarrow{\mathrm{E}}}{\partial t} = -\frac{\partial\overrightarrow{\mathrm{E}}[\xi_i]}{\partial \mathrm{x}_i}, \qquad \frac{\partial\vec{\mathrm{S}}}{\partial t} = -\frac{\partial\vec{\mathrm{S}}[\xi_i]}{\partial \mathrm{x}_i} \tag{134}$$

From (108), it has already been established that the entropy density distribution is $\hat{\mathrm{S}} \equiv -R\hat{\rho}\ln\hat{\rho}$. Since we are considering an isentropic process, the entropy abides the same balance principle as that for mass, momentum, and energy. This will however not be the case in Part II where the entropy will be found in a state of imbalance governed by the second axiom of thermodynamics: nonnegative production of entropy [45; ch.27]. It is found that (133) and (134) reproduce the Euler equations:

$$\frac{\partial\rho}{\partial t} = -\frac{\partial\rho\mathrm{v}_i}{\partial \mathrm{x}_i}, \qquad \frac{\partial\rho\mathrm{v}_i}{\partial t} + \frac{\partial\rho\mathrm{v}_i\mathrm{v}_l}{\partial \mathrm{x}_l} = -\frac{\partial\mathrm{P}}{\partial \mathrm{x}_i} \tag{135}$$

$$\frac{\partial \rho e}{\partial t}+\frac{\partial \rho e \mathrm{v}_i}{\partial \mathrm{x}_i}=-\frac{\partial \mathrm{P} \mathrm{v}_i}{\partial \mathrm{x}_i}, \qquad \frac{\partial \rho \mathrm{s}}{\partial t}=-\frac{\partial \rho \mathrm{s} \mathrm{v}_i}{\partial \mathrm{x}_i} \tag{136}$$

Using the mapping derivative (MD) operator in (81), the evolutions of the mass density, velocity, and internal energy fields may be expressed in the following manner respectively:

$$\mathrm{d}\rho/\mathrm{d}t=\rho\dot{\epsilon}, \qquad \mathrm{d}\mathbf{v}/\mathrm{d}t=\boldsymbol{a}, \qquad \mathrm{d}\varepsilon/\mathrm{d}t=\upsilon \mathrm{P}\dot{\epsilon} \tag{137}$$

Where $\dot{\epsilon}=-\boldsymbol{\nabla}\cdot\mathbf{v}$ and the acceleration is $\boldsymbol{a}=-\upsilon\boldsymbol{\nabla}\mathrm{P}$. It will also be noted that $\mathrm{d}\mathrm{s}/\mathrm{d}t=0$ which again resembles an isentropic process. As a result, the entropy is said to be maximized since the entropy production is zero. Additionally, the MD of the kinetic energy is given by $\mathrm{d}\varrho/\mathrm{d}t=\boldsymbol{a}\cdot\mathbf{v}$. Upon isolating $\dot{\epsilon}$ from the MD of the mass density, then feeding this expression into the MD of the internal energy, while converting ρ to υ, recovers the Gibbs relation: $\mathrm{d}\varepsilon=-\mathrm{P}\mathrm{d}\upsilon$, where $\mathrm{d}\mathrm{s}=0$. The enthalpy total differential is then $\mathrm{d}h=\upsilon\mathrm{d}\mathrm{P}$. A direct connection between the transport equations found in (135) and (136) and the Gibbs relation (GR) has now been uncovered. This is a pinnacle result since the GR was found to be a direct consequence of the fundamental relation (108) derived from the distribution (105). The derivation process is summarized in Figure 9.

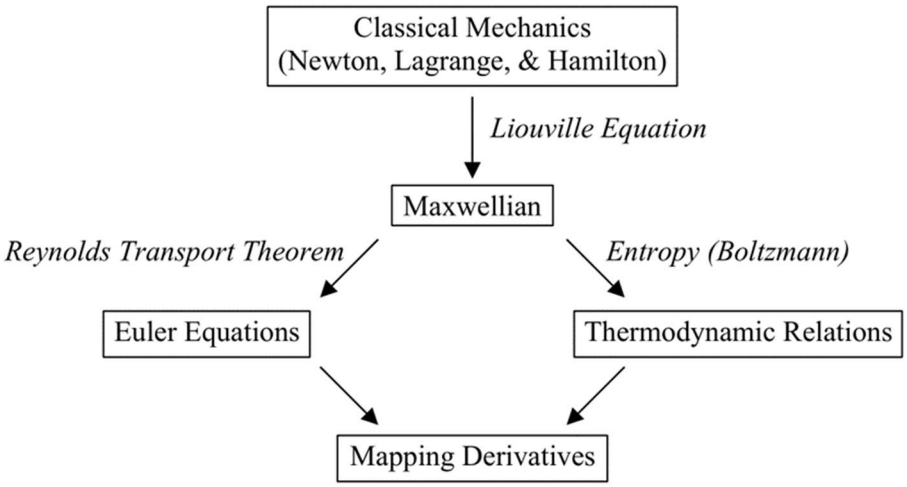

Figure 9 Derivation flow chart

Equations of state will next need to be chosen where there is much flexibility. For the time being, the perfect gas model (monatomic or diatomic) will be chosen so that $\mathrm{P}=\rho\Theta$, $\varepsilon=\mathrm{c}_{\upsilon}\mathrm{T}$, and $h=\mathrm{c}_{\mathrm{P}}\mathrm{T}$ where the specific heat coefficients are constants and independent of temperature. As a result, the mapping derivatives of the temperature and pressure fields are respectively:

$$\mathrm{d}\mathrm{T}/\mathrm{d}t=(\gamma-1)\mathrm{T}\dot{\epsilon}, \qquad \mathrm{d}\mathrm{P}/\mathrm{d}t=\gamma\mathrm{P}\dot{\epsilon} \tag{138}$$

Since $\mathrm{d}\mathrm{P}=\gamma\mathrm{P}\dot{\epsilon}\mathrm{d}t$ and $\mathrm{d}\rho=\rho\dot{\epsilon}\mathrm{d}t$, then the isentropic speed of sound (squared) remains $\mathbb{c}^2=\mathrm{d}\mathrm{P}/\mathrm{d}\rho=\gamma\Theta$. The MD of the enthalpy may now be written as $\mathrm{d}h/\mathrm{d}t=\mathbb{c}^2\dot{\epsilon}$. Referring back to the total energy density distribution (130), it is found that $\overline{\varepsilon}=(\mathrm{c}_{\upsilon}-\frac{3}{2}R)\mathrm{T}$. Upon setting $\overline{\varepsilon}=\varsigma\Theta$, then $\varsigma=(\gamma-1)^{-1}-3/2$; thus concluding the perfect gas model.

The attention will now turn to solving the Euler equations (135) and (136), which may be written in the generalized form:

$$\frac{\partial}{\partial t}\int_{\mathbb{R}^3}\mathrm{F}\,d\Xi = -\frac{\partial}{\partial \mathrm{x}_i}\int_{\mathbb{R}^3}\xi_i\mathrm{F}\,d\Xi \tag{139}$$

Where F is the generalized distribution functional: $\mathrm{F}(\boldsymbol{\xi},\mathbf{x},t)\equiv\mathrm{F}[\boldsymbol{\xi},\rho(\mathbf{x},t),\mathbf{v}(\mathbf{x},t),\varepsilon(\mathbf{x},t)]$, which is inferred as a local Maxwellian [14; p.72]. Assuming the velocity $\boldsymbol{\xi}$ may be quantized into a set $\boldsymbol{\xi}^\alpha$, then the sum should expand to zero:

$$\left(\dot{\mathrm{F}}^1+\xi_i^1\nabla_i\mathrm{F}^1\right)+\left(\dot{\mathrm{F}}^2+\xi_i^2\nabla_i\mathrm{F}^2\right)+\cdots+\left(\dot{\mathrm{F}}^{\mathbb{m}^3}+\xi_i^{\mathbb{m}^3}\nabla_i\mathrm{F}^{\mathbb{m}^3}\right)=0 \tag{140}$$

Each $\mathrm{d}\mathrm{F}^\alpha/\mathrm{d}t$ may therefore be set equal to zero to satisfy the overall equality relation. As a result, we are using the principle of state superposition. For ease of notation, the superscript will be dropped. The objective is to now solve the freestream Boltzmann equation (FBE): $\dot{\mathrm{F}}=-\boldsymbol{\xi}\cdot\boldsymbol{\nabla}\mathrm{F}$. Before doing so, let us first recall the one-to-one coordinate mapping from (80). To apply the mapping derivative to the distribution, we will first convert $\mathrm{F}(\mathbf{x},t)\rightarrow\mathrm{F}[\boldsymbol{\varphi}(\mathbf{x}_\mathrm{o},t),t]$ so that the temporal derivative may be applied while holding $\mathbf{x}_\mathrm{o}$ fixed:

$$\mathrm{d}\mathrm{F}(\mathbf{x},t)/\mathrm{d}t=\dot{\mathrm{F}}(\mathbf{x},t)+\dot{\boldsymbol{\varphi}}(\mathbf{x}_\mathrm{o},t)\cdot\boldsymbol{\nabla}|_{\mathbf{x}_\mathrm{o}=\boldsymbol{\varphi}^{-1}(\mathbf{x},t)}\mathrm{F}(\mathbf{x},t) \tag{141}$$

Upon mapping back into the current configuration, the above operation is completed and the velocity field is once again given by $\boldsymbol{\xi}(\mathbf{x},t)=\dot{\boldsymbol{\varphi}}[\boldsymbol{\varphi}^{-1}(\mathbf{x},t),t]$. Integrating over time yields:

$$\mathbf{u}=\int_{t_\mathrm{o}}^{t}\boldsymbol{\xi}(\mathbf{x},t)\,\mathrm{d}t=\boldsymbol{\varphi}[\boldsymbol{\varphi}^{-1}(\mathbf{x},t),t]-\boldsymbol{\varphi}[\boldsymbol{\varphi}^{-1}(\mathbf{x},t_\mathrm{o}),t_\mathrm{o}]=\mathbf{x}-\mathbf{x}_\mathrm{o} \tag{142}$$

Where $\mathbf{u}$ is the displacement field, being the difference between the current and reference configurations. Again, the assumption is that $\boldsymbol{\xi}$ may be quantized into the set $\boldsymbol{\xi}^\alpha$ meaning the velocities are constant so each possible velocity state is independent of both space and time, per time step. We treat these velocities as occupational states which a portion of the mass, momentum, or energy density may occupy. These quantities, per state, are what change over the time step. In consequence, the molecular velocity field will be uniform and independent of time therefore $\mathbf{u}=\boldsymbol{\xi}(t-t_\mathrm{o})$ so that the motion or mapping is obtained as:

$$\mathbf{x}=\boldsymbol{\varphi}(\mathbf{x}_\mathrm{o},t)=\mathbf{x}_\mathrm{o}+\boldsymbol{\xi}(t-t_\mathrm{o})\ \leftrightarrow\ \mathbf{x}_\mathrm{o}=\boldsymbol{\varphi}^{-1}(\mathbf{x},t)=\mathbf{x}-\boldsymbol{\xi}(t-t_\mathrm{o}) \tag{143}$$

It will be remarked that the function $\boldsymbol{\varphi}$ maps the position $\mathbf{x}$ in reference to the stationary location $\mathbf{x}_\mathrm{o}$ over time, where $\mathbf{x}_\mathrm{o}$ is measured from an absolute frame of reference (Newtonian description). The inverse mapping places the observer with the motion so that it appears $\mathbf{x}_\mathrm{o}$ is in motion given by $\boldsymbol{\varphi}^{-1}$ (Eulerian description). As a result, the spatial coordinate $\mathbf{x}$ has become stationary due to the inverse mapping operation. Please see the one-dimensional motion plotted in Figure 10, given $\varphi(0,0)=\varphi^{-1}(0,0)$ and $\xi=\delta\ell/\delta t$. It is important to note that $\boldsymbol{\varphi}^{-1}$ is not a Galilean transformation (GT) [54; p.13]. If we set $\mathbf{x}_\mathrm{o}=\mathbf{0}$ and $t_\mathrm{o}=0$, then the GT is $\mathbf{x}'[\mathbf{x}(t),t]=\mathbf{x}(t)-\boldsymbol{\xi}t$, where $\mathbf{x}$ is

no longer stationary in comparison to (143). This is because the GT is applied to the Newtonian description, in contrary to the Eulerian. Here, the position $\mathbf{x}'$ is measured from a frame of reference traveling at a constant rate $\boldsymbol{\xi}$ while $\mathbf{x}$ is still measured from an absolute frame of reference. So if $\mathbf{x}(t) = \boldsymbol{\xi}t$, then $\mathbf{x}' = \mathbf{0}$ since the dynamic frame is traveling at the exact same rate as that of the measured position within the absolute frame of reference.

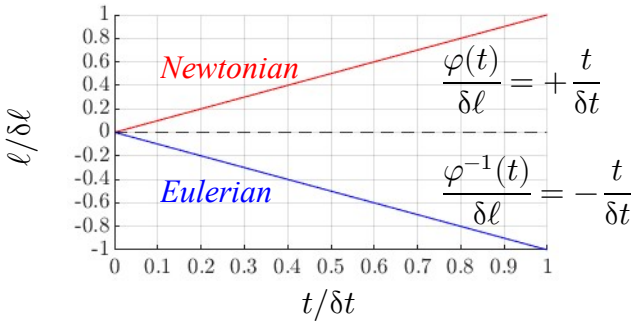

Figure 10 The Newtonian description[8] vs. the Eulerian description of motion

Upon setting $\mathrm{F}(\mathbf{x}, t) = \mathrm{G}[\boldsymbol{\varphi}^{-1}(\mathbf{x}, t)]$ and substituting into the FBE, one arrives at [19; p.530]:

$$\frac{\partial \mathrm{F}}{\partial t} = -\xi_i \frac{\partial \mathrm{F}}{\partial \mathrm{x}_i} = -\xi_i \frac{\partial \mathrm{G}}{\partial \varphi_i^{-1}} \tag{144}$$

Which proves to be a general solution to the FBE. As a result, any function of the form $\mathrm{G}(\mathbf{x}_\mathrm{o})$ subjected to the inverse mapping in (143), is an exact solution to (144). In conclusion, the (assumed) quantized Euler equations have theoretically been solved over a single time step. The temporally advanced distribution values are obtained from the prescribed motion under the condition $\boldsymbol{\xi}\delta t \leq \delta\mathbf{x}$, while holding the observables ρ, $\mathbf{v}$, and ε fixed:

$$\mathrm{F}(\mathbf{x} + \delta\mathbf{x}, t + \delta t) = \mathrm{G}[\boldsymbol{\varphi}^{-1}(\mathbf{x} + \delta\mathbf{x}, t + \delta t)] \tag{145}$$

The system quantities or observables represented by Σ are then theoretically updated through summing the distribution(s) over all possible velocity states at every location in space:

$$\Sigma(\mathbf{x}, t + \delta t) \equiv \mathrm{F}^1(\mathbf{x}, t + \delta t) + \mathrm{F}^2(\mathbf{x}, t + \delta t) + \cdots + \mathrm{F}^{\mathbb{m}^3}(\mathbf{x}, t + \delta t) \tag{146}$$

Since each $\mathrm{dF}^\alpha/\mathrm{d}t = 0$, the solution over each phasetime element is independent of all other elements. As a consequence, this type of finite element formulation does not require assembly of a global matrix nor inversion. To avoid any confusion, it will be noted that this methodology is not a Galerkin method because the residual is exactly zero therefore an integral formulation with the use of a weighting function is not necessary. The algorithm will then consist of time marching exact solutions to the FBE. The solution per element may be written in the usual form of a series expansion being $\mathrm{F}(\mathbf{x}, t) = \boldsymbol{f} \cdot \boldsymbol{g}[\boldsymbol{\varphi}^{-1}(\mathbf{x}, t)]$ where the vector $\boldsymbol{f}$ contains the nodal distribution

[8] In the literature [45,46], the language "Lagrangian description" is more commonly used in contrary to "Newtonian."

values and the vector $\boldsymbol{g}$ is the collection of basis functions. For simplicity, each element may be given its own local coordinate system where $\mathbb{c}_1 = f_1$ is the nodal value at position $\mathbf{x}_1 = \langle 0,0,0 \rangle$. Standard element shapes are a 2-node line element in 1D, a 4-node quadrilateral in 2D, and an 8-node hexahedron in 3D. The general solution in 3D Euclidean space is then:

$$\mathrm{F}(\mathbf{x},t) = \mathbb{c}_1 + (\mathbb{c}_2 x_\mathrm{o} + \mathbb{c}_3 y_\mathrm{o} + \mathbb{c}_4 x_\mathrm{o} y_\mathrm{o} + \mathbb{c}_5 z_\mathrm{o} + \mathbb{c}_6 x_\mathrm{o} z_\mathrm{o} + \mathbb{c}_7 y_\mathrm{o} z_\mathrm{o} + \mathbb{c}_8 x_\mathrm{o} y_\mathrm{o} z_\mathrm{o})|_{\mathbf{x}_\mathrm{o}=\boldsymbol{\varphi}^{-1}(\mathbf{x},t)} \quad (147)$$

At time $t = 0$, the basis functions must satisfy $g_a(\mathbf{x}_b) = \delta_{ab}$ where each $\mathbf{x}_b$ represents the coordinates of each node. Solutions and implementation procedures will be discussed in more detail when performing numerical tests. The generalized polynomial solution per phasetime element may also be written in the form:

$$\mathrm{F}(\mathbf{x},t) = f_1 + \sum_{i=1}^{I}\sum_{j=1}^{J}\sum_{k=1}^{K} \mathbb{C}_{ijk} x_\mathrm{o}^i y_\mathrm{o}^j z_\mathrm{o}^k|_{\mathbf{x}_\mathrm{o}=\boldsymbol{\varphi}^{-1}(\mathbf{x},t)} \quad (148)$$

Where $\mathbb{C}_{ijk}$ is the (rank 3) coefficient tensor. To note, these types of polynomial interpolation functions are constructed according to Pascal's triangle. Please see the Figure below for a phasetime element visualization (in blue):

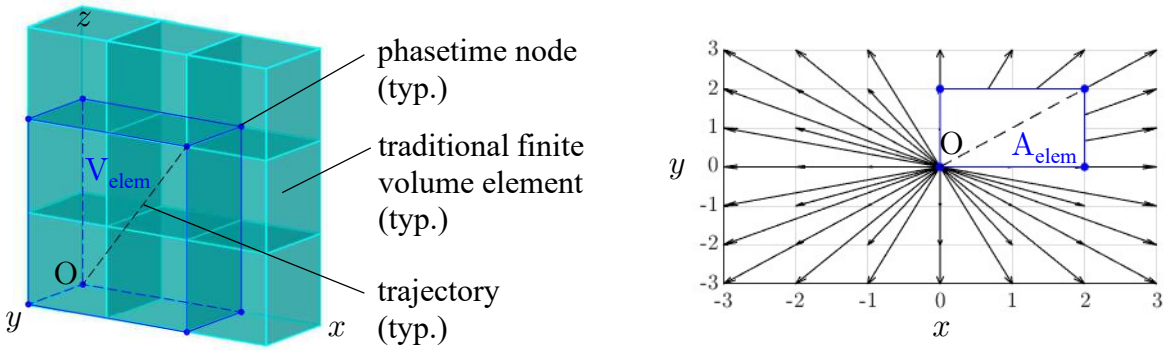

Figure 11 3D phasetime element (left) and 2D phasetime element (right)

If the element is nonuniform, the solutions proposed thus far are still valid. It is insightful however to unveil the general solutions when a coordinate transformation is applied. We will then map the set of points $\mathbf{x}$ into a uniform $\mathbf{y}$. The Jacobian matrix is then $\mathrm{J}_{il}(\mathbf{y}) = \partial \mathrm{x}_i / \partial \mathrm{y}_l$, whose inverse will be denoted $\Delta_{il} = \mathrm{J}_{il}^{-1}(\mathbf{y}) = (\partial \mathrm{y}_i / \partial \mathrm{x}_l)|_{\mathbf{x}\to\mathbf{y}}$. In consequence, the FBE (144) becomes:

$$\frac{\mathrm{dF}}{\mathrm{d}t} = \frac{\partial \mathrm{F}}{\partial t} + \xi_l \Delta_{il} \frac{\partial \mathrm{F}}{\partial \mathrm{y}_i} = 0 \quad (149)$$

One can now identify a new velocity vector as $\xi'_i = \xi_l \Delta_{il}$, so that $\dot{\mathrm{F}} = -\xi'_i \nabla'_i \mathrm{F}$, where the new gradient operator is denoted $\nabla'_i \mathrm{F} = \partial \mathrm{F} / \partial \mathrm{y}_i$. The general solution to (149) is simply the general solution to (144) mapped from $\mathbf{x}$ into $\mathbf{y}$: $\mathrm{F}(\mathbf{y},t) = \mathrm{G}[\boldsymbol{\varphi}^{-1}(\mathbf{x}(\mathbf{y}),t)]$. This elemental coordinate transformation is an alternative option when dealing with nonuniform nodal layouts. More will be discussed on this topic as we proceed further.

The attention will now shift to the inclusion of an applied forcefield, otherwise known as a body force: $\mathbf{b} \equiv \rho \boldsymbol{a}$ $(\mathrm{N}/\mathrm{m}^3)$. The acceleration is being redefined here so $\boldsymbol{a} \neq -\upsilon \boldsymbol{\nabla} \mathrm{P}$. To include this term into our model, the FBE will be rederived from a variational standpoint. One will observe that the variational procedure is analogous to the mapping derivative. The variational time will once again be defined as $t^* = t + \tau$, the position as $\mathbf{x}^* = \mathbf{x} + \boldsymbol{\xi}\tau$, and the velocity $\boldsymbol{\xi}^* = \boldsymbol{\xi} + \boldsymbol{a}\tau$ so that $\mathrm{F}^* = \mathrm{F}(\boldsymbol{\xi} + \boldsymbol{a}\tau, \mathbf{x} + \boldsymbol{\xi}\tau, t + \tau)$. The FBE with the inclusion of a body force may be found through applying the variational operation used in (95) to the perturbed distribution F^* so that:

$$\frac{\partial \mathrm{F}^*}{\partial \tau}\bigg|_{\tau=0} = \left(\frac{\partial \mathrm{F}^*}{\partial t^*}\frac{\partial t^*}{\partial \tau} + \frac{\partial \mathrm{F}^*}{\partial \mathrm{x}_i^*}\frac{\partial \mathrm{x}_i^*}{\partial \tau} + \frac{\partial \mathrm{F}^*}{\partial \xi_i^*}\frac{\partial \xi_i^*}{\partial \tau}\right)\bigg|_{\tau=0} = \frac{\partial \mathrm{F}}{\partial t} + \xi_i \frac{\partial \mathrm{F}}{\partial \mathrm{x}_i} + a_i \frac{\partial \mathrm{F}}{\partial \xi_i} \tag{150}$$

Which is an equivalent formulation of the total time derivative (64). Since $\dot{q}_i \hat{\rho} = -\Theta(\partial \hat{\rho}/\partial \xi_i)$ and using the fact that $\vec{\rho}[\dot{q}_i] = 0$, the mass transport equation is recovered from:

$$\int_{\mathbb{R}^3} \left(\frac{\partial \hat{\rho}}{\partial t} + \xi_i \frac{\partial \hat{\rho}}{\partial \mathrm{x}_i} - \frac{1}{\Theta} a_i \dot{q}_i \hat{\rho}\right) d\Xi = \frac{\partial \rho}{\partial t} + \frac{\partial \rho \mathrm{v}_i}{\partial \mathrm{x}_i} = 0 \tag{151}$$

From the mixed moments $\vec{\mathrm{p}}_i[\dot{q}_l] = \mathrm{P}\delta_{il}$ and $\vec{\mathrm{E}}[\dot{q}_i] = \mathrm{P}\mathrm{v}_i$, the body force appears as:

$$\int_{\mathbb{R}^3} \left(\frac{\partial \hat{\mathrm{p}}_i}{\partial t} + \xi_l \frac{\partial \hat{\mathrm{p}}_i}{\partial \mathrm{x}_l} - \frac{1}{\Theta} a_l \dot{q}_l \hat{\mathrm{p}}_i\right) d\Xi = \frac{\partial \rho \mathrm{v}_i}{\partial t} + \frac{\partial \rho \mathrm{v}_i \mathrm{v}_l}{\partial \mathrm{x}_l} + \frac{\partial \mathrm{P}}{\partial \mathrm{x}_i} - \rho a_i = 0 \tag{152}$$

$$\int_{\mathbb{R}^3} \left(\frac{\partial \hat{\mathrm{E}}}{\partial t} + \xi_i \frac{\partial \hat{\mathrm{E}}}{\partial \mathrm{x}_i} - \frac{1}{\Theta} a_i \dot{q}_i \hat{\mathrm{E}}\right) d\Xi = \frac{\partial \rho e}{\partial t} + \frac{\partial \rho e \mathrm{v}_i}{\partial \mathrm{x}_i} + \frac{\partial \mathrm{P}\mathrm{v}_i}{\partial \mathrm{x}_i} - \rho a_i \mathrm{v}_i = 0 \tag{153}$$

The general solution given $\boldsymbol{a}(t)$ will next be provided. The governing EOM is (150) set equal to zero, which from (151) will be restated as $\dot{\mathrm{F}} + \boldsymbol{\xi} \cdot \boldsymbol{\nabla} \mathrm{F} = (\beta \boldsymbol{a} \cdot \dot{\boldsymbol{q}})\mathrm{F}$. The total solution will next be decomposed as $\mathrm{F}(\mathbf{x}, t) = \mathrm{A}(\mathbf{x}, t)\mathrm{B}(t)$ where A is the solution in the absence of a body force therefore satisfies $\dot{\mathrm{A}} + \boldsymbol{\xi} \cdot \boldsymbol{\nabla} \mathrm{A} = 0$. Upon substituting the decomposition into the EOM, what remains is $\dot{\mathrm{B}} = (\beta \boldsymbol{a} \cdot \dot{\boldsymbol{q}})\mathrm{B}$. Holding $\mathbf{v}$ and T fixed until the end of the time step, the general solution is approximately:

$$\ln \mathrm{B}(t) \approx (\beta \dot{\boldsymbol{q}})|_{t_\circ} \cdot \int_{\delta t} \boldsymbol{a}(t)\, dt \tag{154}$$

To explore this matter further, we'll return to the Newtonian description so that the governing EOM reduces to:

$$\frac{\partial \mathrm{F}}{\partial t} + \boldsymbol{a} \cdot \frac{\partial \mathrm{F}}{\partial \boldsymbol{\xi}} = \dot{\mathrm{F}} - \beta \boldsymbol{a} \cdot \dot{\boldsymbol{q}}_\circ \mathrm{F} = 0 \tag{155}$$

Where the solution has been expressed as $\mathrm{F}(\boldsymbol{\xi}, t) = \mathrm{O}(\boldsymbol{\xi})\mathrm{B}(t)$ and β is held fixed. The initial condition will be set to the initial Maxwellian, i.e. $\mathrm{F}(\boldsymbol{\xi}, 0) = \mathrm{O}(\boldsymbol{\xi}) = (2\pi/\beta)^{-3/2} \exp(-\frac{1}{2}\beta |\dot{\boldsymbol{q}}_\circ|^2)$, where $\dot{\boldsymbol{q}}_\circ = \boldsymbol{\xi} - \mathbf{v}_\circ$. The remaining ODE is then $\dot{\mathrm{B}} = (\beta \boldsymbol{a} \cdot \dot{\boldsymbol{q}}_\circ)\mathrm{B}$, whose general solution without approximation is (154). If the total solution is renormalized over the velocity space, then the final

distribution becomes $\mathrm{F}[\boldsymbol{\xi};\mathbf{v}(t)]=\mathrm{M}[\boldsymbol{\xi};\mathbf{v}(t)]$. The mean velocity is usually found from solving $\dot{\mathbf{v}}=\boldsymbol{a}$ which may now be found from generating the first order moment over the velocity space:

$$\mathbf{v}(t)=\int_{\mathbb{R}^3}\boldsymbol{\xi}\mathrm{F}[\boldsymbol{\xi};\mathbf{v}(t)]\,d\Xi=\mathbf{v}_{\mathrm{o}}+\int_{\delta t}\boldsymbol{a}(t)\,dt \tag{156}$$

Additionally, Newton's 2nd axiom of motion, for this specific case, may be expressed in a form similar to (139):

$$\frac{\partial}{\partial t}\int_{\mathbb{R}^3}\boldsymbol{\xi}\mathrm{F}\,d\Xi=\beta\int_{\mathbb{R}^3}(\boldsymbol{a}\cdot\dot{\boldsymbol{q}})\boldsymbol{\xi}\mathrm{F}\,d\Xi \tag{157}$$

Returning to the Eulerian description, since $\dot{\mathbf{v}}+(\mathbf{v}\cdot\boldsymbol{\nabla})\mathbf{v}=\boldsymbol{a}-\upsilon\boldsymbol{\nabla}\mathrm{P}$, we could split the temporal derivative so that the solution for the velocity field will have two contributions; one from solving $\dot{\mathbf{v}}+(\mathbf{v}\cdot\boldsymbol{\nabla})\mathbf{v}=-\upsilon\boldsymbol{\nabla}\mathrm{P}$ and the other from $\dot{\mathbf{v}}=\boldsymbol{a}$.

As one can observe, extensions to the FBE can be made without causing a tremendous amount of difficulty to the user. Since exact solutions are known, the extensional solutions can usually be found as perturbations of the original solution. This concept will be exploited more in Part II when solving the Navier-Stokes-Fourier equations. To do so, we will now establish the framework.

We'll consider an EOM in a similar form to (65) and (66): $\dot{\mathrm{F}}+\boldsymbol{\xi}\cdot\boldsymbol{\nabla}\mathrm{F}=\mho$, where $\mho$ is analogous to the collision operator $\mathfrak{C}[\mathrm{F}]$. A version of Boltzmann's H-quantity will next be introduced as $\mathsf{H}(\mathrm{F})=\mathrm{F}\ln(\mathrm{F}/f_{\mathrm{o}})$, which will be expanded using a Taylor series about the initial value f_{o}:

$$\mathsf{H}(\mathrm{F})=(\mathrm{F}-f_{\mathrm{o}})+\frac{1}{2f_{\mathrm{o}}}(\mathrm{F}-f_{\mathrm{o}})^2+\mathcal{O}(\mathrm{F}-f_{\mathrm{o}})^3 \tag{158}$$

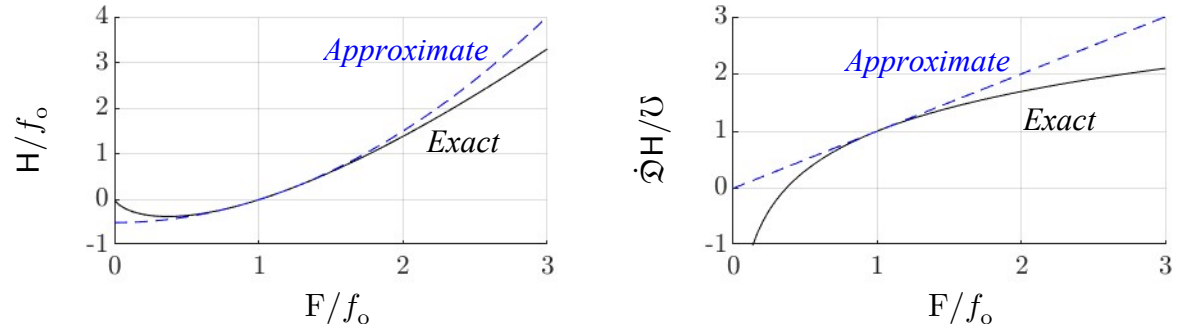

Figure 12 Boltzmann H-quantity vs. Taylor expanded form (left)
Variation in Boltzmann H-quantity vs. Taylor expanded form (right)

A variational principle will newly be established through first defining the perturbed distribution as $\mathrm{F}^*=\mathrm{F}+\mho\tau$. The first order variation in the H-quantity is then $\partial\mathsf{H}^*/\partial\tau|_{\tau=0}=(\mathrm{F}/f_{\mathrm{o}})\mho$, which for future reference will be denoted $\dot{\mathfrak{D}}\mathsf{H}$; see Figure 12. To force this quantity to zero, we'll first integrate over the effective volume, i.e. $\text{⧻}(t)=\prod_{i=1}^{3}\varphi_i(t)$, then integrate over the time step. Upon denoting the nondimensional weight function as $\phi=\mathrm{F}/f_{\mathrm{o}}$, the weak formulation is obtained as:

$$\int_0^{\delta t} \prod_{i=1}^{3} \int_0^{\varphi_i(t)} (\dot{\mathrm{F}} + \mathfrak{A}[\mathrm{F}])\phi \, d\mathrm{x}_i \, dt = \int_0^{\delta t} \prod_{i=1}^{3} \int_0^{\varphi_i(t)} \mho \phi \, d\mathrm{x}_i \, dt \tag{159}$$

To obtain a deeper insight, let us recall the FBE whose solution will be approximated in the form of a series expansion as $\mathrm{F}(\mathbf{x}, t) \approx f_i \psi_i(\mathbf{x}, t)$. We've now introduced a residual into the governing PDE therefore $\dot{\mathrm{F}} + \boldsymbol{\xi} \cdot \boldsymbol{\nabla} \mathrm{F} \neq 0$. As a result, the residual is identified as $\mho$. In an effort to diminish this quantity, we'll multiply the EOM my a vector of weight or test functions ϕ_j then perform the previous integration to obtain the following finite element formulation:

$$f_i \int_{\delta t} \int_{\forall(t)} (\dot{\psi}_i + \mathfrak{A}[\psi_i])\phi_j \, d\forall \, dt = \int_{\delta t} \int_{\forall(t)} \mho \phi_j \, d\forall \, dt \tag{160}$$

Which may be written in the more compact matrix form as $\mathrm{A}_{ji} f_i = \mathrm{b}_j$ or $\mathbf{A} \cdot \boldsymbol{f} = \mathbf{b}$. The Galerkin method will be utilized therefore the test functions will be set equal to the trial functions as derived in (159). If one desired a Petrov-Galerkin approach, the same derivation is performed however the perturbed distribution must be redefined as $\mathrm{F}^* = \mathrm{G} + \mho\tau$, which yields $\phi = \mathrm{G}/f_{\mathrm{o}}$. Within this overall framework, the phasetime elements will take on a similar form to the previous; see Figure 11. However, to obtain exact solutions, a "bow-and-arrow" approach will be implemented which utilizes lower order elements. In one spatial dimension though, the phasetime element is essentially the same, as shown in Figure 13:

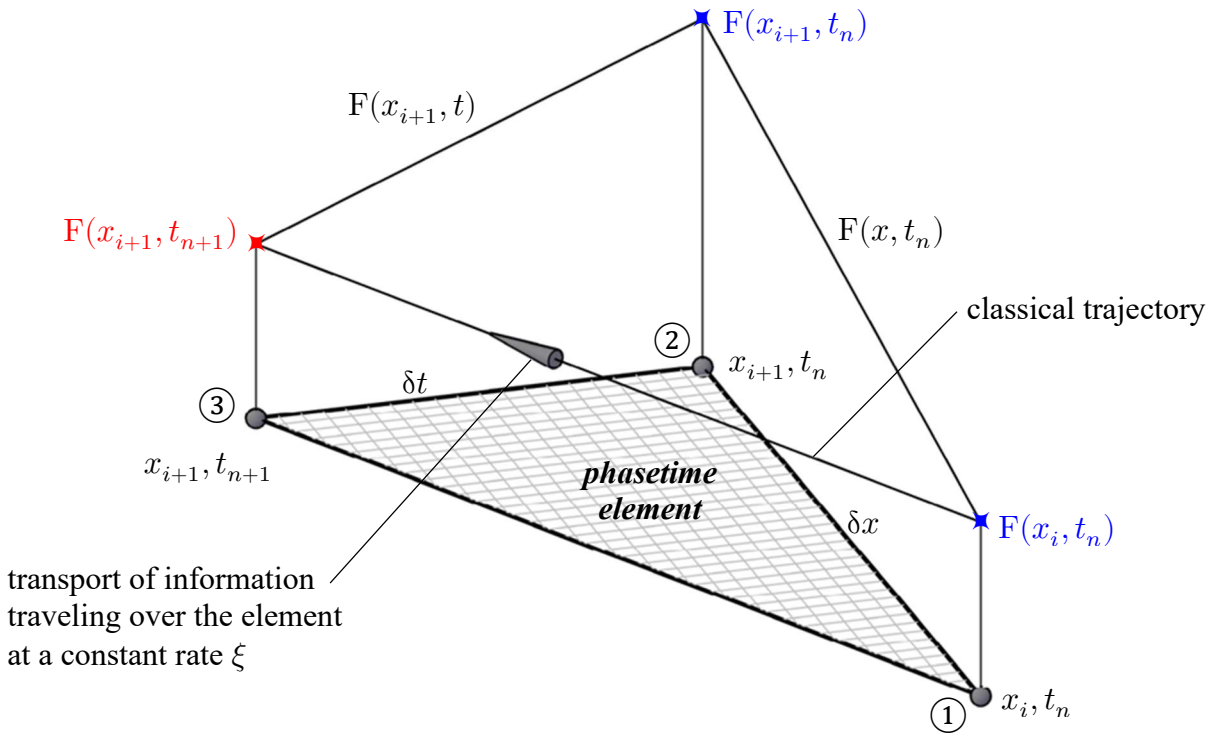

Figure 13 1D phasetime element

Where the nodal values in blue, i.e. $\mathrm{F}(x_i, t_n)$ and $\mathrm{F}(x_{i+1}, t_n)$, are known at the beginning of the

time step and the objective is to solve for the nodal value in red being $\mathrm{F}(x_{i+1}, t_{n+1})$. To accomplish this, we'll begin with first defining the basis functions, which in general, will be linear in both time and space:

$$\psi_i(\mathbf{x}, t) = \psi_i^{\circ} + \boldsymbol{k}_i \cdot \mathbf{x} + \omega_i t \tag{161}$$

Where ψ_i°, $\boldsymbol{k}_i$, and ω_i are constants determined from $\psi_a(\mathbf{x}, t)_b = \delta_{ab}$. The basis functions will then naturally satisfy $\sum_i \psi_i = 1$. In one spatial dimension, the matrix form of (160) is:

$$\begin{bmatrix} \mathrm{A}_{11} & \mathrm{A}_{12} & \mathrm{A}_{13} \\ \mathrm{A}_{21} & \mathrm{A}_{22} & \mathrm{A}_{23} \\ \mathrm{A}_{31} & \mathrm{A}_{32} & \mathrm{A}_{33} \end{bmatrix} \begin{bmatrix} f_1 \\ f_2 \\ f_3 \end{bmatrix} = \begin{bmatrix} \mathrm{b}_1 \\ \mathrm{b}_2 \\ \mathrm{b}_3 \end{bmatrix} \tag{162}$$

Where the nodal values in blue are known, the components in black are computed integrals, and the variables in red are the quantities to be solved for. Therefore, one must rearrange (162) into $\mathbf{A}' \cdot \boldsymbol{f}' = \mathbf{b}'$, where $\boldsymbol{f}' = \langle \mathrm{b}_1, \mathrm{b}_2, f_3 \rangle$. The residual $\mho$ will be held fixed and a local coordinate system will be utilized so that $\mathrm{b}_3 = \frac{1}{3}\xi\delta t^2 \mho$. Since $\det \mathbf{A}' = \frac{1}{3}\xi\delta t$, meaning $\mathbf{A}'$ is invertible, then $\boldsymbol{f}' = \mathbf{A}'^{-1} \cdot \mathbf{b}'$. The final step within this variational procedure is to set $\mho = 0$.

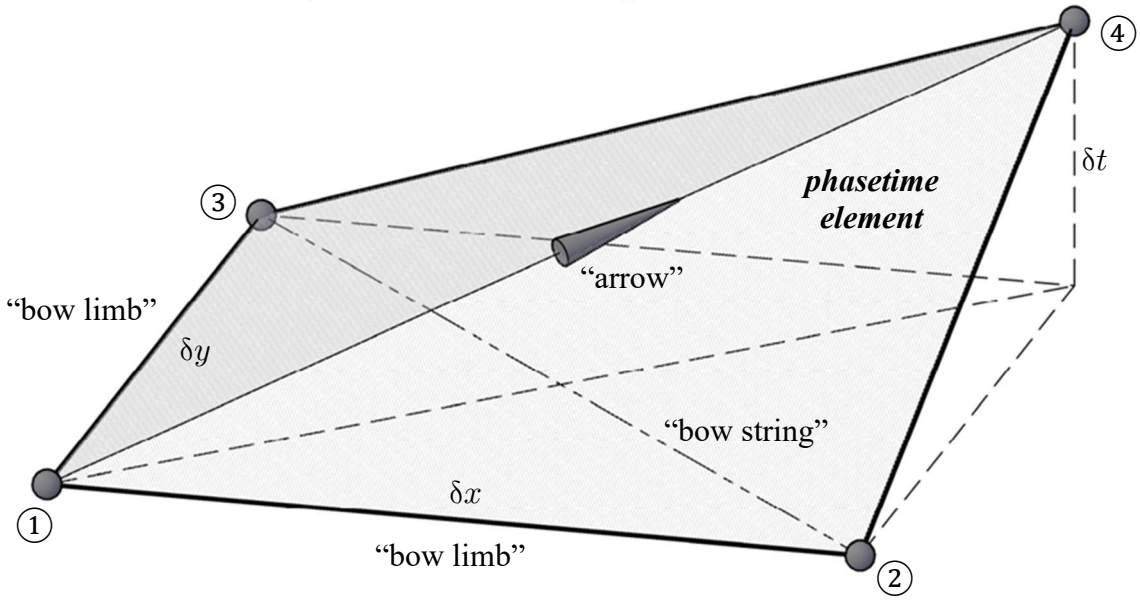

Figure 14 2D phasetime element (bow-and-arrow)

Using this methodology, exact solutions can be obtained in one, two, and three spatial dimensions. This class of solutions are found to be linear forms of (147):

$$\mathrm{F}(\mathbf{x}, t) = \mathfrak{c}_1 + (\mathfrak{c}_2 x_{\mathrm{o}} + \mathfrak{c}_3 y_{\mathrm{o}} + \mathfrak{c}_4 z_{\mathrm{o}})|_{\mathbf{x}_{\mathrm{o}} = \boldsymbol{\varphi}^{-1}(\mathbf{x}, t)} \tag{163}$$

In 2D, a "bow-and-arrow" is formed using four nodes, as shown in Figure 14. In 3D, a "three-pronged slingshot" is formed using five nodes, as shown in Figure 33. One might naturally wonder, should we choose the nonlinear solution (147) or the linear solution (163)? This question is left for future investigation. Before moving onwards, we'll make one last remark. If the governing

EOM is differentiated with respect to $\boldsymbol{\xi}$, then the linear solution (163) satisfies:

$$\frac{\partial}{\partial \xi_k}\left(\frac{\partial \mathrm{F}}{\partial t}\right)+\frac{\partial \mathrm{F}}{\partial \mathrm{x}_k}=\frac{\partial \mathfrak{V}}{\partial \xi_k}-\xi_i\frac{\partial}{\partial \xi_k}\left(\frac{\partial \mathrm{F}}{\partial \mathrm{x}_i}\right)=0 \tag{164}$$

Now that we've established solution procedures within the QVFEM, the requirement regarding nodal layout will next be discussed. My recommendation is to use a structured grid, however, there is no restriction for the grid to be uniform. If we generate an unstructured grid, the choice of nodes to include within each element becomes questionable. The main concern is ensuring proper conveyance of information. One way to generate the grid is to use the "patch-and-match" method. Overall, a uniform grid will be generated, patched into the domain, then fitted (or matched) into an arbitrary geometry. A simple example can be found in Figure 15.

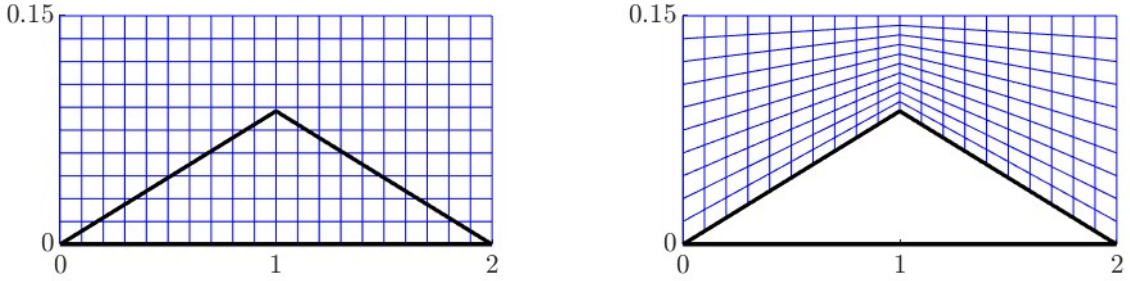

Figure 15 The method of patch (left) and match (right)

If the geometry is complex, then multiple regions can individually be patched and matched:

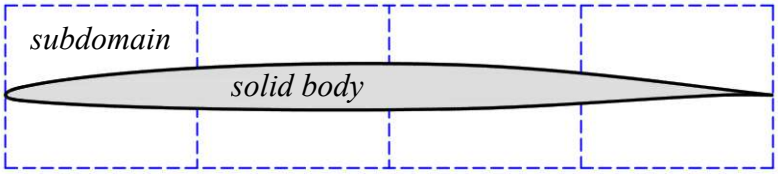

Figure 16 Subdomain example (NACA 66-206)

The next step is to transform $\boldsymbol{\xi}$ into $\boldsymbol{\xi}^{\alpha}$ via quantization so that the density functional $\hat{\rho}$ will be transformed into a discrete mass $\hat{\rho}^{\alpha}$. The same concept will apply to the momentum and energy density functionals. The quantization process will require its own theoretical framework which is established in ch.3.6.

3.5 Thermodynamic Extensions for a Diatomic Ideal Gas

Let us now introduce the total internal energy $\varepsilon=\varepsilon_{\mathrm{tr}}+\overline{\varepsilon}$ where $\overline{\varepsilon}\equiv\varepsilon_{\mathrm{ro}}+\varepsilon_{\mathrm{vi}}+\varepsilon_{\mathrm{el}}$ [50; ch.11]. The energy associated with the electrons (or electronic energy) is beyond the scope of this work however the rotational and vibrational energies will be treated herein. For monatomic molecules $\varepsilon=\varepsilon_{\mathrm{tr}}+\varepsilon_{\mathrm{el}}$ however diatomic molecules may occupy rotational and vibrational energy eigenstates. The translational and rotational energies will be treated classically however the

vibrational energies will need to be treated quantum mechanically. This reasoning is influenced by the work performed by Max Planck, who resolved the "ultraviolet catastrophe," and Albert Einstein's quantum theoretical model of a solid object [51]. Einstein's specific heat prediction proved to be much more accurate in comparison to classical statistical theory. To begin, we'll first review the calculation of the translational energy computed from the second order central moment:

$$\varepsilon_{\text{tr}} = \frac{1}{(2\pi\Theta)^{3/2}} \int_{\mathbb{R}^3} \frac{1}{2} \sum_{i=1}^{3} \dot{q}_i^2 \prod_{l=1}^{3} \exp(-\dot{q}_l^2/2\Theta)\, d\Xi = \frac{3}{2}\Theta \tag{165}$$

Diatomic molecules have two rotational degrees of freedom therefore:

$$\varepsilon_{\text{ro}} = \frac{\mathcal{J}}{2\pi k_{\text{B}}\mathrm{T}} \int_{\mathbb{R}^2} \frac{\mathcal{J}}{2m} \sum_{i=1}^{2} \dot{\theta}_i^2 \prod_{l=1}^{2} \exp\!\big(-\mathcal{J}\dot{\theta}_l^2/2k_{\text{B}}\mathrm{T}\big)\, d\Omega = \Theta \tag{166}$$

Where $\mathcal{J}\ (\mathrm{kg}\cdot\mathrm{m}^2)$ is the moment of inertia of the molecule and $\dot{\theta}\ (1/\mathrm{s})$ is the angular velocity. If $\varepsilon = \varepsilon_{\text{tr}} + \varepsilon_{\text{ro}}$ then $\varepsilon = 5\Theta/2$ and $h = 7\Theta/2$ for a diatomic molecule. Within the perfect gas model, the resulting specific heat coefficients compute to $\mathrm{c}_{\upsilon} = 5R/2$ and $\mathrm{c}_{\mathrm{P}} = 7R/2$ so the specific heat ratio is $\gamma = 7/5$. We'll next draw upon the study of quantum thermodynamics [52] where the vibrational energies will be shown to be quantized. To uncover these energy eigenstates, one must first analytically solve the stationary Schrödinger equation [16; ch.2]:

$$-\frac{\hbar^2}{2m} \sum_{l=1}^{3} \frac{\partial^2 \psi}{\partial \chi_l^2} + \Pi\psi = \mathrm{H}\psi \tag{167}$$

Lets envision two atoms of mass m_1 and m_2 bonded together forming a diatomic molecule. The bond will be modeled as a linear spring with spring constant κ. Restricting the motion to one direction, the position of the center of mass is then $q = (m_1 q_1 + m_2 q_2)/m$ where the total molecular mass is $m = m_1 + m_2$. Differentiating twice with respect to time yields $\dot{\mathrm{p}} = \dot{\mathrm{p}}_1 + \dot{\mathrm{p}}_2$. The EOM for each atom is $\dot{\mathrm{p}}_1 = +\kappa\chi$ and $\dot{\mathrm{p}}_2 = -\kappa\chi$ where $\chi = \ell - \ell_o$, $\ell = q_2 - q_1$, and $\ell_o = q_2^o - q_1^o$. Upon substituting we find that $\dot{\mathrm{p}} = 0$ due to the absence of external force. Since $\ddot{q}_1 = +\kappa\chi/m_1$ and $\ddot{q}_2 = -\kappa\chi/m_2$, then the difference between accelerations may be written as $\mu\ddot{\chi} = -\kappa\chi$ where the reduced mass is denoted $\mu = m_1 m_2/m$. Defining the characteristic vibrational frequency of the diatomic molecule as $\nu = \sqrt{\kappa/\mu}$, the general solution to the recently derived EOM is $\chi(t) = a\cos(\nu t) + b\sin(\nu t)$. The kinetic energy is next found as $\mathrm{K} = \mu \int \ddot{\chi}\, \mathrm{d}\chi = \frac{1}{2}\mu\dot{\chi}^2$ and the potential energy as $\Pi = \kappa \int \chi\, \mathrm{d}\chi = \frac{1}{2}\kappa\chi^2$ so the total energy is $\mathrm{E} = \frac{1}{2}\mu(\dot{\chi}^2 + \nu^2\chi^2)$. The momentum will be defined as $p = \mu\dot{\chi}$ so the Hamiltonian is $\mathrm{H} = \frac{1}{2}(p^2/\mu + \kappa\chi^2)$. We will now assume the molecule has wave properties so the fundamental wave function, which will be derived in the next section, is given as $\psi = \exp[i(p\chi - \mathrm{H}\tau)/\hbar]$. Differentiating with respect to the virtual time τ yields the following operator relation:

$$i\hbar \frac{\partial \psi}{\partial \tau} = \left(\frac{p^2}{2\mu} + \frac{1}{2}\kappa\chi^2\right)\psi \tag{168}$$

Upon holding H fixed, it may now be concluded that the governing differential equation is Schrödinger's model of the quantum harmonic oscillator for a diatomic molecule:

$$-\frac{\hbar^2}{2\mu}\frac{\partial^2\psi}{\partial\chi^2}+\frac{1}{2}\kappa\chi^2\psi=\mathcal{E}_{\text{vi}}\psi \tag{169}$$

It will be noted that the variable χ in this circumstance represents all possible variations from the equilibrium distance between the two atoms connected via a "spring" with spring constant κ. For molecules such as N_2 and O_2, the two bonded atoms are identical therefore $m_1=m_2$ so that $\mu=m/4$ where m is the total molecular mass. The analytical solution per state to the above governing equation is next provided as [16; p.41]:

$$\psi^{\alpha}(\chi)=\frac{1}{(2^{\alpha}\alpha!)^{1/2}}\mathcal{N}^{1/2}\mathcal{H}^{\alpha}\ \forall\ \alpha=0,1,2,... \tag{170}$$

Where $\mathcal{H}^{\alpha}$ is the collection of physicists's Hermite polynomials (in contrary to the probabilist's Hermite polynomials) generated from the distribution $\mathcal{N}(\chi)=(\mu\nu/\pi\hbar)^{1/2}\exp(-\mu\nu\chi^2/\hbar)$:

$$\mathcal{H}^{\alpha}(\chi)=\frac{(-1)^{\alpha}}{\mathcal{N}(\chi)}\frac{\partial^{\alpha}\mathcal{N}(\chi)}{\partial\chi^{\alpha}} \tag{171}$$

To note, the backwards Taylor series expansion of $\mathcal{N}$ may be written in terms of Hermite polynomials thus providing the derivation of the generating formula shown above:

$$\frac{\mathcal{N}(\chi-y)}{\mathcal{N}(\chi)}=\sum_{\alpha=0}^{\infty}\frac{(-y)^{\alpha}}{\alpha!\,\mathcal{N}}\frac{\partial^{\alpha}\mathcal{N}}{\partial\chi^{\alpha}}=\sum_{\alpha=0}^{\infty}\frac{y^{\alpha}}{\alpha!}\mathcal{H}^{\alpha} \tag{172}$$

Most importantly, the associated quantized vibrational energies are $\mathcal{E}_{\text{vi}}^{\alpha}=\hbar\nu(\alpha+1/2)$. Lets recall that (165) and (166) utilized unique probability density functions (PDF) to compute the mean translational and rotational energies respectively. Since the vibrational energies are quantized, it is now necessary to construct a probability mass function (PMF). The vibrational partition function will be evaluated through identifying a geometric series of $\exp(-\nu/\omega)^{\alpha}$ where the general formula is $\sum_{\alpha=0}^{\infty}f^{\alpha}=\frac{1}{1-f}\ \forall\ |f|<1$ and $\omega=k_{\text{B}}\text{T}/\hbar$:

$$\zeta_{\text{vi}}=\sum_{\alpha=0}^{\infty}\exp(-\mathcal{E}_{\text{vi}}^{\alpha}/k_{\text{B}}\text{T})=\frac{\exp(-\nu/2\omega)}{1-\exp(-\nu/\omega)} \tag{173}$$

The mean vibrational energy is next computed from the second order moment of the recently established PMF using the fact that $\sum_{\alpha=0}^{\infty}\alpha f^{\alpha}=\frac{f}{(1-f)^2}\ \forall\ |f|<1$:

$$\mathcal{E}_{\text{vi}}=\frac{1}{\zeta_{\text{vi}}}\sum_{\alpha=0}^{\infty}\exp(-\mathcal{E}_{\text{vi}}^{\alpha}/k_{\text{B}}\text{T})\,\mathcal{E}_{\text{vi}}^{\alpha}=\frac{\hbar\nu}{\exp(\nu/\omega)-1}+\mathcal{E}_{\text{vi}}^{0} \tag{174}$$

Where the ground state energy is $\mathcal{E}_{\text{vi}}^0 = \hbar\nu/2$. Defining $\mathcal{E}_{\text{vi}} = m\varepsilon_{\text{vi}}$, the total specific internal energy of a diatomic molecule (excluding $\varepsilon_{\text{vi}}^0$ and ε_{el}) takes the form:

$$\varepsilon = \frac{5}{2}\Theta + \frac{\hbar\nu}{\exp(\nu/\omega) - 1} \tag{175}$$

Where $\hbar = \hbar/m$ and $\varepsilon_{\text{vi}}^{\alpha} = \hbar\nu(\alpha + 1/2)$ so that $\varepsilon_{\text{vi}}^0 = \hbar\nu/2$. The specific heat coefficient at constant volume may next be computed from $\mathrm{c}_{\upsilon} = \partial\varepsilon/\partial\mathrm{T}$. Denoting $\eta_{\text{vi}} = \nu/\omega$, one finds:

$$\frac{\mathrm{c}_{\upsilon}}{R} = \frac{5}{2} + \frac{\eta_{\text{vi}}^2 \exp\eta_{\text{vi}}}{(\exp\eta_{\text{vi}} - 1)^2} \tag{176}$$

It is important to note that c_{υ} is now a (nonlinear) function of temperature. The characteristic vibrational frequency must be treated with special care otherwise the above expression becomes unstable. Upon defining $\Theta_{\text{vi}} = R\mathrm{T}_{\text{vi}}$, where T_{vi} is a characteristic vibrational temperature, we'll set $\nu = \Theta_{\text{vi}}/\hbar$ so that $\eta_{\text{vi}} = \mathrm{T}_{\text{vi}}/\mathrm{T}$. To compare the above result with experiment, c_{P} data is taken from JANAF for N_2 and O_2 over the temperature range $100\ \mathrm{K} \leq \mathrm{T} \leq 2000\ \mathrm{K}$ at $\mathrm{P} = 1\ \mathrm{bar}$. What is plotted in Figure 17 is the theoretical curve $\mathrm{c}_{\mathrm{P}} = \mathrm{c}_{\upsilon} + R$ and the dashed line identifies $7R/2$. It was found that the theoretical prediction for N_2 agrees fairly well up until ~2000 K while the prediction for O_2 begins to deviate around ~1250 K. To best-fit the data, I set $\mathrm{T}_{\text{vi}}(\mathrm{N}_2) = 3250\ \mathrm{K}$ and $\mathrm{T}_{\text{vi}}(\mathrm{O}_2) = 2150\ \mathrm{K}$ so the frequencies are computed as $\nu(\mathrm{N}_2) \approx 4.255 \cdot 10^{14}\ \mathrm{s}^{-1}$ and $\nu(\mathrm{O}_2) \approx 2.815 \cdot 10^{14}\ \mathrm{s}^{-1}$.

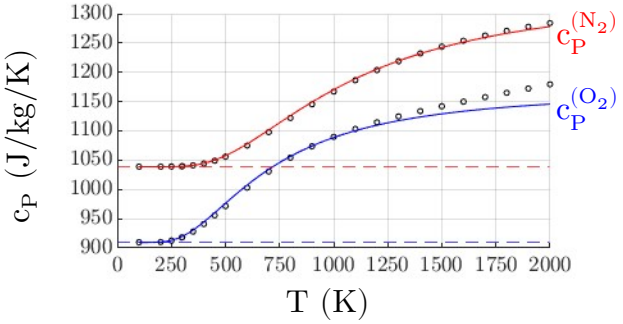

Figure 17 Specific heat coefficient predictions for N_2 and O_2

To extend the range of validity up to 6000 K, a three-term pseudo mean electronic energy will be introduced as:

$$\varepsilon_{\text{el}} \approx \frac{g_1\varepsilon_1 \exp(-\varepsilon_1/\Theta) + g_2\varepsilon_2 \exp(-\varepsilon_2/\Theta)}{1 + g_1 \exp(-\varepsilon_1/\Theta) + g_2 \exp(-\varepsilon_2/\Theta)} \tag{177}$$

Where g_1 and g_2 are the pseudo degeneracies acting as statistical weights and the pseudo electronic energies are denoted ε_1 and ε_2, in addition to the ground state $\varepsilon_0 = 0$. In a similar manner to the vibrational frequency, these energies will be defined in terms of characteristic temperatures so that $\varepsilon_1 = R\mathrm{T}_1$ and $\varepsilon_2 = R\mathrm{T}_2$. Upon defining $\eta_1 = -\mathrm{T}_1/\mathrm{T}$ and $\eta_2 = -\mathrm{T}_2/\mathrm{T}$, the total specific internal energy is:

$$\varepsilon = \frac{5}{2}\Theta + \frac{\Theta_{\text{vi}}}{\exp\eta_{\text{vi}} - 1} + \frac{g_1\Theta_1 \exp\eta_1 + g_2\Theta_2 \exp\eta_2}{1 + g_1 \exp\eta_1 + g_2 \exp\eta_2} \tag{178}$$

The resulting expression for the specific heat coefficient at constant volume is then:

$$\frac{c_v}{R} = \frac{5}{2} + \frac{\eta_{\text{vi}}^2 \exp\eta_{\text{vi}}}{(\exp\eta_{\text{vi}} - 1)^2} + \frac{g_1\eta_1^2 \exp\eta_1 + g_2\eta_2^2 \exp\eta_2 + g_1 g_2(\eta_2 - \eta_1)^2 \exp(\eta_1 + \eta_2)}{(1 + g_1 \exp\eta_1 + g_2 \exp\eta_2)^2} \tag{179}$$

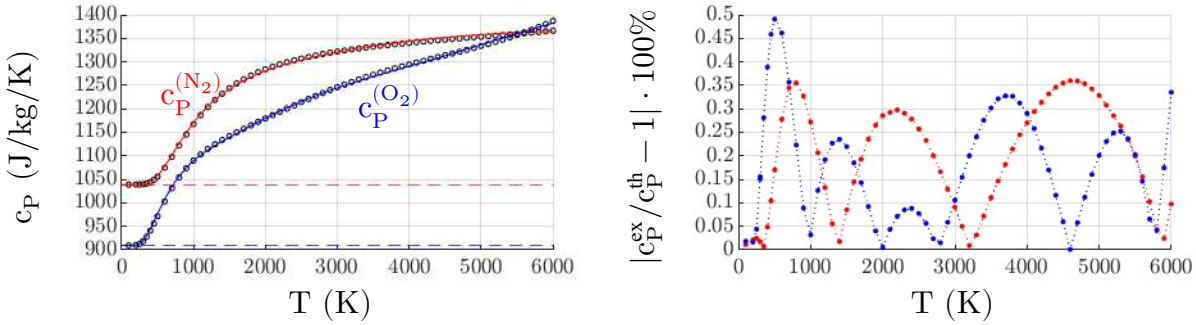

Figure 18 Specific heat coefficient curve fitting for N_2 and O_2

The new results are plotted in Figure 18. It was found that for N_2, the third term in the electronic energy summation was not required. Using the curve fitting parameters provided in Table 1, the maximum percent error for N_2 is ~0.36% and for O_2, ~0.49%. The characteristic temperatures and degeneracies were found using the method of trial and error. To put this temperature range into perspective, it will be noted that on the lower end, the JANAF enthalpy reference temperature is 298.15 K = 77° F; which approximately resembles the temperature of an average day at sea level in the US. On the higher end, the effective temperature of the Sun is ~5772 K ≈ 9930° F. In conclusion, a large temperature range (100 K ≤ T ≤ 6000 K) has successfully been captured while converting the perfect gas model into an ideal gas model. As a result, the specific heat coefficients have become dependent upon temperature for the chemical species N_2 and O_2. The curve fitting parameters can be found in the table below:

	T_{vi}	T_1	T_2	g_1	g_2
N_2	3,250 K	15,000 K	NA	1/4	NA
O_2	2,150 K	10,500 K	31,500 K	10/11	48/11

Table 1 Curve fitting parameters for $c_P(T)$

The incorporation of the rotational, vibrational, and electronic energies into the QVFEM will now be discussed. In reference to the stationary solution (98), the total energy $m\mathcal{E}$ is now:

$$m\mathcal{E}_{\alpha\beta}(\dot{\boldsymbol{q}}, \dot{\boldsymbol{\theta}}) = \tfrac{1}{2}\left(m|\dot{\boldsymbol{q}}|^2 + \mathcal{J}|\dot{\boldsymbol{\theta}}|^2\right) + k_{\text{B}}\left(T_{\text{vi}}\alpha + T_\beta^{\text{el}}\right) \tag{180}$$

Since each type of energy is independent of one another, the total distribution may be decomposed into individual distributions all multiplied together due to the independence of states. Upon

defining the total partition function as $\zeta = \zeta_{\text{tr}}\zeta_{\text{ro}}\zeta_{\text{vi}}\zeta_{\text{el}}$ and recalling $\beta = 1/\Theta$, the associated total energy density distribution is, by definition:

$$\hat{\mathrm{E}} \equiv \rho\zeta^{-1}\exp\left[-\mathcal{E}_{\alpha\beta}(\dot{\boldsymbol{q}},\dot{\boldsymbol{\theta}})/\Theta\right]\left(\tfrac{1}{2}|\boldsymbol{\xi}|^2 + \tfrac{\mathcal{J}}{2m}|\dot{\boldsymbol{\theta}}|^2 + \Theta_{\text{vi}}\alpha + g_\beta\Theta_\beta^{\text{el}}\right) \tag{181}$$

Where $\zeta_{\text{tr}} = (2\pi\Theta)^{3/2}$, $\zeta_{\text{ro}} = 2\pi k_{\text{B}}\mathrm{T}\mathcal{J}^{-1}$, $\zeta_{\text{vi}} = (1-\exp(-\eta_{\text{vi}}))^{-1}$, and $\zeta_{\text{el}} = 1 + g_1\exp\eta_1 + g_2\exp\eta_2$. It will be noted that the ground state vibrational energy is neglected due to physical insignificance. Upon integrating over all possible rotational rates $\dot{\boldsymbol{\theta}}\ \forall\ \Omega \in \mathbb{R}^2$ (2 DOF) and summing over all possible vibrational and electronic energy eigenstates, the above simplifies to:

$$\hat{\upsilon}\hat{\mathrm{E}} = \frac{1}{2}|\boldsymbol{\xi}|^2 + \Theta + \frac{\Theta_{\text{vi}}}{\exp\eta_{\text{vi}} - 1} + \frac{g_1\Theta_1\exp\eta_1 + g_2\Theta_2\exp\eta_2}{1 + g_1\exp\eta_1 + g_2\exp\eta_2} \tag{182}$$

The non-translational internal energy is identified as $\overline{\varepsilon} = (\varepsilon_{\text{ro}} - \varepsilon_{\text{ro}}^0) + (\varepsilon_{\text{vi}} - \varepsilon_{\text{vi}}^0) + (\varepsilon_{\text{el}} - \varepsilon_{\text{el}}^0)$. The general expression for the MD of the temperature field may be found from (137) as $\mathrm{dT}/\mathrm{d}t = \mathrm{c}_{\upsilon}^{-1}\Theta\dot{\epsilon}$. The MD of the pressure remains $\mathrm{dP}/\mathrm{d}t = \gamma\mathrm{P}\dot{\epsilon}$. However c_{υ}, c_{P}, and γ are all dependent upon the temperature. The same concept applies to the isentropic speed of sound ($\mathbb{c}^2 = \gamma\Theta$) and the MD of the enthalpy ($\mathrm{d}h/\mathrm{d}t = \mathbb{c}^2\dot{\epsilon}$). It is important to note that within the ideal gas model $\overline{\varepsilon} \neq \varsigma\Theta$ in contrary to the perfect gas model since the internal energy is no longer a linear function of temperature. In a similar manner to the development of (182), the total entropy density distribution will be defined in the following way:

$$\hat{\upsilon}\hat{\mathrm{S}} = R\ln\upsilon\zeta + \mathrm{T}^{-1}(\tfrac{1}{2}|\dot{\boldsymbol{q}}|^2 + \overline{\varepsilon}) \tag{183}$$

The mean entropy value is then $\mathrm{s} = R\ln\upsilon\zeta + \varepsilon/\mathrm{T}$ and the advective flux is $\vec{\mathrm{S}}[\xi_i] = \rho\mathrm{s}\mathrm{v}_i$. These results are found through using the following mixed moments:

$$\upsilon\vec{\rho}[\xi_i\dot{q}_j] = \Theta\delta_{ij}, \quad \upsilon\vec{\rho}[\xi_i\dot{q}_j\dot{q}_k] = \Theta\mathrm{v}_i\delta_{jk}, \quad \upsilon\vec{\rho}[\xi_i\tfrac{1}{2}|\dot{\boldsymbol{q}}|^2] = \varepsilon_{\text{tr}}\mathrm{v}_i \tag{184}$$

To unveil the entropy evolution, it will be noted that the internal energy may be expressed in the form: $\varepsilon = R\mathrm{T}^2(\partial\ln\zeta/\partial\mathrm{T})$ [50; p.519]. From $\mathrm{ds}/\mathrm{d}t = 0$, we obtain the isentropic relation $R\mathrm{d}\rho/\rho = \mathrm{c}_{\upsilon}\mathrm{dT}/\mathrm{T}$ which balances upon substituting the MD of ρ and T. As a result, the model is in accordance with the first and second axioms of thermodynamics. The theoretical incorporation of the ideal gas model into the QVFEM has now been completed.

In the current literature [50; ch.10], the overall consensus is that hypersonic flowfields within Earth's upper atmosphere may be treated as an ideal gas due to the expected conditions which the chemical composition will experience; as shown in the generalized compressibility chart found in Figure 19. The pressure (blue) and temperature (red) values are specific to N_2 where the critical values were taken from the NIST Chemistry WebBook, SRD 69. The QVFEM is however not restricted to hypersonics. Therefore, a brief introduction will be given on the incorporation of a real gas model. There could also come a time where a real gas model is desired within the analysis of a hypersonic flowfield so we should never say "never."

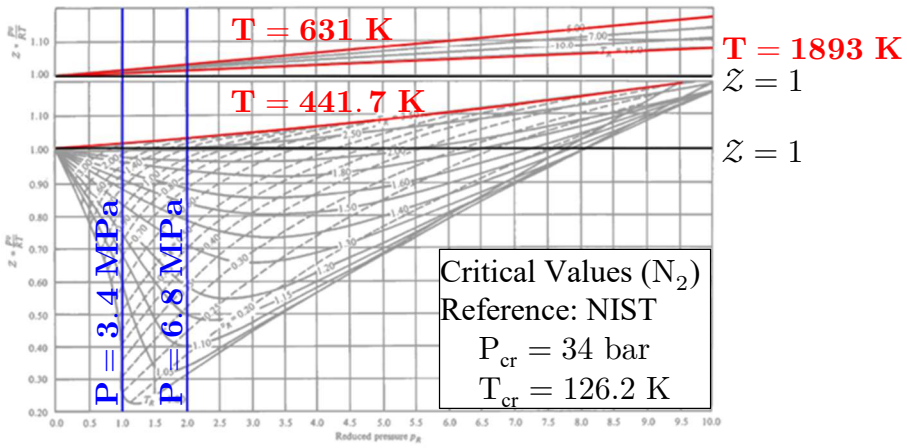

Figure 19 Generalized compressibility chart [53; p.354]

To incorporate real gas effects, the well-known compressibility factor will first be introduced as $\mathcal{Z} \equiv \mathrm{P}_{\text{real}}/\mathrm{P}_{\text{ideal}}$ where $\mathrm{P}_{\text{ideal}} = \rho\Theta$ which entails $\upsilon\mathrm{P} = \mathcal{Z}\Theta$. If the gas is treated as perfect or ideal, then $\mathcal{Z} = 1$. Otherwise, the compressibility factor is typically a function of both temperature and volume (or density). With this general formulation in mind, one example is the Van der Waals EOS, given the number of moles $N = n/N_{\mathrm{A}}$ and molar mass $M = mN_{\mathrm{A}}$, which is commonly expressed as [53; p.346]:

$$(\mathrm{P} + aN^2/\upsilon^2)(\upsilon - bN) = N\mathfrak{R}\mathrm{T} \tag{185}$$

In comparison to $\mathrm{P}_{\text{ideal}}\upsilon = N\mathfrak{R}\mathrm{T}$, the term $+aN^2/\upsilon^2$ accounts for intermolecular interactions and the term $-bN$ incorporates the volume occupied by the molecules within the gas. The coefficients a and b vary between different chemical species. Since $\upsilon\rho = mn = MN$ and $R = \mathfrak{R}/M$, the pressure may be expressed in the following form:

$$\mathrm{P} = \rho\Theta(1 - \beta\rho)^{-1} - \alpha\rho^2 \tag{186}$$

Where the newly introduced coefficients are defined as $\alpha = a/M^2$ and $\beta = b/M$. The Van der Waals compressibility factor is then $\mathcal{Z} = (1 - \beta\rho)^{-1} - \alpha\rho/\Theta$ which is a function of both ρ and T. A similar formulation is the Dieterici EOS where the compressibility factor is $\mathcal{Z} = (1 - \beta\rho)^{-1}\exp(-\alpha\rho/\Theta)$ so the real gas pressure is [53; p.349]:

$$\mathrm{P} = \rho\Theta(1 - \beta\rho)^{-1}\exp(-\alpha\rho/\Theta) \tag{187}$$

To incorporate an EOS such as, for example (186) or (187), $\mathcal{Z}$ will be included within the distribution (124):

$$\hat{\rho}(\boldsymbol{\xi}; \mathbf{v}|\mathcal{Z}\Theta) = \frac{\rho}{(2\pi\mathcal{Z}\Theta)^{3/2}}\exp\left[-\frac{1}{2\mathcal{Z}\Theta}(\boldsymbol{\xi} - \mathbf{v})^{\intercal}\cdot(\boldsymbol{\xi} - \mathbf{v})\right] \tag{188}$$

The above is applicable for the EOM (133) which directly recovers (135) modeling the transport of mass and momentum. In this way, any equation of state may be used for the thermodynamic pressure. Additional considerations would need to be taken into account for the total energy

distribution and entropy since c_υ and c_P may now have dependence upon both ρ and T.

3.6 Quantum Mechanics in Virtual Spacetime

Current velocity discretization methods were discussed in chapter 2.3. What is now desired is a quantization procedure which maintains the mathematical structure of the Maxwellian, maintains all moments exactly without approximation, allows for an unlimited number of sample points, and is based on first principles. Therefore, the method of quantization will first require a theoretical derivation. Here, a reinterpretation of quantum theory will be provided where the Schrödinger equation will be directly derived from classical mechanics; allowing the two theories to exist within harmony with one another. It will be shown that the two actually complement each other. To arrive at such results, we'll draw upon the study of analytical mechanics. This work was inspired by Dr. Kenneth Young's (1947-) special lecture on the principle of least action[9].

Let us first reinstate the variational quantities $\boldsymbol{q}^* = \boldsymbol{q} + \dot{\boldsymbol{q}}\tau$ and $\dot{\boldsymbol{q}}^* = \dot{\boldsymbol{q}} + \ddot{\boldsymbol{q}}\tau$ from (89) and (90), being the perturbed generalized coordinates and rates respectively. The total time derivative presented in (95) will next be applied to the Lagrangian, $\mathrm{L}(\dot{\boldsymbol{q}}, \boldsymbol{q}) = \mathrm{K}(\dot{\boldsymbol{q}}) - \Pi(\boldsymbol{q})$:

$$\frac{\mathbb{d}\mathrm{L}}{\mathbb{d}t} = \frac{\partial \mathrm{L}}{\partial \dot{q}_i}\ddot{q}_i + \frac{\partial \mathrm{L}}{\partial q_i}\dot{q}_i = \mathrm{p}_i\ddot{q}_i + \dot{\mathrm{p}}_i\dot{q}_i = \frac{\mathbb{d}}{\mathbb{d}t}(\mathrm{p}_i\dot{q}_i) \tag{189}$$

Upon integrating by parts, the Euler-Lagrange equation is obtained:

$$\delta\mathrm{H} = \int_{\delta t}\left[\frac{\mathbb{d}}{\mathbb{d}t}\left(\frac{\partial \mathrm{L}}{\partial \dot{q}_i}\right) - \frac{\partial \mathrm{L}}{\partial q_i}\right]\dot{q}_i\,\mathbb{d}t = \left(\frac{\partial \mathrm{L}}{\partial \dot{q}_i}\dot{q}_i - \mathrm{L}\right)\Big|_{\delta t} = 0 \tag{190}$$

Where the Hamiltonian $\mathrm{H}(\mathbf{p}, \boldsymbol{q}) = \mathbf{p}\cdot\dot{\boldsymbol{q}}(\mathbf{p}) - \mathrm{L}[\dot{\boldsymbol{q}}(\mathbf{p}), \boldsymbol{q}]$ is defined by a Legendre transformation. The resulting EOM is of course Newtonian therefore the total energy is a constant of the motion:

$$\frac{\mathbb{d}\mathrm{H}}{\mathbb{d}t} = \frac{\partial \mathrm{H}}{\partial \mathrm{p}_i}\dot{\mathrm{p}}_i + \frac{\partial \mathrm{H}}{\partial q_i}\dot{q}_i = \dot{q}_i\dot{\mathrm{p}}_i - \dot{\mathrm{p}}_i\dot{q}_i = 0 \tag{191}$$

A similar analysis will next be performed, however the variational quantities will be defined in a slightly different manner:

$$\boldsymbol{q}^* = \boldsymbol{q}(t) + \epsilon\boldsymbol{\eta}(t) \tag{192}$$

$$\dot{\boldsymbol{q}}^* = \dot{\boldsymbol{q}}(t) + \epsilon\dot{\boldsymbol{\eta}}(t) \tag{193}$$

Where $\boldsymbol{\eta}$ will be considered a virtual displacement and ϵ is a dimensionless amplitude coefficient. The directional derivative will be found through applying the Gâteaux operator [46; p.46-47, 372-374] to the Lagrangian:

$$\mathfrak{D}\mathrm{L} = \frac{\partial \mathrm{L}^*}{\partial \epsilon}\Big|_{\epsilon=0} = \frac{\partial \mathrm{L}}{\partial q_i}\eta_i + \frac{\partial \mathrm{L}}{\partial \dot{q}_i}\dot{\eta}_i \tag{194}$$

[9] https://youtu.be/IhlSqwZBW1M

Integrating over time and applying the method of integration by parts shows that not only is the total energy conserved, but so is the total action A, so that the variation in total action is zero:

$$\delta \mathrm{A} = \int_{\delta t} \left[\frac{\mathbb{d}}{\mathbb{d}t} \left(\frac{\partial \mathrm{L}}{\partial \dot{q}_i} \right) - \frac{\partial \mathrm{L}}{\partial q_i} \right] \eta_i \, \mathbb{d}t = \frac{\partial \mathrm{L}}{\partial \dot{q}_i} \eta_i \Big|_{\delta t} - \int_{\delta t} \mathfrak{D}\mathrm{L} \, \mathbb{d}t = 0 \tag{195}$$

Since $\mathfrak{D}\mathrm{K} = \mathbf{p} \cdot \dot{\boldsymbol{\eta}}$ and $\mathfrak{D}\Pi = -\dot{\mathbf{p}} \cdot \boldsymbol{\eta}$ then $\mathfrak{D}\mathrm{L}\mathbb{d}t = \mathbb{d}(\mathbf{p} \cdot \boldsymbol{\eta})$. Again, $\boldsymbol{\eta}$ is a virtual displacement so the virtual work is given by $\dot{\mathrm{A}} = (\dot{\mathbf{p}} + \partial \Pi / \partial \boldsymbol{q}) \cdot \boldsymbol{\eta} = 0$, thus abiding D'Alembert's principle. Sir William Hamilton (1805-1865) defined the action in a slightly different manner: $\mathbb{d}\mathbb{S} = \mathfrak{D}\mathrm{L}\mathbb{d}t$. The finite change in Hamilton's action is then:

$$\delta \mathbb{S} = \int_{\delta t} \mathfrak{D}\mathrm{L} \, \mathbb{d}t = \frac{\partial \mathrm{L}}{\partial \dot{q}_i} \eta_i \Big|_{\delta t} - \cancelto{0}{\int_{\delta t} \left[\frac{\mathbb{d}}{\mathbb{d}t} \left(\frac{\partial \mathrm{L}}{\partial \dot{q}_i} \right) - \frac{\partial \mathrm{L}}{\partial q_i} \right] \eta_i \, \mathbb{d}t} \tag{196}$$

To uphold conservation of action, a constraint needs to be applied to the virtual displacement where we must require that $\boldsymbol{\eta}(t_1) = \boldsymbol{\eta}(t_2) = 0$ in order for $\delta \mathbb{S} = 0$. As a result, we've forced the action over $\mathfrak{D}\mathrm{K}$ to equate to the action over $\mathfrak{D}\Pi$ so that the cumulative sum over time of these scalar projections onto the virtual displacements will equal. The act of setting $\mathbb{d}\mathbb{S}/\mathbb{d}t = 0$ means we've utilized Hamilton's principle of stationary action.

Let us next consider a Lagrangian with explicit dependence upon time denoted $\mathrm{L}[\dot{\boldsymbol{q}}(t), \boldsymbol{q}(t), t]$. To find $\mathfrak{D}\mathrm{L}$, the variational time will first be defined as $t^* = t + \epsilon\tau$ where τ is once again the virtual time. It is important to take note that $\boldsymbol{q}^* \neq \boldsymbol{q}(t^*)$ and $\dot{\boldsymbol{q}}^* \neq \dot{\boldsymbol{q}}(t^*)$ in this circumstance which implies $\boldsymbol{\eta}$ is independent of τ. Using (192) and (193), the perturbed Lagrangian is now given by $\mathrm{L}^* = \mathrm{L}(\dot{\boldsymbol{q}} + \epsilon\dot{\boldsymbol{\eta}}, \boldsymbol{q} + \epsilon\boldsymbol{\eta}, t + \epsilon\tau)$ so that the directional derivative is found as:

$$\mathfrak{D}\mathrm{L} = \left(\frac{\partial \mathrm{L}^*}{\partial t^*} \frac{\partial t^*}{\partial \epsilon} + \frac{\partial \mathrm{L}^*}{\partial q_i^*} \frac{\partial q_i^*}{\partial \epsilon} + \frac{\partial \mathrm{L}^*}{\partial \dot{q}_i^*} \frac{\partial \dot{q}_i^*}{\partial \epsilon} \right) \Big|_{\epsilon=0} = \frac{\partial \mathrm{L}}{\partial t} \tau + \frac{\partial \mathrm{L}}{\partial q_i} \eta_i + \frac{\partial \mathrm{L}}{\partial \dot{q}_i} \dot{\eta}_i \tag{197}$$

Performing the usual sequence of integrating over time then applying IBP yields:

$$\delta \mathbb{S} = \int_{\delta t} \mathfrak{D}\mathrm{L} \, \mathbb{d}t = (\mathrm{p}_i \eta_i + \mathrm{L}\tau)|_{\delta t} \tag{198}$$

As a result, the action is now identified as $\mathbb{S} = \mathbf{p} \cdot \boldsymbol{\eta} + \mathrm{L}\tau$. Recalling that $\mathrm{L} = \mathbf{p} \cdot \dot{\boldsymbol{q}} - \mathrm{H}$, the action may next be written in terms of the Hamiltonian. Through denoting the total virtual displacement as $\boldsymbol{\chi} = \boldsymbol{\eta} + \dot{\boldsymbol{q}}\tau$, the virtual action function takes the following fundamental form:

$$\mathbb{S}(\boldsymbol{\chi}, \tau) = \mathbf{p} \cdot \boldsymbol{\chi} - \mathrm{H}\tau \tag{199}$$

From which the virtual Hamilton-Jacobi (H-J) relations may be derived from:

$$-\frac{\partial \mathbb{S}}{\partial \tau} = \mathrm{H}, \qquad \mathbf{p} = \frac{\partial \mathbb{S}}{\partial \boldsymbol{\chi}}, \qquad \mathrm{L} = \frac{\partial \mathbb{S}}{\partial \tau} + \dot{\boldsymbol{q}} \cdot \frac{\partial \mathbb{S}}{\partial \boldsymbol{\chi}} \tag{200}$$

The mathematical structure of the action function is indicative of the phase $\Phi = \boldsymbol{k} \cdot \boldsymbol{\chi} - \omega\tau$ within the generalized wave function $\psi = \exp(i\Phi)$. If we were describing the action of a photon then according to Max Planck (1858-1947) and Albert Einstein (1879-1955), the possible energies which may be occupied by that photon are quantized and given by the Planck-Einstein relation $\mathrm{E} = \hbar\omega$. Louis de Broglie (1892-1987) hypothesized that not only do photons posses wave properties but all matter. With the addition of the de Broglie relation $\mathbf{p} = \hbar\boldsymbol{k}$, the phase takes the form $\Phi = \mathbb{S}/\hbar$ so that the wave function becomes $\psi = \exp(i\mathbb{S}/\hbar)$. Solving for the action in terms of the wave function provides the relation $\mathbb{S} = -i\hbar \ln\psi$. Substituting into the H-J relations yields:

$$i\hbar\frac{\partial\psi}{\partial\tau} = \mathrm{H}\psi, \qquad -i\hbar\frac{\partial\psi}{\partial\boldsymbol{\chi}} = \mathbf{p}\psi \tag{201}$$

Where the LHS of (201) is the virtual Hamiltonian operator and to the right is the associated virtual momentum operator. The Schrödinger equation, named after Erwin Schrödinger (1887-1961), may be directly derived from the recently established wave function $\psi(\boldsymbol{\chi}, \tau) = \exp[i(\mathbf{p} \cdot \boldsymbol{\chi} - \mathrm{H}\tau)/\hbar]$, upon defining the momentum $\mathbf{p} = m\dot{\boldsymbol{q}}$ and the Hamiltonian $\mathrm{H} = |\mathbf{p}|^2/2m + \Pi$:

$$i\hbar\frac{\partial\psi}{\partial\tau} = -\frac{\hbar^2}{2m}\sum_{l=1}^{3}\frac{\partial^2\psi}{\partial\chi_l^2} + \Pi\psi = \mathrm{H}\psi \tag{202}$$

Alternatively, the kinetic energy operator may be directly derived from the known momentum operator. The above will be referred to as the virtual Schrödinger equation. In this work, the Lagrangian will have implicit dependence upon time so we'll set $\tau = 0$. In affect, the action simplifies to $\mathbb{S}(\boldsymbol{\chi}) = \mathbf{p} \cdot \boldsymbol{\chi}$ so the change in action is simply $\delta\mathbb{S} = (\mathbf{p} \cdot \boldsymbol{\chi})|_{\delta t}$. To preserve the action and uphold Hamilton's principle of stationary action, we must require that at the beginning and end of each time step, the virtual displacement in the Newtonian path $\mathfrak{D}\boldsymbol{q} = \boldsymbol{\eta}$ must equate to zero. Since $\boldsymbol{\chi}(\tau = 0) = \boldsymbol{\eta}$, we'll enforce the following condition:

$$\boldsymbol{\chi}(t_i) = \boldsymbol{\chi}(t_{i+1}) = \mathbf{0} \tag{203}$$

It will soon be uncovered that the value $\boldsymbol{\chi} = \mathbf{0}$ is the location of where the moments of the velocity distribution exist and are updated from. Since $\tau = 0$, the phase reduces to $\Phi = \boldsymbol{k} \cdot \boldsymbol{\chi}$. Using the de Broglie relation, the wave function takes the form $\psi(\boldsymbol{\chi}) = \exp(i\mathbf{p} \cdot \boldsymbol{\chi}/\hbar)$, which expands as:

$$\psi(\boldsymbol{\xi}; \mathbf{v}, \boldsymbol{\chi}) = \psi(\boldsymbol{\xi}, \boldsymbol{\chi})\psi^*(\mathbf{v}, \boldsymbol{\chi}) = \exp(i\dot{\boldsymbol{q}} \cdot \boldsymbol{\chi}/\mathfrak{H}) \tag{204}$$

Where $\mathfrak{H} = \hbar/m$ is the specific reduced Planck constant, ψ^* is the complex conjugate wave function, and from the derivation of the Maxwellian: $\dot{\boldsymbol{q}} = \boldsymbol{\xi} - \mathbf{v}$. In ch.3.7, the velocity distributions will be transformed into the virtual space via the continuous Fourier transform (CFT) using the recently derived transformation wave function $\psi(\boldsymbol{\xi}, \boldsymbol{\chi})$.

To demonstrate Hamilton's principle, let us first recall the Maxwellian (98): $\mathfrak{F} = \zeta^{-1}\exp(-\beta\mathcal{E})$. A specific potential will next be defined from the classical harmonic oscillator: $\phi(\boldsymbol{q}) = \frac{1}{2}\omega^2|\boldsymbol{q}|^2$. The total specific energy is then $\mathcal{E}(\dot{\boldsymbol{q}}, \boldsymbol{q}) = \frac{1}{2}(|\dot{\boldsymbol{q}}|^2 + \omega^2|\boldsymbol{q}|^2)$. Upon normalizing the phase space

distribution, the partition function is computed as $\zeta = (2\pi/\beta\omega)^3$. It will be noted that the constraint from (104), i.e. $\vec{\rho}[\mathcal{L}] = 0$, is automatically satisfied. The EOM is then found from (101):

$$\int_{\delta t} (\ddot{q}_i + \omega^2 q_i)\dot{q}_i \mathfrak{F} \, \mathrm{d}t = \int_{\delta t} \dot{\mathcal{E}} \mathfrak{F} \, \mathrm{d}t = 0 \tag{205}$$

Given the initial conditions: $\boldsymbol{q}(0) = \boldsymbol{q}_\mathrm{o}$ and $\dot{\boldsymbol{q}}(0) = \dot{\boldsymbol{q}}_\mathrm{o}$, the solution to $\ddot{\boldsymbol{q}} = -\omega^2 \boldsymbol{q}$, is:

$$\boldsymbol{q}(t) = \boldsymbol{q}_\mathrm{o} \cos(\omega t) + (\dot{\boldsymbol{q}}_\mathrm{o}/\omega) \sin(\omega t) \tag{206}$$

Let us now suppose we are given the set of initial conditions: $\{\boldsymbol{q}_\mathrm{o}^\beta, \dot{\boldsymbol{q}}_\mathrm{o}^\alpha\}$, where the objective is to find the actual path observed $\mathbf{x}$ out of all possible paths $\boldsymbol{y}^{\alpha\beta}$. The solution to the ODE is then:

$$\boldsymbol{y}^{\alpha\beta}(t) = \mathbf{x}(t) + \boldsymbol{q}_\mathrm{o}^\beta \cos(\omega t) + (\dot{\boldsymbol{q}}_\mathrm{o}^\alpha/\omega) \sin(\omega t) \tag{207}$$

Some examples of the variations are plotted in Figure 20 using a five-point integer lattice centered about zero. For plotting purposes, I set $\omega = \pi/\delta t \ \ (\mathrm{s}^{-1})$ and $\delta t = 1/4 \ \ (\mathrm{s})$.

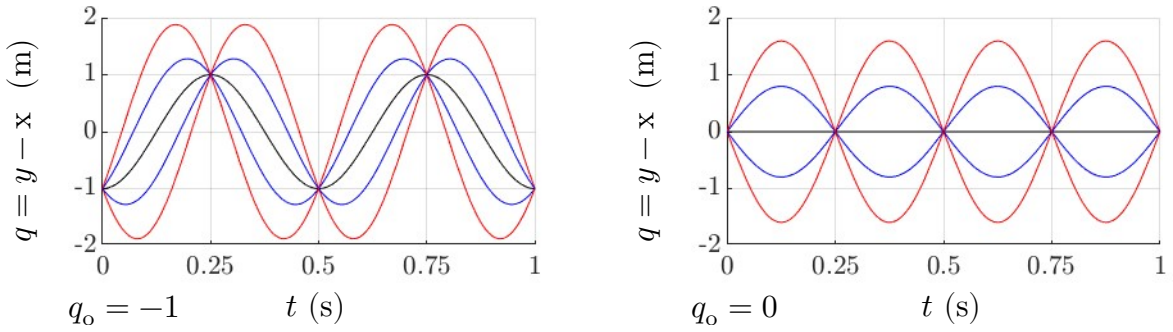

Figure 20 First order variations $q(t)$ in the observed path $\mathrm{x}(t)$

The variational paths are next plotted in Figure 21, where $\mathrm{x}(t)$ satisfies $\dot{\mathrm{x}} + \tau\ddot{\mathrm{x}} = 0$.

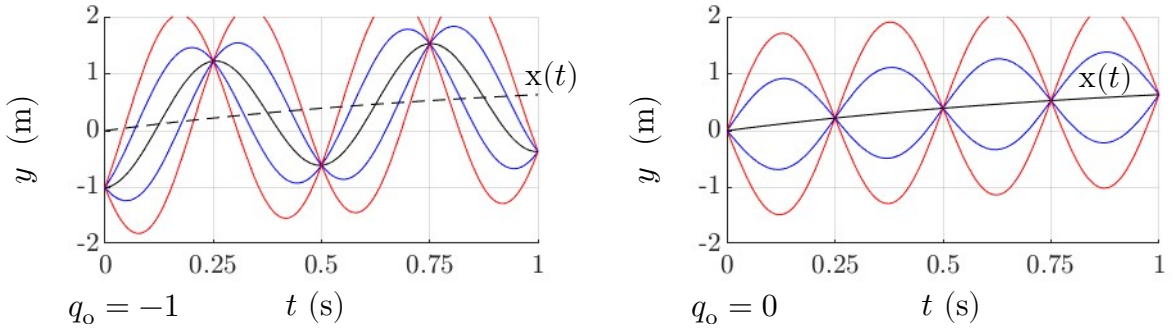

Figure 21 Variational paths $y(t)$

The red curves indicate $\dot{q}_\mathrm{o} = \pm 20 \ \ (\mathrm{m/s})$, the blue curves indicate $\dot{q}_\mathrm{o} = \pm 10 \ \ (\mathrm{m/s})$, and the solid

black curve indicates $\dot{q}_{\mathrm{o}} = 0\ (\mathrm{m/s})$. The path observed is easily found when $q_{\mathrm{o}} = 0$ and $\dot{q}_{\mathrm{o}} = 0$. However, when $q_{\mathrm{o}} = 0$, Hamilton's principle is still satisfied for any $\dot{q}_{\mathrm{o}}$, since:

$$\delta\mathbb{S}/m = (\dot{\boldsymbol{q}} \cdot \boldsymbol{q})|_{n\delta t} - (\dot{\boldsymbol{q}} \cdot \boldsymbol{q})|_{(n-1)\delta t} = 0 \tag{208}$$

Where the variation is the generalized coordinate itself since $\boldsymbol{q} = \boldsymbol{y} - \mathbf{x}$. As a result, one may construct linear approximations to the observed path through connecting the intersection points at the bounds of integration. These concepts are exploited in the finite element method.

3.7 Transformations into Virtual Space

Since we've declared $\mathrm{P} = \rho\Theta$, then the Maxwellian (124) may now be written in the form:

$$\hat{\rho}(\boldsymbol{\xi}; \mathbf{v}|\Theta) = \frac{\rho}{(2\pi\Theta)^{3/2}} \exp\left[-\frac{1}{2\Theta}(\boldsymbol{\xi} - \mathbf{v})^{\mathsf{T}} \cdot (\boldsymbol{\xi} - \mathbf{v})\right] \tag{209}$$

Which satisfies the mass dispersion relation $\partial\hat{\rho}/\partial\Theta = \frac{1}{2}\dot{\nabla}^2\hat{\rho}$ similar to (107). The above isotropic Gaussian is a local Maxwellian where the system quantities or observables ρ, $\mathbf{v}$, and T have spacetime dependence within the current configuration. The LHS of Figure 22 illustrates this distribution at a single point in spacetime where the height of each vertical black solid line represents the amount of mass ρ assigned to the occupational velocity ξ:

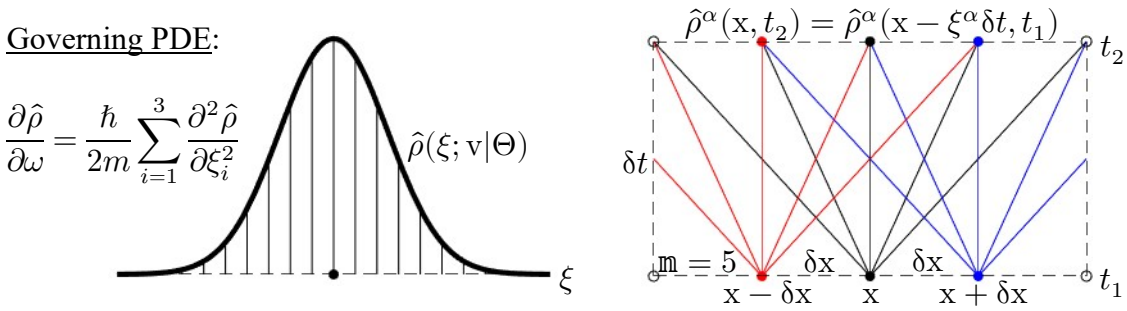

Figure 22 Mass dispersion diagram (left) & characteristic lines from the 1D FBE (right)

Upon defining the thermal frequency $\omega = \Theta/\mathfrak{H} = k_{\mathrm{B}}\mathrm{T}/\hbar$, the governing PDE takes the form: $\partial\hat{\rho}/\partial\omega = \frac{1}{2}\mathfrak{H}\dot{\nabla}^2\hat{\rho}$. The solution will be decomposed as $f(\omega)\psi(\boldsymbol{\xi})$ with the separation constant being $-|\boldsymbol{\chi}|^2/2\mathfrak{H}$, having units of seconds. Solving each ODE yields a single solution of the form: $c(\boldsymbol{\chi})\psi(\boldsymbol{\xi}, \boldsymbol{\chi})f(\omega, \boldsymbol{\chi})$. The total solution can be found through using the principle of state superposition; therefore integrating over all possible virtual displacements $\boldsymbol{\chi}\ \forall\ \mathrm{X} \in \mathbb{R}^3$ gives:

$$\hat{\rho}(\boldsymbol{\xi}; \mathbf{v}|\Theta) = \int_{\mathbb{R}^3} c(\boldsymbol{\chi})\psi(\boldsymbol{\xi}, \boldsymbol{\chi})f(\omega, \boldsymbol{\chi})\, d\mathrm{X} = \frac{\rho}{(2\pi\mathfrak{H})^3}\int_{\mathbb{R}^3}\psi(\boldsymbol{\xi}; \mathbf{v}, \boldsymbol{\chi})f(\omega, \boldsymbol{\chi})\, d\mathrm{X} \tag{210}$$

This operation is a continuous Fourier transform (CFT) where $f(\omega, \boldsymbol{\chi}) = \exp(-m\omega|\boldsymbol{\chi}|^2/2\hbar)$. The normalizing coefficient is obtained through the following inverse Fourier transform, given the "initial" condition $\hat{\rho}(\boldsymbol{\xi}; \mathbf{v}|0) = \rho\delta(\boldsymbol{\xi}; \mathbf{v})$, where $\delta(\boldsymbol{\xi}; \mathbf{v})$ is a Dirac delta function:

$$c(\boldsymbol{\chi}) = \frac{\rho}{(2\pi\mathfrak{H})^3}\int_{\mathbb{R}^3}\psi^*(\boldsymbol{\xi},\boldsymbol{\chi})\delta(\boldsymbol{\xi};\mathbf{v})\,d\Xi = \frac{\rho}{(2\pi\mathfrak{H})^3}\,\psi^*(\mathbf{v},\boldsymbol{\chi}) \tag{211}$$

The Maxwellian has now been shown to be constructed from the recently derived wave function (204). The conjugate PDE stems from (202) provided as ($\partial\breve{\rho}/\partial\tau = 0$):

$$-\frac{\mathfrak{H}^2}{2}\sum_{l=1}^{3}\frac{\partial^2\breve{\rho}(\boldsymbol{\chi})}{\partial\chi_l^2} = \frac{1}{2}\,|\boldsymbol{\xi}|^2\breve{\rho}(\boldsymbol{\chi}) \tag{212}$$

The solution is of course another CFT mapping the distribution from velocity into virtual space:

$$\breve{\rho}(\boldsymbol{\chi},\mathbf{x},t) = \int_{\mathbb{R}^3}\psi(\boldsymbol{\xi},\boldsymbol{\chi})\hat{\rho}(\boldsymbol{\xi},\mathbf{x},t)\,d\Xi = \rho\exp\left(-\frac{\omega}{2\mathfrak{H}}\,|\boldsymbol{\chi}|^2 + \frac{i}{\mathfrak{H}}\,\mathbf{v}\cdot\boldsymbol{\chi}\right) \tag{213}$$

Statisticians and mathematicians would most likely refer to the above as a characteristic function. For the engineers and mechanicians, lets call this a moment generating wave function (MGWF) because $\breve{\rho}$ is a moment generator with wave properties if $\mathbf{v} \neq \mathbf{0}$. In general, the continuous Fourier transform of the function $\mathrm{F}(\boldsymbol{\xi},\mathbf{x},t)$ and the inverse operation are provided respectively:

$$\Psi(\boldsymbol{\chi},\mathbf{x},t) = \int_{\mathbb{R}^3}\psi(\boldsymbol{\xi},\boldsymbol{\chi})\mathrm{F}(\boldsymbol{\xi},\mathbf{x},t)\,d\Xi \tag{214}$$

$$\mathrm{F}(\boldsymbol{\xi},\mathbf{x},t) = \frac{1}{(2\pi\mathfrak{H})^3}\int_{\mathbb{R}^3}\psi^*(\boldsymbol{\xi},\boldsymbol{\chi})\Psi(\boldsymbol{\chi},\mathbf{x},t)\,d\mathrm{X} \tag{215}$$

The benefit of this transformation is that now the m^{th} order moment may be expressed in terms of the following Gâteaux operator, which is a derivative operation, in contrast to integration over the entire real number line:

$$\vec{\mathrm{F}}[\boldsymbol{\xi}^m] = \int_{\mathbb{R}^3}\boldsymbol{\xi}^m\mathrm{F}\,d\Xi = (-i\mathfrak{H})^m\,\frac{\partial^m\Psi}{\partial\boldsymbol{\chi}^m}\bigg|_{\boldsymbol{\chi}=\mathbf{0}} \tag{216}$$

Where the raised power of m denotes a tensor product within the partial derivative. For further investigation, lets first denote a new wave function, $\Psi = \upsilon\breve{\rho}\lambda^{-3}$. The volume λ^3 becomes the partition function so that λ^{-3} acts as the normalizing coefficient. A probability density function will next be defined from the operation $\hat{p} = \sqrt{\Psi^*\Psi} = \lambda^{-3}f$. Upon integrating over all possible virtual displacements $\boldsymbol{\chi}$ and enforcing $\vec{p} = 1$ (Kolmogorov axiom II), the length λ computes to:

$$\lambda = \sqrt{2\pi\mathfrak{H}/\omega} = \sqrt{2\pi\hbar^2/mk_{\mathrm{B}}\mathrm{T}} \tag{217}$$

Which is otherwise known as the thermal de Broglie wavelength associated with an ideal gas model. So, the probability density may now be written as $\hat{p}(\boldsymbol{\chi}|\lambda) = \lambda^{-3}\exp(-\pi|\boldsymbol{\chi}|^2/\lambda^2)$ with variance $\mathfrak{H}/\omega$. The Dirac delta function will next formally be defined as an isotropic Gaussian with a limiting variance approaching zero:

$$\delta(\boldsymbol{\chi}) = \lim_{\Delta\to 0} \mathcal{G}(\boldsymbol{\chi}|\Delta) = \frac{1}{(2\pi)^3} \lim_{\Delta\to 0} \int_{\mathbb{R}^3} \exp\left(-\frac{1}{2}\Delta|\boldsymbol{k}|^2 + i\boldsymbol{k}\cdot\boldsymbol{\chi}\right) d\mathrm{K} \tag{218}$$

Lets note that the three-dimensional case is obtained through use of the factorial operator $\delta(\boldsymbol{\chi}) = \prod_{i=1}^{3} \delta(\chi_i)$ acting on each one-dimensional Dirac delta function. This concept is similar to the Maxwellian (209) due to the equipartition of energy $\prod_{i=1}^{3} \zeta_i^{-1} \exp(-\dot{q}_i^2/2\Theta)$. Each Dirac delta function is orthogonal in the sense that:

$$\int_{\mathbb{R}} \chi^m \delta(\chi)\, d\chi = \begin{cases} 1 \text{ if } m = 0 \\ 0 \text{ if } m > 0 \end{cases} \forall\ m \in \mathbb{Z}^+ \tag{219}$$

Based on this mathematical property, the Gâteaux operator will be redefined as:

$$\vec{\mathrm{F}}[\boldsymbol{\xi}^m] = (-i\mathfrak{H})^m \int_{\mathbb{R}^3} \delta(\boldsymbol{\chi}) \frac{\partial^m \Psi}{\partial \boldsymbol{\chi}^m} d\mathrm{X} \tag{220}$$

Using the virtual or wave form of the Maxwellian (213), the mass density, momentum density, and total energy density (located at $\boldsymbol{\chi} = \mathbf{0}$) may now be expressed as:

$$\rho = \int_{\mathbb{R}^3} \delta(\boldsymbol{\chi}) \breve{\rho}(\boldsymbol{\chi})\, d\mathrm{X}, \qquad \rho\mathbf{v} = -i\mathfrak{H} \int_{\mathbb{R}^3} \delta(\boldsymbol{\chi}) \frac{\partial \breve{\rho}(\boldsymbol{\chi})}{\partial \boldsymbol{\chi}} d\mathrm{X} \tag{221}$$

$$\rho e = -\frac{\mathfrak{H}^2}{2} \int_{\mathbb{R}^3} \delta(\boldsymbol{\chi}) \sum_{l=1}^{3} \frac{\partial^2 \breve{\rho}(\boldsymbol{\chi})}{\partial \chi_l^2} d\mathrm{X} + \overline{\varepsilon} \int_{\mathbb{R}^3} \delta(\boldsymbol{\chi}) \breve{\rho}(\boldsymbol{\chi})\, d\mathrm{X} \tag{222}$$

Where each of these operations conserves the action $\mathbb{S} = m(\boldsymbol{\xi} - \mathbf{v}) \cdot \boldsymbol{\chi}$ and mimics the derived operators as found in (201) and (202). To note, the integral with the Laplacian integrand generates the total specific translational energy denoted $e_{\text{tr}} = \varrho + \varepsilon_{\text{tr}}$ as found in (128). The associated momentum and total energy density moment generating wave functions are respectively:

$$\breve{\mathbf{p}} = \vec{\mathbf{p}}[\psi] = -i\mathfrak{H} \frac{\partial \breve{\rho}(\boldsymbol{\chi})}{\partial \boldsymbol{\chi}} = \breve{\rho}(\boldsymbol{\chi})(\mathbf{v} + i\omega\boldsymbol{\chi}) \tag{223}$$

$$\breve{\mathrm{E}} = \vec{\mathrm{E}}[\psi] = -\frac{\mathfrak{H}^2}{2} \sum_{l=1}^{3} \frac{\partial^2 \breve{\rho}(\boldsymbol{\chi})}{\partial \chi_l^2} + \overline{\varepsilon} \breve{\rho}(\boldsymbol{\chi}) = \breve{\rho}(\boldsymbol{\chi}) \left(e + i\omega\boldsymbol{\chi}\cdot\mathbf{v} - \frac{1}{2}\omega^2|\boldsymbol{\chi}|^2\right) \tag{224}$$

Where the mass density transformation is once again $\breve{\rho} = \vec{\rho}[\psi]$. When $\mathbf{v} = \mathbf{0}$, the the above energy MGWF may be reformulated into the following operator relation:

$$-\frac{\mathfrak{H}^2}{2} \sum_{l=1}^{3} \frac{\partial^2 \breve{\rho}(\boldsymbol{\chi})}{\partial \chi_l^2} + \frac{1}{2}\omega^2|\boldsymbol{\chi}|^2 \breve{\rho}(\boldsymbol{\chi}) = \varepsilon_{\text{tr}} \breve{\rho}(\boldsymbol{\chi}) \tag{225}$$

Quantized solutions to (225) produce quantum harmonic oscillating wave functions. It will be noted that $\hat{p}(\boldsymbol{\chi})$ satisfies this virtual differential equation. Similar to the operation $\breve{\rho}^*\breve{\rho}$ used for $\hat{p}$, the total energy is:

$$e(\boldsymbol{\chi},\mathbf{x},t)=\frac{\sqrt{\breve{\mathrm{E}}^*\breve{\mathrm{E}}}}{\sqrt{\breve{\rho}^*\breve{\rho}}}=\sqrt{e^2-e\omega^2|\boldsymbol{\chi}|^2+\omega^2(\boldsymbol{\chi}\cdot\mathbf{v})^2+\frac{1}{4}\omega^4|\boldsymbol{\chi}|^4} \tag{226}$$

The FBE (144) will next be transformed into the virtual space. The resulting equation of motion will be referred to as ***Lady's equation of motion*** which mimics the structure of the Schrödinger equation (202):

$$\frac{\partial}{\partial t}\Psi(\boldsymbol{\chi},\mathbf{x},t)=i\mathfrak{H}\nabla_l\frac{\partial}{\partial\chi_l}\Psi(\boldsymbol{\chi},\mathbf{x},t) \tag{227}$$

Notice how the velocity $\boldsymbol{\xi}$ has been indirectly transformed into the operator $-i\mathfrak{H}\,\partial/\partial\boldsymbol{\chi}$ as a result from the CFT (214). Lady's EOM may be transformed back to the FBE using the CIFT (215). What makes this operation possible is the fact that when applying IBP, the extrema vanish. So now that the theoretical framework has been established, the process of quantization will next be established within ch.3.8.

3.8 Quantization and the QVFEM Algorithm

The velocities will be quantized as $\boldsymbol{\xi}^\alpha=\mathbb{c}\boldsymbol{\mathcal{z}}^\alpha$ where $\boldsymbol{\mathcal{z}}^\alpha$ is a symmetric integer basis or lattice and $\mathbb{c}\equiv\delta\ell/\delta t$ is a characteristic speed (CS). The number of quantized velocities per dimension $\mathbb{m}$ is always a positive odd integer. So, the total number of velocities in two dimensions is $\mathbb{m}^2$ and in three dimensions $\mathbb{m}^3$. The base integer lattice in one dimension, from which higher dimensional lattices may be constructed, is provided as:

$$\mathcal{z}^\alpha=\{-(\mathbb{m}-1)/2\,,\ldots,-2,-1,0,+1,+2,\ldots,+(\mathbb{m}-1)/2\} \tag{228}$$

The CS per time step, in reference to (209), is determined by finding the distribution with the maximum radius of influence, given by:

$$\mathbb{c}=2(\mathbb{m}-1)^{-1}\max\langle|u\pm\aleph\sqrt{\Theta}|,|v\pm\aleph\sqrt{\Theta}|,|w\pm\aleph\sqrt{\Theta}|\rangle \tag{229}$$

Where $\aleph$ is the number of chosen standard deviations (SD). To properly capture the physics during each time step, it is generally recommended that $3\leq\aleph\leq4$. To note, the above vector is formulated through solving the differential relation $-\sqrt{\Theta}(\partial\hat{\rho}/\partial\xi)=\aleph\hat{\rho}$ for ξ per dimension; similar to a *z*-score. To uphold the stability condition stated in (87) or in other words $\boldsymbol{\xi}\delta t\leq\delta\mathbf{x}$, the time step (per time step) is computed as:

$$\delta t=\mathbb{c}^{-1}\min\langle|\delta x|,|\delta y|,|\delta z|\rangle \tag{230}$$

From the de Broglie relation $\boldsymbol{\xi}^\alpha=\mathfrak{H}\boldsymbol{k}^\alpha$, the wave numbers become $\boldsymbol{k}^\alpha=\mathbb{c}\boldsymbol{\mathcal{z}}^\alpha/\mathfrak{H}=2\pi\boldsymbol{\mathcal{z}}^\alpha/\lambda$ where $\lambda=2\pi\mathfrak{H}/\mathbb{c}$ is the overall wavelength. The step size is given by $\delta\chi=\lambda/\mathbb{m}$ so that the quantized virtual displacements are simply $\boldsymbol{\chi}^\beta=\boldsymbol{\mathcal{z}}^\beta\delta\chi$. Now that $\boldsymbol{\xi}$ and $\boldsymbol{\chi}$ have been quantized

along with space and time, let us now discuss the overall algorithm. Per time step, the QVFEM procedure is provided in the following flow chart:

$$\Psi^{\beta}(\mathbf{x},t) \overset{\text{DIFT}}{\Longrightarrow} \mathrm{F}^{\alpha}(\mathbf{x},t) \overset{\text{EOM}}{\Longrightarrow} \mathrm{F}^{\alpha}(\mathbf{x}+\delta\mathbf{x},t+\delta t) \overset{\text{DFT}}{\Rightarrow} \Psi^{\beta}(\mathbf{x}+\delta\mathbf{x},t+\delta t) \tag{231}$$

As one can observe, the MGWF $\Psi^{\beta}(\mathbf{x},t)$ is first initialized. To compute each "mass" F^{α}, the continuous inverse Fourier transform from (215) will be converted into its discrete counterpart, being the DIFT:

$$\mathrm{F}^{\alpha}(\mathbf{x},t) = \frac{1}{(2\pi\mathfrak{H})^3}\sum_{\beta=1}^{\mathbb{m}^3}\psi^{*}(\boldsymbol{\xi}^{\alpha},\boldsymbol{\chi}^{\beta})\Psi^{\beta}(\mathbf{x},t)\,\delta\chi^3 \tag{232}$$

Where the integral has been converted into a finite sum and the differential $d\mathrm{X}$ has been converted to $\delta\chi^3$ because the step size $\delta\chi = 2\pi\mathfrak{H}/\mathbb{c}\mathbb{m}$ is the same in all three Euclidean dimensions. The transformation matrix is next identified as:

$$\mathrm{Q}^{\alpha\beta} = (2\pi\mathfrak{H})^{-3}\exp(-i\boldsymbol{\xi}^{\alpha}\cdot\boldsymbol{\chi}^{\beta}/\mathfrak{H})\,\delta\chi^3 \tag{233}$$

$$= (\mathbb{c}\mathbb{m})^{-3}\exp(-2\pi i\boldsymbol{z}^{\alpha}\cdot\boldsymbol{z}^{\beta}/\mathbb{m})$$

Which is an $\mathbb{m}^3\times\mathbb{m}^3$ complex matrix containing both real and imaginary parts, i.e. $\exp(\pm i\vartheta) = \cos\vartheta \pm i\sin\vartheta$. It will be noted that $i\boldsymbol{\xi}^{\alpha}\cdot\boldsymbol{\chi}^{\beta}/\mathfrak{H} = (2\pi i/\mathbb{m})(\boldsymbol{z}^{\alpha}\cdot\boldsymbol{z}^{\beta})$ which shows the essence of the DFT. As a result, the DIFT may be written in a more compact form which is optimal for linear algebraic operations:

$$\mathrm{F}^{\alpha}(\mathbf{x},t) = \sum_{\beta=1}^{\mathbb{m}^3}\mathrm{Q}^{\alpha\beta}\Psi^{\beta}(\mathbf{x},t) \tag{234}$$

The matrix representation of the above summation operation is $\mathbf{F} = \mathbf{Q}\cdot\boldsymbol{\Psi}$ where $\mathbf{F}$ and $\boldsymbol{\Psi}$ are both vectors of size $\mathbb{m}^3$ per spatial node. If the matrix $\mathbf{Q}$ is invertible, then the initial MGWF may be recovered exactly without approximation via the operation $\boldsymbol{\Psi} = \mathbf{Q}^{-1}\cdot\mathbf{F}$. This is one of the major benefits of the proposed methodology. Additionally, the user is free to sample as many quantized states (from the unbounded sample space) necessary to achieve numerical stability. Fortunately, the transformation matrix is in fact invertible in this circumstance. It will be noted that $\boldsymbol{\psi}$ and $\boldsymbol{\psi}^{*}$ are both symmetric matrices so that the associated Hermitian matrix is $\boldsymbol{\psi}^{\mathsf{H}} = \boldsymbol{\psi}^{*\mathsf{T}} = \boldsymbol{\psi}^{*}$. It is well known that in the DFT framework $\boldsymbol{\psi}^{\mathsf{H}}\cdot\boldsymbol{\psi} = \boldsymbol{\psi}\cdot\boldsymbol{\psi}^{\mathsf{H}} = \mathbb{m}^3\mathbf{1}$ which proves a matrix inverse exists. Since $\mathbf{Q} = (\mathbb{c}\mathbb{m})^{-3}\boldsymbol{\psi}^{*}$ then $\boldsymbol{\psi}^{\mathsf{H}} = (\mathbb{c}\mathbb{m})^3\mathbf{Q}$ and $\boldsymbol{\psi} = (\mathbb{c}\mathbb{m})^3\mathbf{Q}^{*}$. Substituting into the inverse identity proves that:

$$\mathbf{Q}^{*}\cdot\mathbf{Q} = \mathbf{Q}\cdot\mathbf{Q}^{*} = (\mathbb{c}^2\mathbb{m})^{-3}\mathbf{1} \tag{235}$$

The inverse is identified as $\mathbf{Q}^{-1} = (\mathbb{c}^2\mathbb{m})^3\mathbf{Q}^{*}$ so that the resulting mapping is:

$$\mathbf{F} = (\mathbb{c}\mathbb{m})^{-3}\boldsymbol{\psi}^{*}\cdot\boldsymbol{\Psi} \;\leftrightarrow\; \boldsymbol{\Psi} = \mathbb{c}^3\boldsymbol{\psi}\cdot\mathbf{F} \tag{236}$$

The overall generalized QVFEM algorithm is next summarized in the Table 2:

$\mathbf{x}_{ijk} = \langle x_i, y_j, z_k \rangle$	generate spatial finite element mesh grid
$\Gamma^{\alpha}_{ijk} =$ phase matrix (connectivity)	establish the connectivity matrix $\forall\ (\boldsymbol{\xi}^{\alpha}, \mathbf{x}_{ijk})$
$\rho_{\mathrm{o}}, \mathbf{v}_{\mathrm{o}}, \varepsilon_{\mathrm{o}}$	input initial conditions
for $t = 1 : n_t$	begin time marching
$\mathbb{c} = \cdots$ see (229)	compute the characteristic speed
$\boldsymbol{\xi}^{\alpha} = \mathbb{c}\boldsymbol{z}^{\alpha}$	obtain finite set of quantized velocities
$\delta t = \mathbb{c}^{-1} \min\langle \lvert\delta x\rvert, \lvert\delta y\rvert, \lvert\delta z\rvert \rangle$	compute time step to satisfy (87)
$\lambda = 2\pi\mathfrak{H}/\mathbb{c}$	overall wavelength
$\delta\chi = \lambda/\mathbb{m}$	wavelength step size
$\boldsymbol{\chi}^{\beta} = \boldsymbol{z}^{\beta}\delta\chi$	associated quantized virtual displacements
$\Psi^{\beta}(\mathbf{x}, t)$	initialize moment generating wave functions
$\mathbf{Q} = (\mathbb{c}\mathbb{m})^{-3}\boldsymbol{\psi}^{*}$ and $\mathbf{Q}^{-1} = \mathbb{c}^{3}\boldsymbol{\psi}$	transformation matrix and inverse
$\mathbf{F}(\mathbf{x}, t) = \mathbf{Q} \cdot \boldsymbol{\Psi}(\mathbf{x}, t)$	extract the discrete "masses"
$\mathrm{F}^{\alpha}(\mathbf{x}, t) = \boldsymbol{f}^{\alpha} \cdot \boldsymbol{g}^{\alpha}[\boldsymbol{\varphi}^{-1}(\mathbf{x}, t)]$	apply solution over each phasetime element and extract the temporally advanced distribution values located at $\mathrm{F}^{\alpha\prime} = \mathrm{F}^{\alpha}(\mathbf{x} + \delta\mathbf{x}^{\alpha}, t + \delta t)$ using the phase matrix
$\boldsymbol{\Psi}' = \mathbf{Q}^{-1} \cdot \mathbf{F}'$	update moment generating wave functions
$\Sigma' = \Psi'(\boldsymbol{\chi} = \mathbf{0})$	extract the temporally advanced system quantities from the moment generating wave functions
$\rho_{\mathrm{b}}, \mathbf{v}_{\mathrm{b}}, \varepsilon_{\mathrm{b}}$	apply boundary conditions at the boundaries of analysis
end	end time marching
$\rho(\mathbf{x}, t_{\text{final}}), \mathbf{v}(\mathbf{x}, t_{\text{final}}), \varepsilon(\mathbf{x}, t_{\text{final}})$	export results and plot

Table 2 QVFEM general algorithm

3.9 Numerical Testing

For all numerical simulations shown $\aleph = 4$. To note, the solution to the FBE over a uniform grid simplifies down to $\mathrm{F}^{\alpha}(\mathbf{x}, t + \delta t) = \mathrm{F}^{\alpha}(\mathbf{x} - \boldsymbol{\xi}^{\alpha}\delta t, t)$. Please see an illustration of the characteristic lines in Figure 22 which shows the trajectories for each $\widehat{\rho}^{\alpha}$. In the LBM, this process is known as streaming. For all stationary walls, the normal mean velocity will be manually forced to zero at the end of each time step. More detail on implementation will be given as we proceed. As of now, boundary conditions are restricted to the Dirichlet type. The noble gas argon will be used in all simulations. Since argon is treated as a perfect gas, the temperature is updated at the end of each time step via $\mathrm{T} = \varepsilon/\mathrm{c}_{\upsilon}$. For an ideal gas, however, a first order Taylor series expansion in time will first be applied to the internal energy field:

$$\varepsilon(\mathrm{T}_2) = \varepsilon(\mathrm{T}_1) + \mathrm{c}_{\upsilon}(\mathrm{T}_1)\delta\mathrm{T} + \mathcal{O}(\delta\mathrm{T}^2) \tag{237}$$

Where $\mathrm{T}_1 = \mathrm{T}(\mathbf{x}, t)$, $\mathrm{T}_2 = \mathrm{T}(\mathbf{x}, t + \delta t)$, and $\delta\mathrm{T} = \mathrm{T}_2 - \mathrm{T}_1$. As a result, the updated temperature is expressed as:

$$\mathrm{T}_2 \approx \mathrm{T}_1 + \frac{\varepsilon(\mathrm{T}_2) - \varepsilon(\mathrm{T}_1)}{\mathrm{c}_{\upsilon}(\mathrm{T}_1)} \tag{238}$$

This is the simplest approach when c_v is a nonlinear function of temperature. If desired, higher order expansions may be utilized and implemented into the algorithm.

Sod Shock Tube

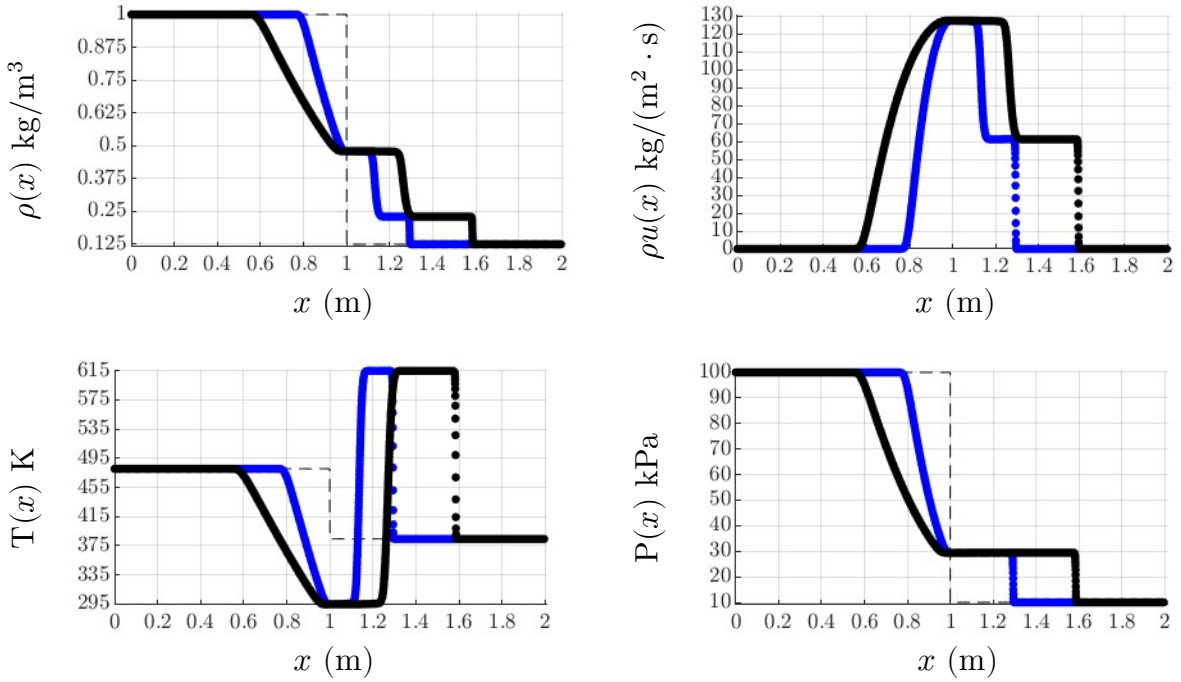

Figure 23 Sod shock tube results at $t \approx 0.5$ ms (blue) and $t \approx 1.0$ ms (black)

Let us envision a two meter long cylindrical tank located within the domain $0 \text{ m} \leq x \leq 2 \text{ m}$. An impermeable barrier exists within the tank interior located at $x = 1$ m at the initial time $t = 0$ s. Both the left region ($0 \text{ m} \leq x < 1 \text{ m}$) and the right region ($1 \text{ m} < x \leq 2 \text{ m}$) will hold in containment a stationary argon gas. The mean velocity of both regions is then $u(x, 0) = 0$. However, the mass density ratio between the two regions is $8 : 1$ and the pressure ratio is $10 : 1$. The ideal gas equation of state will be assumed valid so that $\Theta(x, 0) = v(x, 0)\text{P}(x, 0)$. This experimental setup is known as the Sod shock tube. The initial conditions used are provided below:

Left Region	Right Region
$\rho_{\text{L}}(x, 0) = 1.000 \text{ kg/m}^3$	$\rho_{\text{R}}(x, 0) = 0.125 \text{ kg/m}^3$
$\text{P}_{\text{L}}(x, 0) = 100 \text{ kPa}$	$\text{P}_{\text{R}}(x, 0) = 10 \text{ kPa}$

Table 3 Sod's initial conditions

The simulation begins with an instantaneous uniform destruction of the barrier allowing interaction of the two regions. Due to the pressure gradient, the gas within the left region will move into the right region in a systematic way governed by the one-dimensional form of the Euler equations

(135) and (136). These equations will be solved using the QVFEM over a uniform grid partitioned into two-noded phasetime line elements. If each element is given its own local coordinate system then $x_1 = 0$ and $x_2 = \delta x$ so that $\delta x = x_2 - x_1$. The basis functions are next provided as:

$$g_1 = \mathrm{C}_{11} + \mathrm{C}_{12}(x - \xi t) = 1 - (x - \xi t)/\delta x \tag{239}$$

$$g_2 = \mathrm{C}_{21} + \mathrm{C}_{22}(x - \xi t) = 0 + (x - \xi t)/\delta x \tag{240}$$

Denoting $\delta f = f_2 - f_1$, the solution over each element (per time step) takes the form:

$$\mathrm{F}(x,t) = f_1 g_1 + f_2 g_2 = f_1 + (\delta f/\delta x)(x - \xi t) \tag{241}$$

Where the temporally advanced nodal values are obtained from:

$$\mathrm{F}(x = \delta x, t = \delta t) = f_1 + (1 - \xi \delta t/\delta x)\delta f, \qquad 0 < \xi \delta t/\delta x \leq 1 \tag{242}$$

Since the grid is uniform then $\mathrm{F}(0 + \delta x, 0 + \delta t) = f_1$ thus showing the prescribed motion where $\xi = \delta x/\delta t$. The results of the simulation are shown in Figure 23 over the time interval $[0 : 1]$ ms, where the dashed black line shows the initial condition. It will be noted that $5{,}000$ spatial nodes were used, $\mathbb{m} = 21$, and 425 time steps were required.

The normal shock wave is located at $\varphi_{\mathrm{s}}(t \approx 0.5 \text{ ms}) \approx 1.29$ m and $\varphi_{\mathrm{s}}(t \approx 1.0 \text{ ms}) \approx 1.58$ m. The average shock velocity between these two times is computed as:

$$\frac{\delta \varphi_{\mathrm{s}}}{\delta t} = \frac{1.58 \text{ m} - 1.29 \text{ m}}{1.0 \text{ ms} - 0.5 \text{ ms}} = 580 \text{ m/s} \tag{243}$$

The location of the normal shock wave will next be denoted $x_{\mathrm{s}}^{\pm} = \varphi_{\mathrm{s}}(t) \pm \epsilon$ where ϵ is a "small" perturbation from the mean shock wave location φ_{s}. The average mass located at the "jump" is given by:

$$\overline{m}_{\mathrm{s}} = \int_{x_1}^{x_2} \rho \, dx = \int_{x_1}^{x_{\mathrm{s}}^-} \rho \, dx + \int_{x_{\mathrm{s}}^+}^{x_2} \rho \, dx \tag{244}$$

Where x_1 and x_2 are stationary points located upstream and downstream from the jump respectively. For an observer traveling with the shock wave, the continuity equation becomes $\mathrm{d}\overline{m}_{\mathrm{s}}/\mathrm{d}t = -(\rho_2 u_2 - \rho_1 u_1)$. Using Leibnitz's identity [11; p.69] and the fact that $\dot{x}_1 = \dot{x}_2 = 0$, we may also conclude that:

$$\mathrm{d}\overline{m}_{\mathrm{s}}/\mathrm{d}t = \rho_1 \dot{\varphi}_{\mathrm{s}} - \cancel{\rho_1 \dot{x}_1^{\,0}} + \cancel{\rho_2 \dot{x}_2^{\,0}} - \rho_2 \dot{\varphi}_{\mathrm{s}} + \cancelto{0}{\int_{x_1}^{x_{\mathrm{s}}^-} \dot{\rho} \, dx} + \cancelto{0}{\int_{x_{\mathrm{s}}^+}^{x_2} \dot{\rho} \, dx} \tag{245}$$

The last two terms vanish since the mass density does not change locally with respect to time, both upstream and downstream from the jump. The theoretical shock velocity is then computed as $\dot{\varphi}_{\mathrm{s}} = (\rho_2 u_2 - \rho_1 u_1)/(\rho_2 - \rho_1) \approx 583.3$ m/s, where $\rho_1 \approx 0.23$ kg/m^3, $\rho_2 = 0.125$ kg/m^3, $u_1 \approx 266.3$ m/s, and $u_2 = 0$ m/s. This result is in good agreement with (243) since

$|(\delta\varphi_s/\delta t - \dot{\varphi}_s)/\dot{\varphi}_s| \cdot 100\% \approx 0.57\%$. For further proof, please see Figure 24:

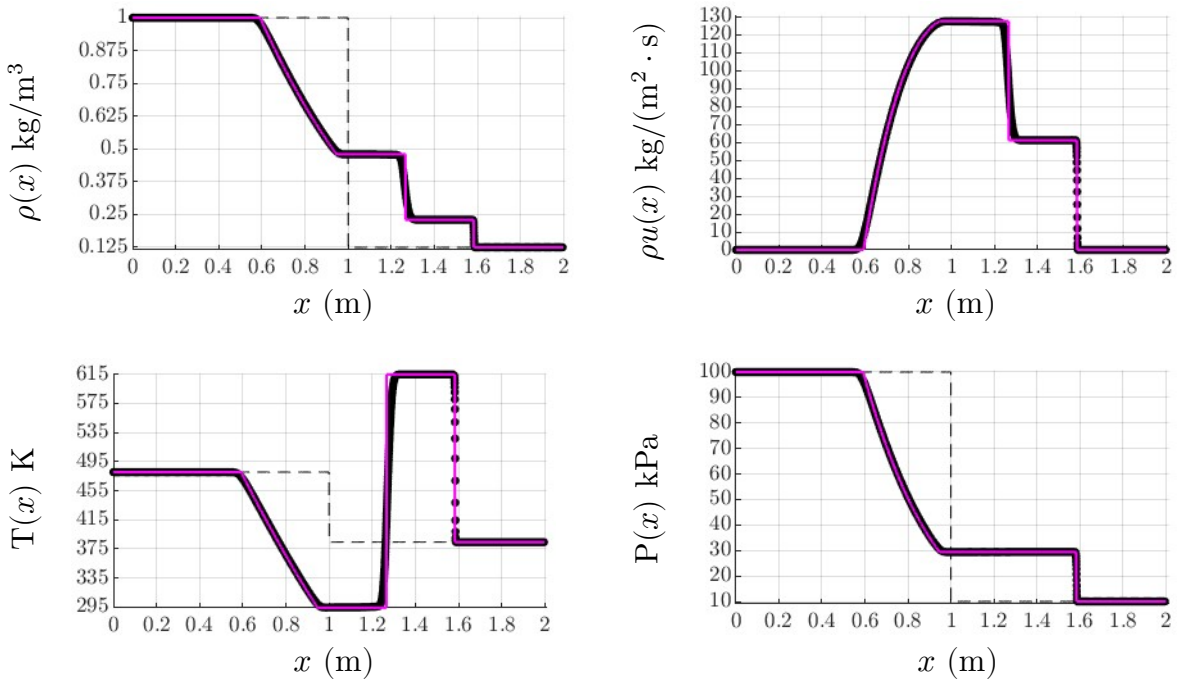

Figure 24 QVFEM prediction (black) vs. analytical solution (magenta) at $t \approx 1.0$ ms (courtesy of Virginia Notaro[10])

Now that the shock velocity has been verified, the simulation will be ran for a longer time period allowing the disturbances to reach the left and right inner walls of the tank. The boundary conditions are simply $u(0\text{ m}, t) = u(2\text{ m}, t) = 0$. The temperature and pressure at the boundaries, as functions of time, are next provided in Figure 25 over the time interval $[0 : 5]$ ms:

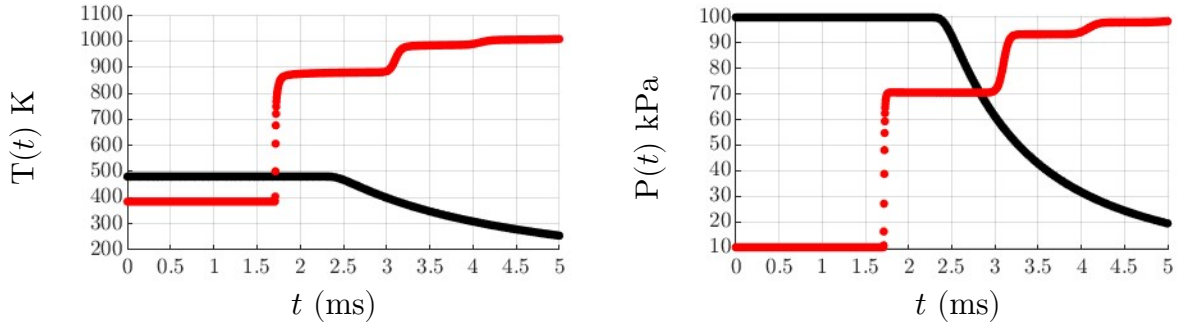

Figure 25 Temperature and pressure at $x = 0$ m (black) and $x = 2$ m (red)

In contrary to the LBM, "bounce-back" or the reflection boundary condition is not implemented at the walls which are considered impermeable and insulated. Since mass nor energy can penetrate, connectivity does not exist therefore a zero is placed within the phase matrix for the applicable

[10] https://www.mathworks.com/matlabcentral/fileexchange/48734-riemannexact-p1-rho1-u1-p4-rho4-u4-tol

distribution values located at or within the vicinity of the positions $x = 0$ m and $x = 2$ m. Upon updating the moments at the end of each time step, the normal mean velocity at the wall is manually forced to zero. This type of boundary treatment will be used throughout all numerical simulations to determine the mechanical and thermal loads acting on boundary surfaces. This type of boundary treatment has yet to be verified and is left for future investigation.

Lax-Type Shock Tube

The next simulation will model a Lax-type shock tube, which is quite similar to Sod's version. Overall, there is approximately a $9:10$ density ratio between the left and right regions and approximately a $7:1$ pressure ratio. Now, ρ_{L} is slightly less than ρ_{R} while $\mathrm{P_L} > \mathrm{P_R}$. Additionally, the left region will be set into motion at a low Mach number of 0.1, resulting in $u_{\mathrm{L}}(x,0) \approx 60$ m/s. The initial conditions are summarized in Table 4.

Left Region	Right Region
$\rho_{\mathrm{L}}(x,0) = 0.445$ kg/m^3	$\rho_{\mathrm{R}}(x,0) = 0.5$ kg/m^3
$\mathrm{M_L}(x,0) = 0.1$	$\mathrm{M_R}(x,0) = 0$
$\mathrm{P_L}(x,0) = 100$ kPa	$\mathrm{P_R}(x,0) \approx 14.3$ kPa

Table 4 Lax's initial conditions (±)

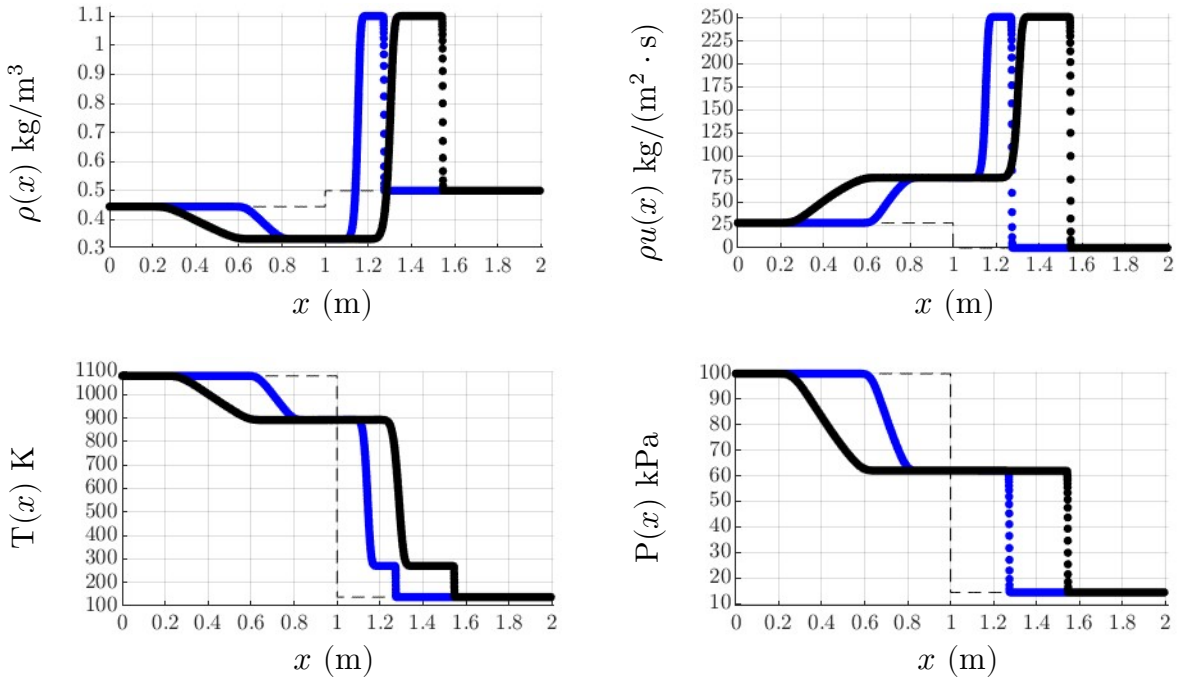

Figure 26 Lax shock tube results at $t \approx 0.65$ ms (blue) and $t \approx 1.3$ ms (black)

It will be noted that 10,000 spatial nodes were used, $\mathbb{m} = 51$, and the results shown in Figure 26 required 510 time steps. The average shock speed in this scenario is $\delta\varphi_s/\delta t \approx 418.5\ \mathrm{m/s}$ and the theoretical value is $\dot{\varphi}_s \approx 418.2\ \mathrm{m/s}$, so that $|(\delta\varphi_s/\delta t - \dot{\varphi}_s)/\dot{\varphi}_s| \cdot 100\% \approx 0.06\%$. Comparing this simulation to the prior, one may conclude that as the number of phasetime elements increase, the error decreases, as one would naturally expect.

Woodward & Colella Double Blast Wave

The next scenario to be simulated is the Woodward and Colella double blast wave problem where the initial conditions are divided up into three different regions:

$$\mathrm{P}(x,0) = 10^6\ \mathrm{Pa} \qquad 0 < x/\ell < 1/10$$

$$\mathrm{P}(x,0) = 10^1\ \mathrm{Pa} \qquad 1/10 < x/\ell < 9/10$$

$$\mathrm{P}(x,0) = 10^5\ \mathrm{Pa} \qquad 9/10 < x/\ell < 1$$

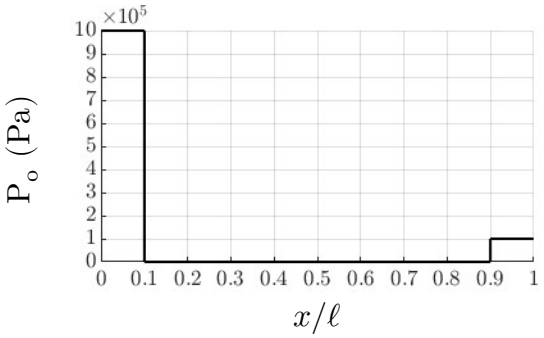

Figure 27 Woodward & Colella's initial conditions ($\ell = 2\ \mathrm{m}$)

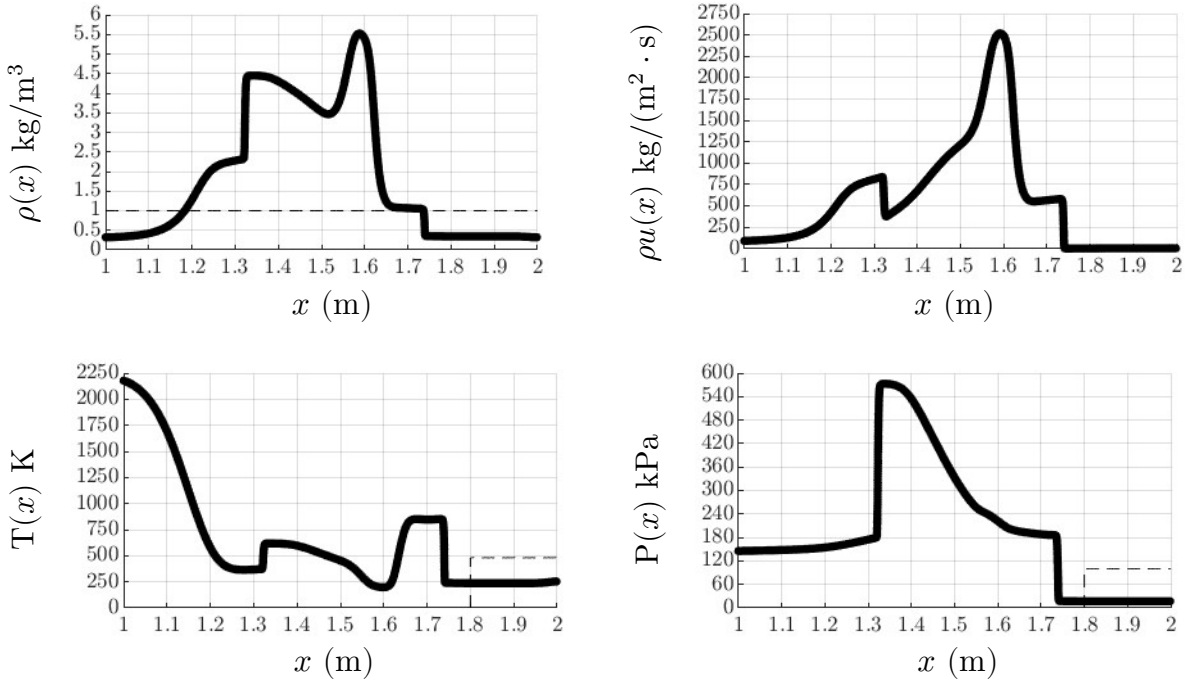

Figure 28 Woodward & Colella's double blast wave results at $t \approx 2.1\ \mathrm{ms}$

What makes this problem so challenging is the $100{,}000 : 1$ pressure ratio between the left and middle regions. For all three regions, the initial density is $\rho(x,0) = 1\ \mathrm{kg/m^3}$ and the velocity

$u(x,0) = 0 \ \mathrm{m/s}$. The velocity at the walls is once again forced to zero, 30,000 spatial nodes were used, $\mathbb{m} = 251$, and the results shown in Figure 28 required 910 time steps. The main concern here is survivability of the algorithm. The code proved satisfactory given enough phasetime information. One may compare the results to [47,62,63,64], which appear to be "smoother" than what others have calculated using other numerical methods.

Fundamental Solution to the Continuity Equation

Here, we will use the theory of continuous Fourier transforms to uncover the fundamental solution to the continuity or mass transport equation. This analytical technique will allow for a deeper understanding of the FBE and why the proposed solutions work as well as they do. To begin, we will introduce the complex propagating wave function $\psi(\boldsymbol{k}, \mathbf{x}, t) = \exp[i(\boldsymbol{k} \cdot \mathbf{x} - \omega t)]$. To solve the FBE, the solution prototype is given as $\mathrm{F}(\boldsymbol{k}, \mathbf{x}, t) = \mathrm{A}(\boldsymbol{k})\psi(\boldsymbol{k}, \mathbf{x}, t)$, where A is the amplitude coefficient having dependence upon the wave numbers. Upon substituting F into the FBE, the dispersion relation is obtained as $\omega(\boldsymbol{k}) = \boldsymbol{k} \cdot \boldsymbol{\xi}$. For the fundamental solution, we set the initial condition to $\mathrm{F}_{\mathrm{o}}(\mathbf{x}) = \hat{\rho}_{\mathrm{o}}\delta(\mathbf{x})$, where $\delta(\mathbf{x})$ is the Dirac delta function centered about $\mathbf{x} = \mathbf{0}$ and $\hat{\rho}_{\mathrm{o}}$ is the initial mass density velocity distribution. The amplitude and total solution for F are obtained from the following CIFT and CFT respectively:

$$\mathrm{A}(\boldsymbol{k}) = \frac{1}{(2\pi)^3} \int_{\mathbb{R}^3} \mathrm{F}_{\mathrm{o}}(\mathbf{x}) \psi_{\mathrm{o}}^{*}(\boldsymbol{k}, \mathbf{x}) \, d\mathcal{X} = \frac{\hat{\rho}_{\mathrm{o}}}{(2\pi)^3} \tag{246}$$

$$\mathrm{F}(\mathbf{x}, t) = \int_{\mathbb{R}^3} \mathrm{A}(\boldsymbol{k}) \psi(\boldsymbol{k}, \mathbf{x}, t) \, d\mathcal{K} = \hat{\rho}_{\mathrm{o}} \delta(\mathbf{x} - \boldsymbol{\xi} t) \tag{247}$$

As one can observe, the inverse mapping (143) reappears in the solution. The final solution for the mass density is then found through generating the zeroth order moment over the velocity space:

$$\rho(\mathbf{x}, t) = \int_{\mathbb{R}^3} \mathrm{F}(\boldsymbol{\xi}, \mathbf{x}, t) \, d\Xi = \frac{\rho_{\mathrm{o}}}{(2\pi\Theta_{\mathrm{o}} t^2)^{3/2}} \exp\left(-\frac{1}{2\Theta_{\mathrm{o}} t^2} |\mathbf{x} - \mathbf{v}_{\mathrm{o}} t|^2 \right) \tag{248}$$

Where the law of constancy of mass is satisfied through integrating over the infinite Euclidean space:

$$\rho_{\mathrm{o}} = \int_{\mathbb{R}^3} \rho(\mathbf{x}, t) \, d\mathcal{X} \tag{249}$$

The associated velocity field can be found through computing the first order moment over the velocity space:

$$\mathbf{v}(\mathbf{x}, t) = v(\mathbf{x}, t) \int_{\mathbb{R}^3} \boldsymbol{\xi} \mathrm{F}(\boldsymbol{\xi}, \mathbf{x}, t) \, d\Xi = \mathbf{x}/t \tag{250}$$

In conclusion, the solution (248) represents the convection process of a point mass dropped within an infinite domain, where the Gaussian is subjected to both advection and diffusion processes:

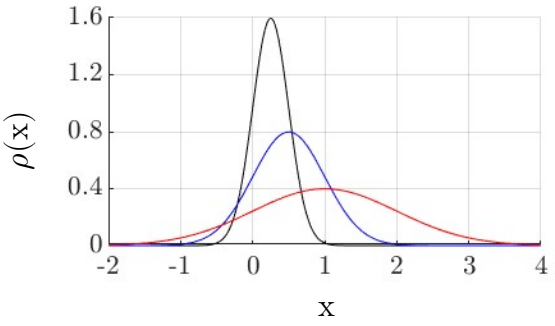

Figure 29 Time evolution of an initial point mass density (black → blue → red)

In conclusion, the dissipation is already included within the framework of the QVFEM, which stems from the use of the velocity distribution; derived ab initio. Therefore, there is no need to include artificial dissipation terms into the governing equations of motion.

Acceleration

Up to now, we have shown that the QVFEM algorithm outputs high-precision accuracy and has the ability to remain stable even throughout the presence of a "strong" shock wave. This final benchmark test case will reach the hypersonic regime through accelerating a flowfield from rest into a stationary wall. The acceleration rate will be constant and the approximation (154) will be utilized, therefore:

$$\mathrm{F}(x,t) \approx [f_1 + (\delta f/\delta x)(x - \xi t)] \exp[(\xi - u)\beta a t] \tag{251}$$

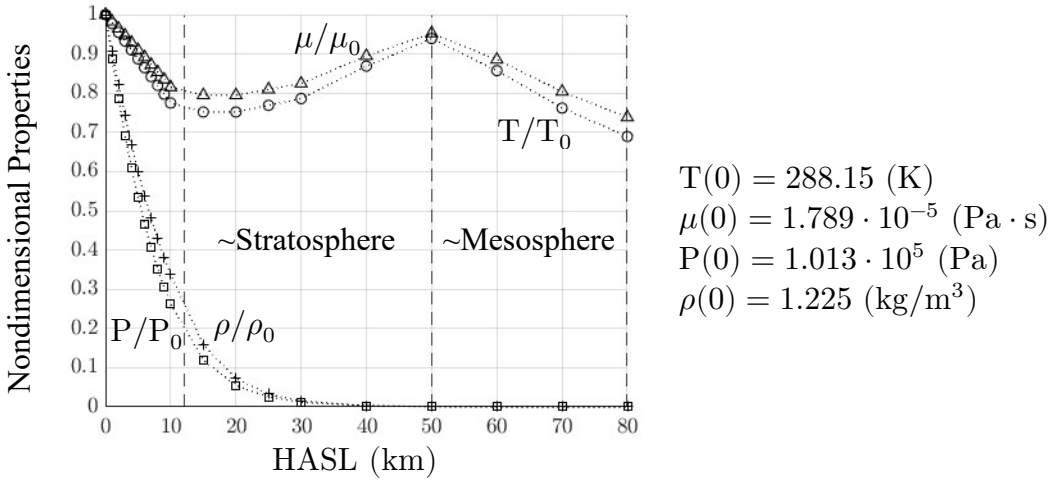

Figure 30 US standard atmosphere vs altitude (data source: The Engineering Toolbox[11])

The initial conditions will be chosen to mimic high-speed flight within Earth's atmosphere; see Figure 30. In regards to the supersonic and hypersonic flight regimes, it is most optimal to fly within regions where the density is the lowest to minimize the mechanical and thermal loads.

[11] https://www.engineeringtoolbox.com/standard-atmosphere-d_604.html

Therefore, the flight elevation above sea level will be set to $30\ \text{km} \approx 100{,}000\ \text{ft}$, where $\rho(30\ \text{km}) \approx 0.02\ \ \text{kg/m}^3$ and $\text{P}(30\ \text{km}) \approx 1{,}200\ \text{Pa}$. For sake of simplicity, argon will remain the gas of analysis. Again, a one-dimensional flow will be accelerated from rest into a stationary wall, located at $x = 2\ \text{m}$, at an aggressive rate of $a = +10^6\ \ \text{m/s}^2$. The results of the simulation are shown in Figure 31. Since the flow is accelerating to the right into the wall, a normal shock wave is produced which travels to the left, away from the wall, while increasing in magnitude. For these computations, 10,000 spatial nodes were used, $\mathbb{m} = 99$, and the total number of time steps required was 2,000. The maximum Mach number achieved at $t \approx 4.0\ \text{ms}$ was almost 13.

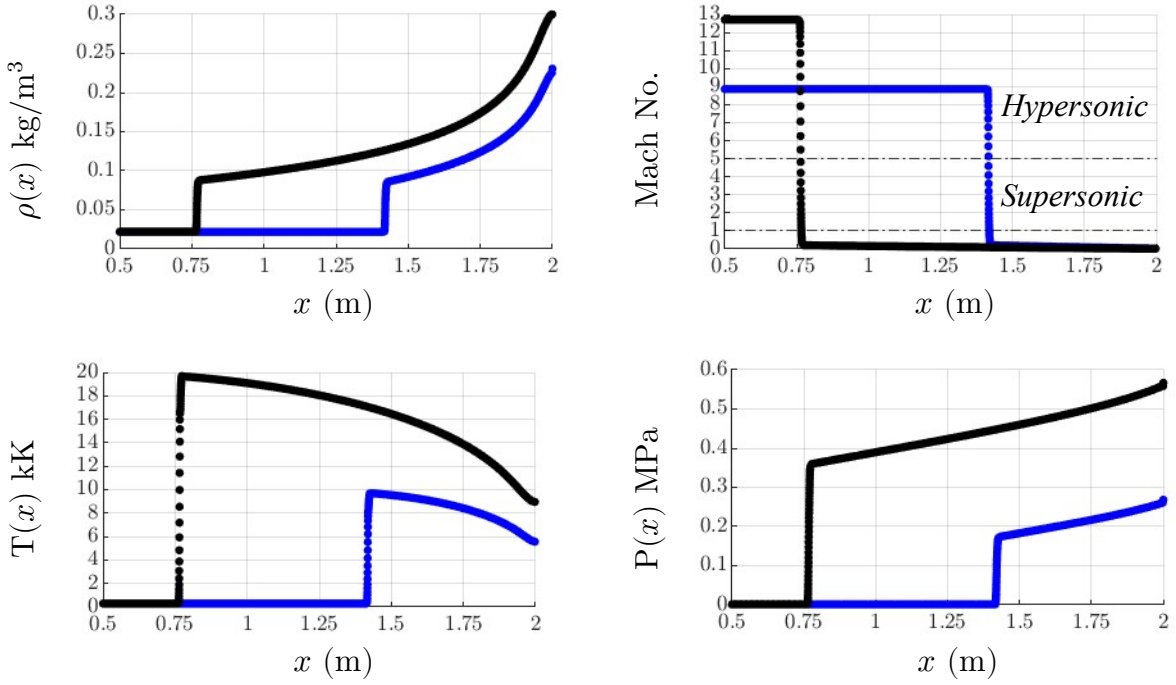

Figure 31 Accelerated flow into wall (RHS) at $t \approx 2.8\ \text{ms}$ (blue) and $t \approx 4.0\ \text{ms}$ (black)

2D Phasetime Element

Future work will include two-dimensional flowfield studies simulated using the QVFEM. The one-dimensional studies were run on my personal desktop computer. However, it will be most optimal to run the 2D test cases on a cluster of high-performance computers. One benefit is that the QVFEM has the same parallelization capabilities as that of the LBM. We will end this chapter by analyzing the nonlinear solution over a 2D quadrilateral element; see Figure 11. The four basis functions are then collected according to Pascal's triangle, provided in the general form:

$$g_i = \text{C}_{i1} + \text{C}_{i2}(x - ut) + \text{C}_{i3}(y - vt) + \text{C}_{i4}(x - ut)(y - vt)\ \ \forall\ i = 1{,}2{,}3{,}4 \tag{252}$$

Where the velocities have been denoted $\xi_1 = u$ and $\xi_2 = v$. Using a local coordinate system for a rectangular element of size $\delta x \times \delta y$, the basis functions are provided as:

$$g_1 = (x - ut)(y - vt)/\delta a - (x - ut)/\delta x - (y - vt)/\delta y + 1 \tag{253}$$

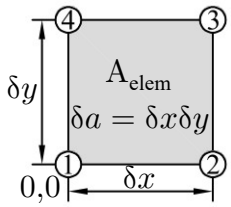

$$g_2 = (x - ut)/\delta x - (x - ut)(y - vt)/\delta a \tag{254}$$

$$g_3 = (x - ut)(y - vt)/\delta a \tag{255}$$

$$g_4 = (y - vt)/\delta y - (x - ut)(y - vt)/\delta a \tag{256}$$

The solution over the phasetime element is then given by:

$$\mathrm{F}(x, y, t) = f_1 g_1 + f_2 g_2 + f_3 g_3 + f_4 g_4 \tag{257}$$

$$= f_1 + \frac{1}{\delta x}(f_2 - f_1)(x - ut) + \frac{1}{\delta y}(f_4 - f_1)(y - vt) + \frac{1}{\delta a}(f_1 - f_2 + f_3 - f_4)(x - ut)(y - vt)$$

The updated value at node #3 is $\mathrm{F}(\delta x, \delta y, \delta t)$, provided as:

$$f_1 + (f_2 - f_1)(1 - \mathtt{C}_x) + (f_4 - f_1)(1 - \mathtt{C}_y) + (f_1 - f_2 + f_3 - f_4)(1 - \mathtt{C}_x)(1 - \mathtt{C}_y) \tag{258}$$

Where the Courant numbers are defined as $\mathtt{C}_x = u\delta t/\delta x$ and $\mathtt{C}_y = v\delta t/\delta y$, which are governed by the constraint (87). If the grid spacing is completely uniform meaning $\delta x = \delta y$, then $\mathtt{C}_x = \mathtt{C}_y = 1$ and $\mathrm{F}(u\delta t, v\delta t, \delta t) = f_1$. If $u = 0$ or $v = 0$, the quadrilateral reduces down to a line element.

3.10 Concluding Remarks

We have thus concluded the foundational framework of the QVFEM. The next chapter will extend the framework over to the Navier-Stokes-Fourier equations. Before doing so, we will lastly discuss the differences between a traditional spacetime finite element formulation and the newly proposed methodology. Beginning with the EOM: $\dot{\mathrm{F}} + \mathfrak{A}[\mathrm{F}] = \mho$, the solution will first be expanded in the more traditional style as $\mathrm{F}(\mathbf{x}, t) = f_i(t)\psi_i(\mathbf{x})$. In this way, space and time are being treated independently in a sense when compared to the expansion used in ch.3.4, i.e. $f_i\psi_i(\mathbf{x}, t)$. Upon substituting, multiplying by $\phi_j(\mathbf{x})$, then integrating over the entire spatial domain, one obtains:

$$\dot{f}_i \int_V \psi_i \phi_j \, d\text{⇿} + f_i \int_V \mathfrak{A}[\psi_i]\phi_j \, d\text{⇿} = \int_V \mho \phi_j \, d\text{⇿} \tag{259}$$

Whose compact matrix form is $\mathrm{A}_{ji}\dot{f}_i + \mathrm{B}_{ji} f_i = \mathrm{c}_j$ or $\mathbf{A} \cdot \dot{\boldsymbol{f}} + \mathbf{B} \cdot \boldsymbol{f} = \mathbf{c}$. Since this is a global approach, the domain and weak form (259) must be partitioned into a system of finite elements, where the nodal values are computed simultaneously. However, the methodology presented in ch.3.4 is a local approach where one node per element is updated based on a stationary potential. If the Galerkin method is used, then the integration bounds do not encompass the entire element but the effective volume, which is a function of time; see (160).

From here, there are two different routes which can be taken. One option is to set $\mho = 0$ so that $\dot{\boldsymbol{f}} = -\mathbf{A}^{-1} \cdot (\mathbf{B} \cdot \boldsymbol{f})$, apply a finite difference scheme to the temporal derivative, then time-march within the algorithm. Alternatively, one could extend the spatial mesh to a spacetime mesh through

setting $f_i(t) = \mathrm{F}_{ik}\zeta_k(t)$. We will next multiply (259) by $\eta_l(t)$, then integrate over all time [65]:

$$\mathrm{F}_{ik}\int_T \dot{\zeta}_k\eta_l\,dt\int_V \psi_i\phi_j\,d\text{-}\!\!\!\text{v} + \mathrm{F}_{ik}\int_T \zeta_k\eta_l\,dt\int_V \mathfrak{A}[\psi_i]\phi_j\,d\text{-}\!\!\!\text{v} = \int_T\int_V \mho\phi_j\eta_l\,d\text{-}\!\!\!\text{v}\,dt \tag{260}$$

Whose compact matrix form is $\mathrm{F}_{ik}(\mathrm{A}_{ji}\mathrm{D}_{kl} + \mathrm{B}_{ji}\mathrm{E}_{kl}) = \mathrm{C}_{jl}$. To solve for all nodal values simultaneously, boundary and initial conditions must be applied then a rank four matrix must be inverted. If the integration is over a time step, then we can time march, for example:

$$\mathrm{F}_{i2} = (\mathrm{A}_{ji}\mathrm{D}_{2l} + \mathrm{B}_{ji}\mathrm{E}_{2l})^{-1}(\mathrm{C}_{jl} - (\mathrm{A}_{ji}\mathrm{D}_{1l} + \mathrm{B}_{ji}\mathrm{E}_{1l})\mathrm{F}_{i1}) \tag{261}$$

On a final note, the QVFEM is not a general finite element methodology and was specifically developed to solve the Euler and Navier-Stokes-Fourier equations. This newly proposed nontraditional framework is a result of the mathematical structure of these equations and the vast landscape of code-friendly analytical solutions.

Chapter 4 – The QVFEM: Part II

The QVFEM was established in Part I with application to Euler's equations of motion for matter in an ideal gaseous state. Part II will extend the framework to incorporate nonequilibrium phenomena including viscous dissipation and thermal conduction. In consequence, the momentum transport equations will now take the form of the Navier-Stokes equations. Additionally, the energy transport equation will now take the form of the Navier-Stokes-Fourier equation containing the stress-flux and heat flux vectors. We can consider the evolutions brought upon by the Euler equations, a first order approximation to the Boltzmann equation. Therefore in this work, a second order approximation will be established theoretically then bridged over into a high-fidelity computational framework.

4.1 Introduction to the Second Order Equations of Motion

To begin, the generalized Eulerian field equations, representative of transport processes, will herein be reviewed. Considering a chemically reacting gas mixture, the species mass transport equations are provided in the form [55]:

$$\dot{\rho}_{\mathscr{j}} + \boldsymbol{\nabla} \cdot (\rho_{\mathscr{j}} \mathbf{v}) = \boldsymbol{\nabla} \cdot (\rho d_{\mathscr{j}} \boldsymbol{\nabla} f_{\mathscr{j}}) + \dot{\wp}_{\mathscr{j}} \;\forall\; \mathscr{j} = 1,2,\dots,n_{\text{sp}} \tag{262}$$

Where the subscript $\mathscr{j}$ indicates the chemical species, $d_{\mathscr{j}}\ (\mathrm{m}^2/\mathrm{s})$ is the mass diffusion coefficient (from Fick's law), $f_{\mathscr{j}} = \upsilon \rho_{\mathscr{j}}$ is the concentration or mass ratio subjected to the constraint $f_1 + f_2 + \cdots + f_{n_{\text{sp}}} = 1$, and $\dot{\wp}_{\mathscr{j}}$ is the mass rate of production due to chemical reactions. The mass density of each individual species is defined from the mass relation $\rho_{\mathscr{j}} \upsilon = m_{\mathscr{j}} n_{\mathscr{j}}$ (no summation) which may also be expressed in terms of the concentration as $\rho_{\mathscr{j}} = \rho f_{\mathscr{j}}$. The total mass density may then be found through summing each individual species density:

$$\rho = \textstyle\sum_{\mathscr{j}} \rho_{\mathscr{j}} = \upsilon^{-1} \sum_{\mathscr{j}} m_{\mathscr{j}} n_{\mathscr{j}} = \rho \sum_{\mathscr{j}} f_{\mathscr{j}} \tag{263}$$

It is critical to note that (262) upholds the condition of constancy of mass, or in other words, the nonrelativistic physical law of mass conservation [20; ch.13]; first discovered by the French chemist Antoine Lavoisier (1743-1794). This simply means that mass is neither created nor destroyed; only subjected to change in form while at rest or during transmission between one location in space to another over time. In this work, a conserved quantity will be defined as a physical property, which when interacting with the environment (in an open system), is technically fully traceable within the structure of spacetime. In other words, from a Newtonian perspective, the conserved information carried by the advection stream is a constant of the motion so may only change in form as carried from one point in spacetime to another, i.e. $\dot{\rho}_{\text{o}} = 0$. In consequence, the summation over all species in (262) recovers the mass continuity equation:

$$\dot{\rho} + \boldsymbol{\nabla} \cdot (\rho \mathbf{v}) = \textstyle\sum_{\mathscr{j}} \dot{\rho}_{\mathscr{j}} + \boldsymbol{\nabla} \cdot \sum_{\mathscr{j}} (\rho_{\mathscr{j}} \mathbf{v}) = \boldsymbol{\nabla} \cdot \sum_{\mathscr{j}} (\rho d_{\mathscr{j}} \boldsymbol{\nabla} f_{\mathscr{j}}) + \sum_{\mathscr{j}} \dot{\wp}_{\mathscr{j}} = 0 \tag{264}$$

Here within Part II, chemical reactions and species diffusion will both be neglected. However, the above EOM is presented to compare the evolution of the mass field, a truly conserved quantity

within the nonrelativistic model, to the evolutions of the mean momentum, energy, and entropy fields which in actuality are subjected to nonconservative changes. This is due to phenomena such as viscous interactions (nonconservative forces) and thermal conduction which both contribute to the total entropy generated within the system. For example, one of Joseph Fourier's (1768-1830) axioms of heat conduction states [56; ch.1]:

> "*When heat is unequally distributed among the different parts of a solid mass, it tends to attain equilibrium, and passes slowly from the parts which are more heated to those which are less; and at the same time it is dissipated at the surface, and lost in the medium or in the void.*"

With this being said, the general formulation modeling the transport of mass, momentum, energy, and entropy (excluding body forces and heat sources) are next provided respectively [46; ch.4]:

$$\frac{\partial \rho}{\partial t} + \frac{\partial \rho \mathrm{v}_i}{\partial \mathrm{x}_i} = 0, \qquad \frac{\partial \rho \mathrm{v}_i}{\partial t} + \frac{\partial \rho \mathrm{v}_i \mathrm{v}_l}{\partial \mathrm{x}_l} + \frac{\partial \Sigma_{il}}{\partial \mathrm{x}_l} = 0 \tag{265}$$

$$\frac{\partial \rho e}{\partial t} + \frac{\partial \rho e \mathrm{v}_i}{\partial \mathrm{x}_i} + \frac{\partial \Sigma_{il} \mathrm{v}_l}{\partial \mathrm{x}_i} + \frac{\partial \mathrm{q}_i}{\partial \mathrm{x}_i} = 0, \qquad \frac{\partial \rho \mathrm{s}}{\partial t} + \frac{\partial \rho \mathrm{s} \mathrm{v}_i}{\partial \mathrm{x}_i} + \frac{\partial \Phi_i}{\partial \mathrm{x}_i} = \dot{\$} \tag{266}$$

Where $\boldsymbol{\Sigma} = \boldsymbol{\Sigma}^{\mathsf{T}}$ is the generalized total stress tensor, $\mathbf{q}$ $(\mathrm{kg/s^3})$ is the generalized heat flux vector which is associated with the generalized heat-entropy flux vector $\boldsymbol{\Phi}$, and $\dot{\$}$ indicates the total rate at which entropy is generated or produced within the system. The mass, momentum, and energy evolutions are subjected to equality relations due to the law of mass continuity [20; ch.13], Newton's laws of motion [1; Book I], and the first law of thermodynamics (1st LoT) [45; ch.26]. These are known as balance laws which are governed by the Reynolds transport theorem, therefore may be written in the general form $\dot{f}_i = -\nabla_l \mathrm{G}_{il}$. Integrating over the control volume then brings about the divergence theorem:

$$\frac{\partial}{\partial t} \int_{\mathcal{V}} f_i \, d\mathrm{V} = - \int_{\mathcal{A}} \delta \mathrm{G}_{il} \, d\mathrm{A}_l \tag{267}$$

So that the temporal rate of change in the total mass, momentum, and energy contained within may be expressed as the cumulative sum of the fluxes acting through each bounding control surface:

$$\dot{m}^{(\mathcal{V})} = \frac{\partial}{\partial t} \int_{\mathcal{V}} \rho \, d\mathrm{V} = - \int_{\mathcal{A}} \delta(\rho \mathrm{v}_i) \, d\mathrm{A}_i \tag{268}$$

$$\dot{\mathrm{p}}_i^{(\mathcal{V})} = \frac{\partial}{\partial t} \int_{\mathcal{V}} \rho \mathrm{v}_i \, d\mathrm{V} = - \int_{\mathcal{A}} \delta(\rho \mathrm{v}_i \mathrm{v}_l + \Sigma_{il}) \, d\mathrm{A}_l \tag{269}$$

$$\dot{\mathrm{E}}^{(\mathcal{V})} = \frac{\partial}{\partial t} \int_{\mathcal{V}} \rho e \, d\mathrm{V} = - \int_{\mathcal{A}} \delta(\rho e \mathrm{v}_i + \Sigma_{il} \mathrm{v}_l + \mathrm{q}_i) \, d\mathrm{A}_i \tag{270}$$

The entropy however, due to the existence of stress and heat flow, is said to be in a state of imbalance. Therefore, the entropy evolution must satisfy the inequality $\dot{\$} \geq 0$ under the second

law of thermodynamics (2nd LoT) [45; ch.27]. The mapping derivative of the mass density remains $\mathrm{d}\rho/\mathrm{d}t = -\rho\nabla_i \mathrm{v}_i$, however, the MD of the velocity, internal energy, and entropy are now:

$$\mathrm{d}\mathrm{v}_i/\mathrm{d}t = -\upsilon\nabla_l \Sigma_{il} \tag{271}$$

$$\mathrm{d}\varepsilon/\mathrm{d}t = -\upsilon(\Sigma_{il}\nabla_i \mathrm{v}_l + \nabla_i \mathrm{q}_i) \tag{272}$$

$$\mathrm{d}\mathrm{s}/\mathrm{d}t = -\upsilon(\nabla_i \Phi_i - \dot{\$}) \tag{273}$$

Which are found from (265-266). From the 2nd LoT, it is also claimed that heat and entropy both flow in the same direction. In consequence, it is postulated that $\mathrm{q}_i = \mathrm{T}\Phi_i$. Well from $\Phi_i = \mathrm{q}_i/\mathrm{T}$, then $\mathrm{T}\nabla_i \Phi_i = \nabla_i \mathrm{q}_i - \mathrm{q}_i \nabla_i \ln \mathrm{T}$, which would then entail:

$$-\upsilon\nabla_i \mathrm{q}_i = \mathrm{T}\mathrm{d}\mathrm{s}/\mathrm{d}t - \upsilon\big(\mathrm{q}_i \nabla_i \ln \mathrm{T} + \mathrm{T}\dot{\$}\big) = \mathrm{d}\varepsilon/\mathrm{d}t + \upsilon\Sigma_{il}\nabla_i \mathrm{v}_l \tag{274}$$

From which the following total differential relation is obtained:

$$\mathrm{d}\varepsilon = \mathrm{T}\mathrm{d}\mathrm{s} - \upsilon\big(\Sigma_{il}\nabla_i \mathrm{v}_l + \mathrm{q}_i \nabla_i \ln \mathrm{T} + \mathrm{T}\dot{\$}\big)\mathrm{d}t \tag{275}$$

Upon defining $\Sigma_{il} = \mathrm{P}\delta_{il} - \sigma_{il}$, where $\sigma_{il} = \sigma_{li}$ is the generalized viscous stress tensor, and noting that $\mathrm{d}\upsilon = \upsilon\nabla_i \mathrm{v}_i \mathrm{d}t$, the total differential of the internal energy (275) may be reformed into:

$$\mathrm{d}\varepsilon = \mathrm{T}\mathrm{d}\mathrm{s} - \mathrm{P}\mathrm{d}\upsilon + \upsilon\big(\sigma_{il}\nabla_i \mathrm{v}_l - \mathrm{q}_i \nabla_i \ln \mathrm{T} - \mathrm{T}\dot{\$}\big)\mathrm{d}t \tag{276}$$

Based on Fourier's axioms of heat conduction [19; p.7], the heat flux vector will next be defined as $\mathrm{q}_i = -\kappa\nabla_i \mathrm{T}$, where $\kappa\ (\mathrm{kg/K}) \cdot (\mathrm{m/s}^3)$ is the coefficient of thermal conductivity. The heat-entropy flux vector may now be written as $\Phi_i = -\kappa\nabla_i \ln \mathrm{T}$. In consequence, the entropy evolution takes on a form of the Clausius-Duhem inequality [46; p.169]:

$$\dot{\$} = \rho\mathrm{d}\mathrm{s}/\mathrm{d}t - \nabla_i(\kappa\nabla_i \ln \mathrm{T}) \geq 0 \tag{277}$$

Where the 2nd LoT states that the above difference must always be nonnegative. To satisfy the 1st LoT through recovering the Gibbs relation, it will be postulated that the total rate of entropy production must be:

$$\dot{\$} = \sigma_{il}(\nabla_i \mathrm{v}_l)\mathrm{T}^{-1} + \kappa|\boldsymbol{\nabla} \ln \mathrm{T}|^2 \tag{278}$$

Well the term $\kappa^{-1}|\boldsymbol{\Phi}|^2 = \kappa|\boldsymbol{\nabla} \ln \mathrm{T}|^2$ is always positive ✓. We must now require the contraction $\sigma_{il}\nabla_i \mathrm{v}_l$ to also yield strictly positive values. This thermodynamic restriction will be revisited upon deriving the viscous stress tensor. The MD of the entropy field may now be expressed in the form:

$$\mathrm{d}\mathrm{s}/\mathrm{d}t = \upsilon(\sigma_{il}\nabla_i \mathrm{v}_l - \nabla_i \mathrm{q}_i)\mathrm{T}^{-1} \tag{279}$$

What has been presented thus far is a general overview of the relevant continuum mechanics and thermodynamics. The equations of motion and constitutive relations will next be derived in a more

rigorous fashion based on the study of statistical mechanics; in contrary to the Coleman-Noll procedure [45; ch.39].

4.2 Theoretical Framework

The Navier-Stokes-Fourier equations will be derived directly from the Euler equations utilized in chapter 3, therefore Part II is a direct extension of Part I. The method presented was inspired by [23] however a direct recovery of the governing evolution equations will herein be sought after. The MD will first be recast as a variation over the finite time interval δt. So, the variational time and position vector field will be defined respectively as $t^* = t + \epsilon\delta t$ and $\mathbf{x}^* = \mathbf{x} + \epsilon\boldsymbol{\xi}\delta t$. The perturbed distribution is then denoted $\mathrm{F}^* = \mathrm{F}(\mathbf{x} + \epsilon\boldsymbol{\xi}\delta t, t + \epsilon\delta t)$. The directional derivative of the generalized distribution may now be found through applying the Gâteaux operator [46; p.46-47, 372-374]:

$$\mathfrak{D}\mathrm{F} = (\mathrm{d}\mathrm{F}^*/\mathrm{d}\epsilon)|_{\epsilon=0} = (\dot{\mathrm{F}} + \xi_i\nabla_i\mathrm{F})\delta t \tag{280}$$

In consequence, we may conclude that $\mathrm{d}\mathrm{F}/\mathrm{d}t = \mathfrak{D}\mathrm{F}/\delta t$, where cross multiplying yields $\mathrm{d}\mathrm{F}\delta t = \mathfrak{D}\mathrm{F}\mathrm{d}t$. If $\mathfrak{D}\mathrm{F}$ is independent of time, then upon integration, one finds $\delta\mathrm{F} = \mathfrak{D}\mathrm{F}$, otherwise:

$$\delta\mathrm{F} = \frac{1}{\delta t}\int_{t_1}^{t_2}\mathfrak{D}\mathrm{F}\,\mathrm{d}t = \int_{t_1}^{t_2}(\dot{\mathrm{F}} + \xi_i\nabla_i\mathrm{F})\,\mathrm{d}t \tag{281}$$

The variation in the distribution will be related to a generalized change via the master relation:

$$\Delta[\![\mathrm{F}]\!] = \epsilon\mathfrak{D}\mathrm{F} \tag{282}$$

An alternate formulation is taken from Chapman and Enskog [15; ch.7]: $\epsilon\mathrm{d}\mathrm{F} = \mathscr{J}[\mathrm{F},\mathrm{G}]\mathrm{d}t$, where $\mathscr{J}[\mathrm{F},\mathrm{G}]$ represents the two-body Boltzmann collision integral. Following this work, we will enforce the constraints: $\overrightarrow{\Delta}[\![\hat{\rho}]\!] \equiv 0$, $\overrightarrow{\Delta}[\![\hat{\mathbf{p}}]\!] \equiv \mathbf{0}$, and $\overrightarrow{\Delta}[\![\hat{\mathrm{E}}]\!] \equiv 0$. These conditions of solubility are enforced to uphold the established balance laws of mass, momentum, and energy. The generalized distribution F and the operator $\mathfrak{D}$ will next be expanded using the following perturbation series:

$$\mathrm{F} = \mathrm{F}^{\mathbb{0}} + \epsilon\mathrm{F}^{\mathbb{1}} + \epsilon^2\mathrm{F}^{\mathbb{2}} + \mathcal{O}(\epsilon^3) \tag{283}$$

$$\epsilon\mathfrak{D} = \epsilon\mathfrak{D}_{\mathbb{1}} + \epsilon^2\mathfrak{D}_{\mathbb{2}} + \mathcal{O}(\epsilon^3) \tag{284}$$

$$\epsilon\mathfrak{D}\mathrm{F} = \epsilon\mathfrak{D}_{\mathbb{1}}\mathrm{F}^{\mathbb{0}} + \epsilon^2(\mathfrak{D}_{\mathbb{2}}\mathrm{F}^{\mathbb{0}} + \mathfrak{D}_{\mathbb{1}}\mathrm{F}^{\mathbb{1}}) + \mathcal{O}(\epsilon^3) \tag{285}$$

The notation $\mathrm{F}^{\mathbb{0}}$ refers to the equilibrium distributions utilized in Part I:

$$\hat{\rho}^{\mathbb{0}} = \rho\zeta_{\mathrm{tr}}^{-1}\exp(-\tfrac{1}{2}\beta|\dot{\boldsymbol{q}}|^2) \tag{286}$$

$$\hat{\mathbf{p}}^{\mathbb{0}} = \hat{\rho}^{\mathbb{0}}\boldsymbol{\xi} \tag{287}$$

$$\hat{\upsilon}^{\mathbb{0}}\hat{\mathrm{E}}^{\mathbb{0}} = \tfrac{1}{2}|\boldsymbol{\xi}|^2 + \overline{\varepsilon} \tag{288}$$

$$\hat{\upsilon}^{\mathbb{0}}\hat{\mathrm{S}}^{\mathbb{0}} = R\ln\upsilon\zeta + (\tfrac{1}{2}|\dot{\boldsymbol{q}}|^2 + \overline{\varepsilon})\mathrm{T}^{-1} \tag{289}$$

The notation $\mathrm{F}^{\mathbb{1}}$ indicates the first perturbation from equilibrium, which must satisfy the solubility constraints: $\vec{\rho}^{\mathbb{1}} = 0$, $\vec{\mathbf{p}}^{\mathbb{1}} = \mathbf{0}$, $\vec{\mathrm{E}}^{\mathbb{1}} = 0$, and $\vec{\mathrm{S}}^{\mathbb{1}} = 0$. Based on (280), the variations are:

$$\mathfrak{D}_{\mathbb{I}}\mathrm{F} = (\partial_{\mathbb{I}}\mathrm{F} + \xi_i\nabla_i\mathrm{F})\delta t \;\forall\; \mathbb{I} = 1{,}2 \tag{290}$$

Where the subscript $\mathbb{1}$ simply refers to the isentropic evolutions provided by the Euler equations and the subscript $\mathbb{2}$ refers to an evolution involving entropy production. For ease of notation, the partial temporal derivatives are written as $\partial_{\mathbb{I}}\mathrm{F} = \partial_{\mathbb{I}}\mathrm{F}/\partial t \;\forall\; \mathbb{I} = 1{,}2$. It will be noted that these derivatives do not indicate different time scales but varying levels of description regarding transport processes. Substituting (283) and (285) into (282) obtains:

$$\epsilon\mathfrak{D}_{\mathbb{1}}\mathrm{F}^{\mathbb{0}} + \epsilon^2(\mathfrak{D}_{\mathbb{2}}\mathrm{F}^{\mathbb{0}} + \mathfrak{D}_{\mathbb{1}}\mathrm{F}^{\mathbb{1}}) = \Delta[\![\mathrm{F}^{\mathbb{0}} + \epsilon\mathrm{F}^{\mathbb{1}} + \epsilon^2\mathrm{F}^{\mathbb{2}}]\!] \tag{291}$$

The varying orders of ϵ will be separated from 0^{th} to 2^{nd} order to obtain the following hierarchy:

$$\mathcal{O}(\epsilon^0)\text{:} \qquad \Delta[\![\mathrm{F}^{\mathbb{0}}]\!] = 0 \tag{292}$$

$$\mathcal{O}(\epsilon^1)\text{:} \qquad \mathfrak{D}_{\mathbb{1}}\mathrm{F}^{\mathbb{0}} = \Delta[\![\mathrm{F}^{\mathbb{1}}]\!] \tag{293}$$

$$\mathcal{O}(\epsilon^2)\text{:} \qquad \mathfrak{D}_{\mathbb{2}}\mathrm{F}^{\mathbb{0}} + \mathfrak{D}_{\mathbb{1}}\mathrm{F}^{\mathbb{1}} = \Delta[\![\mathrm{F}^{\mathbb{2}}]\!] \tag{294}$$

Overall, the velocity distribution is derived from solving (292), which is then fed into (293) to uncover the first order change. Both $\mathrm{F}^{\mathbb{0}}$ and $\mathrm{F}^{\mathbb{1}}$ are then fed into (294), which is representative of the second order change. The operation of integrating the EOM (293) over the velocity space $\boldsymbol{\xi} \;\forall\; \Xi \in \mathbb{R}^3$, under the constraint $\overrightarrow{\Delta}[\![\mathrm{F}^{\mathbb{1}}]\!] = 0$, yields:

$$\partial_{\mathbb{1}}\vec{\rho}^{\mathbb{0}} = -\nabla_i\vec{\rho}^{\mathbb{0}}[\xi_i] \qquad \partial_{\mathbb{1}}\vec{\mathrm{p}}_i^{\mathbb{0}} = -\nabla_l\vec{\mathrm{p}}_i^{\mathbb{0}}[\xi_l] \tag{295}$$

$$\partial_{\mathbb{1}}\vec{\mathrm{E}}^{\mathbb{0}} = -\nabla_i\vec{\mathrm{E}}^{\mathbb{0}}[\xi_i] \qquad \partial_{\mathbb{1}}\vec{\mathrm{S}}^{\mathbb{0}} = -\nabla_i\vec{\mathrm{S}}^{\mathbb{0}}[\xi_i] \tag{296}$$

Which recovers the set of Euler equations:

$$\partial_{\mathbb{1}}\rho = -\nabla_i(\rho\mathrm{v}_i), \qquad \partial_{\mathbb{1}}(\rho\mathrm{v}_i) + \nabla_l(\rho\mathrm{v}_i\mathrm{v}_l) = -\nabla_i\mathrm{P} \tag{297}$$

$$\partial_{\mathbb{1}}(\rho e) + \nabla_i(\rho e\mathrm{v}_i) = -\nabla_i(\mathrm{P}\mathrm{v}_i), \qquad \partial_{\mathbb{1}}(\rho\mathrm{s}) = -\nabla_i(\rho\mathrm{s}\mathrm{v}_i) \tag{298}$$

From which the following first order evolutions are obtained:

$$\partial_{\mathbb{1}}\mathrm{v}_i = -\mathrm{v}_l\nabla_l\mathrm{v}_i - \upsilon\nabla_i\mathrm{P} \qquad \partial_{\mathbb{1}}e = -\mathrm{v}_i\nabla_i e - \upsilon\nabla_i(\mathrm{P}\mathrm{v}_i) \tag{299}$$

$$\partial_{\mathbb{1}}\varepsilon = -\mathrm{v}_i\nabla_i\varepsilon - \Theta\nabla_i\mathrm{v}_i \qquad \partial_{\mathbb{1}}h = -\mathrm{v}_i\nabla_i h - \gamma\Theta\nabla_i\mathrm{v}_i \tag{300}$$

$$\partial_{\mathbb{1}}\mathrm{T} = -\mathrm{v}_i\nabla_i\mathrm{T} - \mathrm{c}_{\upsilon}^{-1}\Theta\nabla_i\mathrm{v}_i \qquad \partial_{\mathbb{1}}\mathrm{P} = -\mathrm{v}_i\nabla_i\mathrm{P} - \gamma\mathrm{P}\nabla_i\mathrm{v}_i \tag{301}$$

$$\partial_{\mathbb{1}}\varrho = -\mathrm{v}_i(\nabla_i\varrho + \upsilon\nabla_i\mathrm{P}) \qquad \partial_{\mathbb{1}}\mathrm{s} = -\mathrm{v}_i\nabla_i\mathrm{s} \tag{302}$$

We'll next return to (293) and multiply by the newly introduced dissipation function ð (nondimensional) which will be set equal to the generalized first perturbation from equilibrium:

$$ð\mathfrak{D}_{\mathbb{1}}\mathrm{F}^{\mathbb{0}} = \tau(\partial_{\mathbb{1}}\mathrm{F}^{\mathbb{0}} + \xi_i\nabla_i\mathrm{F}^{\mathbb{0}}) = ðΔ[\![\mathrm{F}^{\mathbb{1}}]\!] = -\mathrm{F}^{\mathbb{1}} \tag{303}$$

Where the dissipation time is defined as $\tau = ðδt$. One may notice that we've adopted the BGK collision operator if we redefine (66) according to the master relation (282):

$$\epsilon\mathrm{dF}/\mathrm{d}t = -(\mathrm{F} - \mathrm{F}^{\mathbb{0}})\tau^{-1} \tag{304}$$

Similar to (284), the total differential expands as $\epsilon\mathrm{dF} = \epsilon\mathrm{d}_{\mathbb{1}}\mathrm{F} + \epsilon^2\mathrm{d}_{\mathbb{2}}\mathrm{F} + \mathcal{O}(\epsilon^3)$. Upon substituting (283) and $\epsilon\mathrm{dF}$ into (304), one finds a similar hierarchy in comparison to (293-294):

$$\mathcal{O}(\epsilon^1)\text{:} \qquad \mathrm{F}^{\mathbb{1}}\mathrm{d}t = -\tau\mathrm{d}_{\mathbb{1}}\mathrm{F}^{\mathbb{0}} \tag{305}$$

$$\mathcal{O}(\epsilon^2)\text{:} \qquad \mathrm{F}^{\mathbb{2}}\mathrm{d}t = -\tau(\mathrm{d}_{\mathbb{2}}\mathrm{F}^{\mathbb{0}} + \mathrm{d}_{\mathbb{1}}\mathrm{F}^{\mathbb{1}}) \tag{306}$$

The EOM (294) will then expand into what will be referred to as ***Leo's equation of motion***:

$$\partial_{\mathbb{2}}\mathrm{F}^{\mathbb{0}} + \xi_i\nabla_i\mathrm{F}^{\mathbb{0}} - \partial_{\mathbb{1}}[\tau(\partial_{\mathbb{1}}\mathrm{F}^{\mathbb{0}} + \xi_l\nabla_l\mathrm{F}^{\mathbb{0}})] - \xi_i\nabla_i[\tau(\partial_{\mathbb{1}}\mathrm{F}^{\mathbb{0}} + \xi_l\nabla_l\mathrm{F}^{\mathbb{0}})] = Δ[\![\mathrm{F}^{\mathbb{2}}]\!]δt^{-1} \tag{307}$$

The objective is to now recover a form of the transport equations (265-266). This will be accomplished through integrating (307) over the velocity space then utilizing the isentropic evolutions (299-302) to convert the subscript $\mathbb{1}$ temporal derivatives into spatial gradients. To begin, the Maxwellian $\hat{\rho}^{\mathbb{0}}$ from (286) will first replace $\mathrm{F}^{\mathbb{0}}$. The zeroth to third order raw moments are provided in ch.3.4. The fourth order raw moment will here be needed, i.e. $\vec{\rho}^{\mathbb{0}}[\xi_i\xi_j\xi_k\xi_l]$:

$$\rho\mathrm{v}_i\mathrm{v}_j\mathrm{v}_k\mathrm{v}_l + \mathrm{P}(\mathrm{v}_i\mathrm{v}_j\delta_{kl} + \mathrm{v}_i\mathrm{v}_k\delta_{jl} + \mathrm{v}_i\mathrm{v}_l\delta_{jk} + \mathrm{v}_j\mathrm{v}_k\delta_{il} + \mathrm{v}_j\mathrm{v}_l\delta_{ik} + \mathrm{v}_k\mathrm{v}_l\delta_{ij}) + \mathrm{P}\Theta\delta_{ijkl} \tag{308}$$

Where the fourth order Kronecker delta tensor is provided in ch.1.2. We will also need some partial moments, which may be computed from the raw moments, e.g.:

$$\vec{\rho}^{\mathbb{0}}[\xi_i\xi_l\tfrac{1}{2}|\boldsymbol{\xi}|^2] = \rho(\varrho + \tfrac{7}{2}\Theta)\mathrm{v}_i\mathrm{v}_l + \mathrm{P}(\varrho + \tfrac{5}{2}\Theta)\delta_{il} \tag{309}$$

As mentioned in Part I, odd order central moments compute to zero while the necessary even ones are $\vec{\rho}^{\mathbb{0}}[q_iq_l] = \mathrm{P}\delta_{il}$ and $\vec{\rho}^{\mathbb{0}}[q_iq_jq_kq_l] = \mathrm{P}\Theta\delta_{ijkl}$. Some useful mixed moments are $\vec{\rho}^{\mathbb{0}}[\xi_i\dot{q}_l] = \mathrm{P}\delta_{il}$ and $\vec{\rho}^{\mathbb{0}}[\xi_i\dot{q}_j\dot{q}_k] = \mathrm{P}\mathrm{v}_i\delta_{jk}$, in addition to:

$$\vec{\rho}^{\mathbb{0}}[\xi_i\xi_j\dot{q}_k\dot{q}_l] = \mathrm{P}(\mathrm{v}_i\mathrm{v}_j\delta_{kl} + \Theta\delta_{ijkl}) \tag{310}$$

$$\vec{\rho}^{\mathbb{0}}[\xi_i\xi_l\tfrac{1}{2}|\dot{\boldsymbol{q}}|^2] = \mathrm{P}(\tfrac{3}{2}\mathrm{v}_i\mathrm{v}_l + \tfrac{5}{2}\Theta\delta_{il}) \tag{311}$$

Referring back to Leo's EOM (307), we'll generate the moment while enforcing $\overrightarrow{\Delta}[\![\hat{\rho}^{\mathbb{2}}]\!] = 0$:

$$\partial_{\mathbb{2}}\vec{\rho}^{\mathbb{0}} + \nabla_i\vec{\rho}^{\mathbb{0}}[\xi_i] - \nabla_i[\tau(\partial_{\mathbb{1}}\vec{\rho}^{\mathbb{0}}[\xi_i] + \nabla_l\vec{\rho}^{\mathbb{0}}[\xi_i\xi_l])] = 0 \tag{312}$$

Upon substituting the relevant moments, we obtain $\partial_{\mathbb{1}}\rho = \partial_{\mathbb{2}}\rho$ therefore the mass density field remains conserved ✓. The same procedure will next be applied to the momentum distribution through replacing $\mathrm{F}^{\mathbb{0}}$ with (287), generating the moment, and enforcing $\overrightarrow{\Delta}[\![\hat{\mathbf{p}}^{\mathbb{2}}]\!] = \mathbf{0}$:

$$\partial_{\mathbb{2}}\vec{\mathrm{p}}_i^{\mathbb{0}} + \nabla_j\vec{\mathrm{p}}_i^{\mathbb{0}}[\xi_j] - \nabla_j[\tau(\partial_{\mathbb{1}}\vec{\mathrm{p}}_i^{\mathbb{0}}[\xi_j] + \nabla_k\vec{\mathrm{p}}_i^{\mathbb{0}}[\xi_j\xi_k])] = 0 \tag{313}$$

The raw form of the viscous stress tensor is identified as:

$$\sigma_{ij} = \tau[\partial_{\mathbb{1}}(\rho\mathrm{v}_i\mathrm{v}_j) + (\partial_{\mathbb{1}}\mathrm{P})\delta_{ij} + \nabla_k(\rho\mathrm{v}_i\mathrm{v}_j\mathrm{v}_k) + \nabla_j(\mathrm{P}\mathrm{v}_i) + \nabla_i(\mathrm{P}\mathrm{v}_j) + \nabla_k(\mathrm{P}\mathrm{v}_k)\delta_{ij}] \tag{314}$$

The conversion from the isentropic temporal evolutions into spatial gradients is:

$$\partial_{\mathbb{1}}(\rho\mathrm{v}_i\mathrm{v}_j) + (\partial_{\mathbb{1}}\mathrm{P})\delta_{ij}$$

$$= -\nabla_k(\rho\mathrm{v}_i\mathrm{v}_j\mathrm{v}_k) - (\mathrm{v}_i\nabla_j\mathrm{P} + \mathrm{v}_j\nabla_i\mathrm{P} + \mathrm{v}_k(\nabla_k\mathrm{P})\delta_{ij}) - \gamma\mathrm{P}(\nabla_k\mathrm{v}_k)\delta_{ij} \tag{315}$$

Substituting and simplifying recovers the Navier-Stokes (NS) viscous stress tensor [45; ch.45]:

$$\sigma_{ij} = \mu(\nabla_i\mathrm{v}_j + \nabla_j\mathrm{v}_i - \tfrac{2}{3}(\nabla_k\mathrm{v}_k)\delta_{ij}) + \eta(\nabla_k\mathrm{v}_k)\delta_{ij} \tag{316}$$

Where the coefficients of shearing and dilatational viscosity are identified respectively as:

$$\mu = \mathrm{P}\tau, \qquad \eta = \mu(\tfrac{5}{3} - \gamma) \tag{317}$$

The two are related via the relation $\varsigma = \eta - \frac{2}{3}\mu = \mu(1-\gamma)$ and the total stress tensor is:

$$\Sigma_{il} = \mathrm{P}\delta_{il} - \mu(\nabla_i\mathrm{v}_l + \nabla_l\mathrm{v}_i) - \varsigma(\nabla_k\mathrm{v}_k)\delta_{il} \tag{318}$$

From which the total pressure may be found through $\frac{1}{3}\Sigma_{ii} = \mathrm{P} - \eta\nabla_l\mathrm{v}_l$. For a monatomic perfect gas, where only translational modes of internal energy are relevant, $\eta(\gamma = \frac{5}{3}) = 0$ and the total pressure reduces down to the hydrostatic pressure. It can now be inferred that the coefficient of dilatational viscosity is directly related to non-translational modes of internal energy such as rotation, vibration, etc. So for a diatomic perfect gas, $\eta(\gamma = \frac{7}{5}) = \frac{4}{15}\mu$. The theoretical predictions for the viscosity ratio $\mathfrak{T} = \eta/\mu$ are shown in Figure 32 for N_2 (red) and O_2 (blue), where the black dashed line indicates $4/15$. This nondimensional quantity will for future reference be referred to as ***Tracey's number***. It is found that for this particular application $\eta < \mu$.

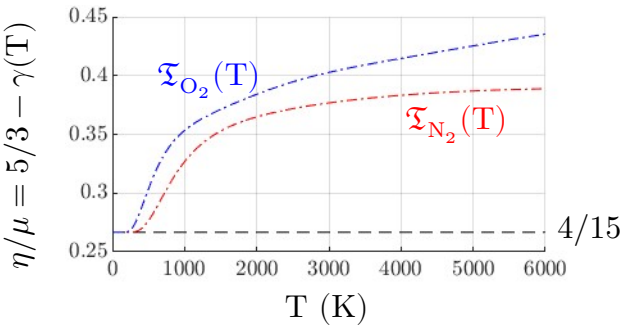

Figure 32 Dilatational viscosity coefficient predictions for N_2 and O_2

Referring back to (317), others have found a similar result, e.g. [31,34]. The dissipation time can be expressed as $\tau = \mu \mathrm{P}^{-1}$, however η is not guaranteed to match experimental data. The discussion in [45; ch.45.4] states that in general $\mathfrak{T} > 1$, which contradicts our prediction shown in Figure 32. Modifications to the expression obtained for η will be left for future work. Some numerical estimates can be found in [57,68].

To recap, thus far we've derived the Navier-Stokes equations for a compressible viscous gas:

$$\partial_{\mathbb{2}} \rho + \nabla_i (\rho \mathrm{v}_i) = 0 \tag{319}$$

$$\partial_{\mathbb{2}} (\rho \mathrm{v}_i) + \nabla_l [\rho \mathrm{v}_i \mathrm{v}_l - \mu(\nabla_i \mathrm{v}_l + \nabla_l \mathrm{v}_i)] + \nabla_i (\mathrm{P} - \varsigma \nabla_k \mathrm{v}_k) = 0 \tag{320}$$

Where Cauchy's tetrahedron [45; p.137] can now be visualized on the phasetime element:

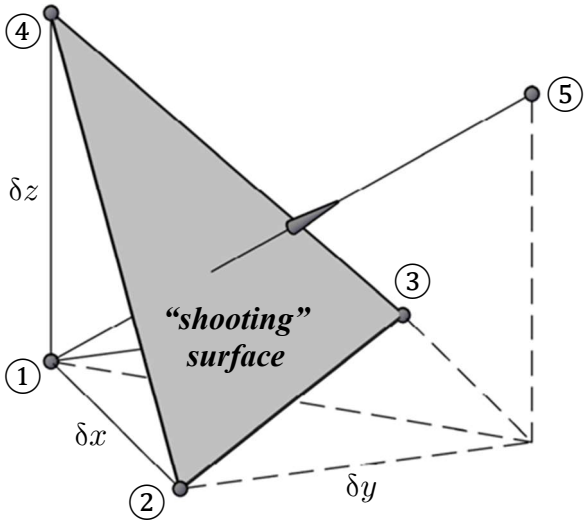

Figure 33 3D phasetime element (three-pronged slingshot)

The attention will next turn to the entropy evolution. The first perturbation from equilibrium will be found through multiplying (293) by the variational dissipation function $\eth^*$:

$$\eth^{*}\mathfrak{D}_{\mathbb{1}}\hat{\mathrm{S}}^{\mathbb{0}}=\tau^{*}(\partial_{\mathbb{1}}\hat{\mathrm{S}}^{\mathbb{0}}+\xi_{i}\nabla_{i}\hat{\mathrm{S}}^{\mathbb{0}})=\eth^{*}\Delta[\![\hat{\mathrm{S}}^{\mathbb{1}}]\!]=-\hat{\mathrm{S}}^{\mathbb{1}} \tag{321}$$

Where the variational dissipation time is $\tau^{*}=\eth^{*}\delta t=\tau(1+\dot{\tau})$. Leo's EOM then becomes:

$$\partial_{\mathbb{2}}\hat{\mathrm{S}}^{\mathbb{0}}+\xi_{i}\nabla_{i}\hat{\mathrm{S}}^{\mathbb{0}}-\partial_{\mathbb{1}}[\tau^{*}(\partial_{\mathbb{1}}\hat{\mathrm{S}}^{\mathbb{0}}+\xi_{l}\nabla_{l}\hat{\mathrm{S}}^{\mathbb{0}})]-\xi_{i}\nabla_{i}[\tau^{*}(\partial_{\mathbb{1}}\hat{\mathrm{S}}^{\mathbb{0}}+\xi_{l}\nabla_{l}\hat{\mathrm{S}}^{\mathbb{0}})]=\Delta[\![\hat{\mathrm{S}}^{\mathbb{2}}]\!]\delta t^{-1} \tag{322}$$

The next step is to integrate over the velocity space which yields:

$$\partial_{\mathbb{2}}\vec{\mathrm{S}}^{\mathbb{0}}+\nabla_{i}\vec{\mathrm{S}}^{\mathbb{0}}[\xi_{i}]-\nabla_{i}[\tau^{*}(\partial_{\mathbb{1}}\vec{\mathrm{S}}^{\mathbb{0}}[\xi_{i}]+\nabla_{l}\vec{\mathrm{S}}^{\mathbb{0}}[\xi_{i}\xi_{l}])]=\overrightarrow{\Delta}[\![\hat{\mathrm{S}}^{\mathbb{2}}]\!]\delta t^{-1}=\dot{\$} \tag{323}$$

It is important to note that for the entropy, $\overrightarrow{\Delta}[\![\hat{\mathrm{S}}^{\mathbb{2}}]\!]\neq 0$ but must equate to the rate of entropy production multiplied over the time interval, i.e. $\overrightarrow{\Delta}[\![\hat{\mathrm{S}}^{\mathbb{2}}]\!]=\dot{\$}\delta t$, as shown in (323). The zeroth order moment is reviewed as $\vec{\mathrm{S}}^{\mathbb{0}}=\rho\mathrm{s}$, where the entropy is $\mathrm{s}=R\ln\upsilon\zeta+\varepsilon/\mathrm{T}$. The first order moment is simply $\vec{\mathrm{S}}^{\mathbb{0}}[\xi_{i}]=\rho\mathrm{s}\mathrm{v}_{i}$ and the second is presented as:

$$\vec{\mathrm{S}}^{\mathbb{0}}[\xi_{i}\xi_{l}]=\rho\mathrm{s}(\mathrm{v}_{i}\mathrm{v}_{l}+\Theta\delta_{il})+R\mathrm{P}\delta_{il} \tag{324}$$

Upon substituting these moments into (323), the raw form of the heat-entropy flux vector becomes:

$$\Phi_{i}=-\tau^{*}[\partial_{\mathbb{1}}(\rho\mathrm{s}\mathrm{v}_{i})+\nabla_{l}(\rho\mathrm{s}\mathrm{v}_{i}\mathrm{v}_{l})+\nabla_{i}(\mathrm{P}\mathrm{s})+R\nabla_{i}\mathrm{P}] \tag{325}$$

Where the conversion from the isentropic temporal evolutions into spatial gradients is:

$$\partial_{\mathbb{1}}(\rho\mathrm{s}\mathrm{v}_{i})=-\nabla_{l}(\rho\mathrm{s}\mathrm{v}_{i}\mathrm{v}_{l})-\mathrm{s}\nabla_{i}\mathrm{P} \tag{326}$$

Substituting and simplifying recovers the hypothesized heat-entropy flux vector (266):

$$\Phi_{i}=-\tau^{*}(\mathrm{P}\nabla_{i}\mathrm{s}+R\nabla_{i}\mathrm{P})=-\kappa\nabla_{i}\ln\mathrm{T}=\mathrm{q}_{i}\mathrm{T}^{-1} \tag{327}$$

Where the coefficient of thermal conductivity is identified as:

$$\kappa=\mathrm{c}_{\mathrm{P}}\mu(1+\dot{\tau}) \tag{328}$$

The Prandtl number is then:

$$\mathtt{P}=\mathrm{c}_{\mathrm{P}}\mu/\kappa=(1+\dot{\tau})^{-1} \tag{329}$$

As a result, the rate of dissipation may be reformed in terms of the Prandtl number: $\dot{\tau}=\mathtt{P}^{-1}-1$. Let us now recall the dissipation function $\eth=\tau/\delta t$ and its variational form $\eth^{*}=\tau^{*}/\delta t$, where $\tau^{*}=\tau(1+\dot{\tau})$ and $\eth^{*}=\eth(1+\dot{\tau})$. If τ were a function of time, then the corresponding rate must be $\dot{\tau}=\dot{\eth}\delta t$. Feeding this relation into the variational dissipation function unveils $\eth^{*}=\eth+\dot{\eth}\tau$, so that the Prandtl number may take the fundamental form: $\mathtt{P}=\eth/\eth^{*}$; thus providing some further insight into these newly introduced parameters. The expression for the entropy $\mathrm{s}=R\ln\upsilon\zeta+\varepsilon/\mathrm{T}$, will next be fed into (323), restated in the form:

$$\partial_{\mathbb{2}}(\rho \mathrm{s}) + \nabla_i(\rho \mathrm{s} \mathrm{v}_i) + \nabla_i \Phi_i = \dot{\$} \tag{330}$$

From which the rate of entropy production is obtained exactly as postulated in (278):

$$\dot{\$} = \sigma_{il}(\nabla_i \mathrm{v}_l)\mathrm{T}^{-1} + \kappa(\nabla_i \ln \mathrm{T})(\nabla_i \ln \mathrm{T}) \geq 0 \tag{331}$$

It is already apparent that $\kappa|\boldsymbol{\nabla} \ln \mathrm{T}|^2 \geq 0$ since $\kappa \geq 0$ and $|\boldsymbol{\nabla} \ln \mathrm{T}|^2 \geq 0$. We'll next examine the contraction $\sigma_{il}\nabla_i \mathrm{v}_l$ through first decomposing the velocity gradient into symmetric & skew parts:

$$\nabla_i \mathrm{v}_l = \mathrm{A}_{il} + \mathrm{B}_{il} = \tfrac{1}{2}(\nabla_i \mathrm{v}_l + \nabla_l \mathrm{v}_i) + \tfrac{1}{2}(\nabla_i \mathrm{v}_l - \nabla_l \mathrm{v}_i) \tag{332}$$

Since $2\mathrm{A}_{il} = \nabla_i \mathrm{v}_l + \nabla_l \mathrm{v}_i$ and $\mathrm{A}_{ll} = \nabla_l \mathrm{v}_l$, then the NS viscous stress tensor may be written in terms of the symmetric tensor $\mathrm{A}_{il} = \mathrm{A}_{li}$, therefore $\sigma_{il} = 2\mu \mathrm{A}_{il} + \varsigma \mathrm{A}_{kk}\delta_{il}$. The contraction is now:

$$\sigma_{il}(\nabla_i \mathrm{v}_l)/\mu = 2\mathrm{A}_{il}\nabla_i \mathrm{v}_l + (\mathfrak{T} - \tfrac{2}{3})(\mathrm{A}_{kk})^2 \geq 0 \tag{333}$$

Using comma notation, the shear and dilatational parts respectively expand as follows:

$$2\mathrm{A}_{il}\nabla_i \mathrm{v}_l = 2(u_{,x}^2 + v_{,y}^2 + w_{,z}^2) + (u_{,y} + v_{,x})^2 + (v_{,z} + w_{,y})^2 + (u_{,z} + w_{,x})^2 \geq 0 \tag{334}$$

$$(\mathrm{A}_{kk})^2 = (\nabla_k \mathrm{v}_k)^2 = (u_{,x} + v_{,y} + w_{,z})^2 \geq 0 \tag{335}$$

Since $\mu \geq 0$ and $\eta \geq 0$, the minimum value for Tracey's number is $\mathfrak{T}_{\text{min}} = 0$ so we must prove:

$$2\mathrm{A}_{il}\nabla_i \mathrm{v}_l \geq \tfrac{2}{3}(\mathrm{A}_{kk})^2 \tag{336}$$

$$\tfrac{3}{1}(u_{,x}^2 + v_{,y}^2 + w_{,z}^2) + \tfrac{3}{2}(u_{,y} + v_{,x})^2 + \tfrac{3}{2}(v_{,z} + w_{,y})^2 + \tfrac{3}{2}(u_{,z} + w_{,x})^2$$

$$\geq (u_{,x} + v_{,y} + w_{,z})^2 \tag{337}$$

Well the Cauchy-Schwarz inequality states that [12; p.5]:

$$(a_1^2 + a_2^2 + a_3^2)(b_1^2 + b_2^2 + b_3^2) \geq (a_1 b_1 + a_2 b_2 + a_3 b_3)^2 \tag{338}$$

Upon setting $a_1 = u_{,x}$, $a_2 = v_{,y}$, $a_3 = w_{,z}$, and $b_1 = b_2 = b_3 = 1$, the above simplifies down to:

$$3(u_{,x}^2 + v_{,y}^2 + w_{,z}^2) \geq (u_{,x} + v_{,y} + w_{,z})^2 \tag{339}$$

As a result, (333) is in accordance with the 2nd LoT ✓. As proven in ch.4.1, we've maintained the Gibbs relation (112) where the entropy differential is $\mathrm{d}\mathrm{s} = \upsilon \mathrm{T}^{-1}(\sigma_{il}\nabla_i \mathrm{v}_l - \nabla_i \mathrm{q}_i)\mathrm{d}t$, so that:

$$\mathrm{d}\varepsilon = \upsilon(\sigma_{il}\nabla_i \mathrm{v}_l - \nabla_i \mathrm{q}_i)\mathrm{d}t - \mathrm{P}\mathrm{d}\upsilon$$

$$= \upsilon(2\mu\,\mathrm{dev}(\mathrm{A}_{il})\,\nabla_i \mathrm{v}_l - \nabla_i \mathrm{q}_i)\mathrm{d}t - \upsilon \mathrm{A}_{kk}(\mathrm{P} - \eta \mathrm{A}_{ll})\mathrm{d}t \tag{340}$$

One can interpret that $2\nu\,\mathrm{dev}(\mathrm{A}_{il})\,(\nabla_i \mathrm{v}_l)\mathrm{d}t$ represents the heat generated due to viscous interactions (friction), the term $-\upsilon(\nabla_i \mathrm{q}_i)\mathrm{d}t$ is indicative of the heat transfer due to the temperature gradient, and $\upsilon\eta(\mathrm{A}_{kk})^2\mathrm{d}t$ affects the work response which is now no longer equal and opposite. To note, $\nu = \upsilon\mu$, $\mathrm{dev}(\mathrm{A}_{il}) = \mathrm{A}_{il} - \frac{1}{3}\mathrm{A}_{kk}\delta_{il}$, and $\sigma_{il} = 2\mu\,\mathrm{dev}(\mathrm{A}_{il}) + \eta \mathrm{A}_{kk}\delta_{il}$.

To unify the entropy and momentum evolutions in the total energy equation, we'll first revisit (303), which provides the following two relations:

$$\eth\mathfrak{D}_{\mathbb{1}}\hat{\mathrm{E}}^{\mathbb{0}} = \tau(\partial_{\mathbb{1}}\hat{\mathrm{E}}^{\mathbb{0}} + \xi_i \nabla_i \hat{\mathrm{E}}^{\mathbb{0}}) = \eth\Delta[\![\hat{\mathrm{E}}^{\mathbb{1}}]\!] \tag{341}$$

$$\mathrm{T}\dot{\tau}\eth\mathfrak{D}_{\mathbb{1}}\hat{\mathrm{S}}^{\mathbb{0}} = \mathbb{t}\mathrm{T}(\partial_{\mathbb{1}}\hat{\mathrm{S}}^{\mathbb{0}} + \xi_i \nabla_i \hat{\mathrm{S}}^{\mathbb{0}}) = \mathrm{T}\dot{\tau}\eth\Delta[\![\hat{\mathrm{S}}^{\mathbb{1}}]\!] \tag{342}$$

Upon combining, where $\mathbb{t} = \dot{\tau}\tau$, the first perturbation in the energy distribution is then:

$$\eth\mathfrak{D}_{\mathbb{1}}\hat{\mathrm{E}}^{\mathbb{0}} + \mathrm{T}\dot{\tau}\eth\mathfrak{D}_{\mathbb{1}}\hat{\mathrm{S}}^{\mathbb{0}} = \eth\Delta[\![\hat{\mathrm{E}}^{\mathbb{1}}]\!] + \mathrm{T}\dot{\tau}\eth\Delta[\![\hat{\mathrm{S}}^{\mathbb{1}}]\!] = -\hat{\mathrm{E}}^{\mathbb{1}}$$

$$= \tau(\partial_{\mathbb{1}}\hat{\mathrm{E}}^{\mathbb{0}} + \xi_i \nabla_i \hat{\mathrm{E}}^{\mathbb{0}}) + \mathbb{t}\mathrm{T}(\partial_{\mathbb{1}}\hat{\mathrm{S}}^{\mathbb{0}} + \xi_i \nabla_i \hat{\mathrm{S}}^{\mathbb{0}}) \tag{343}$$

Under the constraint $\overrightarrow{\Delta}[\![\hat{\mathrm{E}}^{\mathbb{2}}]\!] = 0$, the energy evolution may now be represented in the form:

$$\partial_{\mathbb{2}}\overrightarrow{\mathrm{E}}^{\mathbb{0}} + \nabla_i \overrightarrow{\mathrm{E}}^{\mathbb{0}}[\xi_i] - \nabla_i\big[\tau\big(\partial_{\mathbb{1}}\overrightarrow{\mathrm{E}}^{\mathbb{0}}[\xi_i] + \nabla_l \overrightarrow{\mathrm{E}}^{\mathbb{0}}[\xi_i\xi_l]\big) + \mathbb{t}\mathrm{T}\big(\partial_{\mathbb{1}}\vec{\mathrm{S}}^{\mathbb{0}}[\xi_i] + \nabla_l \vec{\mathrm{S}}^{\mathbb{0}}[\xi_i\xi_l]\big)\big] = 0 \tag{344}$$

Recalling from Part I, the first two moments are $\overrightarrow{\mathrm{E}}^{\mathbb{0}} = \rho e$ and $\overrightarrow{\mathrm{E}}^{\mathbb{0}}[\xi_i] = \mathrm{H}\mathrm{v}_i$, where $\mathrm{H} = \rho e + \mathrm{P}$ is the total enthalpy density. The third order moment is next provided in the form:

$$\overrightarrow{\mathrm{E}}^{\mathbb{0}}[\xi_i\xi_l] = (\mathrm{H} + \mathrm{P})\mathrm{v}_i\mathrm{v}_l + \mathrm{H}\Theta\delta_{il} \tag{345}$$

So that the raw form of the stress flux vector minus the heat flux vector is identified as:

$$\sigma_{il}\mathrm{v}_l - \mathrm{q}_i = \tau[\partial_{\mathbb{1}}(\mathrm{H}\mathrm{v}_i) + \nabla_l(\mathrm{H}\mathrm{v}_i\mathrm{v}_l) + \nabla_l(\mathrm{P}\mathrm{v}_i\mathrm{v}_l) + \nabla_i(\mathrm{H}\Theta)] + \dot{\tau}\mu\mathrm{c}_{\mathrm{P}}\nabla_i\mathrm{T} \tag{346}$$

The conversion from the isentropic temporal evolutions into spatial gradients is provided as:

$$\partial_{\mathbb{1}}(\mathrm{H}\mathrm{v}_i) = -\nabla_l(\mathrm{H}\mathrm{v}_i\mathrm{v}_l) - \mathrm{v}_i\mathrm{v}_l\nabla_l\mathrm{P} - \gamma\mathrm{P}\mathrm{v}_i\nabla_l\mathrm{v}_l - \upsilon\mathrm{H}\nabla_i\mathrm{P} \tag{347}$$

Substituting and simplifying recovers the N-S stress flux vector minus the Fourier heat flux vector:

$$\sigma_{il}\mathrm{v}_l - \mathrm{q}_i = \mu(\nabla_i\mathrm{v}_l + \nabla_l\mathrm{v}_i)\mathrm{v}_l + \varsigma(\nabla_k\mathrm{v}_k)\mathrm{v}_i + \kappa\nabla_i\mathrm{T} \tag{348}$$

The final form of the energy evolution then becomes:

$$\partial_{\mathbb{2}}(\rho e) + \nabla_i(\mathrm{H}\mathrm{v}_i) = \nabla_i(\sigma_{il}\mathrm{v}_l + \kappa\nabla_i\mathrm{T}) \tag{349}$$

In conclusion, the transport equations (265-266) have fully been derived from a statistical standpoint. From here we must uncover expressions for the dissipation time $\tau = \mu \mathrm{P}^{-1}$ and the rate of dissipation $\dot{\tau} = \kappa(\mathrm{c_P}\mu)^{-1} - 1$. Theoretical predictions of the transport coefficients are beyond the scope of this work therefore Sutherland's law[12] [59] will briefly be reviewed:

$$\mu = \frac{\mu_0(\mathfrak{s}_\mu + \mathrm{T}_0)}{\mathrm{T}_0^{3/2}} \frac{\mathrm{T}^{3/2}}{(\mathfrak{s}_\mu + \mathrm{T})}, \qquad \kappa = \frac{\kappa_0(\mathfrak{s}_\kappa + \mathrm{T}_0)}{\mathrm{T}_0^{3/2}} \frac{\mathrm{T}^{3/2}}{(\mathfrak{s}_\kappa + \mathrm{T})} \tag{350}$$

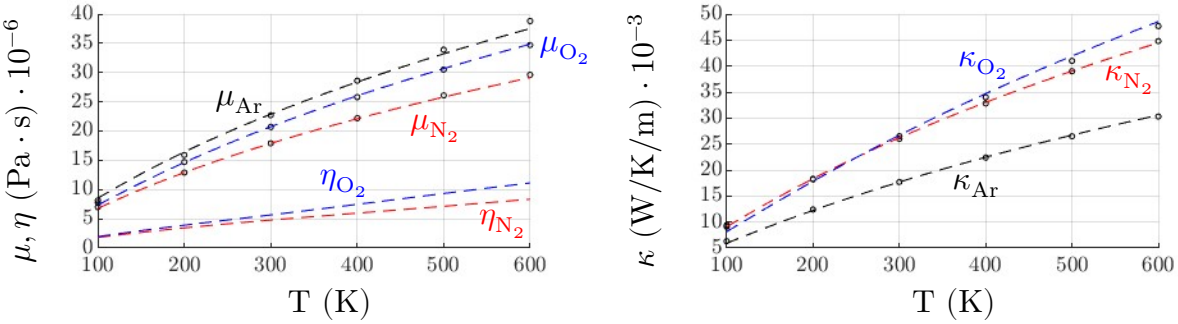

Figure 34 Viscosity (left) and thermal conductivity (right)
via Sutherland's law for Ar, $\mathrm{N_2}$, and $\mathrm{O_2}$
(data source: CRC Handbook of Chemistry and Physics [17])

Some data taken from [17; p.6-229,6-241] is shown in Figure 34 and compared to Sutherland's predictions over the temperature range $100\ \mathrm{K} \leq \mathrm{T} \leq 600\ \mathrm{K}$. Even though this range is relatively small, there is good agreement between Sutherland's formulas and the experimental data. We can also compare (61) and (350) to obtain a deeper understanding; see [15; p.223].

4.3 Analytical Expressions for the First Perturbation

Here, we will scrub down our theoretical formulations and find analytical expressions for the first perturbation from equilibrium. To begin, the generalized velocity distribution will be expressed as $\mathrm{F} = \mathrm{F}^{\mathbb{0}} + \mathrm{F}^{\mathbb{1}}$, which is governed by the EOM (294):

$$\dot{\mathrm{F}} + \boldsymbol{\xi} \cdot \boldsymbol{\nabla} \mathrm{F} = (\dot{\mathrm{F}}^{\mathbb{0}} + \boldsymbol{\xi} \cdot \boldsymbol{\nabla} \mathrm{F}^{\mathbb{0}}) + (\dot{\mathrm{F}}^{\mathbb{1}} + \boldsymbol{\xi} \cdot \boldsymbol{\nabla} \mathrm{F}^{\mathbb{1}}) = \Delta[\![\mathrm{F}^{\mathbb{2}}]\!] \delta t^{-1} \tag{351}$$

It has been well established and proven that $\overline{\mathrm{F}}^{\mathbb{1}} = 0$ and theoretically $\overline{\Delta}[\![\mathrm{F}^{\mathbb{2}}]\!] = 0$ (except for the entropy). In regards to the mass, momentum, and energy evolutions, the terms $\dot{\mathrm{F}}^{\mathbb{1}}$ and $\Delta[\![\mathrm{F}^{\mathbb{2}}]\!]\delta t^{-1}$ are then negligible and will be removed from (351). The reduced EOM is then:

$$\dot{\mathrm{F}}^{\mathbb{0}} + \boldsymbol{\xi} \cdot \boldsymbol{\nabla} \mathrm{F}^{\mathbb{0}} + \boldsymbol{\xi} \cdot \boldsymbol{\nabla} \mathrm{F}^{\mathbb{1}} = 0 \tag{352}$$

The objective is to now uncover expressions for $\mathrm{F}^{\mathbb{1}}$ in terms of the velocity gradient tensor $\nabla_l \mathrm{v}_i$ and the temperature gradient vector $\nabla_i \mathrm{T}$. From (303), it was established that the first perturbation

[12] https://doc.comsol.com/5.5/doc/com.comsol.help.cfd/cfd_ug_fluidflow_high_mach.08.27.html

is $\mathrm{F}^{\mathbb{1}} \equiv -\tau(\partial_{\mathbb{1}}\mathrm{F}^{\mathbb{0}} + \boldsymbol{\xi}\cdot\boldsymbol{\nabla}\mathrm{F}^{\mathbb{0}})$, so that the total distribution is by definition:

$$\mathrm{F} \equiv \mathrm{F}^{\mathbb{0}} - \tau(\partial_{\mathbb{1}}\mathrm{F}^{\mathbb{0}} + \xi_i\nabla_i\mathrm{F}^{\mathbb{0}}) \tag{353}$$

The derivatives $\partial_{\mathbb{1}}\mathrm{F}^{\mathbb{0}}$ and $\nabla_i\mathrm{F}^{\mathbb{0}}$ will be expanded through identifying the zeroth order functional:

$$\mathrm{F}^{\mathbb{0}}(\boldsymbol{\xi},\mathbf{x},t) = \mathrm{F}^{\mathbb{0}}[\boldsymbol{\xi},\rho(\mathbf{x},t),\mathbf{v}(\mathbf{x},t),\mathrm{T}(\mathbf{x},t)] \tag{354}$$

In consequence, the first order perturbation will expand as:

$$-\frac{1}{\tau}\mathrm{F}^{\mathbb{1}} \equiv \frac{\partial\mathrm{F}^{\mathbb{0}}}{\partial\rho}(\partial_{\mathbb{1}}\rho + \xi_i\nabla_i\rho) + \frac{\partial\mathrm{F}^{\mathbb{0}}}{\partial\mathrm{v}_i}(\partial_{\mathbb{1}}\mathrm{v}_i + \xi_l\nabla_l\mathrm{v}_i) + \frac{\partial\mathrm{F}^{\mathbb{0}}}{\partial\mathrm{T}}(\partial_{\mathbb{1}}\mathrm{T} + \xi_i\nabla_i\mathrm{T}) \tag{355}$$

$$= \left(\dot{q}_i\frac{\partial\mathrm{F}^{\mathbb{0}}}{\partial\rho} - \frac{\Theta}{\rho}\frac{\partial\mathrm{F}^{\mathbb{0}}}{\partial\mathrm{v}_i}\right)\nabla_i\rho + \left(\dot{q}_l\frac{\partial\mathrm{F}^{\mathbb{0}}}{\partial\mathrm{v}_i} - \rho\frac{\partial\mathrm{F}^{\mathbb{0}}}{\partial\rho}\delta_{il} - \frac{\Theta}{\mathrm{c}_{\upsilon}}\frac{\partial\mathrm{F}^{\mathbb{0}}}{\partial\mathrm{T}}\delta_{il}\right)\nabla_l\mathrm{v}_i + \left(\dot{q}_i\frac{\partial\mathrm{F}^{\mathbb{0}}}{\partial\mathrm{T}} - R\frac{\partial\mathrm{F}^{\mathbb{0}}}{\partial\mathrm{v}_i}\right)\nabla_i\mathrm{T}$$

Utilizing the isentropic evolutions, the advective spacetime evolutions are converted via:

$$\partial_{\mathbb{1}}\rho + \xi_i\nabla_i\rho = \dot{q}_i\nabla_i\rho - \rho\nabla_i\mathrm{v}_i \tag{356}$$

$$\partial_{\mathbb{1}}\mathrm{v}_i + \xi_l\nabla_l\mathrm{v}_i = \dot{q}_l\nabla_l\mathrm{v}_i - \upsilon\nabla_i\mathrm{P} \tag{357}$$

$$\partial_{\mathbb{1}}\mathrm{T} + \xi_i\nabla_i\mathrm{T} = \dot{q}_i\nabla_i\mathrm{T} - \mathrm{c}_{\upsilon}^{-1}\Theta\nabla_i\mathrm{v}_i \tag{358}$$

As one can observe, the temporal derivatives have once again been transformed into strictly spatial gradients, as done in ch.4.2. Upon setting $\mathrm{F}^{\mathbb{0}} = \hat{\rho}^{\mathbb{0}}$, the partial derivatives in (355) are:

$$\partial\hat{\rho}^{\mathbb{0}}/\partial\rho = \upsilon\hat{\rho}^{\mathbb{0}}, \qquad \partial\hat{\rho}^{\mathbb{0}}/\partial\mathrm{v}_i = \beta\dot{q}_i\hat{\rho}^{\mathbb{0}}, \qquad \partial\hat{\rho}^{\mathbb{0}}/\partial\mathrm{T} = R\beta^2\mathcal{L}\hat{\rho}^{\mathbb{0}} \tag{359}$$

Where $\mathcal{L} = \frac{1}{2}|\dot{\boldsymbol{q}}|^2 - \varepsilon_{\text{tr}}$ is the specific Lagrangian and $\beta = \Theta^{-1}$. Feeding (359) into (355) yields:

$$\mathrm{F}^{\mathbb{1},\mathbb{0}} = -\tau\beta(\dot{q}_i\dot{q}_l - \tfrac{1}{2}(\gamma-1)|\dot{\boldsymbol{q}}|^2\delta_{il} - \mathfrak{T}\varepsilon_{\text{tr}}\delta_{il})\nabla_l\mathrm{v}_i - \tau\beta(\tfrac{1}{2}|\dot{\boldsymbol{q}}|^2 - h_{\text{tr}})\dot{q}_i\nabla_i\ln\mathrm{T} \tag{360}$$

For a monatomic perfect gas, meaning $\mathrm{c}_{\upsilon} = 3R/2$, $\gamma = 5/3$, and $\mathfrak{T} = 0$, then (360) simplifies to:

$$\mathrm{F}^{\mathbb{1},\mathbb{0}}_{\mathrm{Ar}} = -\tau\beta(\dot{q}_i\dot{q}_l - \tfrac{1}{3}|\dot{\boldsymbol{q}}|^2\delta_{il})\nabla_l\mathrm{v}_i - \tau\beta(\tfrac{1}{2}|\dot{\boldsymbol{q}}|^2 - \tfrac{5}{2}\Theta)\dot{q}_i\nabla_i\ln\mathrm{T} \tag{361}$$

Thus being a similar expression found in [15; p.119]. We'll next define the quantities:

$$\varkappa_i = (\tfrac{1}{2}|\dot{\boldsymbol{q}}|^2 - h_{\text{tr}})\dot{q}_i\mathrm{T}^{-1} \tag{362}$$

$$\mathcal{L}_{il} = \dot{q}_i\dot{q}_l - \tfrac{1}{2}(\gamma-1)|\dot{\boldsymbol{q}}|^2\delta_{il} - \mathfrak{T}\varepsilon_{\text{tr}}\delta_{il} \tag{363}$$

So that (360) may be written in the more compact form:

$$\mathrm{F}^{\mathbb{1},\mathbb{0}} = -\tau\beta(\mathcal{L}_{il}\nabla_l \mathrm{v}_i + \varkappa_i \nabla_i \mathrm{T}) \tag{364}$$

From a numerical standpoint, we will simply set $\hat{\rho}^{\mathbb{1}} = 0$, meaning $\hat{\rho} = \hat{\rho}^{\mathbb{0}}$, which is governed by:

$$\partial\vec{\rho} + \nabla_i \vec{\rho}[\xi_i] = \partial\rho + \nabla_i(\rho \mathrm{v}_i) = 0 \tag{365}$$

In contrary, the momentum density velocity distribution expands as $\hat{\mathbf{p}} = \hat{\mathbf{p}}^{\mathbb{0}} + \hat{\mathbf{p}}^{\mathbb{1}}$, where the first perturbation is simply:

$$\hat{\mathrm{p}}_i^{\mathbb{1}} = -(\tau\beta\nabla_l \mathrm{v}_k)\mathcal{L}_{kl}\hat{\mathrm{p}}_i^{\mathbb{0}} \tag{366}$$

The term containing the temperature gradient has been dropped since the heat flux vector does not appear in the momentum evolution (320). The first two moments over the Lagrange tensor are:

$$\vec{\mathrm{p}}_i^{\mathbb{0}}[\mathcal{L}_{jk}] = 0 \tag{367}$$

$$\vec{\mathrm{p}}_i^{\mathbb{0}}[\xi_j \mathcal{L}_{kl}] = \mathrm{P}\Theta(\delta_{ijkl} - \gamma\delta_{ij}\delta_{kl}) \tag{368}$$

$$\delta_{ijkl} - \gamma\delta_{ij}\delta_{kl} = (\delta_{ik}\delta_{jl} + \delta_{il}\delta_{jk} - \tfrac{2}{3}\delta_{ij}\delta_{kl}) + \mathfrak{T}\delta_{ij}\delta_{kl} \tag{369}$$

In consequence $\vec{\mathbf{p}}^{\mathbb{1}} = \mathbf{0}$ as expected. The stress tensor will next be expressed as:

$$\sigma_{ij} = \mathrm{M}_{ijkl}\nabla_l \mathrm{v}_k \tag{370}$$

Where M_{ijkl} is the viscosity tensor, similar to the elasticity tensor [45; p.300]:

$$\mathrm{M}_{ijkl} = \tau\beta\vec{\mathrm{p}}_i^{\mathbb{0}}[\xi_j\mathcal{L}_{kl}] = \mu(\delta_{ijkl} - \gamma\delta_{ij}\delta_{kl}) = \mu(\delta_{ik}\delta_{jl} + \delta_{il}\delta_{jk}) + \varsigma\delta_{ij}\delta_{kl} \tag{371}$$

The first order moment of (366) is next computed as:

$$\vec{\mathrm{p}}_i^{\mathbb{1}}[\xi_j] = -(\tau\beta\nabla_l \mathrm{v}_k)\vec{\mathrm{p}}_i^{\mathbb{0}}[\xi_j\mathcal{L}_{kl}] = -\mathrm{M}_{ijkl}\nabla_l \mathrm{v}_k = -\sigma_{ij} \tag{372}$$

The Navier-Stokes momentum equation is then recovered from (352):

$$\partial\vec{\mathrm{p}}_i^{\mathbb{0}} + \nabla_l \vec{\mathrm{p}}_i[\xi_l] = \partial(\rho \mathrm{v}_i) + \nabla_l(\rho \mathrm{v}_i \mathrm{v}_l + \mathrm{P}\delta_{il} - \sigma_{il}) = 0 \tag{373}$$

We'll next discuss the computation of both the velocity gradient tensor and the temperature gradient vector found in (364), where each may be treated in the same manner. If one were to compute these quantities, then a nonlocal approach will work best. We'll consider χ to be the center position within a one-dimensional lattice and λ_α as the step length. A first order Taylor series expansion of the function $\mathrm{T}(\chi)$ is then:

$$\mathrm{T}(\chi + \lambda_\alpha) = \mathrm{T}(\chi) + \lambda_\alpha \mathrm{T}'(\chi) + \mathcal{O}(\lambda_\alpha^2) \tag{374}$$

It may be concluded that a first order finite difference scheme approximates the gradient:

$$\frac{\partial \mathrm{T}}{\partial \chi} \approx \frac{\mathrm{T}(\chi + \lambda_\alpha) - \mathrm{T}(\chi)}{\lambda_\alpha} \tag{375}$$

Summing over all possible steps $\forall\ \alpha = 1,2,\dots,n$ then provides a more accurate description:

$$\frac{\partial \mathrm{T}}{\partial \chi} \approx \frac{1}{n}\sum_{\alpha=1}^{n} \frac{\mathrm{T}(\chi + \lambda_\alpha) - \mathrm{T}(\chi)}{\lambda_\alpha} \tag{376}$$

The exact definition of the derivative is recovered in the limit as the step size approaches zero:

$$\frac{\partial \mathrm{T}}{\partial \chi} = \frac{1}{n}\sum_{\alpha=1}^{n} \lim_{\lambda_\alpha \to 0} \frac{\mathrm{T}(\chi + \lambda_\alpha) - \mathrm{T}(\chi)}{\lambda_\alpha} \tag{377}$$

Each finite difference $\delta_\alpha \mathrm{T} = \mathrm{T}(\chi + \lambda_\alpha) - \mathrm{T}(\chi)$ is weighted proportional to λ_α^{-1} when n is finite. If we define the weight as $k_\alpha = (n\lambda_\alpha)^{-1}$, then (376) may be written in the more compact form:

$$\frac{\partial \mathrm{T}}{\partial \chi} \approx \sum_{\alpha=1}^{n} k_\alpha \delta_\alpha \mathrm{T} \tag{378}$$

Please see Figure 35 (left) showing the absolute value of the weights as a function of the distance from χ; which refers to $\lambda = 0$. As one can observe, finite differences located nearer to χ are weighted more heavily in comparison to the ones located farther away since:

$$\lim_{\lambda_\alpha \to 0^{\pm}} |k_\alpha| = \infty, \qquad \lim_{\lambda_\alpha \to \pm\infty} |k_\alpha| = 0 \tag{379}$$

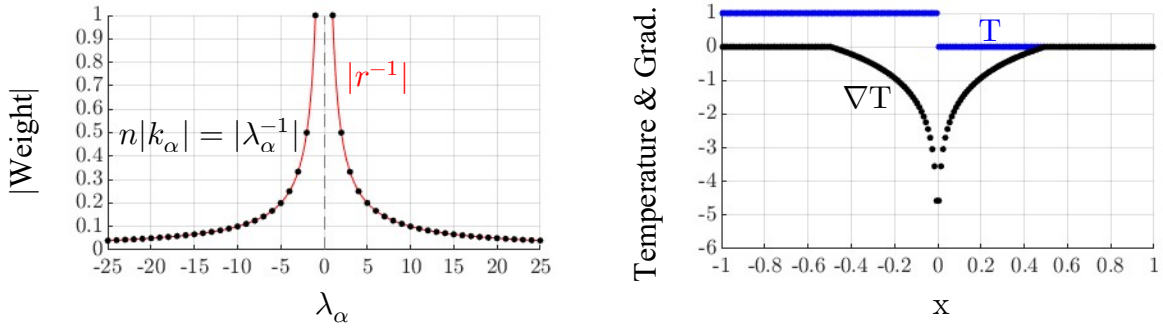

Figure 35 Finite difference weights (left) and gradient approximation at discontinuity (right)

To the right within Figure 35 is a numerical approximation of the gradient, using (376), of a function containing a jump discontinuity. As a result, the proposed methodology shows to be successful in capturing the derivative through using a simple nonlocal approach. Figure 36 provides additional examples where the analytical solutions are in red. It will be noted that $\mathcal{H}_{10}$ refers to the 10th order probabilist's Hermite polynomial. Additionally, for nodes located within the vicinity of a boundary, a reflective scheme is utilized. In other words, when there is a loss of connectivity, the lattice derivative is not set to zero but to the value of the opposing side.

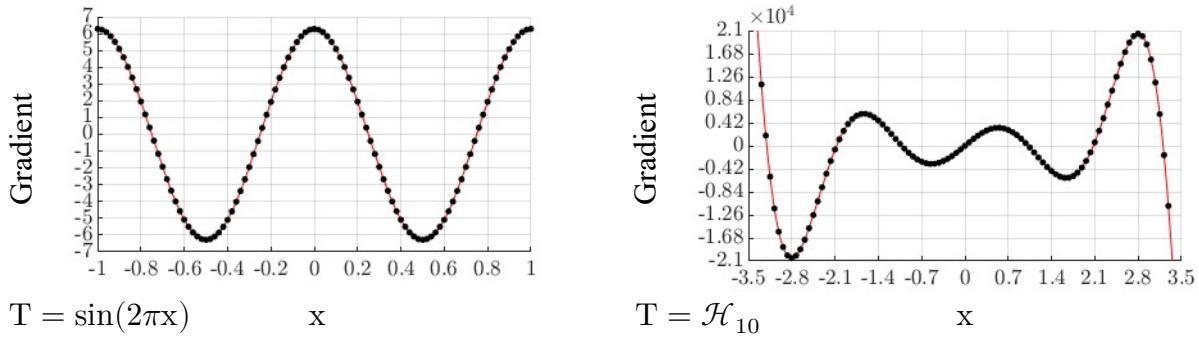

Figure 36 Gradient approximations of smooth analytical functions

In conclusion, analytical expressions for the first perturbation have been obtained. If desired, the same methodology can be applied to uncover $\hat{\mathrm{E}}^{\mathbb{1}}$ and $\hat{\mathrm{S}}^{\mathbb{1}}$. Additionally, a reliable method has been established to numerically compute the gradients. However, this methodology will not be used within the QVFEM, where the stress and heat flux will be treated at the mesoscopic level.

4.4 Finite Element Formulation

We will herein provide a finite element formulation of Leo's EOM (352). To begin, we'll denote an observable by Σ whose variational form is $\Sigma^* = \Sigma + \tau\partial_{\mathbb{1}}\Sigma$. The isentropic temporal derivative of the distribution may now be found through the following variational operation:

$$\partial_{\mathbb{1}}\mathrm{F} = (\partial \mathrm{F}^*/\partial\tau)|_{\tau=0} = \nu\mathrm{F} \tag{380}$$

Where from here on out, $\mathrm{F} = \mathrm{F}^{\mathbb{0}}$. Denoting $\delta = 1 - \nu\tau$, Leo's EOM will be expressed as:

$$\dot{\mathrm{F}} + \xi_i\nabla_i(\delta\mathrm{F}) = \xi_i\xi_l\nabla_i(\tau\nabla_l\mathrm{F}) \tag{381}$$

If we set the "drift" velocity to $\mu_i = \delta\xi_i$ and denote the diffusion tensor as $\mathrm{D}_{ij} = \xi_i\xi_j\tau$, then Leo's EOM will take the form of the Fokker-Planck equation:

$$\dot{\mathrm{F}} + \nabla_i(\mu_i\mathrm{F}) = \nabla_i(\mathrm{D}_{il}\nabla_l\mathrm{F}) \tag{382}$$

Which is then directly connected to the N-S momentum equation through replacing F with $\hat{\mathbf{p}}$. If we hold ν and τ constant, the dispersion relation is computed as:

$$\omega = (\delta - i\tau\omega_\infty)\omega_\infty \tag{383}$$

Where the freestream version is recovered when $\tau = 0$, i.e. $\omega_\infty = \boldsymbol{k}\cdot\boldsymbol{\xi}$, and the group velocity is:

$$\partial\omega/\partial\boldsymbol{k} = (\delta - 2i\tau\omega_\infty)\boldsymbol{\xi} \tag{384}$$

The associated complex propagating wave function (introduced in ch.3.9) will now take the form:

$$\psi(\boldsymbol{k},\mathbf{x},t) = \exp[i\boldsymbol{k}\cdot(\mathbf{x}-\delta\boldsymbol{\xi}t) - \tau(\boldsymbol{k}\cdot\boldsymbol{\xi})^2 t] \tag{385}$$

$$= \psi_\infty \exp[-i(\omega-\omega_\infty)t]$$

Where the freestream version is $\psi_\infty = \exp[i\boldsymbol{k}\cdot(\mathbf{x}-\boldsymbol{\xi}t)]$. One can observe that two additional contributions have been added; one which directly modifies the advection velocity $\boldsymbol{\xi}$, as found in $\exp(i\nu\tau\omega_\infty t)$, and the other is $\exp(-\tau\omega_\infty^2 t)$, which directly affects the amplitude of the wave. This analysis gives us hints towards the solution structure. Again, holding ν and τ constant, the solution will next be decomposed as $\mathrm{F}(\mathbf{x},t) = \mathrm{G}[\boldsymbol{\varphi}^{-1}(\mathbf{x},t)]\mathrm{Q}(t)$, where the inverse mapping is redefined as $\boldsymbol{\varphi}^{-1}(\mathbf{x},t) = \mathbf{x} - \delta\boldsymbol{\xi}t$. Leo's EOM (381) will then simplify to:

$$\dot{\mathrm{F}} + \delta\xi_i\nabla_i\mathrm{F} - \tau\xi_i\xi_l\nabla_i\nabla_l\mathrm{F} = \mathrm{G}\dot{\mathrm{Q}} + \mathrm{Q}\cancelto{0}{\left(\dot{\mathrm{G}} + \delta\xi_i\nabla_i\mathrm{G}\right)} - \tau\xi_i\xi_l(\nabla_i\nabla_l\mathrm{G})\mathrm{Q} = 0 \tag{386}$$

We'll next divide by $\mathrm{F} = \mathrm{GQ}$ and utilize the solution (385) to uncover the eigen-relations:

$$\frac{1}{\mathrm{Q}}\frac{dQ}{dt} = \frac{\tau\xi_i\xi_l}{\mathrm{G}}\frac{\partial^2\mathrm{G}}{\partial\varphi_i^{-1}\varphi_l^{-1}} = -\tau(k_j\xi_j)^2 \tag{387}$$

The general solution over the element can then be expressed as a real Fourier series:

$$\mathrm{F}(\mathbf{x},t) = \mathrm{A}_0 + \sum_{\alpha=1}^{\infty}\sum_{\beta=1}^{\infty}\sum_{\gamma=1}^{\infty}(\mathrm{A}_{\alpha\beta\gamma}\cos\Phi_{\alpha\beta\gamma} + \mathrm{B}_{\alpha\beta\gamma}\sin\Phi_{\alpha\beta\gamma})\exp(-\Omega_{\alpha\beta\gamma}t) \tag{388}$$

$$\Phi_{\alpha\beta\gamma} = \frac{\alpha\pi}{a}(x-\delta ut) + \frac{\beta\pi}{b}(y-\delta vt) + \frac{\gamma\pi}{c}(z-\delta wt) \tag{389}$$

$$\Omega_{\alpha\beta\gamma} = \tau\left(\frac{\alpha\pi u}{a} + \frac{\beta\pi v}{b} + \frac{\gamma\pi w}{c}\right)^2 \tag{390}$$

The rank three tensors $\mathrm{A}_{\alpha\beta\gamma}$ and $\mathrm{B}_{\alpha\beta\gamma}$ store the Fourier or normalizing coefficients, the velocity vector is denoted $\boldsymbol{\xi} = \langle u,v,w\rangle$, and the constants $\boldsymbol{l} = \langle a,b,c\rangle$ are the length, width, and height of the reference element. If the grid is uniform, then $\boldsymbol{l} = \langle\delta x,\delta y,\delta z\rangle$. To compute the coefficients, which represent the amplitude of each wave function, we must integrate over the element. In order to perform a proper integration over an arbitrary shaped element sampled from a nonuniform grid, a coordinate transformation must be applied where the set of points $\mathbf{x}$ are mapped into a uniform $\mathbf{y}$. In consequence, the governing EOM (381) will now take the following form:

$$\frac{\partial\mathrm{F}}{\partial t} + \left(\delta\xi_b' - \tau\xi_a'\frac{\partial\xi_b'}{\partial\mathrm{y}_a}\right)\frac{\partial\mathrm{F}}{\partial\mathrm{y}_b} = \tau\xi_a'\xi_b'\frac{\partial^2\mathrm{F}}{\partial\mathrm{y}_a\partial\mathrm{y}_b} \tag{391}$$

Where $\boldsymbol{\xi}' = \boldsymbol{\Delta}\cdot\boldsymbol{\xi}$ and $\boldsymbol{\Delta} = (\partial\mathbf{y}/\partial\mathbf{x})|_{\mathbf{x}\to\mathbf{y}}$; see ch.3.4. The solution to (391) is simply (388) mapped into $\mathbf{y}$, i.e. $\mathrm{F}(\mathbf{y},t) = \mathrm{F}[\mathbf{x}(\mathbf{y}),t]$. This type of solution, regardless of the grid geometry, requires special care. The construction procedure is as follows. We'll begin with the initial

condition prescribed by the polynomial interpolation (147):

$$\mathrm{I}[\mathbf{x}(\mathbf{y})] = \mathfrak{c}_1 + (\mathfrak{c}_2 x + \mathfrak{c}_3 y + \mathfrak{c}_4 xy + \mathfrak{c}_5 z + \mathfrak{c}_6 xz + \mathfrak{c}_7 yz + \mathfrak{c}_8 xyz)|_{\mathbf{x}\to\mathbf{y}} \tag{392}$$

Where the interpolation coefficients $\mathfrak{c}_i$ are yet to be determined. We will next enforce:

$$\prod_{i=1}^{3} \int_0^{l_i} (\mathrm{F}[\mathbf{x}(\mathbf{y}), 0] - \mathrm{I}[\mathbf{x}(\mathbf{y})])\Psi \, d\mathrm{y}_i = 0 \tag{393}$$

Where Ψ represents 1, $\cos\Phi_{\alpha\beta\gamma}$, and $\sin\Phi_{\alpha\beta\gamma}$. Since (388) is not a standard Fourier series [19; ch.7.3], the orthogonal properties of the cosine and sine functions cannot be typically utilized to obtain explicit expressions for A_0, $\mathrm{A}_{\alpha\beta\gamma}$, and $\mathrm{B}_{\alpha\beta\gamma}$. Instead, a matrix may be assembled using (393) then inverted to compute the wave amplitudes. We will next require that the variation at the nodal points be zero meaning $\mathrm{F}[\mathbf{x}(\mathbf{y}_i), 0] = f_i$, where $\boldsymbol{f}$ is the vector of nodal distribution values. Therefore, the interpolation coefficients will be computed directly from (388) at $t = 0$, after obtaining the Fourier coefficients, which are dependent upon $\mathfrak{c}_i$.

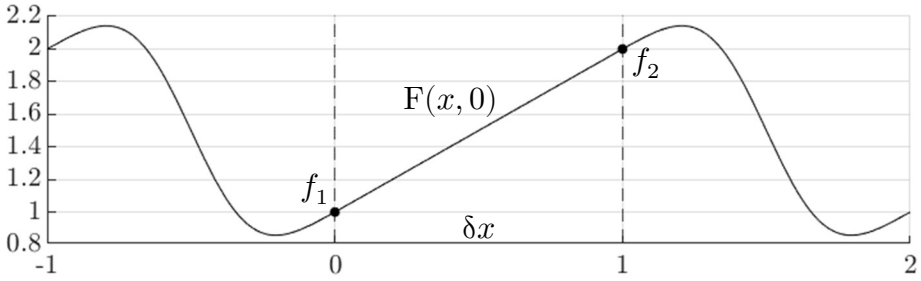

Figure 37 Fourier series interpolation over a 1D element

An analytical solution in 1D is shown in Figure 38, which can be compared with the first order solution shown in Figure 13. The linear solutions are next provided as:

$$\mathrm{F}(x, y, z, t) = \mathfrak{c}_1 + \mathfrak{c}_2(x - \delta u t) + \mathfrak{c}_3(y - \delta v t) + \mathfrak{c}_4(z - \delta w t) \tag{394}$$

However, the linearized form causes all terms within the Hessian $\nabla_i \nabla_l \mathrm{F}$ to vanish therefore (394) does not resemble the full essence of Leo's EOM. This is an elegant result however because the modified motion $\boldsymbol{\varphi}(\mathbf{x}_\mathrm{o}, t) = \mathbf{x}_\mathrm{o} + \delta\boldsymbol{\xi} t$ was once predicted by Newton [1; Book II], who said:

> *If a body is resisted in the ratio of its velocity, the motion lost by resistance is as the space gone over in its motion.*

The finite element formulation of (381) is next given as:

$$f_i \int_{\delta t} \int_{\mathscr{v}(t)} [(\dot{\psi}_i + \mu_a \psi_{i,a})\phi_j + \mathrm{D}_{ab}\psi_{i,a}\phi_{j,b}] \, d\mathscr{v} \, dt = \int_{\delta t} \int_{\mathscr{v}(t)} \mho \phi_j \, d\mathscr{v} \, dt \tag{395}$$

Which is analogous to the freestream version (160) and once again ν and τ have been held fixed. To note, integration by parts has been applied to $\psi_{i,ab}\phi_j$ where the boundary terms were neglected. This process is directly related through defining $\mathrm{F}^* = f_i\psi_i + \epsilon_k\phi_k$, then finding the first order variation in the scalar quantity shown below:

$$\frac{1}{2}\xi_a\xi_b\frac{\mathbb{d}}{\mathbb{d}\epsilon_j}\left(\frac{\partial \mathrm{F}^*}{\partial \mathrm{x}_a}\frac{\partial \mathrm{F}^*}{\partial \mathrm{x}_b}\right)\Bigg|_{\boldsymbol{\epsilon}=\mathbf{0}} = f_i\xi_a\xi_b\psi_{i,a}\phi_{j,b} \tag{396}$$

For a comparison to the LBE, the linear one-dimensional solution is provided as:

$$\mathrm{F}(x,t) = f_1 + (\delta f/\delta x)(x - \delta\xi t) \tag{397}$$

For a uniform grid, meaning $\delta x = \xi\delta t$, the updated nodal value is:

$$f_3 = (1-\nu\tau)f_1 + \nu\tau f_2 \tag{398}$$

One can now compare this solution to the LBE (68). One major difference is that in this framework, a multistage algorithm must be utilized, where the first order evolution must first be computed. Once ν is known, the second order evolution may next be approximated.

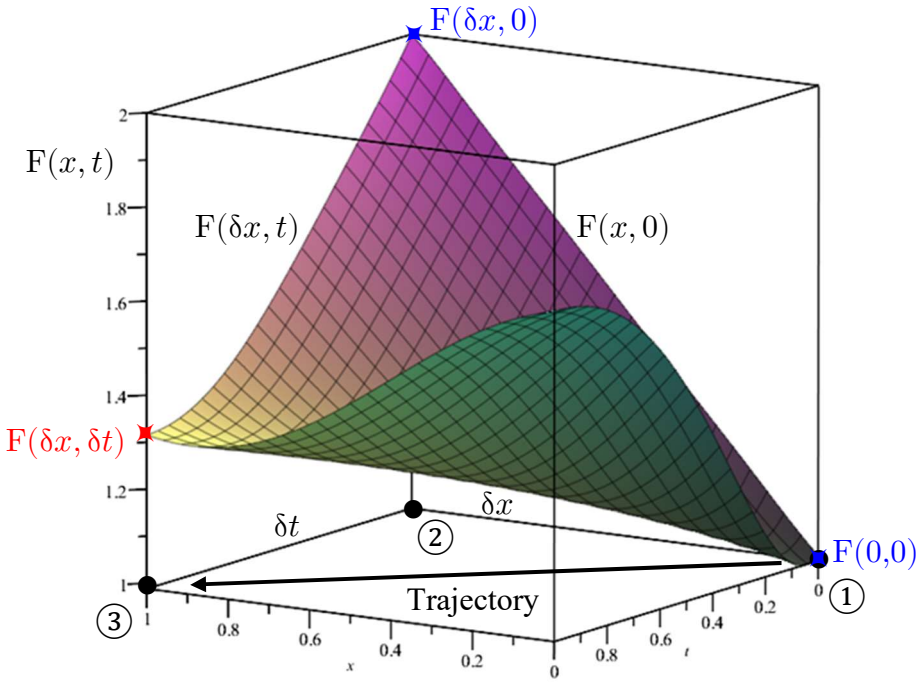

Figure 38 Second order spacetime solution over a phasetime element

4.5 Testing the Theory

To begin, let us first state the equations of motion to be numerically solved:

$$\partial\hat{\rho} + \xi_i \nabla_i \hat{\rho} = 0 \tag{399}$$

$$\partial\hat{\mathrm{p}}_i + \xi_l \nabla_l \hat{\mathrm{p}}_i = \xi_k \nabla_k [\tau(\nu(\hat{\mathrm{p}}_i) + \xi_l \nabla_l \hat{\mathrm{p}}_i)] \tag{400}$$

$$\partial\hat{\mathrm{E}} + \xi_i \nabla_i \hat{\mathrm{E}} = \xi_l \nabla_l [\tau(\nu(\hat{\mathrm{E}}) + \xi_i \nabla_i \hat{\mathrm{E}})] \tag{401}$$

Where $\nu(\hat{\mathrm{p}}_i) = \partial_{\mathbb{1}} \hat{\mathrm{p}}_i$ and $\nu(\hat{\mathrm{E}}) = \partial_{\mathbb{1}} \hat{\mathrm{E}}$. Upon integrating over the velocity space, we obtain the following set of Navier-Stokes-Fourier equations:

$$\partial\rho + \nabla_i(\rho \mathrm{v}_i) = 0 \tag{402}$$

$$\partial(\rho \mathrm{v}_i) + \nabla_l(\rho \mathrm{v}_i \mathrm{v}_l + \mathrm{P}\delta_{il}) = \nabla_l[\mu(\nabla_i \mathrm{v}_l + \nabla_l \mathrm{v}_i) + \varsigma \nabla_k \mathrm{v}_k \delta_{il}] \tag{403}$$

$$\partial(\rho e) + \nabla_i[(\rho e + \mathrm{P})\mathrm{v}_i] = \nabla_l[\mu(\nabla_i \mathrm{v}_l + \nabla_l \mathrm{v}_i)\mathrm{v}_i + \varsigma(\nabla_k \mathrm{v}_k)\mathrm{v}_l + \kappa \nabla_l \mathrm{T}] \tag{404}$$

Where $\mu = \mathrm{P}\tau$, $\varsigma = \eta - \frac{2}{3}\mu$, $\eta = \mu(\frac{5}{3} - \gamma)$, and $\kappa = \mathrm{c}_{\mathrm{P}}\mu$. Therefore, the Prandtl number in this model is unity. For an adjustable Prandtl number, the derived theoretical model is:

$$\partial\hat{\mathrm{E}} + \xi_i \nabla_i \hat{\mathrm{E}} = \xi_l \nabla_l [\tau(\nu(\hat{\mathrm{E}}) + \xi_i \nabla_i \hat{\mathrm{E}}) + \mathbb{t}\mathrm{T}(\nu(\hat{\mathrm{S}}) + \xi_i \nabla_i \hat{\mathrm{S}})] \tag{405}$$

Since the additional contribution is in terms of the entropy distribution, solutions to the EOM (405) become more difficult to obtain. We could consider solving the entropy evolution:

$$\partial\hat{\mathrm{S}} + \xi_i \nabla_i \hat{\mathrm{S}} = \xi_l \nabla_l [\tau^*(\nu(\hat{\mathrm{S}}) + \xi_i \nabla_i \hat{\mathrm{S}})] + \, ? \tag{406}$$

However, we will need to uncover an expression for the rate of entropy production in distribution form. Also keep in mind, we would now need to solve for the temperature in terms of the entropy. We'll next return to (400) and (401), and investigate further the coefficients η and κ. Well, the coefficient of dilatational viscosity may be expressed as:

$$\upsilon\eta = (\mathbb{o}_{\mathrm{tr}}^2 - \mathbb{o}^2)\tau \tag{407}$$

Where the speed of sound (squared) is $\mathbb{o}^2 = \gamma\Theta$ therefore $\mathbb{o}_{\mathrm{tr}}^2 = \frac{5}{3}\Theta$. So if $\mathbb{o} = \mathbb{o}_{\mathrm{tr}}$, then $\eta = 0$. In order to fit experimental data, let us hypothetically modify the first order pressure evolution (301):

$$\partial_{\mathbb{1}} \mathrm{P} = -\mathrm{v}_i \nabla_i \mathrm{P} - \epsilon\gamma \mathrm{P} \nabla_i \mathrm{v}_i \tag{408}$$

As a result, Tracey's number becomes $\mathfrak{T} = \frac{5}{3} - \epsilon\gamma$. We'll next identify an entropy quantity, which will be referred to as ***Cooper's entropy density***: $\mathrm{C} = -(\epsilon - 1)\gamma R\rho$, so that (408) becomes:

$$\mathrm{d}_{\mathbb{1}}\mathrm{P} = -(\gamma\mathrm{P} - \mathrm{CT})\nabla_i \mathrm{v}_i \mathrm{d}t \tag{409}$$

The minimum value of this new quantity is $\mathrm{C}_{\text{min}} = \mathrm{C}(\epsilon = 1) = 0$ therefore $\mathfrak{T}_{\text{min}} = \frac{5}{3} - \gamma$. Future investigation is required to validate this theory and determine how to modify (400).

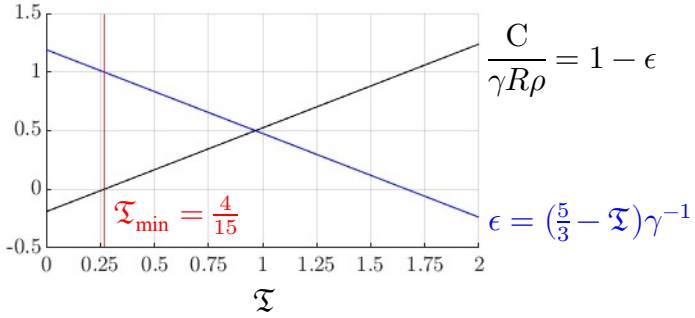

Figure 39 Cooper's entropy density for a diatomic perfect gas ($\gamma = 7/5$)

Let us next revisit (272) in regards to a stationary perfect gas with uniform density:

$$\dot{\varepsilon} = -\upsilon \boldsymbol{\nabla} \cdot \mathbf{q} \;\Rightarrow\; \dot{\mathrm{T}} = \boldsymbol{\nabla} \cdot (\alpha \boldsymbol{\nabla} \mathrm{T}) \tag{410}$$

Where $\alpha = \upsilon\kappa/\mathrm{c}_\upsilon$ and $\mathbf{q} = -\kappa\boldsymbol{\nabla}\mathrm{T}$. If $\kappa = \mathrm{c}_\mathrm{P}\mu$, then $\alpha = \mathbb{c}^2\tau$ and the heat flux vector may be expressed as:

$$\upsilon\mathbf{q} = -\alpha\boldsymbol{\nabla}\varepsilon \tag{411}$$

We'll next consider the case when $\kappa = \mathrm{c}_\mathrm{P}\mu(1 + \dot{\tau})$. Therefore, $\alpha = \mathbb{b}^2\tau$, where $\mathbb{b}^2 = (1 + \dot{\tau})\mathbb{c}^2$. The additional contribution could possibly be associated to the second sound wave [66,67]. The speed of second sound is then denoted $\mathbb{b}$. Again, this is only speculation.

Now that we've discussed some future avenues of work, we will return to testing (399-401). To do so, we must uncover expressions for the operator $\nu \equiv \partial_{\mathbb{1}}$. Referring back to (380), the isentropic temporal derivative will be expanded in a similar fashion to (355):

$$\frac{\partial_{\mathbb{1}}\mathrm{F}}{\partial t} = \frac{\partial \mathrm{F}}{\partial \rho}\frac{\partial_{\mathbb{1}}\rho}{\partial t} + \frac{\partial \mathrm{F}}{\partial \mathrm{v}_i}\frac{\partial_{\mathbb{1}}\mathrm{v}_i}{\partial t} + \frac{\partial \mathrm{F}}{\partial \mathrm{T}}\frac{\partial_{\mathbb{1}}\mathrm{T}}{\partial t} = \nu\mathrm{F} \tag{412}$$

Where a simple forward difference scheme will be used to approximate the virtual changes:

$$\nu \approx \frac{1}{\delta t}\left(\frac{\partial \mathrm{F}}{\partial \rho}\delta_{\mathbb{1}}\rho + \frac{\partial \mathrm{F}}{\partial \mathrm{v}_i}\delta_{\mathbb{1}}\mathrm{v}_i + \frac{\partial \mathrm{F}}{\partial \mathrm{T}}\delta_{\mathbb{1}}\mathrm{T}\right) \tag{413}$$

Using the derivative relations (359), $\partial_{\mathbb{1}}\hat{\mathbf{p}}$ is found as:

$$\frac{\partial_{\mathbb{1}}\hat{\mathrm{p}}_i}{\partial t} = \left(\upsilon\frac{\partial_{\mathbb{1}}\rho}{\partial t} + \beta\dot{q}_l\frac{\partial_{\mathbb{1}}\mathrm{v}_l}{\partial t} + R\beta^2\mathcal{L}\frac{\partial_{\mathbb{1}}\mathrm{T}}{\partial t}\right)\hat{\mathrm{p}}_i \tag{414}$$

The derivative relations for the total energy density distribution are next provided in the form:

$$\frac{\partial \hat{\mathrm{E}}}{\partial \rho} = \upsilon \hat{\mathrm{E}}, \qquad \frac{\partial \hat{\mathrm{E}}}{\partial \mathrm{v}_i} = \beta \dot{q}_i \hat{\mathrm{E}}, \qquad \frac{\partial \hat{\mathrm{E}}}{\partial \mathrm{T}} = (R\beta^2 \mathcal{L} + \overline{\mathrm{c}}_{\upsilon} \mathcal{E}^{-1}) \hat{\mathrm{E}} \tag{415}$$

Where $\mathcal{E} = \frac{1}{2}|\boldsymbol{\xi}|^2 + \overline{\varepsilon}$ and $\overline{\mathrm{c}}_{\upsilon} = \partial \overline{\varepsilon} / \partial \mathrm{T}$, therefore, $\partial_{\mathbb{1}} \hat{\mathrm{E}}$ expands as:

$$\frac{\partial_{\mathbb{1}} \ln \hat{\mathrm{E}}}{\partial t} = \upsilon \frac{\partial_{\mathbb{1}} \rho}{\partial t} + \beta \dot{q}_i \frac{\partial_{\mathbb{1}} \mathrm{v}_i}{\partial t} + (R\beta^2 \mathcal{L} + \overline{\mathrm{c}}_{\upsilon} \mathcal{E}^{-1}) \frac{\partial_{\mathbb{1}} \mathrm{T}}{\partial t} \tag{416}$$

Even though we will not include the entropy evolution into our simulation, the derivatives with respect to the observables, will be provided for future reference ($\mathcal{Q} = \mathcal{L} + \mathrm{Ts}$):

$$\frac{\partial \hat{\mathrm{S}}}{\partial \rho} = \upsilon (1 - \Theta \mathcal{Q}^{-1}) \hat{\mathrm{S}}, \qquad \frac{\partial \hat{\mathrm{S}}}{\partial \mathrm{v}_i} = \beta \dot{q}_i (1 - \Theta \mathcal{Q}^{-1}) \hat{\mathrm{S}} \tag{417}$$

$$\frac{\partial \hat{\mathrm{S}}}{\partial \mathrm{T}} = R\beta^2 \mathcal{L} (1 - \Theta \mathcal{Q}^{-1}) \hat{\mathrm{S}} + \overline{\mathrm{c}}_{\upsilon} \mathcal{Q}^{-1} \hat{\mathrm{S}} \tag{418}$$

The exact same Sod setup will be used from ch.3.9. However, the simulation will be ran for a longer time duration to allow for the nonequilibrium effects to be observed. The modified algorithm can be found in Table 5. In one spatial dimension, for argon, the mass and energy distributions are respectively:

$$\hat{\rho} = \rho \zeta^{-1} \exp(-\tfrac{1}{2} \beta \dot{q}^2) \tag{419}$$

$$\hat{\mathrm{E}} = (\tfrac{1}{2} \xi^2 + \Theta) \hat{\rho} \tag{420}$$

Where $\zeta = (2\pi\Theta)^{1/2}$, $\dot{q} = \xi - u$, $\mathcal{L} = \frac{1}{2}(\dot{q}^2 - \Theta)$, $\mathcal{E} = \frac{1}{2}\xi^2 + \Theta$, and $\overline{\mathrm{c}}_{\upsilon} = R$. Since the motion is given by $\varphi^{-1}(x,t) = x - (1 - \nu\tau)\xi t$, the velocity is in actuality dependent upon position. To satisfy the CFL requirement, the factor of safety was set to $\sigma = 0.5$. The end result of the simulation is shown in Figure 40 at $t \approx 5.6438$ ms. The first and second order solutions are compared in Figures 41 and 42.

$\mathbf{x}_{ijk} = \langle x_i, y_j, z_k \rangle$	generate spatial finite element mesh grid
$\Gamma_{ijk}^{\alpha} =$ phase matrix (connectivity)	establish the connectivity matrix $\forall\ (\boldsymbol{\xi}^{\alpha}, \mathbf{x}_{ijk})$
$\rho_{\mathrm{o}}, \mathbf{v}_{\mathrm{o}}, \varepsilon_{\mathrm{o}}$	input initial conditions
for $t = 1 : n_t$	begin time marching
$\mathbb{c} = \cdots$ see (229)	compute the characteristic speed
$\boldsymbol{\xi}^{\alpha} = \mathbb{c}\boldsymbol{z}^{\alpha}$	obtain finite set of quantized velocities
$\delta t = \sigma \mathbb{c}^{-1} \min\langle \lvert\delta x\rvert, \lvert\delta y\rvert, \lvert\delta z\rvert \rangle$	compute time step to satisfy (87) apply factor of safety $0 < \sigma < 1$
$\lambda = 2\pi\mathfrak{H}/\mathbb{c}$	overall wavelength
$\delta\chi = \lambda/\mathbb{m}$	wavelength step size
$\boldsymbol{\chi}^{\beta} = \boldsymbol{z}^{\beta}\delta\chi$	associated quantized virtual displacements
$\Psi^{\beta}(\mathbf{x}, t)$	initialize moment generating wave functions
$\mathbf{Q} = (\mathbb{c}\mathbb{m})^{-3}\boldsymbol{\psi}^{*}$ and $\mathbf{Q}^{-1} = \mathbb{c}^{3}\boldsymbol{\psi}$	transformation matrix and inverse
$\mathbf{F}(\mathbf{x}, t) = \mathbf{Q} \cdot \boldsymbol{\Psi}(\mathbf{x}, t)$	extract the discrete "masses"
$\mathrm{F}^{\alpha}(\mathbf{x}, t) = \boldsymbol{f}^{\alpha} \cdot \boldsymbol{g}^{\alpha}[\boldsymbol{\varphi}^{-1}(\mathbf{x}, t)]$	apply solution over each phasetime element and extract the temporally advanced distribution values located at $\mathrm{F}^{\alpha\prime} = \mathrm{F}^{\alpha}(\mathbf{x} + \delta\mathbf{x}^{\alpha}, t + \delta t)$ using the phase matrix
$\boldsymbol{\Psi}' = \mathbf{Q}^{-1} \cdot \mathbf{F}'$	update moment generating wave functions
$\Sigma' = \Psi'(\boldsymbol{\chi} = \mathbf{0})$	extract the temporally advanced system quantities from the moment generating wave functions
$\partial_{\mathbb{1}}\Sigma/\partial t \approx \delta_{\mathbb{1}}\Sigma/\delta t$	compute isentropic changes then reset the observables
$\tau = \mu \mathrm{P}^{-1}$	initialize the dissipation time
$\mathrm{F}^{\alpha}(\mathbf{x}, t) = \cdots$ see (388)	apply the second order solution
$\boldsymbol{\Psi}' = \mathbf{Q}^{-1} \cdot \mathbf{F}'$	update moment generating wave functions
$\Sigma' = \Psi'(\boldsymbol{\chi} = \mathbf{0})$	extract the temporally advanced system quantities from the moment generating wave functions
$\rho_{\mathrm{b}}, \mathbf{v}_{\mathrm{b}}, \varepsilon_{\mathrm{b}}$	apply boundary conditions at the boundaries of analysis
end	end time marching
$\rho(\mathbf{x}, t_{\text{final}}), \mathbf{v}(\mathbf{x}, t_{\text{final}}), \varepsilon(\mathbf{x}, t_{\text{final}})$	export results and plot

Table 5 QVFEM modified algorithm

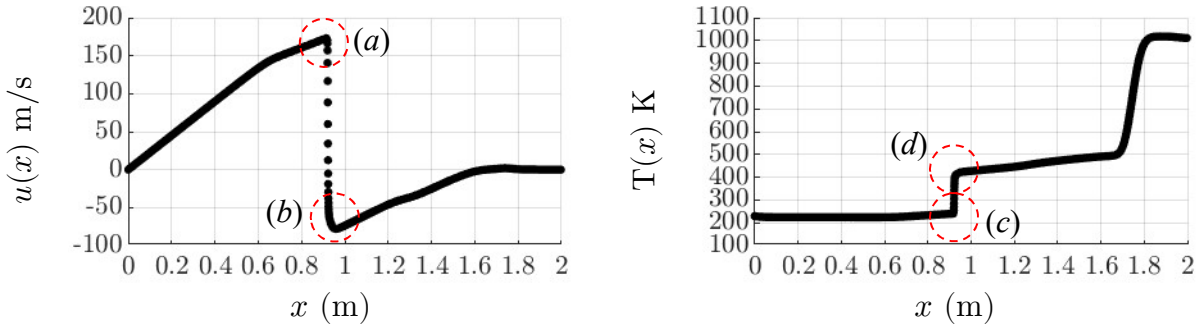

Figure 40 Modified Sod shock tube results at $t \approx 5.6438$ ms

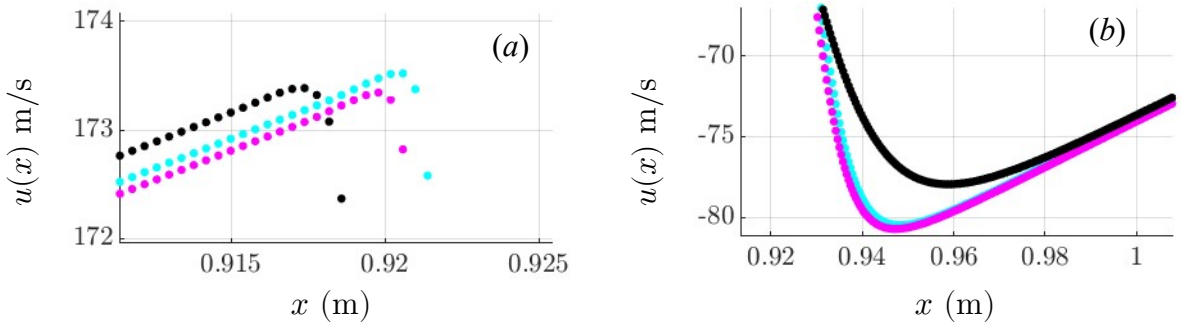

Figure 41 Velocity comparison between the first order solution, shown at $t \approx 5.6419$ ms (cyan) and $t \approx 5.6440$ ms (magenta), and the second order solution at $t \approx 5.6438$ ms

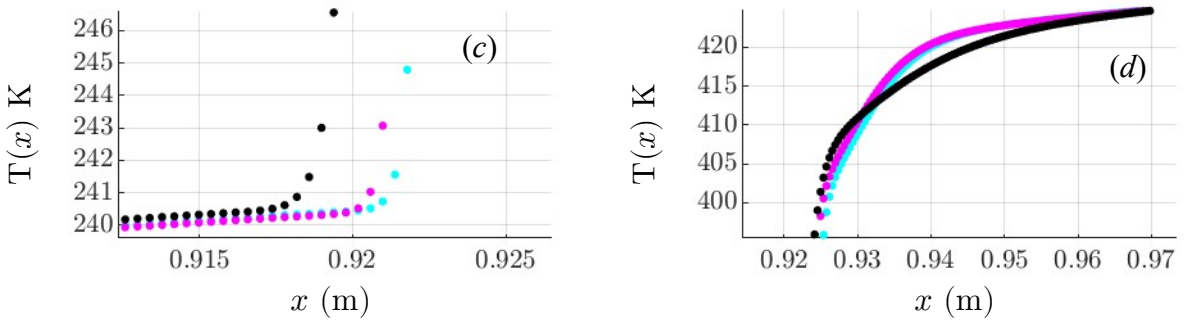

Figure 42 Temperature comparison between the first order solution, shown at $t \approx 5.6419$ ms (cyan) and $t \approx 5.6440$ ms (magenta), and the second order solution at $t \approx 5.6438$ ms

Chapter 5 – Conclusions & Future Directions

Within this work, the following was accomplished:

- Development of a new quantization procedure ab initio which maintains the structure of the Gaussian and allows for an unlimited number of sample points
- Derived Leo's equation of motion, which when integrated over the velocity space, directly recovers the Navier-Stokes-Fourier equations
- A new finite element was discovered which was coined the phasetime element
- Overall, a new finite element method was developed to solve the Euler and Navier-Stokes-Fourier equations

The foundations of the QVFEM have now been laid. Future work will be invested in high-performance computing on two- and three-dimensional test cases. This is a key step for future development. Based on the results in ch.3.9 and ch.4.5, the proposed methodology shows much promise. As of now, boundary conditions are restricted to the Dirichlet type, which have yet to be verified. The implementation of other boundary constraints, e.g. Neumann conditions, is left for future work. Computational grids must be structured but allow for a nonuniform layout. Therefore, one cannot triangulate a mesh; which is one slight disadvantage.

Due to the complexity of the NSF equations, I believe with more testing, we can show that the QVFEM is the approach to be adopted for numerical simulations of flowfields. We have now given the LBM a proper continuum treatment, where Leo's EOM directly represents the governing evolution equations. I hope this work begins a new paradigm shift in CFD, where computational solutions will be more accessible, accurate, and reliable. Future avenues of exploration may entail:

- Extend the framework to incorporate a chemically reacting gas mixture
- Account for gas-surface interactions [69; ch.4]
- Extensions for plasma physics

Appendix

Within ch.2.3, it was briefly mentioned that the LB algorithm does not align with the Chapman-Enskog perturbation analysis, therefore, does not directly represent approximate solutions to the Navier-Stokes equations. The details will be provided herein.

Chapman-Enskog Methodology

To begin, we'll recall the generalized Boltzmann equation (29), whose two-body form, in the absence of both external and internal forces, is provided as:

$$\frac{\partial \mathfrak{F}_1}{\partial t} + \dot{\boldsymbol{q}}_1 \cdot \frac{\partial \mathfrak{F}_1}{\partial \boldsymbol{q}_1} + \pi \varnothing^2 \int_{\mathbb{R}^3} |\dot{\boldsymbol{q}}_2| \delta\mathfrak{F} \, d\dot{\mathcal{Q}}_2 = 0 \tag{421}$$

Where the details of the molecular interactions are taken from ch.2.2. Since $d\dot{\mathcal{Q}}_1 d\dot{\mathcal{Q}}_2 = d\dot{\mathcal{X}}_1 d\dot{\mathcal{X}}_2$ and $\dot{\boldsymbol{q}}_1 = \dot{\mathbf{x}}_1$, then $d\dot{\mathcal{Q}}_2 = d\dot{\mathcal{X}}_2$. For ease of notation, we'll reassign the coordinate variables to $\mathbf{x}_1 = \mathbf{x}$, $\mathbf{x}_2 = \mathbf{y}$, and $\boldsymbol{q}_2 = \boldsymbol{\eta}$. Additionally, we'll set $\mathfrak{F}_1 = \mathrm{F}$. To satisfy Boltzmann's H-theorem [15; ch.4], the variation (34) must be slightly modified, such that:

$$\delta\mathfrak{F} = -(\mathrm{F}'\mathrm{G}' - \mathrm{F}\mathrm{G}) \tag{422}$$

As a result, (421) will take the more usual form [15; ch.7] for the hard-sphere case:

$$\frac{\partial \mathrm{F}}{\partial t} + \dot{\mathrm{x}}_i \frac{\partial \mathrm{F}}{\partial \mathrm{x}_i} = \pi \varnothing^2 \int_{\mathbb{R}^3} |\dot{\boldsymbol{\eta}}| (\mathrm{F}'\mathrm{G}' - \mathrm{F}\mathrm{G}) \, d\dot{\mathcal{Y}} \tag{423}$$

We'll next recall the derived mean-free path length from ch.2.2, i.e. $\ell_{\mathrm{c}} = m(\sqrt{2}\pi\varnothing^2\rho)^{-1}$. Upon defining a volumetric quantity $\mathcal{V} = m(\sqrt{2}\rho)^{-1} = \pi\varnothing^2\ell_{\mathrm{c}}$ and multiplying (423) by a characteristic length ℓ, one obtains:

$$\mathfrak{K}\left(\frac{\partial \mathrm{F}}{\partial t} + \dot{\mathrm{x}}_i \frac{\partial \mathrm{F}}{\partial \mathrm{x}_i}\right) = \mathcal{A} \int_{\mathbb{R}^3} |\dot{\boldsymbol{\eta}}| (\mathrm{F}'\mathrm{G}' - \mathrm{F}\mathrm{G}) \, d\dot{\mathcal{Y}} \tag{424}$$

Where $\mathfrak{K} = \ell_{\mathrm{c}}/\ell$ is the Knudsen number and $\mathcal{V} = \mathcal{A}\ell$ therefore $\mathcal{A} = \pi\varnothing^2\mathfrak{K}$. The compact form of (424) can then be written as $\mathfrak{K}(\mathrm{d}\mathrm{F}/\mathrm{d}t) = \mathcal{J}[\mathrm{F}, \mathrm{G}]$. From here, we will expand the distribution and the partial time derivative according to Chapman and Enskog [15; ch.7]:

$$\mathrm{F} = \mathrm{F}^{\mathbb{0}} + \mathfrak{K}\mathrm{F}^{\mathbb{1}} + \mathcal{O}(\mathfrak{K}^2) \tag{425}$$

$$\dot{\mathrm{F}} = \partial_{\mathbb{1}}\mathrm{F} + \mathfrak{K}\partial_{\mathbb{2}}\mathrm{F} + \mathcal{O}(\mathfrak{K}^2) \tag{426}$$

For ease of notation, the partial time derivatives have been written as $\partial_{\mathbb{I}}\mathrm{F} = \partial_{\mathbb{I}}\mathrm{F}/\partial t \;\forall\; \mathbb{I} = 1,2$. As mentioned in ch.4.2, these derivatives do not indicate different time scales but varying levels of description regarding transport processes. In contrary to typical perturbation methods [19; ch.14], which are used to approximate solutions to differential equations, this unique methodology

is used to derive higher order evolution equations, which involve the production of entropy. For example, the first order evolutions of the velocity and internal energy fields are provided in (299) and (300) respectively, while the second order evolutions are:

$$\rho\partial_{\mathbb{2}}\mathrm{v}_i = \nabla_l\sigma_{il} \tag{427}$$

$$\rho\partial_{\mathbb{2}}\varepsilon = \sigma_{il}\nabla_i\mathrm{v}_l + \nabla_i(\kappa\nabla_i\mathrm{T}) \tag{428}$$

In regards to the entropy, the first order evolution can be found in (302), while the second order evolution can be expressed as $\partial_{\mathbb{2}}\varepsilon = \mathrm{T}\partial_{\mathbb{2}}\mathrm{s}$. One may now construct the total evolutions from the expansion $\partial = \partial_{\mathbb{1}} + \partial_{\mathbb{2}}$. In consequence, $\partial\varepsilon = \partial_{\mathbb{1}}\varepsilon + \mathrm{T}\partial_{\mathbb{2}}\mathrm{s}$. We'll now feed (425) and (426), in addition to $\mathrm{G} = \mathrm{G}^{\mathbb{0}} + \mathfrak{K}\mathrm{G}^{\mathbb{1}}$, into (424), then separate the terms according to the Knudsen number:

$$\mathcal{O}(\mathfrak{K}^0)\text{:} \qquad \mathscr{J}[\mathfrak{F}^{\mathbb{0}}] = 0 \tag{429}$$

$$\mathcal{O}(\mathfrak{K}^1)\text{:} \qquad \partial_{\mathbb{1}}\mathrm{F}^{\mathbb{0}} + \dot{\mathrm{x}}_i\nabla_i\mathrm{F}^{\mathbb{0}} = \mathscr{J}[\mathfrak{F}^{\mathbb{1}}] \tag{430}$$

$$\mathcal{O}(\mathfrak{K}^2)\text{:} \qquad \partial_{\mathbb{2}}\mathrm{F}^{\mathbb{0}} + \partial_{\mathbb{1}}\mathrm{F}^{\mathbb{1}} + \dot{\mathrm{x}}_i\nabla_i\mathrm{F}^{\mathbb{1}} = \mathscr{J}[\mathfrak{F}^{\mathbb{2}}] \tag{431}$$

To explain the collision terms, since $\mathfrak{F} = \mathrm{FG}$, then the total distribution expands as:

$$\mathfrak{F} = \mathfrak{F}^{\mathbb{0}} + \mathfrak{K}\mathfrak{F}^{\mathbb{1}} + \mathfrak{K}^2\mathfrak{F}^{\mathbb{2}} \tag{432}$$

$$= \mathrm{F}^{\mathbb{0}}\mathrm{G}^{\mathbb{0}} + \mathfrak{K}(\mathrm{F}^{\mathbb{1}}\mathrm{G}^{\mathbb{0}} + \mathrm{F}^{\mathbb{0}}\mathrm{G}^{\mathbb{1}}) + \mathfrak{K}^2\mathrm{F}^{\mathbb{1}}\mathrm{G}^{\mathbb{1}}$$

It is easy to observe that $\mathfrak{F}^{\mathbb{0}} = \mathrm{F}^{\mathbb{0}}\mathrm{G}^{\mathbb{0}}$, $\mathfrak{F}^{\mathbb{2}} = \mathrm{F}^{\mathbb{1}}\mathrm{G}^{\mathbb{1}}$, and $\mathfrak{F}^{\mathbb{1}}$ expands as:

$$\mathfrak{F}^{\mathbb{1}} = \mathrm{F}^{\mathbb{1}}\mathrm{G}^{\mathbb{0}} + \mathrm{F}^{\mathbb{0}}\mathrm{G}^{\mathbb{1}} = \mathfrak{F}^{\mathbb{0}}(\mathrm{F}^{\mathbb{1},\mathbb{0}} + \mathrm{G}^{\mathbb{1},\mathbb{0}}) = \mathfrak{F}^{\mathbb{0}}\mathfrak{F}^{\mathbb{1},\mathbb{0}} \tag{433}$$

Where $\mathrm{F}^{\mathbb{1},\mathbb{0}} = \mathrm{F}^{\mathbb{1}}/\mathrm{F}^{\mathbb{0}}$ and $\mathrm{G}^{\mathbb{1},\mathbb{0}} = \mathrm{G}^{\mathbb{1}}/\mathrm{G}^{\mathbb{0}}$ so that $\mathfrak{F}^{\mathbb{1},\mathbb{0}} = \mathfrak{F}^{\mathbb{1}}/\mathfrak{F}^{\mathbb{0}}$. Referring back to the master relation (282), it will be recognized that we've here set $\Delta[\![\mathrm{F}]\!] = \mathscr{J}[\mathrm{F},\mathrm{G}]\delta t$. We'll next feed (433) into (430), while utilizing (303), to obtain:

$$-\frac{1}{\tau}\mathrm{F}^{\mathbb{1}} = \mathcal{A}\int_{\mathbb{R}^3}|\dot{\boldsymbol{\eta}}|(\mathrm{F}^{\mathbb{1},\mathbb{0}\prime} + \mathrm{G}^{\mathbb{1},\mathbb{0}\prime} - \mathrm{F}^{\mathbb{1},\mathbb{0}} - \mathrm{G}^{\mathbb{1},\mathbb{0}})\mathfrak{F}^{\mathbb{0}}\,d\dot{\mathcal{Y}} \tag{434}$$

It will be reminded that the solution to (429) yields the relation $\mathfrak{F}^{\mathbb{0}} = \mathfrak{F}^{\mathbb{0}\prime}$. The BGK operator was developed after the publication of [15], however, Chapman and Enskog used a similar formulation to determine an expression for $\mathrm{F}^{\mathbb{1}}$; see (364): $\mathrm{F}^{\mathbb{1},\mathbb{0}} = -\tau\beta\mathcal{L}_{il}(\nabla_l\mathrm{v}_i)$. For the sake of simplicity, we've neglected the temperature gradient and the Lagrange tensor is taken from (361):

$$\mathcal{L}_{il} = \mathrm{dev}(\dot{q}_i\dot{q}_l) = \dot{q}_i\dot{q}_l - \tfrac{1}{3}|\dot{\boldsymbol{q}}|^2\delta_{il} \tag{435}$$

However, the function τ now has dependence upon $\dot{\mathbf{x}}$. Upon defining the individual perturbations

as $\mathrm{F}^{\mathbb{1},\mathbb{0}} = -\beta(\nabla_l \mathrm{v}_i)\tau_1 \mathrm{M}_{il}$ and $\mathrm{G}^{\mathbb{1},\mathbb{0}} = -\beta(\nabla_l \mathrm{v}_i)\tau_2 \mathrm{N}_{il}$, then feeding into (434), we obtain the constraint equation used by Chapman and Enskog [15; ch.7]:

$$\mathrm{M}_{ij}\mathrm{F}^{\mathbb{0}} = \mathcal{A}\int_{\mathbb{R}^3} |\dot{\boldsymbol{\eta}}|(\tau_1 \mathrm{M}_{ij} + \tau_2 \mathrm{N}_{ij} - \tau_1' \mathrm{M}_{ij}' - \tau_2' \mathrm{N}_{ij}')\mathfrak{F}^{\mathbb{0}}\, d\dot{\mathcal{Y}} \tag{436}$$

The NS viscous stress tensor will next be expressed in the following form:

$$\sigma_{ij} = -\int_{\mathbb{R}^3} \dot{q}_i \dot{q}_j \mathrm{F}^{\mathbb{1}}\, d\dot{\mathcal{Q}} = \beta(\nabla_l \mathrm{v}_k)\int_{\mathbb{R}^3} \tau \dot{q}_i \dot{q}_j \,\mathrm{dev}(\dot{q}_k \dot{q}_l)\,\mathrm{F}^{\mathbb{0}}\, d\dot{\mathcal{Q}} \tag{437}$$

$$= \frac{1}{5}\beta\,\mathrm{dev}(\mathrm{A}_{ij})\int_{\mathbb{R}^3} \tau\,\mathrm{dev}(\dot{q}_k \dot{q}_l)\,\mathrm{dev}(\dot{q}_k \dot{q}_l)\,\mathrm{F}^{\mathbb{0}}\, d\dot{\mathcal{Q}}$$

Where the integral theorem found within [15; ch.1] has been implemented, $\mathrm{A}_{ij} = \frac{1}{2}(\nabla_i \mathrm{v}_j + \nabla_j \mathrm{v}_i)$ is the symmetric part of the velocity gradient tensor, and $\mathrm{dev}(\mathrm{A}_{ij}) = \mathrm{A}_{ij} - \frac{1}{3}\mathrm{A}_{kk}\delta_{ij}$. Since the molecules only possess translational degrees of freedom, the coefficient of dilatational viscosity is zero. The NS viscous stress tensor may then be expressed as $\sigma_{ij} = 2\mu\,\mathrm{dev}(\mathrm{A}_{ij})$. Through utilizing (437), the coefficient of shearing viscosity may now be identified as:

$$\mu = \frac{1}{10}\beta\int_{\mathbb{R}^3} \tau\,\mathrm{dev}(\dot{q}_k \dot{q}_l)\,\mathrm{dev}(\dot{q}_k \dot{q}_l)\,\mathrm{F}^{\mathbb{0}}\, d\dot{\mathcal{Q}} \tag{438}$$

The final step is to expand τ into a series, plug into (436), then solve for the coefficients. Upon multiplying (436) by $\mathrm{M}_{ij}\phi_\alpha d\dot{\mathcal{X}}$, then integrating, one obtains the governing constraint equation:

$$\int_{\mathbb{R}^3} \mathrm{M}_{ij}\mathrm{M}_{ij}\phi_\alpha \mathrm{F}^{\mathbb{0}}\, d\dot{\mathcal{X}} = \mathcal{A}\int_{\mathbb{R}^3} \mathrm{M}_{ij}\phi_\alpha \int_{\mathbb{R}^3} |\dot{\boldsymbol{\eta}}|(\tau_1 \mathrm{M}_{ij} + \tau_2 \mathrm{N}_{ij} - \tau_1' \mathrm{M}_{ij}' - \tau_2' \mathrm{N}_{ij}')\mathfrak{F}^{\mathbb{0}}\, d\dot{\mathcal{Y}} d\dot{\mathcal{X}} \tag{439}$$

The remaining process is far beyond the scope of our purpose here, which is to show the overall Chapman-Enskog methodology. A similar procedure can be performed for the coefficient of thermal conductivity in addition to mass diffusion coefficients involving a gas mixture. On a final note, we'll briefly discuss the Boltzmann H-theorem. To do so, we must first identify the following symmetry properties of the collision integral [14; ch.4]:

$$\int_{\mathbb{R}^3}\int_{\mathbb{R}^3} \psi(\dot{\mathbf{x}})|\dot{\boldsymbol{\eta}}|\delta\mathfrak{F}\, d\dot{\mathcal{Y}} d\dot{\mathcal{X}} = \int_{\mathbb{R}^3}\int_{\mathbb{R}^3} \psi(\dot{\mathbf{y}})|\dot{\boldsymbol{\eta}}|\delta\mathfrak{F}\, d\dot{\mathcal{Y}} d\dot{\mathcal{X}} \tag{440}$$

$$= -\int_{\mathbb{R}^3}\int_{\mathbb{R}^3} \psi'|\dot{\boldsymbol{\eta}}|\delta\mathfrak{F}\, d\dot{\mathcal{Y}}' d\dot{\mathcal{X}}' = -\int_{\mathbb{R}^3}\int_{\mathbb{R}^3} \psi'|\dot{\boldsymbol{\eta}}|\delta\mathfrak{F}\, d\dot{\mathcal{Y}} d\dot{\mathcal{X}}$$

If we define the post-collision velocities as $\dot{\mathbf{x}}' = \dot{\mathbf{x}} + (\boldsymbol{\epsilon}\cdot\dot{\boldsymbol{\eta}})\boldsymbol{\epsilon}$ and $\dot{\mathbf{y}}' = \dot{\mathbf{y}} - (\boldsymbol{\epsilon}\cdot\dot{\boldsymbol{\eta}})\boldsymbol{\epsilon}$, where the vector $\boldsymbol{\epsilon}$ is the apse direction, then the momentum balance (41) is automatically satisfied [14; ch.3].

We next find that $d\dot{\mathcal{X}}' d\dot{\mathcal{Y}}' = d\dot{\mathcal{X}} d\dot{\mathcal{Y}}$ iff $|\boldsymbol{\epsilon}| = 1$, which would then also satisfy the energy balance (42). In consequence, we obtain the following identity:

$$\int_{\mathbb{R}^3} \psi(\dot{\mathbf{x}}) \mathcal{J}[\mathfrak{F}]\, d\dot{\mathcal{X}} = \frac{1}{4} \int_{\mathbb{R}^3} [\psi(\dot{\mathbf{x}}) + \psi(\dot{\mathbf{y}}) - \psi(\dot{\mathbf{x}}') - \psi(\dot{\mathbf{y}}')] \mathcal{J}[\mathfrak{F}]\, d\dot{\mathcal{X}} \tag{441}$$

The H-quantity will next be defined as $\mathsf{H} = \mathrm{F} \ln \mathrm{F}$, where Boltzmann's H-theorem states:

$$\int_{\mathbb{R}^3} \Big(\frac{\partial \mathsf{H}}{\partial t} + \dot{\mathrm{x}}_i \frac{\partial \mathsf{H}}{\partial \mathrm{x}_i} \Big)\, d\dot{\mathcal{X}} \leq 0 \tag{442}$$

Since $\mathrm{d}\mathsf{H} = (\ln \mathrm{F} + 1)\mathrm{dF}$, then upon dividing by $\mathrm{d}t$ and recalling (423), one obtains:

$$\frac{\partial \mathsf{H}}{\partial t} + \dot{\mathrm{x}}_i \frac{\partial \mathsf{H}}{\partial \mathrm{x}_i} = \pi \varnothing^2 (\ln \mathrm{F} + 1) \int_{\mathbb{R}^3} |\dot{\boldsymbol{\eta}}| (\mathrm{F}' \mathrm{G}' - \mathrm{FG})\, d\dot{\mathcal{Y}} \tag{443}$$

Lastly, we'll multiply by $d\dot{\mathcal{X}}$, integrate, and implement the identity (441):

$$\int_{\mathbb{R}^3} \Big(\frac{\partial \mathsf{H}}{\partial t} + \dot{\mathrm{x}}_i \frac{\partial \mathsf{H}}{\partial \mathrm{x}_i} \Big)\, d\dot{\mathcal{X}} = \pi \varnothing^2 \int_{\mathbb{R}^3} \int_{\mathbb{R}^3} (\ln \mathrm{F} + 1) |\dot{\boldsymbol{\eta}}| (\mathrm{F}' \mathrm{G}' - \mathrm{FG})\, d\dot{\mathcal{Y}}\, d\dot{\mathcal{X}} \tag{444}$$

$$= \frac{1}{4} \pi \varnothing^2 \int_{\mathbb{R}^3} \int_{\mathbb{R}^3} |\dot{\boldsymbol{\eta}}| (\ln \mathfrak{F} - \ln \mathfrak{F}')(\mathfrak{F}' - \mathfrak{F})\, d\dot{\mathcal{Y}}\, d\dot{\mathcal{X}} \leq 0$$

Since $\ln(\mathfrak{F}/\mathfrak{F}')\,(\mathfrak{F}' - \mathfrak{F}) \leq 0$, the above inequality is satisfied, hence the choice of sign in (422).

Lattice Boltzmann Interpretation

There are two different routes which may be taken. The first will analyze the LBE (68):

$$(\ell_{\mathrm{c}}/\ell)(\mathrm{F} - \mathrm{F}_{\mathrm{o}}) = -(\delta t/\Delta t)(\mathrm{F}_{\mathrm{o}} - \mathrm{M}_{\mathrm{o}}) \tag{445}$$

Where the relaxation time has been expressed as $\tau = \mathfrak{K} \Delta t$, which is no longer dependent upon $\boldsymbol{\xi}$. In contrary to (69), a second order Taylor series will now be applied to the solution:

$$\mathrm{F}[\mathbf{x}(t), t] = \mathrm{F}(\mathbf{x}_{\mathrm{o}}, t_{\mathrm{o}}) + \mathrm{d}\mathrm{F}/\mathrm{d}t|_{t_{\mathrm{o}}}\, \delta t + \tfrac{1}{2} \mathrm{d}^2\mathrm{F}/\mathrm{d}t^2|_{t_{\mathrm{o}}}\, \delta t^2 + \mathcal{O}(\delta t^3) \tag{446}$$

Upon combining the LBE (445) and the expansion (446), one may generally state:

$$\mathfrak{K} \left(\mathrm{d}\mathrm{F}/\mathrm{d}t + \frac{1}{2} \delta t\, \mathrm{d}^2\mathrm{F}/\mathrm{d}t^2 \right) \approx -\frac{1}{\Delta t} (\mathrm{F} - \mathrm{M}) \tag{447}$$

Since $\mathrm{d}\mathrm{F}/\mathrm{d}t = \dot{\mathrm{F}} + \xi_i \nabla_i \mathrm{F}$, then $\mathrm{d}^2\mathrm{F}/\mathrm{d}t^2 = \ddot{\mathrm{F}} + 2\xi_i \nabla_i \dot{\mathrm{F}} + \xi_i \xi_l \nabla_i \nabla_l \mathrm{F}$. From here, (425) and (426) are fed into (447) and the terms are separated according to the Knudsen number. Using this

ad hoc methodology, the coefficient of kinematic viscosity is interpreted as $\nu = \Theta(\Delta t - \frac{1}{2}\delta t)$. The resulting mathematical structure of the NS viscous stress tensor, varies throughout the literature. For example, [23] recovers (316) $\forall\ \eta = 0$, while [7; ch.4] uncovers terms which are cubic in velocity $\forall\ \eta = \frac{2}{3}\mu$. Regardless, this procedure is not incorporated within the LB algorithm but is an interpretation of the LBE. The second route of analysis begins with the EOM (66):

$$\mathfrak{K}(\dot{\mathrm{F}} + \boldsymbol{\xi} \cdot \boldsymbol{\nabla}\mathrm{F}) = -\Delta t^{-1}(\mathrm{F} - \mathrm{M}) \tag{448}$$

Given $\ell_{\mathrm{c}} = \overline{v}t_{\mathrm{c}}$, then a set of nondimensional quantities are identified as: $\grave{t} = tt_{\mathrm{c}}^{-1}$, $\grave{\mathrm{x}}_i = \mathrm{x}_i(\xi_i t_{\mathrm{c}})^{-1}$ (no summation), and $\grave{v} = \overline{v}\Delta t/\ell$. Therefore, (448) may also be expressed in the form:

$$\grave{v}\big(\partial\mathrm{F}/\partial\grave{t} + \textstyle\sum_{i=1}^{3} \partial\mathrm{F}/\partial\grave{\mathrm{x}}_i\big) = -(\mathrm{F} - \mathrm{M}) \tag{449}$$

Upon substituting (425) and (426) into (448), one may find expressions for $\mathrm{F}^{\mathbb{I}}\ \forall\ \mathbb{I} = 1{,}2$:

$$\mathrm{F}^{\mathbb{1}} = -(\partial_{\mathbb{1}}\mathrm{F}^{\mathbb{0}} + \xi_i\nabla_i\mathrm{F}^{\mathbb{0}})\Delta t \tag{450}$$

$$\mathrm{F}^{\mathbb{2}} = -(\partial_{\mathbb{2}}\mathrm{F}^{\mathbb{0}} + \partial_{\mathbb{1}}\mathrm{F}^{\mathbb{1}} + \xi_i\nabla_i\mathrm{F}^{\mathbb{1}})\Delta t \tag{451}$$

In this more general framework, one finds $\nu = \Theta\Delta t$; see for example [31]. One may now construct the total evolution equation as:

$$\dot{\mathrm{F}}^{\mathbb{0}} + \xi_i\nabla_i\mathrm{F} = \mathscr{J}[\mathfrak{F}] - \partial_{\mathbb{1}}\mathrm{F}^{\mathbb{1}} \tag{452}$$

Where from (430) and (431), $\mathscr{J}[\mathfrak{F}^{\mathbb{I}}] = -\mathrm{F}^{\mathbb{I}}\Delta t^{-1}$. Additionally, $\mathrm{F} = \mathrm{F}^{\mathbb{0}} + \mathrm{F}^{\mathbb{1}}$, $\dot{\mathrm{F}}^{\mathbb{0}} = \partial_{\mathbb{1}}\mathrm{F}^{\mathbb{0}} + \partial_{\mathbb{2}}\mathrm{F}^{\mathbb{0}}$, and $\mathscr{J}[\mathfrak{F}] = \mathscr{J}[\mathfrak{F}^{\mathbb{0}}] + \mathscr{J}[\mathfrak{F}^{\mathbb{1}}] + \mathscr{J}[\mathfrak{F}^{\mathbb{2}}]$. Upon multiplying by ϕ, in reference to (71), then integrating over the velocity space, we uncover a weak form of Leo's EOM:

$$\int_{\mathbb{R}^3} (\dot{\mathrm{F}}^{\mathbb{0}} + \xi_i\nabla_i\mathrm{F})\phi\, d\Xi = 0 \tag{453}$$

Which is in actuality the governing EOM for fluid and gas simulations; in contrary to (66). If one were to solve (66) over a phasetime element, the exact solution is simply: $\mathrm{F} = \mathrm{F}^{\mathbb{0}} + \mathrm{F}^{\mathbb{1}}$, where $\mathrm{F}^{\mathbb{1}} = \mathrm{F}^{\mathbb{0}}\exp(-\mathfrak{t})$ and $\mathrm{F}^{\mathbb{0}}$ satisfies $\dot{\mathrm{F}}^{\mathbb{0}} = -\xi_i\nabla_i\mathrm{F}^{\mathbb{0}}$. As one can observe, the first order evolution is nonexistent; in contrary to the solutions to Leo's EOM provided in ch.4.4. Therefore, the BGK solution is not directly related to the stress tensor nor heat flux vector.

Relation to the QVFEM Derivation

The theoretical framework established in ch.4.2 is quite analogous to the Chapman-Enskog methodology shown here, where the total evolution operator is given by $\partial = \partial_{\mathbb{1}} + \partial_{\mathbb{2}}$. However, we considered $\partial_{\mathbb{2}}$ as the total evolution operator and arrived at a similar result. This goes to show that this perturbation procedure is not mathematically rigorous and should not be assumed to be naturally built into the Boltzmann equation. At this current point in time, a direct connection to the NS equations has never been found. To reconcile the two procedures, one could set each evolution

to $\partial_{\mathbb{I}}\mathrm{F}^{\mathbb{O}} = -\xi_i \nabla_i \mathrm{F}^{\mathbb{I}}$ so that the total evolution is found from $\dot{\mathrm{F}}^{\mathbb{O}} = \partial_{\mathbb{1}}\mathrm{F}^{\mathbb{O}} + \partial_{\mathbb{2}}\mathrm{F}^{\mathbb{O}}$. Alternatively, we can use the Reynolds transport theorem, such that: $\dot{\mathrm{F}}^{\mathbb{O}} = -\nabla_i \mathrm{g}_i$, where the flux vector is defined as $\mathrm{g}_i = \xi_i \mathrm{F}$.

Bibliography

[1] Newton, I. (2021). *The mathematical principles of natural philosophy*. Phoemixx Classics Ebooks.

[2] Euler, L. (1757). Principes généraux du mouvement des fluides. *Mémoires de l'académie des sciences de Berlin*, 274-315.

[3] Navier, C. (1822). *Mémoire sur les lois du mouvement des fluides* (pp. 389-440). éditeur inconnu.

[4] Stokes, G. G. (2007). On the theories of the internal friction of fluids in motion, and of the equilibrium and motion of elastic solids.

[5] Bistafa, S. R. (2017). On the development of the Navier-Stokes equation by Navier. *Revista Brasileira de Ensino de Física*, *40*.

[6] Sheng, W. (2020). A revisit of Navier–Stokes equation. *European Journal of Mechanics-B/Fluids*, *80*, 60-71.

[7] Krüger, T., Kusumaatmaja, H., Kuzmin, A., Shardt, O., Silva, G., & Viggen, E. M. (2017). The lattice Boltzmann method. *Springer International Publishing*, *10*(978-3), 4-15.

[8] Mohamad, A. A. (2011). *Lattice boltzmann method* (Vol. 70). London: Springer.

[9] Goldstein, H., Poole, C., & Safko, J. (2002). Classical mechanics.

[10] Kasdin, N. J., & Paley, D. A. (2011). *Engineering dynamics: a comprehensive introduction*. Princeton University Press.

[11] Casella, G., & Berger, R. L. (2021). *Statistical inference*. Cengage Learning.

[12] Pearson, C. E., & Saunders, H. (1987). Handbook of Applied Mathematics.

[13] Marion, J. B. (1985). Classical dynamics of particles and systems. *(No Title)*.

[14] Harris, S. (2004). *An introduction to the theory of the Boltzmann equation*. Courier Corporation.

[15] Chapman, S., & Cowling, T. G. (1990). *The mathematical theory of non-uniform gases: an account of the kinetic theory of viscosity, thermal conduction and diffusion in gases*. Cambridge university press.

[16] Griffiths, D. J., & Schroeter, D. F. (2018). *Introduction to quantum mechanics*. Cambridge university press.

[17] Haynes, W. M. (Ed.). (2014). *CRC handbook of chemistry and physics*. CRC press.

[18] Einstein, A. (1915). Investigations on the Theory of the Brownian Movement.

[19] Haberman, R. (2004). Applied partial differential equations with Fourier series and boundary value problems. *(No Title)*.

[20] Lavoisier, A. L. (1806). *Elements of chemistry in a new systematic order containing all the modern discoveries* (Vol. 1). Evert Duyckinck, no. 110 Pearl-Street, and James and Thomas Ronalds, no. 188 Pearl-Street.

[21] Perumal, D. A., & Dass, A. K. (2015). A Review on the development of lattice Boltzmann computation of macro fluid flows and heat transfer. *Alexandria Engineering Journal*, *54*(4), 955-971.

[22] Dellar, P. J. (2001). Bulk and shear viscosities in lattice Boltzmann equations. *Physical Review E*, *64*(3), 031203.

[23] Coelho, R. C., Ilha, A., Doria, M. M., Pereira, R. M., & Aibe, V. Y. (2014). Lattice boltzmann method for bosons and fermions and the fourth-order hermite polynomial expansion. *Physical Review E*, *89*(4), 043302.

[24] Mei, R., Luo, L. S., Lallemand, P., & d'Humières, D. (2006). Consistent initial conditions for lattice Boltzmann simulations. *Computers & Fluids*, *35*(8-9), 855-862.

[25] Wei, X., Li, W., Mueller, K., & Kaufman, A. E. (2004). The Lattice-Boltzmann method for simulating gaseous phenomena. *IEEE Transactions on Visualization and Computer Graphics*, *10*(2), 164-176.

[26] Petersen, K. J., & Brinkerhoff, J. R. (2021). On the lattice Boltzmann method and its application to turbulent, multiphase flows of various fluids including cryogens: A review. *Physics of Fluids*, *33*(4).

[27] Hosseini, S. A., Atif, M., Ansumali, S., & Karlin, I. V. (2023). Entropic lattice Boltzmann methods: A review. *Computers & Fluids*, 105884.

[28] Babinsky, H., & Harvey, J. K. (Eds.). (2011). *Shock wave-boundary-layer interactions* (Vol. 32). Cambridge University Press.

[29] So, R. M. C., Fu, S. C., & Leung, R. C. K. (2010). Finite difference lattice Boltzmann method for compressible thermal fluids. *AIAA journal*, *48*(6), 1059-1071.

[30] Misztal, M. K., Hernandez-Garcia, A., Matin, R., Sørensen, H. O., & Mathiesen, J. (2015). Detailed analysis of the lattice Boltzmann method on unstructured grids. *Journal of Computational Physics*, *297*, 316-339.

[31] Li, Q., He, Y. L., Wang, Y., & Tao, W. Q. (2007). Erratum: Coupled double-distribution-function lattice Boltzmann method for the compressible Navier-Stokes equations [Phys. Rev. E 76, 056705 (2007)]. *Physical Review E*, *76*(6), 069902.

[32] Liu, Q., Feng, X. B., & Lu, C. W. (2019). Simulating high-Mach-number compressible flows with shock waves via Hermite-expansion-based lattice Boltzmann method. *Physica A: Statistical Mechanics and its Applications*, *533*, 122062.

[33] Qiu, R. F., Zhu, C. X., Chen, R. Q., Zhu, J. F., & You, Y. C. (2018). A double-distribution-function lattice Boltzmann model for high-speed compressible viscous flows. *Computers & Fluids*, *166*, 24-31.

[34] WANG, Y., He, Y. L., Zhao, T. S., Tang, G. H., & Tao, W. Q. (2007). Implicit-explicit finite-difference lattice Boltzmann method for compressible flows. *International Journal of Modern Physics C*, *18*(12), 1961-1983.

[35] Pieraccini, S., & Puppo, G. (2007). Implicit–explicit schemes for BGK kinetic equations. *Journal of Scientific Computing*, *32*, 1-28.

[36] Qu, K., Shu, C., & Chew, Y. T. (2007). Alternative method to construct equilibrium distribution functions in lattice-Boltzmann method simulation of inviscid compressible flows at high Mach number. *Physical Review E*, *75*(3), 036706.

[37] Rathan, S., & Raju, G. N. (2018). A modified fifth-order WENO scheme for hyperbolic conservation laws. *Computers & Mathematics with Applications*, *75*(5), 1531-1549.

[38] Pareschi, L., & Russo, G. (2005). Implicit–explicit Runge–Kutta schemes and applications to hyperbolic systems with relaxation. *Journal of Scientific computing*, *25*, 129-155.

[39] Shan, X. (2016). The mathematical structure of the lattices of the lattice Boltzmann method. *Journal of Computational Science*, *17*, 475-481.

[40] Shan, X. (2010). General solution of lattices for Cartesian lattice Bhatanagar-Gross-Krook models. *Physical Review E*, *81*(3), 036702.

[41] Shan, X., & He, X. (1998). Discretization of the velocity space in the solution of the Boltzmann equation. *Physical Review Letters*, *80*(1), 65.

[42] Sayler, H. M. (2019). *Hypersonic weapons: Background and issues for Congress*. Congressional Research Service.

[43] Fu, L. (2019). A very-high-order TENO scheme for all-speed gas dynamics and turbulence. *Computer Physics Communications*, *244*, 117-131.

[44] Ji, Z., Liang, T., & Fu, L. (2023). High-Order Finite-Volume TENO Schemes with Dual

ENO-Like Stencil Selection for Unstructured Meshes. *Journal of Scientific Computing*, *95*(3), 76.

[45] Gurtin, M. E., Fried, E., & Anand, L. (2010). *The mechanics and thermodynamics of continua*. Cambridge university press.

[46] Holzapfel, G. A. (2002). Nonlinear solid mechanics: a continuum approach for engineering science.

[47] Huynh, H. (1995). Accurate upwind schemes for the Euler equations. In *12th Computational Fluid Dynamics Conference* (p. 1737).

[48] Kashyap, D., & Dass, A. K. (2020). Benchmark compressible flow simulation based on lattice Boltzmann method. *Materials Today: Proceedings*, *28*, 2522-2526.

[49] Anderson, J. D., & Wendt, J. (1995). *Computational fluid dynamics* (Vol. 206, p. 332). New York: McGraw-hill.

[50] Anderson, J. D. (1989). *Hypersonic and high temperature gas dynamics*. Aiaa.

[51] Einstein, A. (1907). Planck's theory of radiation and the theory of specific heat. *Ann. Phys*, *22*, 180-190.

[52] Hatsopoulos, G. N., & Gyftopoulos, E. P. (1979). *Thermionic energy conversion. Volume II. Theory, technology, and application* (No. DOE/TIC-11035). MIT Press, Cambridge, MA.

[53] Gyftopoulos, E. P., & Beretta, G. P. (2005). *Thermodynamics: foundations and applications*. Courier Corporation.

[54] Friedman, M. (1972). *Foundations of Space-Time Theories* (Doctoral dissertation, Princeton University).

[55] Gnoffo, P. A. (1989). *Conservation equations and physical models for hypersonic air flows in thermal and chemical nonequilibrium* (Vol. 2867). National Aeronautics and Space Administration, Office of Management, Scientific and Technical Information Division.

[56] Baron Fourier, J. B. J. (2003). *The analytical theory of heat*. Courier Corporation.

[57] Cramer, M. S. (2012). Numerical estimates for the bulk viscosity of ideal gases. *Physics of fluids*, *24*(6).

[58] Cockburn, B., Lin, S. Y., & Shu, C. W. (1989). TVB Runge-Kutta local projection discontinuous Galerkin finite element method for conservation laws III: one-dimensional systems. *Journal of computational Physics*, *84*(1), 90-113.

[59] Sutherland, W. (1893). LII. The viscosity of gases and molecular force. *The London, Edinburgh, and Dublin Philosophical Magazine and Journal of Science*, *36*(223), 507-531.

[60] Jaiswal, S. (2021). Isogeometric schemes in rarefied gas dynamics context. *Computer Methods in Applied Mechanics and Engineering*, *383*, 113926.

[61] Villani, C. (2002). A review of mathematical topics in collisional kinetic theory. *Handbook of mathematical fluid dynamics*, *1*(71-305), 3-8.

[62] Huynh, H. T. (1995). Accurate upwind methods for the Euler equations. *SIAM Journal on Numerical Analysis*, *32*(5), 1565-1619.

[63] Toro, E. F., & Vázquez-Cendón, M. E. (2012). Flux splitting schemes for the Euler equations. *Computers & Fluids*, *70*, 1-12.

[64] Toro, E. F. (1989). A weighted average flux method for hyperbolic conservation laws. *Proceedings of the Royal Society of London. A. Mathematical and Physical Sciences*, *423*(1865), 401-418.

[65] Hulbert, G. M., & Hughes, T. J. (1990). Space-time finite element methods for second-order hyperbolic equations. *Computer methods in applied mechanics and engineering*, *84*(3), 327-348.

[66] Chen, W. (2021). Heat transfer at speed of sound. *International Journal of Heat and Mass Transfer*, *177*, 121529.

[67] Lopez Molina, J. A., Rivera, M. J., & Berjano, E. (2014). Fourier, hyperbolic and relativistic heat transfer equations: a comparative analytical study. *Proceedings of the Royal Society A: Mathematical, Physical and Engineering Sciences*, *470*(2172), 20140547.

[68] Jaeger, F., Matar, O. K., & Müller, E. A. (2018). Bulk viscosity of molecular fluids. *The Journal of chemical physics*, *148*(17).

[69] Sharipov, F. (2015). *Rarefied gas dynamics: fundamentals for research and practice*. John Wiley & Sons.